VYSOKÉ UČENÍ TECHNICKÉ V BRNĚ

Fakulta chemická

habilitační práce v oboru

Chemie a technologie ochrany životního prostředí

VYUŽITÍ MOŽNOSTÍ, KTERÉ PŘINESLA TECHNIKA VYSOKOROZLIŠOVACÍ AAS S KONTINUÁLNÍM ZDROJEM ZÁŘENÍ DO VÝZKUMU MATERIÁLŮ ŽIVOTNÍHO PROSTŘEDÍ

RNDr. Ondřej Zvěřina, Ph.D.

Brno 2024

Děkuji všem, se kterými jsem měl možnost spolupracovat na výzkumu, a také všem těm, kteří mě podporovali a inspirovali.

Obsah

1. Úvod

Výskytu potenciálně toxických prvků je věnována velká pozornost, motivovaná potřebou chránit lidské zdraví a životní prostředí. Do této široké skupiny prvků patří ryze toxické kovy a nekovy (zejména arsen, kadmium, olovo a rtuť) i prvky esenciální, byť toxické ve vyšším množství (selen, zinek, železo a mnohé další). Postupné prohlubování znalostí o výskytu a dopadu těchto prvků v prostředí zvyšuje nároky na metody jejich stanovení. Proto je nezbytné průběžné zdokonalování souvisejících analytických postupů.

Atomová absorpční spektrometrie (AAS) je tradiční a zaužívaná technika prvkové analýzy. Komerčně dostupná je již od 60. let 20. století, načež se záhy stala zlatým standardem díky své robustnosti, širokému rozsahu stanovitelných prvků a dostupnosti metodických postupů. Koncem minulého století se však AAS ocitla pod tlakem nových „konkurenčních“ analytických technik, založených na indukčně vázaném plazmatu ve spojení s optickou nebo hmotnostní spektrometrií. Oproti klasické AAS nabídly tyto techniky nesporné výhody a v současné době jde již o metody první volby.

Od nultých let tohoto století však AAS zažívá znovuoživení zájmu díky představení komerčně dostupných AA spektrometrů s vysokým rozlišením (*high-resolution continuum source*, HR-CS). Tato technologie otevřela zbrusu nové možnosti pro analýzu složek životního prostředí; umožňuje například měřit více prvků současně, stanovit i některé nekovové prvky, nebo zajistit spolehlivější výsledky díky lepší korekci interferencí. Předložená práce využívá nových možností vysokorozlišovací AAS v environmentální analýze, což je – vzhledem k povaze a rozmanitosti přírodních materiálů – mimořádně náročná analytická disciplína.

2. Cíle habilitační práce

Cílem této práce je **prohlubovat nové možnosti analýzy materiálů životního prostředí**, které přineslo začlenění vysokého rozlišení a kontinuálního zdroje záření (HR-CS) do atomové absorpční spektrometrie (AAS). **Inovativní postupy, založené na HR-CS AAS, jsou demonstrovány na analýze různých složek prostředí: rostlin, půd, potravinářských surovin i biologických materiálů**.

Pro zasazení inovací do náležitého kontextu úvodní část práce popisuje dosavadní vývoj atomové absorpční spektrometrie. Z fundamentálních základů této techniky totiž vyplývají i jistá omezení, znesnadňující analýzu přírodních materiálů. Jde především o její omezení na jednoprvkovou analýzu (přičemž v ekologických studiích jsou důležité vztahy mezi různými prvky), její úzký pracovní rozsah (když obsahy prvků v různě exponovaných materiálech vykazují řádové rozdíly) a omezená kontrola interferencí (protože přírodní materiály obsahují mnohé rušivé složky).

Druhá a hlavní část habilitační **práce předkládá řešení těchto překážek environmentální analýzy**. Jsou představeny nově vyvinuté analytické metody, které – s využitím potenciálu HR-CS – výše uvedená omezení překonávají. Ze souboru komentovaných prací je přitom patrné, že se nejedná o prosté aplikace nové techniky, ale systematické noření se do možností, které technika pro studium zkoumaných materiálů nabízí. Specifické jsou v tomto ohledu už příprava vzorku, hledání vhodných vlnových délek a podmínek pro měření zájmových prvků ve zkoumaných materiálech, nebo adaptace citlivosti pro přizpůsobení metod specifickým účelům.

Mezi představené přínosy patří například nový způsob odečítání signálu, jenž umožňuje stanovení analytů v rostlinných materiálech v nebývale širokém koncentračním rozpětí. V kombinaci s (rovněž nově popsanými) metodami víceprvkové analýzy je tak možné současné stanovení kontaminujících a referenčních prvků, umožňující zhodnocení úrovně kontaminace prostředí. Dále jsou popsány nové metody analýzy těžko stanovitelných prvků, například fosforu.

Ke splnění vytyčených cílů bylo vybráno a komentováno 9 autorských publikací. V některých kapitolách je navíc odkazováno na vybrané bakalářské, diplomové a disertační práce, které vznikly pod mým vedením – zejména pro zasazení vyvinutých metod do náležitého kontextu. Prezentováno je také několik dosud nepublikovaných výsledků.

3. Seznam komentovaných prací

I. **Zvěřina, O**; Brůhová, L; Coufalík, P; Stringer, CD; Rieger, J; Goessler, W, 2024. *Multi-element analysis (Pb, Al, Fe) of Antarctic flora using HR-CS ETAAS with an extended working range.* SPECTROCHIMICA ACTA PART B-ATOMIC SPECTROSCOPY. 10.1016/j.sab.2024.106979

II. Coufalík, P; Vašinka, M; Krmíček, L; Ševčík, R; **Zvěřina, O**; Brůhová, L; Komárek, J, 2024. *Toxic metals in cyanobacterial mat of Big Lachman Lake, James Ross Island, Antarctica.* ENVIRONMENTAL MONITORING AND ASSESSMENT. 10.1007/s10661-023-12224-3

III. **Zvěřina, O**; Vychytilová, M; Rieger, J; Goessler, W, 2023. *Fast and simultaneous determination of zinc and iron using HR-CS GF-AAS in vegetables and plant material.* SPECTROCHIMICA ACTA PART B-ATOMIC SPECTROSCOPY. 10.1016/j.sab.2023.106616

IV. Coufalík, P; **Zvěřina, O**; Sádovská, K; Komárek, J, 2023. *UV-photochemical vapor generation coupled to hydride generation AAS in the study of dietary intake of Se, Hg, Cd, and Pb from fish.* JOURNAL OF FOOD COMPOSITION AND ANALYSIS. 10.1016/j.jfca.2023.105668

V. Kosečková, P; **Zvěřina, O** ✉; Pechová, M; Krulíková, M; Duborská, E; Borkovcová, M, 2022. *Mineral profile of cricket powders, some edible insect species and their implication for gastronomy.* JOURNAL OF FOOD COMPOSITION AND ANALYSIS. 10.1016/j.jfca.2021.104340

VI. **Zvěřina, O**; Venclíček, O; Kuta, J; Coufalík, P; Hagarová, I; Brat, K, 2021. *A simple dilute-and-shoot procedure for the determination of platinum in human pleural effusions using HR-CS GF-AAS.* JOURNAL OF TRACE ELEMENTS IN MEDICINE AND BIOLOGY. 10.1016/j.jtemb.2021.126869

VII. Brtnický, M; Pecina, V; Galiová, MV; Prokeš, L; **Zvěřina, O**; Juřička, D; Klimánek, M; Kynický, J, 2020. *The impact of tourism on extremely visited volcanic island: Link between environmental pollution and transportation modes.* CHEMOSPHERE. 10.1016/j.chemosphere.2020.126118

VIII. **Zvěřina, O**; Coufalík, P; Šimůnek, J; Kachlík, P; Chlupová, R; Pavelková, J, 2020. *Inorganic pollutants in the indoor environment of the Moravian Library: assessment of Cd, Pb, Cu, and Zn in total suspended particles and dust using HR-CS GF-AAS.* ENVIRONMENTAL MONITORING AND ASSESSMENT. 10.1007/s10661-020-08748-7

IX. **Zvěřina, O**; Kuta, J; Coufalík, P; Kosečková, P; Komárek, J, 2019. *Simultaneous determination of cadmium and iron in different kinds of cereal flakes using high-resolution continuum source atomic absorption spectrometry.* FOOD CHEMISTRY. 10.1016/j.foodchem.2019.125084

4. Atomová absorpční spektrometrie

Principem AAS je měření absorpce záření volnými atomy sledovaného prvku. Současná instrumentace v hlavních obrysech udržuje uspořádání definované před šedesáti lety. Relativně nedávno však byly představeny přístroje využívající inovativní technologie, o jejichž přínosech pro analýzu složek životního prostředí tato práce pojednává. Pro náležité vysvětlení významu těchto inovací však bude užitečné začít od samotných základů. Následující kapitoly jsou proto věnovány hlavním milníkům a průlomům ve vývoji techniky AAS.

4.1. Od pozorování slunce po moderní atomovou spektrometrii

Kořeny optické spektroskopie sahají do období vědecké revoluce v 17. století a jsou spjaty zejména s Isaacem Newtonem, který popsal rozklad slunečního záření do barevného spektra pomocí hranolu. Významnou českou stopu v prvopočátcích spektroskopie zanechal Jan Marek Marci z Kronlandu (Lanškrouna), působící jako profesor na Karlo-Ferdinandově univerzitě v Praze. Na základě svých pozorování sepsal tzv. Knihu o Duze (1648), v níž popsal různé optické jevy včetně principu vzniku duhy skrze dvojlom světla na vodních kapkách v atmosféře. Také Marci experimentoval s rozkladem světla pomocí hranolu do spektra, přičemž si povšiml, že vzniklé monochromatické světlo již nelze dále rozložit a popsal také difrakci světla pomocí mřížky. Někdy proto bývá označován **Marci jako první spektroskopista** (Štoll 1996; Welz and Sperling 2008).

Objev *absorpční* spektrometrie úzce souvisí s pozorováním slunečního záření, v jehož rozloženém spektru William Wollaston rozpoznal sérii tmavých čar (1802), tedy **první popsané absorpční spektrum**. Tyto čáry později zkoumal Joseph Fraunhofer a nejvýraznější z nich označil písmeny; od červené části spektra A až K. Výrazně žlutá sodíková čára 589 nm se dodnes označuje jako čára D. Původ těchto tmavých spektrálních čar vysvětlil David Brewster (1820) jakožto absorpci některých složek jinak spojitého světla ve sluneční atmosféře (Shah et al. 2020; Koirtyohann 1991).

V první polovině 19. století začali badatelé zkoumat spektra generovaná pomocí elektrických oblouků a jisker a několik také začalo využívat plameny jakožto excitační zdroje pro emisní spektrometrii. Ve dvacátých letech John Herschel a William Talbot systematicky zaznamenávali spektra solí různých prvků v plameni a identifikovali jednotlivé alkalické kovy na základě zbarvení plamene. Položili tím základy pro práci Gustava Kirchhoffa a Roberta Bunsena, kteří s využitím Bunsenova kahanu, jež díky průzračnému plameni umožnil lepší pozorování spekter, prohloubili dosavadní pochopení principů absorpce a emise záření prvky (1859-1961).

Systematicky zkoumali *zvraty čar* ve spektrech mnoha alkalických kovů a kovů alkalických zemin a předvedli, že žlutá spektrální čára emitovaná sodíkem je totožná s Fraunhoferovou čarou D ve slunečním spektru. Kirchhoff předpokládal, že ostatní Fraunhoferovy čáry jsou způsobeny absorpcí záření dalšími prvky a také zformuloval myšlenku, že hmota dokáže **emitovat záření určité vlnové délky a záření o stejné vlnové délce také absorbovat**. Postupně přiřadili i další čáry jednotlivým prvkům (kromě sodíku ve spektru prokázali přítomnost draslíku, vápníku a železa), dále objevili cesium a rubidium. Atomová spektroskopie se rychle stala hlavní metodou **prokazování nových prvků**. Tímto postupem William Crookes objevil thalium (1861) a Ferdinand Reich a Hieronymus Richter indium (1863). Ve slunečním spektru byla také vedle sodíkové linie rozpoznána nová výrazná žlutá čára 587 nm a přiřazena novému prvku, pojmenovanému helium, jehož výskyt nebyl tehdy nikde krom slunce pozorován. Po doplnění periodické tabulky o řadu nových prvků, obzvlášť pak jinými způsoby těžko rozlišitelných přechodných kovů, se ale tato analytická metoda příliš nerozvíjela (Welz and Sperling 1999; Shah et al. 2020).

Atomová spektra však umožnila rozvoj kvantové teorie, která je zpětně pomohla vysvětlit. Bohrův model atomu (1913) stál na myšlence, že atomy se nevyskytují v náhodných, ale v přesně definovaných energetických stavech. Absorpcí kvanta energie přechází atom (elektron) do excitovaného stavu, ze kterého po 10^{-9} až 10^{-8} sekundy relaxuje zpět do základního stavu, přičemž rozdílovou energii emituje. Skutečnost, že absorpce záření je exponenciálně závislá na koncentraci již dříve popsal August Beer (1852).

Půda pro nástup AAS byla tedy připravena. Mimo astronomii však metoda nedosáhla popularity. Její rozmach přišel až v šedesátých letech, kdy Alan Walsh stál u zrodu prvních moderních přístrojů pro AAS.

4.2. Moderní atomová spektrometrie

Ačkoli fundamentální popis přístroje pro AAS v roce 1955 publikovali i další autoři, hlavní zásluhy a otcovství metody jsou přikládány Australanovi **Alanu Walshovi**. Nejen, že jím vytvořený koncept obsahoval některé důležité prvky opomenuté ostatními, ale svým nasazením prolomil prvotní nezájem o novou techniku a zasadil se o její rozšíření do praxe. Na začátku, v roce 1952, byl jednoduchý nákres konceptu se sodíkovou lampou, Mekerovým kahanem, spektroskopem a detektorem záření. O jedenáct let později byl představen Model 303, první komerčně dostupný přístroj pro AAS od firmy Perkin-Elmer (L'vov 2005; Walsh 1999).

Jako klíčové pro vznik AAS uvádí Walsh svoje zkušenosti se spektrochemickou analýzou kovů, následované mnohaletým využívám infračervené spektrometrie pro studium molekul. Zaujal ho

zaběhlý zvyk, zkoumat molekuly na základě absorpčních spekter, zatímco atomy na základě emise. Když ke svému překvapení nenašel pro tento úzus žádné argumenty[1], pustil se do mnohaletého vývoje absorpčního spektrometru. Hlavní výhody měření absorpce spatřoval v její relativní nezávislosti na teplotě atomových par a excitačním potenciálu a také v menších potížích se samoabsorpcí (Walsh 1974). Díky znalosti modulace signálu v IČ spektrometrii začlenil modulaci světelného svazku i do svého přístroje. Přerušované propouštění zdrojového záření přes absorpční prostředí umožnilo odečíst emisní spektrum plamene, a tedy měřit čistou absorpci. Tento zásadní prvek jeho tehdejší konkurenti nepoužili a pro vyplývající potíže vývoj časem opustili (Alkemade and Milatz 1955).

V období rozmachu AAS v 60. a 70. letech byly Walshem nastavené základy zdokonalovány. Základní prvky instrumentace klasické AAS jsou stručně popsány na následujících stranách. Výraznější technologický průlom přineslo představení komerčně dostupných přístrojů pro vysokorozlišovací AAS na začátku 21. století.

4.2.1. Atomizátory

Jelikož pouze volné atomy prvků mohou absorbovat charakteristické záření, je nutné jejich převedení na volné atomy v *atomizátoru*. Walsh jako atomizátor pro AAS vyzdvihoval plamen (*flame* AAS, resp. F-AAS).

Praktické provedení vypadá tak, že kapalný vzorek je kapilárou nasáván do přístroje, kde je nejprve zmlžovačem převeden na co nejjemnější aerosol, který vstupuje do plamene. Během krátkého průchodu plamenem dochází k vypaření rozpouštědla a atomizaci analytu. Volné atomy zachycují záření lampy a tato míra zeslabení se odečítá jako **absorbance**.

Oproti tehdy populárním jiskrovým zdrojům má plamen nižší teplotu, což je pro měření absorbance výhodou. Nižší teplota atomové páry vede totiž k vyššímu podílu atomů v základním stavu, tedy k jednodušším spektrům a vyšší citlivosti díky převaze přechodů mezi základním a prvním excitovaným stavem.

Brzy však začal být zřejmý nedostatek, že při atomizaci v nízkoteplotním plameni některé prvky nejsou plně atomizovány, což vede k nízké citlivosti a interferencím. První přístroje využívaly pro plamen směs svítiplyn-vzduch s teplotou kolem 1800 °C, což nebylo dostatečné pro měření prvků jako je vápník ve složitých matricích. Přes prvotní obavy z bezpečnosti se acetylen brzy

[1] Preference emise nad absorpcí měla spíš historické opodstatnění; je snazší detekovat slabé světlo na tmavém pozadí než naopak, obzvlášť pak při detekci fotografickou deskou, kdy malé ztmavnutí na jinak čiré desce je zřetelnější než téměř černý proužek na zcela černé vyvolané desce (Welz et al. 2005).

prosadil jako standardní palivo a plamen acetylen–vzduch s teplotou kolem 2300 °C řadu potíží vyřešil. Pro měření některých těžko atomizovatelných prvků, jako je např. hliník, bylo zapotřebí najít ještě teplejší plamen, ovšem ne příliš rychle hořící. Tím se stal plamen acetylen – oxid dusný, který zavedl Walshův kolega J. B. Willis a který s teplotou kolem 2800 °C umožňoval stanovení více než 65 prvků (Walsh 1974; Willis 1965; 1997).

Mezitím ve vzdáleném a politicky uzavřeném Rusku rozvíjel zcela nový typ atomizátoru Boris L'vov. Nadšen Walshovou první publikací chtěl ověřit myšlenku atomové absorpce, k dispozici měl však jen sodíkovou lampu a hranol – ne už hořák. Zkusil tedy atomizovat špetku soli v grafitové peci a záření lampy, procházející pecí, pozoroval přes hranol. Tomuto experimentu obětoval svoji letní dovolenou, když se ale před jeho očima sodíková spektrální čára postupně vytratila, pochopil, že absorpce půjde měřit i bezplamenovou technikou (L'vov 2005). Jeho publikace se – podobně jako Walshovy – setkaly s vlažným přijetím, přestože atomizátor poskytoval řádově lepší citlivost. Nadšení se mu podařilo rozšířit až během návštěvy první mezinárodní konference o AAS v Praze (1967). První komerčně dostupný **elektrotermický atomizátor** byl představen v roce 1970. Vycházel ze zjednodušené verze navržené Massmanem, kdy se vzorek vkládal dovnitř relativně pomalu ohřívané grafitové kyvety. Rozvoj elektrotermické techniky (ET-AAS, nebo GF-AAS z *graphite furnace*) přinesl nový impuls právě v době, kdy se začínalo zdát, že vývoj AAS ustal – v lehce skepticky pojmenovaném článku „*AAS–stagnant or pregnant?"* vkládal Walsh do tohoto elektrotermického atomizátoru velké naděje. Technika skutečně oživila zájem o AAS, jelikož přinesla až o tři řády lepší citlivost oproti atomizaci v plameni. Grafitová kyveta byla později doplněna o platformu, která zpožďuje atomizaci analytu do fáze již dostatečně vytemperovaného prostoru kyvety.

Použití platformy se stalo jedním ze základních pilířů konceptu, který popsal Walter Slavin jako STPF: *stabilized temperature platform furnace* (Slavin et al. 1981). Jde o soubor podmínek zajišťujících ideální průběh analýzy v ET-AAS. Zahrnuje atomizaci za izotermických podmínek, dobře definovaný povrch grafitu, účinnou korekci pozadí, zastavený průtok inertního plynu během atomizace, použití chemických modifikátorů a vyhodnocování signálu na základě plochy píku.

Pro analýzu materiálů životního prostředí znamenala elektrotermická technika výrazný přínos. Její citlivost umožnila detekovat rizikové prvky, které se v prostředí vyskytují v nízkých, byť relevantních koncentracích. Metoda ET-AAS například umožnila stanovení a s ním i kontrolu vysoce toxických prvků, jakými jsou olovo a kadmium – a to i v povrchových vodách a potravinách.

4.2.2. Průběh analýzy ET-AAS

Typická analýza v ET-AAS probíhá následovně. Na platformu grafitové kyvety automatický dávkovač napipetuje vzorek o objemu jednotek až desítek mikrolitrů, načež je spuštěn **teplotní program**. Vzorek je postupně vysušen a poté je během *pyrolýzy* za zvýšené teploty odstraněna větší část matrice, přičemž analyt zůstává na platformě. K jeho převedení na volné atomy dochází při *atomizaci*, kdy se teplota rychle zvýší nad teplotu varu měřeného prvku a měří se signál (absorbance), který má charakter pulzu. V závěrečné fázi je kyveta vyčištěna od zbytků vzorku dalším krátkým nárůstem teploty. Cyklus trvá jednu až dvě minuty.

Pro zlepšení průběhu měření se často využívají chemické **modifikátory**. Slouží k odstranění rušivých vlivů a pro lepší separaci analytu od matrice při atomizaci. Modifikátory nejčastěji stabilizují analyt a umožňují vyšší teplotu pyrolýzy pro účinnější odstranění doprovodných složek. Pro těkavé prvky Cd a Pb se osvědčil fosfátový modifikátor, univerzálnější jsou modifikátory na bázi palladia, které stabilizují více než 20 prvků. Využívají se také *permanentní* modifikátory, jako je W, Ir, nebo Zr, které pokryjí grafitový povrch vrstvou karbidů a vydrží v kyvetě po mnoho analýz.

4.2.3. Zdroje záření

Zdroj záření musí poskytovat vysokou intenzitu především v UV oblasti spektra, kde se nachází většina analyticky významných čar. V prvních letech vývoje Walsh pracoval s různými zdroji záření. **Kontinuální zdroj však brzy opustil**, protože neposkytoval dostatečnou citlivost, zejména kvůli nedostatečnému rozlišení Littrowova monochromátoru. Na detektor se dostávalo příliš mnoho neabsorbovaného záření blízkých vlnových délek a absorpce analytu se proto podílela na celkové absorpci jen málo. Walsh kontinuální zdroj záření pro svůj spektrometr zavrhl, když si dopočítal, že dostatečné vymezení spektrální čáry by vyžadovalo monochromátor s rozlišovací schopností 2 pm, což se jevilo nereálné. Potřeboval tedy použít zdroj záření s co nejostřejší emisní čárou, která by byla absorbována výhradně analytem. Monochromátor by pouze oddělil tuto čáru od dalších emitovaných vlnových délek a rozptýleného záření (Walsh 1974).

Dutá katoda byla v té době již dlouho známa – jako zdroj záření ji představil v roce 1916 Friedrich Paschen –, ale pro potřeby AAS ji bylo nutné zdokonalit, do čehož se Walsh s kolegy pustili. V původní verzi například vyžadovala neustálý proplach argonem. Právě **dutokatodové lampy** udělaly z AAS citlivou a vysoce selektivní metodu, byť za cenu jejího omezení měřit vždy pouze jeden prvek. Velice ostrá emisní čára dutokatodové lampy – podstatně užší než absorpční profil čáry analytu – vede k lineárnějším kalibračním závislostem než při použití zdrojů záření se širším

profilem, jako jsou jiskry a oblouky. Později byly představeny také bezelektrodové výbojky poskytující vyšší intenzitu, zejména vhodné pro měření v nízkých vlnových délkách.

4.2.4. Korekce pozadí

Již od prvních pokusů bylo zřejmé, že záření lampy není absorbováno pouze měřeným prvkem, ale také *nespecificky* – hlavně rozptylem záření na částicích a absorpčními pásy molekul. První nepříliš přesné korekce pozadí vycházely z měření *blízké čáry* jiného prvku nebo *neabsorbujících čar* analytu. V roce 1965 bylo navrženo využití kontinuálního záření deuteriové lampy, jejíž absorpce je měřena v oblasti analytické čáry vymezené šířkou štěrbiny monochromátoru. Výhodou tohoto řešení bylo, že šlo snadno implementovat do prvního AAS přístroje Perkin-Elmer Model 303. Zjevnou nevýhodou odečtu průměrné absorpce v oblasti analytické čáry byla nepřesná korekce strukturovaného pozadí a překorigování signálu v přítomnosti blízkého silně absorbujícího prvku (Welz and Sperling 1999). Přesto je deuteriová korekce pozadí dodnes využívána.

Později byly vyvinuty pokročilejší techniky korekce pozadí, měřící jeho úroveň co nejblíž analytické čáře. Efekt samozvratu emisní čáry výbojky, kdy vysokoproudý pulz vede k výraznému rozšíření čáry a zároveň k samoabsorpci v jejím středu, využívá korekce typu Smith-Hieftje (Smith and Hieftje 1983).

Ještě účinnější korekční systém využívá *Zeemanova jevu*, založeném na štěpení energetických hladin atomů v silném magnetickém poli. Prvotní řešení aplikovala magnetické pole na zdroj záření. Po letech postupného vývoje se ukázalo, že nejlepší výsledky přináší aplikace paralelně orientovaného proměnného magnetického pole přímo na atomizátor. Během zapnutí magnetu je díky „rozestoupení“ tzv. σ-složek spektrální čáry možno měřit samotné pozadí v místě analytické čáry, přičemž π-složky při této konfiguraci chybí (Otruba et al. 1978).

4.3. Vysokorozlišovací AAS s kontinuálním zdrojem záření

Úvodní neúspěchy s kontinuálními zdroji záření neodradily řadu výzkumníků od snahy o jejich využití v AAS; vidina víceprvkové analýzy a přesnější korekce pozadí byla silnou motivací. Slibná se v tomto směru ukázala **kombinace xenonové výbojky a monochromátoru echelle** mřížky s vysokým rozlišením (Keliher and Wohlers 1974). Předpovědi z osmdesátých let hlásaly, že AAS s kontinuálním zdrojem záření přinese možnosti srovnatelné s tehdy novými metodami ICP-OES a ICP-MS – a to při nižších nákladech. Walshovu obavu o „stagnující a nepregnantní“ AAS rozptylovaly prognózy tím, že metoda přinese revoluci v absorpčním i emisním měření, takže se naopak těhotenství blíží konci a jeho výsledkem budou možná i dvojčata (Marshall et

al. 1986). Vývoj však nepostupoval tak rychle a stejná „těhotenská“ metafora fungovala ještě i v posledním mileniálním čísle journalu Spectrochimica Acta, věnovaném tehdy nedávno zesnulému Alanu Walshovi. Podle Bernarda Welze se jako slibné vývojové větve AAS jevily přímá analýza pevných látek – a právě kontinuální zdroje záření. O průlom se zasloužila zejména vědecká skupina Helmuta Becker-Rosse, která na rozdíl od většiny ostatních nešla cestou kombinování dostupných komponent, ale vyvíjela svoje vlastní součástky na základě přesně definovaných požadavků (Becker-Roß et al. 1996); kromě zdroje záření také monochromátor se speciálním uspořádáním.

První komerčně dostupný přístroj, vycházející z jejich konceptu, byl spektrometr ContrAA 300, představený firmou Analytik Jena v roce 2003 (Becker-Ross et al. 2006). Verze s elektrotermickou atomizací přišla v roce 2007. Uspořádání spektrometru znázorňuje Obrázek 1. Pro techniku vysokorozlišovací AAS s kontinuálním zdrojem záření, tedy *high-resolution continuum source*, se vžila zkratka HR-CS AAS.

Zjednodušeně by se dalo říci, že oproti tradiční AAS s čárovým zdrojem záření (nově odlišované jako *line source* AAS, LS-AAS), která sleduje závislost absorbance na čase, **HR-CS přidává třetí rozměr – vlnovou délku**. Podle původního záměru to přineslo přesnější korekci pozadí, mimo jiné díky možnosti matematického odečtu strukturovaného molekulárního pozadí. Zároveň se otevřely dveře pro sledování nekovů a detekci vícero prvků současně.

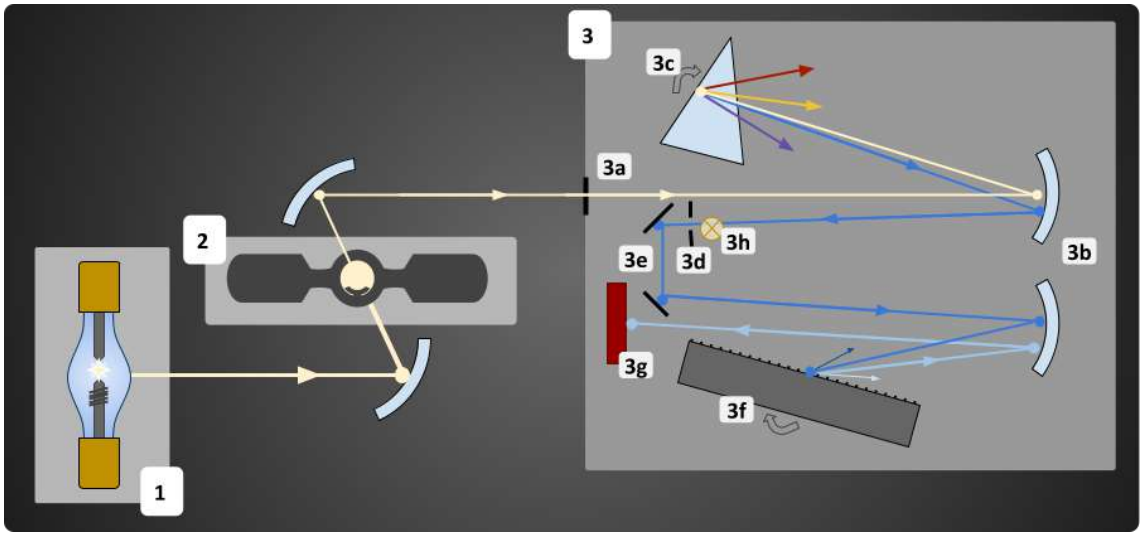

Obrázek 1: Schéma HR-CS ET-AAS instrumentace: 1) xenonová vysokotlaká výbojka, 2) atomizátor, 3) dvojitý monochromátor s vysokým rozlišením; 3a) vstupní štěrbina, 3b) parabolická zrcadla, 3c) Littrowův hranol pro separaci řádů spektra, 3d) meziclona 30 µm, 3e) zrcadla, 3f) echelle mřížka, 3g) CCD detektor, 3h) neonová lampa.

4.3.1. Xe výbojka jakožto zdroj kontinuálního záření

Problémem tradičních zdrojů kontinuálního záření byla jejich slabá intenzita zejména v UV oblasti spektra, kde se nachází většina významných analytických čar. Dostatečnou intenzitu poskytla speciální xenonová výbojka s krátkým obloukem, provozovaná v tzv. *hot-spot* režimu, kdy mezi elektrodami vzniká vysoce intenzivní plazmový výboj o teplotě přes 10 000 K. Toho je dosaženo díky speciálním materiálům elektrod, jejich blízkosti <1 mm a vysokému tlaku xenonu. Protože se plazmová skvrna pohybuje, její záření je sledováno pohyblivým piezoelektricky řízeným zrcátkem a neustále směřováno do vstupní štěrbiny monochromátoru. Kvůli výkonu 300 W je nutné chlazení výbojky vodním okruhem. Poskytovaná intenzita vztažená na 1 nm je asi o dva řády vyšší než u dutokatodové výbojky, a to i v oblasti pod 200 nm. Díky tomu je i pro prvky jako je As a Se dosahováno citlivosti minimálně srovnatelné s čárovými zdroji (Welz et al. 2005; Becker-Ross et al. 2006)

4.3.2. Monochromátor s vysokým rozlišením

Nároky kladené na rozlišení spektrometru jsou u HR-CS AAS vysoké. Pro správně fungující korekci pozadí je nutný současný záznam analytické čáry i jejího spektrálního okolí. Klasické mřížkové spektrometry konfigurace Czerny-Turner svými vlastnostmi nevyhovují. Nynější přístroje jsou založeny na konstrukci DEMON (*double echelle monochromator*, viz obrázek 1), sestávající z hranolového předmonochromátoru a echelle mřížky. Záření xenonové výbojky je tedy nejprve rozloženo pomocí otočného hranolu v Littrowově konfiguraci a pouze jeho malá výseč prochází štěrbinou do echelle monochromátoru s vysokým rozlišením.

Detektorem záření je lineární CCD snímač. Současné přístroje využívají snímače s 588 pixely, z nichž 200 slouží pro analytické účely, tj. zaznamenávání analytické čáry a jejího blízkého spektrálního okolí. Ostatní pixely slouží pro interní funkce přístroje, jako korekce fluktuace záření lampy.

Poskytované spektrální rozlišení optického systému je lepší než 2 pm na 1 pixel. Detektor pokrývá spektrální interval 0,2 až 0,3 nm v závislosti na vlnové délce.

U monochromátoru je nutné i přesné seřízení absolutní vlnové délky. Pro reprodukovatelné výsledky musí být vlnová délka nastavena s přesností v řádu femtometrů (Welz et al. 2010b). Ke kalibraci slouží neonová lampa, vestavěná mezi hranol a echelle monochromátor; neonová lampa poskytuje relativně úzké spektrální čáry, vhodné pro vnitřní kalibraci.

4.3.3. Korekce pozadí v HR-CS AAS

Matrice přírodních materiálů jsou komplexní a kromě analytů obsahují složky více nebo méně rušící stanovení. I pokud je vzorek před analýzou mineralizován, a tedy je odstraněna většina matrice, v roztoku mineralizátu je analyt stále v přítomnosti dalších minerálních látek a také například kyseliny použité k mineralizaci. Mnohé z těchto složek se při měření projevují specifickou nebo nespecifickou absorpcí, které je pro dosažení správných a přesných výsledků nutné eliminovat. K tomu slouží korekce pozadí, jejíž princip je v HR-CS AAS jiný oproti klasické AAS. Tato málo nápadná inovace je z praktického hlediska vrcholně významná.

V úvodní části byl popsán význam modulace záření lampy v klasické AAS, se kterou přišel Alan Walsh. Modulace (přerušování záření lampy) byla zajišťována buď mechanicky – rotujícím segmentem –, nebo střídavým napájením lampy. V okamžicích, kdy lampa nesvítila, bylo možné sledovat záření samotného atomizátoru. Modulace signálu přinesla větší specificitu, protože emise samotného atomizátoru – ať už zářícího plamene, nebo doruda rozžhavené grafitové kyvety – byla automaticky odečtena.

Ve vysokorozlišovací AAS něco takového není nutné. Důvodem je o jeden až dva řády vyšší intenzita záření xenonové lampy, která činí příspěvek záření atomizátoru zanedbatelný. Zadruhé, i případný intenzivní zářivý přechod by neovlivnil měření, pokud by jeho vlnová délka přesně nekorespondovala s analytickou čarou – a i v takovém případě by byl celkem účinně odstraněn interním korekčním systémem.

Důležitým faktorem při korekci pozadí je kolísání záření lampy. Intenzitu záření lampy neustále sledují „neanalytické“ pixely detektoru. Kolísání intenzity záření je tedy sledováno zároveň s měřením a jeho korekce je díky tomu velice přesná. Navíc, protože světlo je sledováno až za atomizátorem, korekce zahrnuje také veškeré změny v optické propustnosti prostředí, tedy *nespecifickou* absorpci. Matematicky je následně celé pozadí „srovnáno do roviny“; vyrovnány jsou: vyzařované spektrum xenonové výbojky, charakteristická intenzita odlesku echelle mřížky, průběžně se měnící transmitance celého prostředí (Welz et al. 2005; 2010b).

Po korekci souvislého záření může ve spektru zůstat kromě čáry analytu ještě **strukturované pozadí**, způsobené absorpcí molekul, případně přítomností dalších prvků ve vzorku. Pokud žádný z absorpčních pásů nepřekrývá analytickou čáru, není třeba zasahovat. V případě, že k překryvu dochází, je někdy možné úpravou teplotního programu dosáhnout rozdělení analytu a interferentu v čase (v případě elektrotermické atomizace). Další možností je odečtení korekčního spektra samotné interferující molekuly (Becker-Ross et al. 2000).

Strukturované pozadí se často vyskytuje při měření vzorků obsahujících vysoké množství fosforu (například hub, cereálií a olejnin). Vznikající molekuly monoxidu fosforu (PO) se projevují jemnými absorpčními pásy, které přímo překrývající některé významné analytické čáry. Další interferující molekuly se mohou objevovat při vysokém obsahu síry (mořské řasy, cibuloviny) nebo křemíku ve vzorku (zejména při analýze půd nebo obilovin – např. rýže).

4.3.4. Aplikace a postavení HR-CS AAS v environmentální analýze

Technika **HR-CS AAS se nejčastěji využívá ve stopové a ultrastopové prvkové analýze**. Ve verzi s plamenovou atomizací je vhodná ke kvantifikaci prvků v koncentrační hladině přibližně mg/l, zatímco ve spojení s elektrotermickým atomizátorem dosahuje o tři řády lepší citlivosti, tedy µg/l. Stejně jako u klasické LS-AAS je možné její spojení s hydridovou technikou pro analýzu hydridotvorných prvků, nebo s metodou studených par pro detekci rtuti.

Z přehledových studií vyplývá, že většina publikovaných prací využívá elektrotermický atomizátor (70 %), následovaný plamenovým (24 %) (Resano et al. 2019). Asi 30 % prací se věnuje přímé analýze pevných vzorků (*solid sampling, SS*), pro jejichž vnášení do grafitové kyvety existuje komerčně dostupné řešení. Díky přesné korekci pozadí, možnosti používání chemických modifikátorů a kalibraci vodnými roztoky patří SS HR-CS ET-AAS mezi zdaleka nejčastější techniky přímé analýzy pevných vzorků (Machado et al. 2020; Pasias et al. 2021) a objevují se stále nové aplikace převážně v environmentální analýze (Bacon et al. 2024).

Asi čtvrtina publikovaných studií se věnuje studiu molekul. Prvky, které se stanovují na základě absorpčních pásů svých diatomických molekul, jsou nejčastěji fluor jako CaF nebo GaF, síra jako CS, fosfor jako PO, nebo chlor, tvořící celou plejádu využitelných molekul: AlCl, InCl, SrCl, CaCl, GaCl a MgCl (Resano et al. 2019). Formálně se pak jedná o *molekulovou* absorpční spektrometrii, HR-CS MAS.

Analytické laboratoře mají možnost volby mezi řadou různých spektrometrických metod pro prvkovou analýzu a volí v závislosti na svých požadavcích, možnostech a v neposlední řadě také na rozpočtu. Na poli environmentální analýzy je AAS využívána nejčastěji pro analýzu rostlinných materiálů (Hossain et al. 2021), poněkud méně pro analýzu půd a vod. Hlavními alternativami k AAS jsou metody založené na indukčně vázaném plazmatu (ICP). V sedmdesátých letech přišly komerčně dostupné optické emisní spektrometry s indukčně vázaným plazmatem (ICP-OES) a v osmdesátých pak hmotnostní spektrometry (ICP-MS). Obě tyto techniky poskytují výhodu víceprvkového měření, přičemž citlivost ICP-OES je blízká plamenové AAS a ICP-MS pro většinu prvků dokonce překonává ET-AAS. Praktický je jejich široký dynamický rozsah. Tyto techniky jsou v současnosti využívány pro prvkovou analýzu

nejčastěji (Hossain et al. 2021; Douvris et al. 2023). Jejich pořizovací i provozní náklady jsou vyšší, vyplácejí se proto v laboratořích s vysokou prostupností vzorků. V posledních dekádách se navíc objevily emisní spektrometry využívající mikrovlnné indukční plazma (MIP-OES), které sice nedosahují citlivostí F-AAS ani ICP-OES, avšak stále s výhodami víceprvkové analýzy a při velmi příznivých provozních nákladech (Douvris et al. 2023).

Široká dostupnost HR-CS AAS v nultých letech a její nové možnosti znovu oživily zájem o AAS, jak je patrné z literární analýzy (Obrázek 2). V rozmezí let 2001 až 2023 bylo publikováno 587 prací s tematikou HR-CS AAS, které nasbíraly 11 260 citací (resp. 6 527 bez autocitací). Publikace jsou na portálu Web of Science nejčastěji indexovány v následujících oblastech výzkumu: *Chemistry* (62 %), *Spectroscopy* (35 %), *Food Science Technology* (14 %), *Environmental Sciences Ecology* (7 %), *Biochemistry Molecular Biology* (6 %), *Engineering* (5 %) a *Nutrition Dietetics* (4 %).

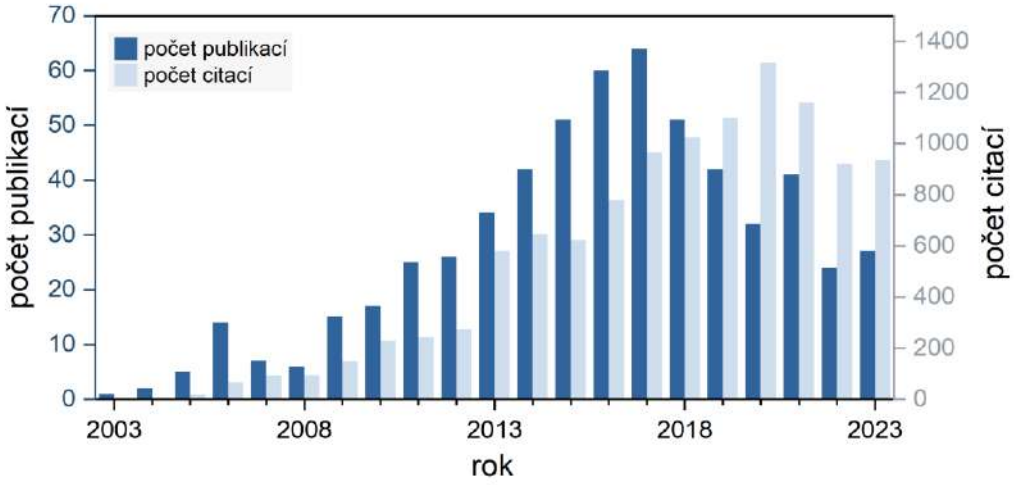

Obrázek 2: Počet publikací a citací na portálu Web of Science s klíčovým heslem high-resolution continuum source AAS.

Po dvaceti letech v běžném provozu už nelze HR-CS AAS považovat tak docela za novinku. Dozrála v plnohodnotnou nástupnici LS-AAS a na trhu je aktuálně třetí generace spektrometrů. Dokladem takového přechodu je, že v poslední dekádě se téměř pětina publikací vyskytuje v aplikovaných časopisech, věnovaných nejčastěji klinické a environmentální analýze a analýze potravin (Resano et al. 2019; Patriarca et al. 2023; Bacon et al. 2024).

Podobně tomu je i publikací, o které se opírá tato habilitační práce: některé byly zveřejněny ve fundamentálních spektroskopických časopisech, větší část však v časopisech zaměřených na environmentální analýzu. Právě v analýze rostlin, půd a dalších přírodnin spočívá hlavní směr využití HR-CS AAS – a její potenciál v tomto směru se nadále rozvíjí, což je cílem i této předložené práce.

5. Nové možnosti, které HR-CS AAS přinesla do analýzy složek životního prostředí

Rostliny, půdy, sedimenty i potravinové suroviny jsou komplexní materiály a vzhledem k jejich charakteru není jejich analýza přímočará. Tato část se věnuje konkrétním novým možnostem, které pro jejich analýzu technika vysokorozlišovací AAS přináší. Následující **čtyři kapitoly vysvětlují přínosy habilitační práce** v jednotlivých oblastech zájmu, kterými jsou:

- Víceprvková analýza
- Korekce strukturovaného pozadí
- Rozšiřování dynamického rozsahu měření
- Nekovy a další těžko stanovitelné prvky

Každá kapitola obsahuje komentáře k autorským publikacím, které se dané oblasti věnují. Odkazovaných devět publikací je k nalezení v příloze. V některých případech se dílčí aspekty vyvinutých metod promítají do více kapitol. Pro úplnost jsou uváděny i bakalářské, diplomové a disertační práce mnou vedených/konzultovaných studentů, které rozvíjely daná témata. Je uvedena i malá část dosud nepublikovaných výsledků, které dokreslují aktuální směr výzkumu.

5.1. Víceprvková analýza

Omezení měřit vždy pouze jeden prvek značně znevýhodňuje klasickou AAS oproti mnohým ostatním metodám elementární analýzy. V HR-CS AAS se otevřely možnosti stanovení několika prvků současně. Tři z přiložených prací se přímo zaměřují na toto téma a další dvě se ho dotýkají okrajově.

Byť jsou současné víceprvkové možnosti v AAS novinkou, je nutné zmínit, že v minulosti se vyráběly i speciální víceprvkové AA spektrometry založené na klasickém principu – např. Perkin-Elmer SIMAA využíval kombinaci několika čárových zdrojů záření a plošného CCD detektoru. Přes jejich popularitu mezi uživateli se již nevyrábějí. Právě v ohledu víceprvkové analýzy si mnozí od nasazení kontinuálních zdrojů záření – a tedy možnosti pozorování absorpčních čar v libovolné části spektra – slibovali průlom. Je však třeba konstatovat, že prozatím nevznikl žádný skutečně multiprvkový přístroj. Jak bylo popsáno v úvodu, dostupná HR-CS AAS instrumentace monitoruje spektrální interval 0,2–1 nm a simultánně tedy mohou

být měřeny pouze spektrální čáry vyskytující se v tomto intervalu. Přes toto omezení již bylo publikováno mnoho víceprvkových metod. V některých případech šlo dokonce o současné stanovení čtyř prvků (Ozbek 2019; Resano et al. 2013). Vzhledem k časové náročnosti měření pomocí elektrotermické AAS je výsledná úspora času výrazná. Jde ale i o šetření na energii a materiálu. O zájmu uživatelů o víceprvkovou analýzu svědčí přehledový článek, který popisuje přes padesát publikací (Pasias et al. 2021), přičemž od jeho vydání přibyly další.

Pro víceprvkové stanovení musí být splněny následující podmínky:

a) Zvolené analytické čáry musí ležet v monitorovaném spektrálním intervalu,

b) citlivost analytických čar musí odpovídat koncentraci prvků ve vzorku,

c) teplotní program musí být optimalizován vzhledem k různým vlastnostem prvků,

d) pochopitelně je také nutná účelnost měření oněch prvků ve zkoumaném materiálu.

Tak například kadmium a olovo patří k nejrizikovějším toxickým prvkům a zároveň k prvkům nejčastěji stanovovaným pomocí ET-AAS. V prostředí se vyskytují ve stopových koncentracích a jejich detekce vyžaduje využití nejcitlivějších analytických čar. V okolí primárních čar obou prvků se vyskytují sekundární čáry[2] několika dalších potenciálně významných prvků, které mohou být měřeny současně. Většina okolních čar náleží přechodným prvkům, jako jsou železo, hliník, kobalt, nikl. Protože olovo i kadmium jsou těkavé prvky, tyto okolní čáry nejsou při běžně nízkých atomizačních teplotách patrné (a tedy například neinterferují v LS-AAS). Při dostatečně vysoké atomizační teplotě se však linie prvků objeví a je možné je využít pro analytické účely. Tabulka 1 uvádí vybrané spektrální čáry v okolí rezonančních čar olova a kadmia a také v oblasti jediné dostupné sekundární čáry zinku.

Přínos práce v oblasti víceprvkové analýzy spočívá ve vyvinutí nových metod pro environmentální analýzu. Metody jsou relevantní pro praxi, byly prověřeny na velkém množství reálných vzorků a jsou snadno adaptovatelné v laboratořích s odpovídajícím vybavením. Poslouží k následujícím účelům:

- Posouzení kontaminace prostředí na základě analýzy biologických indikátorů (v tomto případě lišejníků). Komplexní analytická metoda s vysokou citlivostí stanovuje toxické olovo a současně s ním i referenční prvky hliník a železo. Tato kombinace umožňuje zhodnocení míry kontaminace prostředí na základě výpočtu obohacovacích faktorů.

[2] Sekundární čáry jsou nerezonanční spektrální čáry prvků, které vůči primárním čarám vykazují nižší citlivost. Ta se vyjadřuje nejčastěji jako *relativní citlivost*, tj. podílem citlivosti dané spektrální čáry vůči primární čáře prvku.

- Hodnocení obsahu esenciálních a často nedostatkových prvků železa a zinku v potravinářských surovinách. Rychlá jednoduchá metoda je optimalizována pro analýzu rostlin a zeleniny.
- Sledování dvou prvků v cereáliích, a sice toxického kadmia (cereálie jsou jeho hlavním zdrojem pro běžnou populaci) a železa, jehož obsah je důležitým nutričním parametrem.

Tabulka 1: Vybrané spektrální čáry prvků v okolí primárních čar Pb a Cd a sekundární čáry Zn

prvek	vlnová délka (relativní citlivost)	prvek	vlnová délka (relativní citlivost)	prvek	vlnová délka (relativní citlivost)
Al	216,883 nm (5,6 %)	Sn	228,668 nm (2,9 %)	V	307,382 nm (3,8 %)
W	216,948 nm (16 %)	Fe	228,725 nm (0,91 %)	Sm	307,392 nm (0,48 %)
Ru	216,977 nm (1,1 %)	Ni	228,733 nm (0,27 %)	Tb	307,471 nm (1,3 %)
Al	216,984 nm (0,19 %)	Re	228,751 nm (100 %)	Fe	307,572 nm (0,043 %)
Pb	217,001 nm (100 %)	Ru	228,768 nm (0,83 %)	**Zn**	307,590 nm (0,02 %)
Ru	217,006 nm (0,71 %)	Co	228,781 nm (0,91 %)	Tb	307,572 nm (1,1 %)
V	217,074 nm (2,8 %)	**Cd**	228,802 nm (100 %)	Tb	307,905 nm (1,5 %)
Fe	217,130 nm (0,33 %)	Sc	228,805 nm (6,3 %)		
Sn	217,132 nm (0,031 %)	Ni	228,840 nm (0,42 %)		
Os	217,165 nm (2,9 %)	Pt	228,927 nm (2,9 %)		

Kromě současného (*simultánního*) stanovení více prvků existuje i tzv. *sekvenční* postup, kdy se nejprve stanovuje těkavý prvek a v druhém odděleném atomizačním kroku je přeladěna vlnová délka do jiné oblasti spektra. Přeladění monochromátoru však zabere určitý čas a je nutné i vychladnutí atomizátoru mezi jednotlivými atomizacemi. Sekvenční postup proto neskýtá velké výhody při roztokové analýze, poněkud výhodnější může být v případě pevného dávkování v SS HR-CS ET-AAS.

5.1.1. Simultánní stanovení kadmia a železa v cereáliích

Jedna z prvních simultánních metod využívající současnou instrumentaci se věnovala stanovení kadmia spolu se železem v cereáliích. Skupina Becker-Rosse je měřila pomocí prototypu HR-CS spektrometru s dávkováním pevných vzorků (Dos Santos et al. 2009).

Jedná se o smysluplnou aplikaci, jelikož cereálie a cereální produkty představují významný zdroj kadmia pro člověka. Při pravidelném příjmu se kadmium může kumulovat v těle a při vysokých dávkách poškodit ledviny jakožto cílový orgán, vést k osteoporóze nebo rozvoji rakoviny. Železo

je naopak esenciální a zároveň nejčastěji deficitní prvek. Je důležité pro tvorbu hemoglobinu a jeho dlouhodobě snížený příjem může vést k anémii z nedostatku železa. I když schopnost obilnin kumulovat železo z půdy je omezena – a omezena je také schopnost člověka toto železo vstřebat kvůli obsahu antinutričních látek jako jsou fytáty –, jsou cereální produkty, jakožto základní potraviny, jeho důležitým zdrojem. Cereálie se proto železem také často fortifikují.

Jak je patrné z tabulky 1, v blízkosti rezonanční čáry kadmia se nachází sekundární čára železa s citlivostí 0,91 %, což se ukazuje jako vhodná citlivost vzhledem k jeho množství v cereáliích. Cílem studie ***Simultaneous determination of cadmium and iron in different kinds of cereal flakes using high-resolution continuum source atomic absorption*** (příloha IX) bylo vyvinout rutinně použitelnou metodu pro jejich simultánní stanovení obou prvků pomocí roztokové analýzy a HR-CS ET-AAS.

Podmínkou víceprvkového stanovení je, že teplotní program grafitové pece musí reflektovat různou teplotní stabilitu analyzovaných prvků. Je proto nutné si uvědomit, že kadmium je oproti železu výrazně těkavější. Jelikož rozdíl v atomizačních teplotách prvků je značný (přes tisíc stupňů), bylo možné atomizaci rozdělit do dvou kroků, kdy se nejprve při teplotě 1250 °C (4 sekundy) atomizuje kadmium, přičemž železo zůstává na platformě stabilní až do zvýšení teploty na 2325 °C (5 sekund). Každý prvek je tak atomizován za optimálních podmínek (tedy podle STPF konceptu). Díky tomu je dosaženo nejvyšší možné citlivosti a také přesnosti, jelikož k atomizaci dochází vždy za konstantních teplotních podmínek. Lineární kalibrační rozsahy byly 0,05–2 µg Cd/l a 25–500 µg Fe/l, což odpovídalo koncentracím prvků v mineralizátech vzorků (kdy faktor zředění z pevné do kapalné fáze byl asi 1:100). Analyzováno bylo 25 vzorků 10 různých druhů cereálních vloček. Nejvyšší obsah železa byl stanoven v amarantových vločkách (66,2 mg/kg), přičemž ty vykazovaly i nejvyšší poměr železa ku kadmiu. Nejvyšší obsah kadmia, 0,15 mg/kg, pozorovaný v ovesných vločkách, dokonce přesahoval limitní hodnotu 0,1 mg/kg pro cereálie (The European Commission 2023). Dokládá to potřebu vhodných a citlivých analytických metod.

Tato metoda je nyní rutinně využívána. Její možnosti byly dále rozvíjeny například v disertační práci Mgr. Pavlíny Kosečkové, Ph.D. ***Stopové prvky u jednostranně založených diet***, již jsem vedl (obhájena 2022). Další aplikaci nalezla při analýze jedlého hmyzu, který se po nedávné legislativní úpravě stal obchodovatelnou potravinou tzv. nového typu. Ve studii ***Mineral profile of cricket powders, some edible insect species and their implication for gastronomy*** (příloha V) byly tímto způsobem analyzovány vzorky čtyř populárních druhů jedlého hmyzu a také vzorky cvrččího prášku. Ten produkuje již několik českých výrobců a používá se obdobně jako obyčejná pšeničná mouka. Ukazuje se, že oproti mouce má vyšší obsah železa (patrně i lépe vstřebatelného) a přitom nižší obsah kadmia. Část výsledků pro uvedenou publikaci vznikla

v rámci diplomové práce Mgr. Martiny Krulíkové ***Jedlý hmyz jako potravina budoucnosti***, již jsem vedl (obhájena 2022). Ve spolupráci s uvedenými dvěma studentkami byl na základě naměřených dat připraven příspěvek do soutěže farmaceutické společnosti Angelini Pharma: Angelini University Award. Příspěvek byl oceněn prvním místem.

5.1.2. Simultánní stanovení železa a zinku v rostlinných materiálech a zelenině

Dietární význam železa jakožto nejčastěji deficitního prvku byl již zmíněn. Zinek je v tomto ohledu v těsném závěsu. Obsah obou prvků v potravinách je proto důležitý nutriční parametr a důležité jsou tedy i metody pro jejich přesné stanovení.

V rámci studie ***Fast and simultaneous determination of zinc and iron using HR-CS GF-AAS in vegetables and plant material*** (příloha III) byla proto vyvinuta metoda jejich současného stanovení v rostlinném materiálu a zelenině.

Železo vykazuje přes 500 absorpčních čar, které se velice různí svojí citlivostí a je tedy snadné najít linii s vhodnou citlivostí pro daný účel, nezatíženou spektrálními interferencemi. Naopak, stanovení zinku pomocí ET-AAS je komplikovanější. Zinek má totiž pouze dvě využitelné absorpční čáry, přičemž rezonanční čára 213.859 nm patří k vůbec nejcitlivějším v AAS, což paradoxně komplikuje její využití; kvůli extrémní citlivosti měření vyžaduje silné ředění vzorků, v důsledku je náchylné ke kontaminacím a také fluktuace slepých pokusů bývají vysoké. Naproti tomu sekundární čára zinku 307,588 nm má citlivost pouhých 0,02 %. V klasické LS-AAS, kde měření při této vlnové délce ještě znesnadňovala velmi slabá intenzita lampy, nacházela proto jeho sekundární linie jen minimální využití. Vysoká intenzita záření xenonové výbojky, spolu s minimálními interferencemi v těchto relativně vysokých vlnových délkách, umožňují stanovení zinku v koncentracích řádu mg/l. V těsné blízkosti se nachází čára železa (307,572 nm, viz tab. 1) s citlivostí 0,043 %, která v praxi umožňuje jeho stanovení v koncentracích v řádu mg/l. Pro daný účel se ukázala kombinace těchto dvou čar jako ideální.

Při vývoji metody simultánního stanovení zinku a železa bylo nutné vzít v úvahu jejich rozdílnou těkavost. I v tomto případě bylo možné rozdělit atomizaci do oddělených kroků, poskytujících ideální a konstantní podmínky pro každý z obou prvků. Případný překryv čar v případě obzvlášť vysokých koncentrací je v tomto případě ošetřen výskytem píků v rozdílných časech (Obrázek 3).

V práci byla zkoumána závislost počtu pixelů využitých k integraci signálu. Integrace většího počtu pixelů může vést ke zlepšení citlivosti, protože pokrývají větší část profilu spektrální čáry. Signál se do určitého počtu zapojených pixelů zesiluje rychleji než šum, ideální počet pixelů je

závislý na instrumentaci a vlastnostech spektrální čáry (Heitmann et al. 2007). Standardní je integrace 3 pixelů, tzn. centrálního pixelu (CP) na středu čáry a dvou okolních přilehlých (CP±1). Zde sledovaná oblast kolem 307 nm je jen málo zatížena interferencemi a odečítání signálu bylo jen minimálně rušeno šumem. Proto bylo možné rozšířit oblast registrace signálu na 5 pixelů (tzn. centrálního pixelu CP±2 okolních). Pět pixelů pokrývá většinu plochy píků a jejich snímání vedlo ke zlepšení charakteristické koncentrace o 20 % pro zinek a o 30 % pro železo.

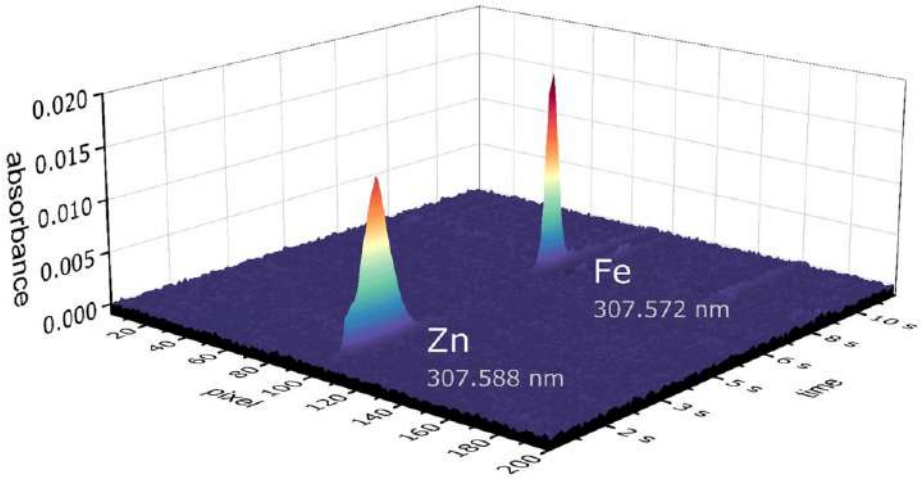

Obrázek 3: Trojrozměrné absorpční spektrum (x = vlnová délka, resp. číslo pixelu, y = absorbance, z = čas) získané při simultánním stanovení Zn a Fe. Měřený mineralizát vzorku salátu v tomto případě obsahoval 1 mg/l Zn a 3 mg/l Fe.

Doba trvání teplotního programu byla 88 sekund, celý proces včetně dávkování vzorku a chlazení pece byl kratší než 2 minuty. Správnost metody byla ověřena pomocí několika certifikovaných referenčních materiálů a bylo dosaženo také velmi blízké shody s metodou ICP-MS, pomocí které byla část vzorků také proměřena.

Výsledný pracovní rozsah metody (0,06–5 mg Zn/l a 0,2–10 mg Fe/l) dobře korespondoval s koncentracemi prvků v mineralizátech vzorků, kterými byly různé druhy zeleniny a hub. Metoda se prokázala jako použitelná v rutinní analýze více než sta vzorků získaných od lokálních zahrádkářů a z obchodní sítě. Saláty například obsahovaly obou prvků výrazně větší množství než mrkev, přičemž jen malé rozdíly byly pozorovány v obsahu prvků mezi doma pěstovanou a kupovanou zeleninou. Jejich mírně vyšší obsah v domácích výpěstcích byl vysvětlen většinou nižším obsahem vody oproti kupovaným produktům.

Publikace vznikla v rámci mezinárodního projektu ***Potenciálně toxické prvky v houbách a zelenině pěstovaných ve městech v Rakousku a České republice*** (MŠMT Mobility,

8J21AT006). Tématu se věnovala také diplomová práce Mgr. Moniky Vychytilové s názvem ***Domácí zelenina: obsah esenciálních a toxických prvků***, jejíž jsem školitel (obhájena 2023). Práce závěrem konstatovala, že časté přesvědčení laické veřejnosti o vyšší nutriční hodnotě domácí zeleniny nelze na základě dosažených výsledků potvrdit.

5.1.3. Simultánní stanovení olova, hliníku a železa v antarktické flóře

Dokonce tři prvky současně je možné stanovit pomocí metody, která byla vyvinuta pro analýzu rostlinného materiálu – konkrétně pro environmentální monitoring ekosystému antarktického ostrova. Olovo, hliník a železo byly stanoveny simultánně pomocí metody popsané v publikaci ***Multi-element analysis (Pb, Al, Fe) of Antarctic flora using HR-CS ETAAS with an extended working range*** (příloha I).

Zkoumanými materiály zde byly lišejníky, mechy, tráva a houby, vzorkované na ostrově Nelson, ležícím v souostroví Jižní Shetlandy. Zájmovým prvkem studie bylo olovo, které patří mezi kontaminanty životního prostředí s výrazným potenciálem poškozovat ekosystémy. V důsledku jeho masivního využívání, zejména jako historické příměsi do benzínu, se stalo všudypřítomným polutantem, a to i v natolik odlehlé oblasti, jakou je Antarktida (McConnell et al. 2014). Kromě dálkového přenosu se do ekosystémů Antarktidy dostává také z lokálních zdrojů, kterými jsou provoz vědeckých stanic (kterých je aktuálně přes 80, z toho 40 s celoročním provozem (COMNAP Secretariat 2017)) a rozmáhající se turismus (za sezónu navštíví oblast přes 70 tisíc turistů (IAATO 2020)). Obě tyto aktivity ovlivňují zejména příbřežní oblasti, kde je koncentrována většina biodiverzity.

Protože antarktický regolit (svrchní pokryv, striktně vzato se ani nejedná o půdu) obsahuje příliš málo organického materiálu, a tím pádem vykazuje malou retenci prvků, pro indikaci znečištění se ukázaly vhodnější kumulativní organismy, jako jsou mechy a lišejníky (Zvěřina et al. 2014; 2018; Coufalík et al. 2015). Tyto nižší rostliny jsou často využívané jako bioindikátory; díky své schopnosti kumulovat atmosférické polutanty věrně reflektují stav prostředí (Bargagli 2008). Navíc, protože přímá měření jsou v Antarktidě komplikována drsnými podmínkami, je využití těchto přírodních indikátorů praktické.

Kromě stanovení zájmových prvků – v tomto případě olova – je v podobných environmentálních studiích důležitá i znalost obsahu referenčních prvků. Nemobilní prvky jako hliník nebo železo slouží pro výpočty ekologických indexů, například obohacovacích faktorů (Ferreira et al. 2022).

Jak je patrné z výše uvedené tabulky 1, dvě sekundární čáry hliníku (216,883 a 216,984 nm) a jedna čára železa (217,130 nm) se nacházejí v těsné blízkosti primární čáry olova (217,001 nm). Na rozdíl od olova jde o tepelně stabilní prvky a pro jejich atomizaci je nutná náležitá teplota. Při

atomizaci na 2 500 °C jsou jejich spektrální čáry pozorovatelné v detekčním okně přístroje a jsou využitelné pro jejich stanovení. Spektrum získané měřením vzorku lišejníku pomocí vyvinuté metody je na obrázku 4.

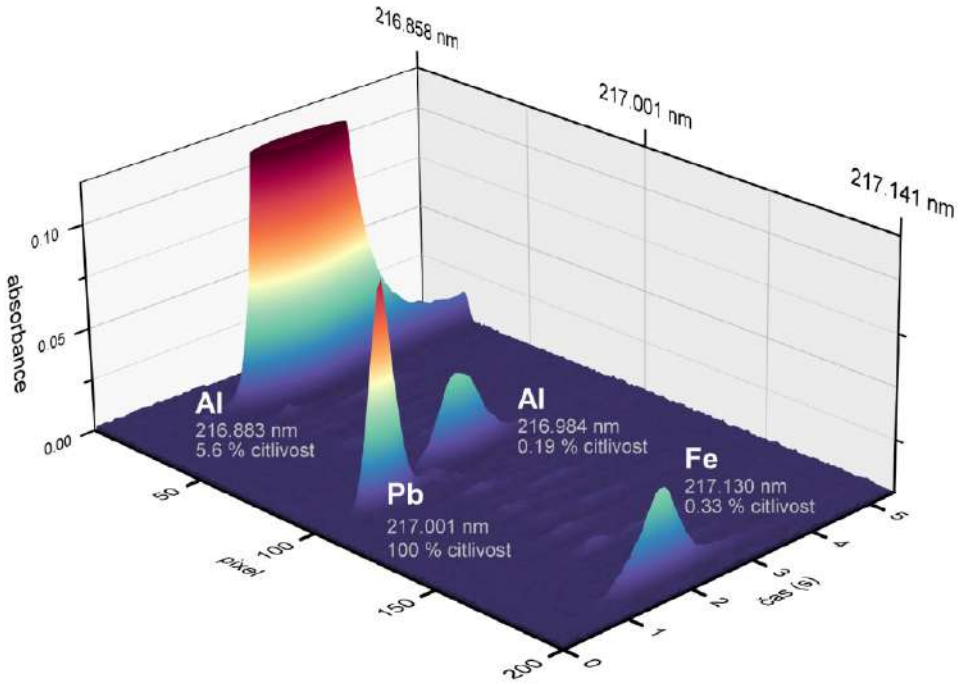

Obrázek 4: Absorpční spektrum simultánního stanovení tří prvků ve vzorku lišejníku.

Vysoká atomizační teplota však již není ideální pro těkavé olovo, které atomizuje rychle a vzniklý oblak jeho atomů se rychle rozpíná a uniká z atomizátoru, čímž dochází ke snížení citlivosti. V uvedené publikaci byl prověřován přístup, který k omezení tohoto jevu využila skupina španělských autorů (Bustos et al. 2022). Autoři využili pro víceprvkovou analýzu pomalý nárůst teploty při atomizaci – pouhých 400 °C/s –, což umožňuje delší setrvání atomů těkavějšího prvku v atomizátoru, než dojde k přílišnému záhřevu kyvety. Tím dosáhli zvýšení citlivosti pro těkavý prvek. Naše experimenty však ukázaly, že přístup může vést k nesprávným výsledkům. Málo zjevná příčina spočívá v tom, že teplotní chování prvků u jednoduchých kalibračních roztoků a komplexních reálných vzorků se může lišit – a velmi často se opravdu liší. Pokud se píky prvků při analýze vzorku a kalibrantu objevují v různém čase, tedy za různé teploty, si jejich plochy při stejné koncentraci nemohou odpovídat. V tom tkví fundamentální problém tohoto přístupu – je v rozporu s STPF konceptem, vysvětleným v úvodní kapitole. Ukazuje se, že znalost historie je důležitá v době novinek a změn. K dosažení správných výsledků ve víceprvkové analýze ET-AAS – byť za cenu snížení citlivosti těkavých prvků – bude tedy nevyhnutelné používat rychlý ohřev (anebo vícekrokovou atomizaci, popsanou v předchozích kapitolách). Ve výsledné

metodě byla proto nastavena rychlost nárůstu teploty 1500 °C/s, vedoucí k atomizaci za izotermních podmínek.

Co se výsledků týče, naměřené obsahy prvků v antarktických houbách a trávě představují jedny z prvních publikovaných dat o jejich prvkovém složení. Výsledky studie svědčí o minimální kontaminaci ekosystému ostrova Nelson olovem. Ostrov přitom sousedí s Ostrovem Krále Jiřího, který tvoří dopravní uzel souostroví Jižní Shetlandy. Bioindikátory však ukazují na relativně malou zátěž tohoto přiléhajícího ostrova, patrně danou minimálním provozem přímo v jeho oblasti. Hodnoty proto mohou sloužit jako referenční pozadí tohoto antarktického regionu.

Vzhledem k výrazně odlišným poměrům olova a hliníku (jakožto referenčního nemobilního prvku) u čtyř zkoumaných materiálů se ukazuje, že právě lišejníky představují vhodné ekologické indikátory. Nejvyšší poměr Pb/Al poukazuje na schopnost kumulovat polutanty při minimální kontaminaci částicemi půdy a prachu.

Tato studie vznikla v rámci projektu AKTION Česká republika - Rakousko s názvem ***Výzkum potenciálně toxických prvků v antarktické suchozemské flóře*** (AKTION 96p6, MŠMT). Prvotnímu vývoji metody byla věnovaná bakalářská práce Bc. Lenky Brůhové s názvem ***Současné stanovení více prvků metodou HR-CS GFAAS ve vzorcích lišejníků*** (2022, PřF MU), která se věnovala optimalizaci teplotního programu a testování různých chemických modifikátorů. Metoda byla dále rozvíjena v její diplomové práci ***Pokročilé postupy simultánního stanovení prvků metodou HR-CS GF-AAS***, přičemž u obou prací figuruji jako konzultant. Na úrovní poradce jsem na vývoji dalších víceprvkových metod spolupracoval také s kolegy z FCH VUT, například v rámci diplomové práce Romana Jurnečky ***Vývoj metod simultánní analýzy na přístroji HR–CS–ET–AAS a jejich využití v environmentální analýze*** (obhájeno 2023, FCH VUT).

5.2. Korekce strukturovaného pozadí

Materiály životního prostředí představují často komplikované matrice. Obsahují četné složky, které mohou rušit měření, a jejich množství se navíc různí vzorek od vzorku. Metody zamýšlené pro jejich analýzu proto musí být robustní vůči interferencím.

O způsobu korekce *nespecifického* průběžného pozadí v HR-CS AAS již bylo pojednáno. V praxi se příliš neliší od řešení v klasické AAS – jen díky tomu, že záření není modulované, vykazuje nižší šum a poněkud lepší přesnost (Welz et al. 2005). Protože silné nespecifické pozadí komplikuje přesný odečet absorbance analytu, je namístě usilovat o jeho snížení. K tomu slouží totožné prostředky jako u klasické ET-AAS, tzn. optimalizace teplotního programu, případně použití chemických modifikátorů.

Obzvlášť problematické na korekci je ale jemně strukturované pozadí. Nejčastěji ho způsobují diatomické molekuly s vysokou disociační energií – typicky monoxidy fosforu (PO) a dusíku (NO). V HR-CS AAS je možné uložit referenční spektrum interferentu a následně ho odečítat od spekter při měření vzorků korekční metodou LSBC (*least-squares background correction*). Referenční spektrum lze získat měřením interferentu bez analytu – tedy například dávkováním čistého roztoku fosforečnanu nebo dusičnanu. Někdy lze dokonce spektrum interferentu odečíst přímo během analýzy vzorku, pokud je jejich absorpční pás alespoň částečně oddělen od analytické čáry v čase (v takovém případě se uloží příslušný časový výsek). Referenční spektrum – nebo i kombinace několika takových spekter – je poté odečteno korekční metodou LSBC. Postup poprvé popsala skupina Helmuta Becker-Rosse právě za účelem eliminace PO a NO pásů při stanovení arsenu a selenu (Becker-Ross et al. 2000).

Přínos práce v této oblasti spočívá zejména v popsání nepřímé závislosti výskytu strukturovaného pozadí na přídavku chemického modifikátoru. Komplikované spektrální interference, které často provází analýzy rostlinných materiálů s vysokým obsahem fosforu, se ukázaly dobře potlačitelné nadbytkem modifikátoru na bázi palladia. Případnou „zbytkovou“ interferenci je možné korigovat odečtem referenčního spektra, jak popisují níže komentované publikace. Výsledkem je možnost detekce toxických prvků arsenu, kadmia a olova osvobozená od rušivých vlivů matrice.

5.2.1. Odečet referenčního spektra

Jako ukázka korekce strukturovaného pozadí poslouží spektra na obrázku 5. Pocházejí z analýzy obsahu arsenu jakožto kontaminantu průmyslově vyráběné kyseliny fosforečné. Kontrola čistoty

kyseliny fosforečné byla zájmem bakalářské práce Veroniky Halfarové ***Analýza prvků v kyselině fosforečné metodami ICP-OES a AAS*** (obhájena 2023 na PřF MU), kde jsem se jako konzultant podílel na vývoji metodiky pro AAS.

Jde o zajímavý problém, protože právě fosfor je hlavní interferent při stanovení arsenu metodami atomové absorpční spektrometrie – kvůli strukturovanému absorpčnímu pozadí molekul PO v oblasti 193 nm. Míra nespecifického pozadí byla omezena ředěním vzorků v poměru 1:100. I po tomto zředění bylo nutné strukturované pozadí korigovat odečtem referenčního spektra, získaného měřením vysoce čisté kyseliny. Jak je vidět na obrázku 5, korekce výrazně potlačila strukturovaného pozadí.

Dosahovaná mez detekce je v nízkých desítkách µg/l, což se ukázalo jako dostatečné pro daný účel. Nicméně pro potřeby analýzy arsenu ve složkách životního prostředí, kde se vyskytuje ve stopových množstvích, je zpravidla nutné využití citlivějšího přístupu – generování těkavých forem (viz další kapitoly).

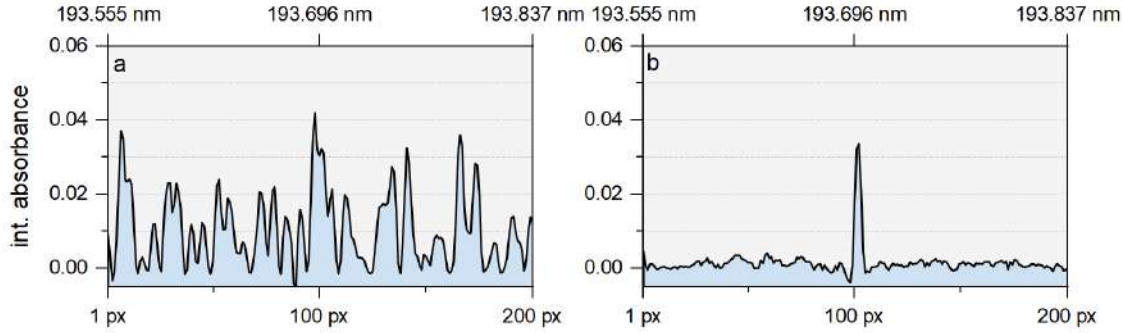

Obrázek 5: Dvojrozměrné spektrum (integrovaná absorbance podle vlnové délky) při stanovení 1000 µg/l arsenu (193,696 nm) ve zředěné kyselině fosforečné a) bez korekce a b) s LSBC korekcí.

Právě interference monoxidu fosforu (PO) bývá z nejčastěji řešených v literatuře. Je obecně známo, že stanovení olova na rezonanční čáře 217,001 nm je v LS-AAS v podstatě nemožné při použití fosfátového modifikátoru. S LSBC korekcí v HR-CS AAS je však taková analýza proveditelná (Borges et al. 2014). Molekula PO vykazuje neobvykle mnoho rotačně-vibračních přechodů a kromě primární čáry olova a arsenu interferuje také v oblasti hlavní čáry kadmia (228,802 nm). Některé z nejvýraznějších přechodů molekuly bývají využívány dokonce k nepřímému stanovení koncentrace fosforu (Bechlin et al. 2014; Pomarolli et al. 2020).

5.2.2. Korekce interferencí při analýze rostlinného materiálu a cereálií

Interference PO například rušily současné stanovení kadmia a železa v již zmiňované publikaci věnující se cereáliím (příloha IX). Molekuly PO se tvoří za teplot mezi atomizační teplotou kadmia a železa, přesto se výskyt absorpčního pásu nepodařil optimalizací teplotního programu posunout tak, aby nedocházelo k jeho překryvu s čarou železa. Příspěvek PO falešně zvyšoval signál železa až o 10 %. Bylo proto zaznamenáno referenční spektrum interferentu měřením roztoku NaH_2PO_4. Jeho následným odečtem byla interference zcela eliminována, viz Obrázek 6.

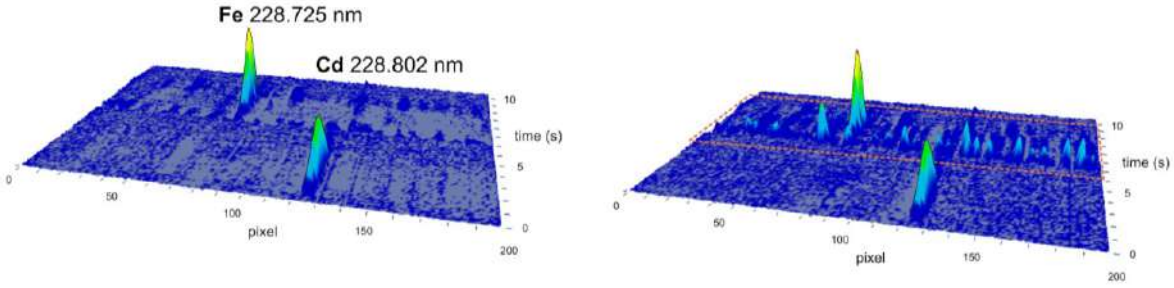

Obrázek 6: Spektrum získané při simultánním stanovení kadmia a železa v cereáliích. Vlevo je výsledné spektrum po aplikaci LSBC korekce a vpravo pro srovnání původní spektrum před korekcí s vyznačeným strukturovaným pozadím.

Výsledky několika studií naznačily možnost chemického potlačení interferencí PO s využitím modifikátorů matrice. Některá činidla totiž silně ovlivňují rovnováhu mezi atomizací (atomárního) fosforu a jeho vaporizací ve formě monoxidu. Bez přídavku modifikátorů se jen malé množství fosforu vyskytuje v atomární formě, a to dokonce i za vysokých atomizačních teplot 2 700 °C (Resano et al. 2009). Přednostní tvorbu atomárního fosforu podporují modifikátory na bázi palladia, ruthenia, iridia a wolframu (Lepri et al. 2006; de Campos et al. 2011; Pomarolli et al. 2020).

Některé rostlinné materiály obsahují relativně vysoké množství fosforu, který způsobuje interference. Možnost potlačení interferencí byla proto zkoumána a rozvíjena v již zmíněné studii věnované analýze antarktické flóry (příloha I). V příslušné metodě byla totiž monitorována vlnová délka v oblasti rezonanční čáry olova 217,001 nm, která je výrazně zasažena absorpčními pásy PO.

Obrázek 7 ilustruje analýzu houby *Arrhenia antarctica*, která byla kvůli vysokému obsahu fosforu zatížena obzvlášť silnou interferencí. Měření bylo opakováno s různými přídavky $Pd/Mg(NO_3)_2$ modifkátoru. Postupný útlum interference s přídavkem modifikátoru je zřejmý. Na základě tohoto a dalších experimentů byl jako efektivní přídavek modifikátoru vyhodnocen jeho

poměr vůči mineralizátu 1:1,5. V některých případech to postačovalo k úplné eliminaci strukturovaného pozadí. V případě extrémně silných interferencí – jako ve zde ilustrované analýze houby – bylo nutné zbytek interference eliminovat metodou LSBC.

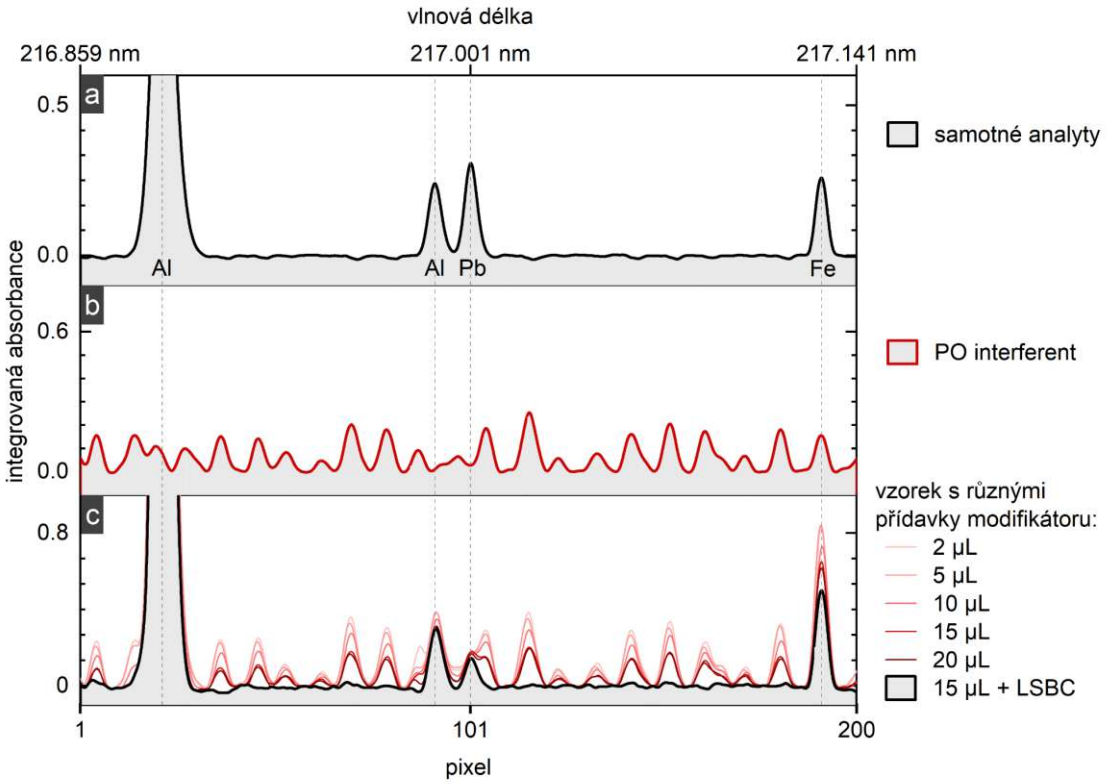

Obrázek 7: Spektra získaná měřením a) jednoduchého roztoku analytů, b) referenční spektrum samotného interferentu získané měřením roztoku fosforečnanu amonného (tzn. absorpční pásy PO), c) spektrum získané měřením mineralizátu houby, vykazující silné interference, se znázorněním vlivu přídavku Pd-modifikátoru a LSBC korekce pozadí.

5.3. Rozšíření dynamického rozsahu měření

Dynamický rozsah atomové absorpční spektrometrie je úzký 2 až 3 řády, což ji v kontextu ostatních technik znevýhodňuje. Detekovatelnost analytu se většinou pohybuje na úrovni *charakteristické koncentrace*, tzn. takové, která vyvolává absorbanci 0,0044. Jelikož absorbance je záporným dekadickým logaritmem transmitance, znamená to zeslabení původního světelného toku o 1 %. Při absorbanci A=1 je již pohlceno 90 % záření a při absorbanci A=2 již na detektor dopadá pouhé 1 % původního záření. To vede nejen ke zhoršování poměru signál-šum, ale navíc, jelikož stále větší podíl dopadajícího záření tvoří rozptýlené záření, se snižuje i podíl záření, který je skutečně absorbován analytem. Dosažení širokého kalibračního rozsahu je tak fundamentálně omezeno. Pro měření koncentrací nad horní hranicí pracovního rozsahu je tedy nutné vzorky ředit, nebo dávkovat menší objemy vzorku (v případě ET-AAS).

Variantou je využívání sekundárních spektrálních čar s nižší citlivostí. V LS-AAS jejich využití nebývalo příliš populární, zejména proto, že vykazovaly horší poměr signál-šum, kvůli nižší intenzitě emise sekundárních čar výbojek. Neklesala proto pouze citlivost na straně absorpce v atomizátoru, ale také intenzita zdrojového záření. Obavy panovaly také z interferencí, protože spektrální okolí zřídkakdy využívaných čar je méně probádané. Oba tyto argumenty odpadají s použitím HR-CS instrumentace, jelikož xenonová výbojka poskytuje podobně vysokou intenzitu při všech vlnových délkách a případné spektrální interference jsou ihned zjevné.

Vysoké rozlišení přineslo ještě další způsob, jak dynamický rozsah rozšířit směrem do vyšších koncentrací: tlumením signálu tzv. WSA přístupem (*wavelength-selected absorbance*). Tento přístup spočívá v odečítání absorbance na křídlech spektrální čáry namísto na jejím středu. U snímání absorbance na křídlech dochází k „saturaci“ signálu podstatně později. Je tak možné dosáhnout širokého dynamického rozsahu (Heitmann et al. 2007). Pochopitelně, využívání krajních pixelů rozšiřuje linearitu za cenu ztráty citlivosti. U klasické LS-AAS toto není dost dobře možné; záření úzké emisní čáry dutokatodové výbojky se na středu absorpční čáry brzy plně absorbuje.

Reálné vzorky často obsahují analyty ve větším rozpětí koncentrací než pojme běžný kalibrační rozsah AAS. V takových případech bývá nutné jejich ředění *ad hoc*. S ohledem na to, jak omezující úzký dynamický rozsah v praxi je, je až s podivem, že relativně málo studií zkoumalo

možnosti jeho rozšíření (Fernández-López et al. 2018; Hesse et al. 2015; Bechlin et al. 2014; Welz et al. 2010a; Gómez-Nieto et al. 2015).

Přínos práce v oblasti rozšiřování dynamického rozsahu spočívá v rozvinutí metod, jejichž citlivost a pracovní rozsah jsou uzpůsobeny analýze konkrétních materiálů; jde například o polétavý prach, biologické tekutiny, půdy i rostlinné materiály. V níže komentovaných publikacích jsou popsány metody s citlivostí přizpůsobenou například detekci zinku v indoorovém ovzduší, platině v séru, nebo různých kovů v půdách. Obzvlášť široký dynamický rozsah vyžadovala analýza rostlinných materiálů z Antarktidy (lišejníků, mechů, hub a trávy). Variabilita obsahu prvků v těchto materiálech byla extrémně široká, odpovídající míře jejich expozice i stáří jednotlivých exemplářů. Vyvinutá metoda, pokrývající celý vyžadovaný koncentrační rozsah, je založena na unikátní kombinaci simultánního snímání více spektrálních čar stejného prvku s přístupem WSA. Takovéto řešení bylo představeno vůbec poprvé.

5.3.1. Regulace příliš vysoké citlivosti měření pomocí WSA

Problematika absorpčních čar zinku již byla diskutována a byla popsána i metoda pro jeho stanovení v koncentraci nad 0,06 mg/l, využívající jeho jedinou sekundární čáru s citlivostí 0,02 %. Pro stanovení nižších koncentrací je však nevyhnutelné využít jeho rezonanční čáru. Vzhledem k její enormní citlivosti to však znamená práci na úrovni koncentrací <μg/l, což vzhledem k všudypřítomnosti zinku v prostředí není ideální ani snadné v běžných laboratořích. Někteří autoři pro tento účel dokonce uzavírali spektrometr do speciálního kabinetu s filtrovaným vzduchem splňujícím čistotu třídy 100 (Schlemmer and Petek 2000). Nutné mnohonásobné ředění vzorků (a související vysoké nároky na jakost demineralizované vody a použitých chemikálií) činí tento přístup nadmíru nepraktickým.

Tento problém byl řešen v práci ***Inorganic pollutants in the indoor environment of the Moravian Library: assessment of Cd, Pb, Cu, and Zn in total suspended particles and dust using HR-CS GF-AAS*** (příloha VIII). Projekt si kladl za cíl zhodnotit kvalitu vnitřního prostředí Moravské zemské knihovny a jejich depozitářů s ohledem na výskyt vybraných kovů. Polétavý prach byl vzorkován pomocí filtračního systému v různých částech knihovny: v čítárně, depozitáři i externím skladu knih. Analyzován byl také prach vznikající při strojovém čištění svazků. Navzorkovaný prach byl mineralizován pomocí mikrovlnného rozkladného systému.

S ohledem na koncentraci zinku v mineralizátech byla vyvinuta metoda využívající jeho rezonanční čáru, avšak s citlivostí regulovanou čtením signálu na křídlech čáry. Namísto standardního odečítání signálu pomocí centrálního a dvou přilehlých pixelů (CP±1) byl signál odečítán pouze na křídlech čáry. Testováno bylo odečítání signálu ve vzdálenosti ±2, ±3 a ±4

pixelů od středu čáry, viz Obrázek 8. Citlivost stanovení tím byla snížena 4-, 20- a 50krát. Nakonec byla zvolena varianta středního tlumení signálu (±3 px) v kombinaci s dávkováním 5 µl vzorku. Získaná kalibrační závislost vykazovala skvělou linearitu v rozmezí 1 až 100 µg/l, což právě odpovídalo potřebám analýzy.

Ze čtyř sledovaných prvků (Pb, Cd, Cu a Zn) byla koncentrace zinku v polétavém prachu v knihovně nejvyšší (medián 21 ng/m^3, za Zn následovaly Pb > Cu > Cd), což se nevymyká typickému složení vnitřního prachu (Niu et al. 2021; Rasmussen et al. 2013). V prachu získaném přímo z knih byl pozorován poměrně vysoký obsah olova (až 700 mg/kg), naznačující souvislost s olověnou liteřinou. Nejvyšší koncentrace olova v polétavém prachu, naměřená v externím skladu knih, byla 15 ng Pb/m^3, což je stále bezpečně pod hygienickými limity.

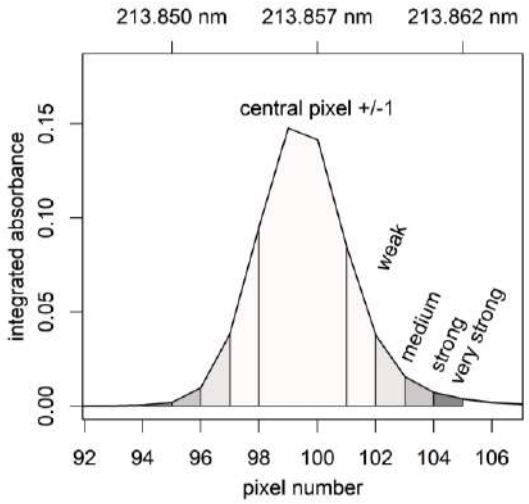

Obrázek 8: Profil primární absorpční čáry Zn s vyznačenými způsoby odečítání signálu

Regulace příliš silného signálu odečtem na křídlech čáry (WSA přístup) se ukazuje jako vhodná v situacích, kdy není možné využít alternativní analytickou čáru s nižší citlivostí. Také umožňuje se vyhnout přílišným ředěním vzorků.

Popsaný postup našel uplatnění i při již zmíněné kontrole čistoty chemikálií; metoda byla adaptována a použita pro analýzu různých šarží kyseliny fosforečné v bakalářské práci *Analýza prvků v kyselině fosforečné metodami ICP-OES a AAS*.

5.3.2. Regulace citlivosti využitím sekundárních čar

V případech, kdy je pro analyt k dispozici více spektrálních čar, může být výhodnějším způsobem snížení citlivosti právě jejich využití oproti přístupu WSA. Výhodou oproti WSA může být lepší reprodukovatelnost a teoreticky i nižší riziko interferencí. Lepší reprodukovatelnost měření je dána odečítáním signálu ze středu čáry a ne šikmé plochy křídla, což – byť při femtometrové přesnosti nastavení vlnové délky – vede k mírně zhoršené reprodukovatelnosti.

Adaptace pracovního rozsahu pro potřeby analýzy biologických vzorků byla předmětem studie ***A simple dilute-and-shoot procedure for the determination of platinum in human pleural effusions using HR-CS GF-AAS*** (příloha VI). Motivací projektu byl zájem lékařů z Kliniky nemocí plicních a tuberkulózy znát průběžnou koncentraci cytostatik u pacientů s rakovinou plic, komplikovanou tvorbou pleurálního výpotku. Jde o stav, kdy se v pohrudničním prostoru hromadí velké množství tekutiny, kterou je nutné pravidelně odsávat. V případě současného podávání platinových cytostatik je tedy žádoucí dobré načasované podávání léčiva a odsávání výpotku. V některých případech totiž může být výhodné výpotek záměrně neodstraňovat, ale třeba ho alespoň část ponechat pro zachování terapeutického působení přítomného léčiva.

Protože se využívaná léčiva – cisplatina a karboplatina – postupně vážou na bílkoviny, bylo zájmem také stanovení podílu volného léčiva, nevázaného na bílkovinu. Volná platina byla v tomto případě stanovena po ultrafiltraci výpotku na membráně s cut-off limitem 20 kDa.

S ohledem na potřebu rychlého získání výsledků byla vyvinuta metoda přímého dávkování výpotku po pouhém zředění detergentem Triton X-100 – tedy bez mineralizace vzorku.

Problém je, že plicní výpotky jsou složením podobné séru, a tedy obsahují vysokou koncentraci bílkovin (stanoveno bylo 34±6 g/l). Po měření tak zůstává v kyvetě značné množství nespáleného uhlíkatého rezidua. Nahromaděné uhlíkaté zbytky časem blokují optickou průchodnost kyvety a ovlivňují také rozprostření dávkovaného roztoku po platformě. Pro odstranění uhlíkatých zbytků bylo do teplotního programu začleněno *spalování matrice v kyslíku* (oxygen ashing). Při této proceduře je za teploty 500 °C do kyvety přiváděn kyslík, čímž dochází ke spálení organické matrice. Další krok pyrolýzy – už opět s argonem jako inertním plynem – byl nastaven na 1300 °C a sloužil k odstranění solí. Jak je patrné z obrázku 9, spalování v kyslíku účinně vyřešilo problém a umožnilo přímou analýzu vzorků bez předchozí mineralizace. Teplotní program trval 164 sekund. Životnost kyvety přitom nebyla výrazně ovlivněna.

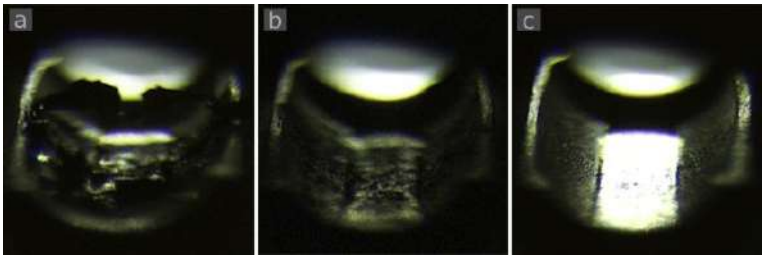

Obrázek 9: Pohled do grafitové kyvety: a) po pěti odpalech výpotku zředěného 1+3, b) po třiceti odpalech filtrátu výpotku, c) po stovce odpalů zředěného (1+3) výpotku za použití spalování v kyslíku.

Koncentrace platiny ve výpotcích byla dle očekávání velice variabilní, protože vzorky byly průběžně odebírány v časovém rozmezí 24 hodin po podání léčiva a také proto, že ultrafiltrát volné frakce platiny obsahoval často jen malý zlomek její celkové koncentrace.

Byly proto testovány analytické parametry různých čar Pt, jejichž citlivost se lišila od 100 do 28 %. Jak je patrné z obrázku 10, všechny čáry poskytovaly vysoce lineární kalibrační závislosti v širokém rozsahu koncentrací od mikrogramů až po miligram na litr.

Vzhledem k celkovému množství analytu ve vzorcích (od desítek µg/l až do 5 mg/l) vyhovovala svojí citlivostí a rozsahem sekundární spektrální čára 292,979 nm (s citlivostí 28 % vůči primární čáře). Za zmínku stojí poznatek, že v její blízkosti leží čára železa, které je tedy možno simultánně stanovit. Její citlivost (0,56 %) přitom odpovídá fyziologické koncentraci Fe v séru.

Koncentrace volné platiny v ultrafiltrátech byla krátce po podání taktéž v řádu mg/l, byť během 24 hodin klesala často až k jednotkám µg/l. Cisplatina se na bílkoviny váže poněkud rychleji než karboplatina (van der Vijgh 1991). Vývoj koncentrací platiny v čase se i u pozorovaných pacientů výrazně lišil v závislosti na podaném cytostatiku.

Pokud je zájmem měřit vysoké a zároveň i velmi nízké koncentrace, jako vhodné řešení se jeví použití primární čáry s druhým kalibračním rozsahem měřeným na jejích křídlech – tedy klasický přístup rozšířený o metodu WSA. Při měření celkového množství Pt může být praktičtější využití sekundární čáry s vyšším rozsahem, byť nižší citlivostí.

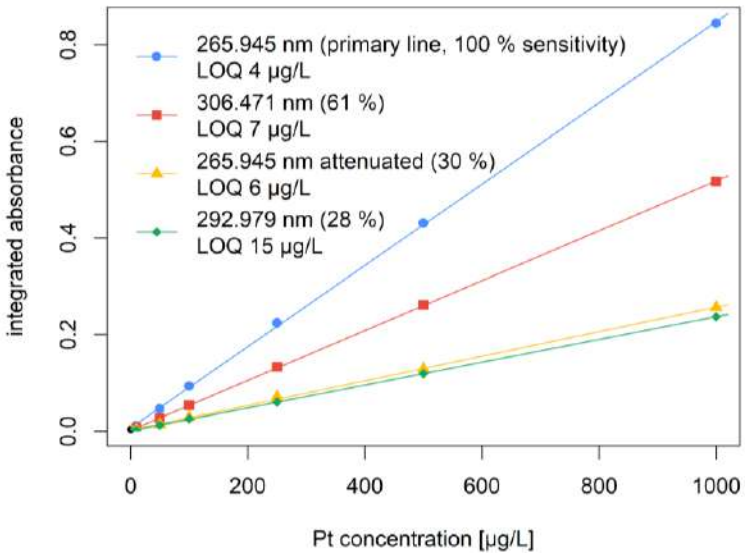

Obrázek 10: Kalibrační závislosti pro platinu s použitím jejích různých spektrálních čar.

5.3.3. Využití sekundárních čar v analýze půd

Využití sekundárních čar je obzvlášť praktické při analýze půd. Zájmové stopové prvky se v nich běžně vyskytují v relativně vysokých koncentracích, často vyžadujících ředění vzorků. Jednoduchou změnou vlnové délky na některou z dostupných čar s odpovídající citlivostí lze předejít ručnímu ředění vzorků. Ostatní parametry metody, jako je teplotní program, zůstávají beze změn.

Z dříve popsaných důvodů (vysoký šum, neznámé spektrální okolí) nebyly sekundární čáry v klasické LS-AAS příliš populární a pravděpodobně ze setrvačnosti jsou jen zřídka využívány i v HR-CS AAS. Prozatím bylo publikováno relativně málo metod s jejich využitím, pomineme-li metody simultánního víceprvkového stanovení (de Andrade et al. 2017; Gómez-Nieto et al. 2023; Araujo et al. 2013).

Praktické využití sekundárních čar bylo demonstrováno ve studii ***The impact of tourism on extremely visited volcanic island: Link between environmental pollution and transportation modes*** (příloha VII). V půdách vulkanického ostrova Santorini v Egejském moři byly sledovány kovy v souvislosti s intenzivním turismem v oblasti (tento populární řecký ostrov navštíví ročně 2 miliony turistů).

Koncentrace prvků v mineralizátech půd se lišily od velmi nízkých, vyžadujících plnou citlivost (kadmium, olovo) až po takové, jako je měď, jejíž měření na rezonanční čáře by vyžadovalo deseti- až stonásobné ředění. Namísto individuálního ředění celé sady vzorků byla citlivost

adaptována sekundárními čarami. V technice ET-AAS lze také v omezeném rozsahu měnit objem vzorku nanášený na platformu – toho bylo využito k „jemnému“ doladění rozsahu.

Po orientačním určení koncentrací kovů byly zvoleny čáry: Cd 228,802 nm (citlivost 100 %), Co 242,493 nm (citlivost 45 %), Cr 425,433 nm (33 %), Cu 216,509 (13 %) a Pb 283,306 (42 %). Vzorky byly dávkovány na platformu v objemech 6 až 20 µl.

Studie nalezla výraznou antropogenní kontaminaci, zejména mědí, chromem a olovem, soustředěnou především do oblasti letiště. Rostoucí intenzita turismu tak může v budoucnu vést k další degradací půd a dá se očekávat negativní dopad na kvalitu zde hojně produkovaného vína.

Na základě zkušeností lze konstatovat, že sekundární čáry jsou metodou první volby, pokud je třeba snížit citlivost stanovení a/nebo rozšířit pracovní rozsah. Některé prvky vykazují vysoké množství absorpčních čar – např. zde analyzované prvky: Co 575, Cr 193, Pb 41, Cu 32 a Cd 3 (Welz et al. 2010b). Oproti LS-AAS je lze využívat bez kompromisů.

5.3.4. Kombinace možných přístupů při analýze antarktické flóry

Výrazného rozšíření dynamického rozsahu bylo dosaženo zkombinováním obou možných přístupů – využitím sekundárních čar i odečítáním absorbance na jejich křídlech. V již zmiňované studii antarktické flóry (příloha I) byly simultánně stanoveny tři prvky; spolu s olovem také hliník a železo. Pro hliník byly přitom v měřeném úseku spektra dostupné hned dvě jeho sekundární čáry s výrazně odlišnou citlivostí (viz Obrázek 11). Citlivější čára 216,883 nm vykazuje relativní citlivost 5,6 % (vztaženo na primární čáru prvku), zatímco méně citlivá 216,984 nm pouze 0,19 %, tedy je asi 30krát slabší.

Obě tyto čáry byly využity pro analytické účely. V závislosti na koncentraci hliníku byl signál odečítán:

- na citlivější čáře pro koncentrace 20 µg/l až 5 mg/l,
- na méně citlivé čáře, poskytující lineární odezvu až do 100 mg/l, nebo
- na křídlech méně citlivé čáry pro obzvlášť vysoké koncentrace do 500 mg/l (Obrázek 11).

Vhodný způsob odečtu byl automaticky vybírán na základě jednoduchého kritéria při zpracování výsledků. Výsledkem bylo dosažení dynamického rozsahu přesahujícího čtyři řády. Celý tento rozsah byl přitom potřebný vzhledem k nárokům analýzy. Obsahy hliníku v rostlinných vzorcích se výrazně lišily v závislosti na obsahu minerálních částic, takže koncentrace hliníku v mineralizátech pokrývaly celý kalibrační rozsah.

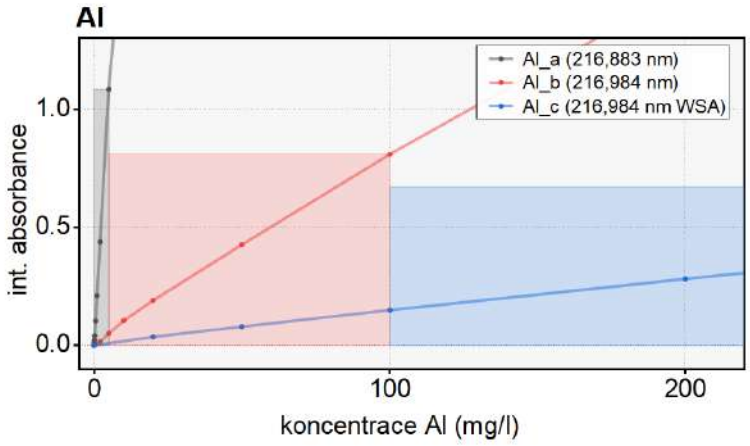

Obrázek 11: Kalibrační rozsahy hliníku, kombinující dvě spektrální čáry a odečítání signálu na křídle čáry pro dosažení širokého dynamického rozsahu. Jednotlivé pracovní rozsahy jsou vyznačeny obdélníky.

I když by se mohlo zdát, že grafitová kyveta je vhodná pouze pro stopovou analýzu, tato studie ukazuje, že je možné bez omezení měřit i tak vysoké koncentrace prvků, jako jsou desetiny gramu na litr. Také by se dalo namítnout, že vyšší obsahy je možné pohodlně měřit s plamenovou atomizací. V případě hliníku však taková analýza vyžaduje vysokoteplotní plamen acetylen – oxid dusný, který není dostupný v každé AAS laboratoři. Navíc – a to zejména – informace o obsahu tohoto referenčního prvku je s malým úsilím dostupná už při měření olova, tedy zájmového kontaminantu.

Lze očekávat, že umožní-li budoucí přístroje monitorování širší oblasti spektra (a tedy i většího množství prvků současně), právě takovéto kombinování jejich čar povede k obecnému rozšíření dynamického rozsahu. Využití vícero spektrálních čar pro kalibraci jednoho prvku se tedy má předpoklad stát běžným přístupem. Na rozdíl od např. měření intenzity emise je totiž absorpční měření vždy omezeno svým přirozeným rozsahem.

5.4. Nekovy a další těžko stanovitelné prvky

Záření kontinuálního zdroje pokrývá spektrum od 185 do 900 nm a je tedy možné měřit absorpci na vlnových délkách, pro které dříve nebyly dostupné čárové zdroje, nebo neposkytovaly dostatečnou citlivost. Ukázkovým příkladem je fosfor. Intenzivní emise výbojky také potlačuje dříve rušivé příspěvky záření ze samotného atomizátoru, toto téma je diskutováno v případě stanovení vápníku. Vysoký poměr signál-šum je výhodou při stopových stanoveních, jak je demonstrováno na příkladu hydridotvorných prvků arsenu a selenu.

Přínosy práce v oblasti analýzy těžko stanovitelných prvků zahrnují vyvinutí jednoduše aplikovatelné metody stanovení fosforu v hmyzu (a dalších matricích) a nového způsobu stanovení selenu v rybách pomocí kombinace fotochemického a chemického generování jeho těkavých sloučenin ve spojení s detekcí vysokorozlišovací AAS. Objasněna byla také specifika stanovení vápníku plamenovou technikou v rostlinných materiálech a potravinách, což jsou matrice silně rušící jeho stanovení.

5.4.1. Stanovení fosforu

Stanovení fosforu je náročné pro většinu analytických technik. V případě AAS jeho stanovení komplikují následující faktory.

- Rezonanční čáry fosforu, jakožto typického nekovu, leží ve vzdálené UV oblasti, a proto jsou pro běžné spektrometry nedostupné. Nezbývá než použít méně citlivé sekundární čáry.
- Dutokatodové lampy pro fosfor patřily k těm s nejnižší intenzitou, což v kombinaci se slabšími sekundárními čarami vedlo k chabému poměru signálu k šumu v klasické LS-AAS (de Campos et al. 2011).
- Spektrální oblast kolem 213 nm, kde se nachází dostupné sekundární čáry, je silně rušena absorpčními pásy již zmíněných problematických molekul monoxidu fosforu. Molekuly PO vykazují jemnou rotační strukturu, která se přímo překrývá s používaným nerezonančním dubletem fosforu, což komplikuje měření (de Campos et al. 2011; Lepri et al. 2006; Pomarolli et al. 2020; Welz et al. 2005). Fosfor je tedy prvek s raritní vlastností: interferuje sám sobě. Dřívější metody proto často poskytovaly nepravdivé výsledky.

Vysokorozlišovací AAS umožnila pochopit tyto interference a fosfor stanovit správně s lepší citlivostí. Xenonová výbojka poskytuje i na sekundární čáře vysokou intenzitu záření a případná interference PO molekul je zjevná. Autoři, kteří pomohli objasnit chování fosforu v grafitové kyvetě pomocí HR-CS AAS, záležitost popsali následovně: „*the story about the determination of phosphorus by conventional ETAAS at the 213.547/213.618 nm non-resonance doublet has to be re-written*“ (Lepri et al. 2006; Resano et al. 2009). Přesto není stanovení fosforu pomocí HR-CS ET-AAS příliš často uváděno, nejspíš kvůli historicky špatným zkušenostem z LS-AAS.

Snaha byla vytvořit jednoduše aplikovatelnou metodu, tzn. například vyhnout se používání permanentních modifikátorů, které využívali jiní autoři. Ve výsledné metodě je klíčová kombinace palladnatého modifikátoru a vysoké atomizační teploty. Potvrdilo se, že přídavek modifikátoru (1 g/L Pd v 0,6 g/L $Mg(NO_3)_2$) potlačuje tvorbu PO a podporuje atomizaci volného fosforu. Jako optimální množství se jeví 15 µl modifikátoru na 10 µl vzorku; menší množství vedlo k nižší citlivosti, zatímco větší přebytek vedl k novým spektrálním interferencím (viz Obrázek 12b). Ze spekter na obrázku 12b a 12c je patrné, že okolí nejcitlivější dostupné čáry fosforu 213,618 nm není díky tomu zatíženo interferencemi plynoucími z absorpce PO pásů – a tedy ani „ztrátami“ fosforu v jejich podobě. Podobný účinek potlačování jejich tvorby byl popsán i pro modifikátory na bázi Ir a Ru (Pomarolli et al. 2020), které se používají pro permanentní pokrytí platformy.

Fosfor je alternativně možné kvantifikovat na základě molekulové absorpce právě PO pásů (tedy pomocí HR-CS *M*AS – *molekulové* namísto atomové absorpce). K přednostní tvorbě molekulární formy během atomizace přispívají modifikátory jako zlato nebo vápník (Pomarolli et al. 2020). Lze použít nižší teploty vaporizace, což prodlužuje životnost kyvety, avšak výměnou za nižší citlivost a vyšší riziko spektrálních interferencí (Resano et al. 2009). Tento postup by však v našem případě nepostačoval svojí citlivostí – měření *atomové* absorpce fosforu je několikanásobně citlivější (Resano et al. 2009).

Zajímavostí je, že citlivost stanovení fosforu na základě jeho atomové absorpce je funkcí atomizační teploty. Dostupná čára totiž vychází z excitovaného stavu a vyšší teplota přispívá k vyšší populaci tohoto stavu. Při optimalizaci atomizační teploty proto nebyl dosažen ideální stav – signál v testované oblasti 2100 až 2800 °C setrvale roste (viz Obrázek 12a). Dokonce i navýšení atomizační teploty z 2600 na 2700 °C vede ke zvýšení signálu o třicet procent a na 2800 °C pak o dalších dvacet. Protože však používání takto vysoké teploty vede ke zkrácení životnosti kyvety, byla nakonec zvolena teplota 2700 °C – podobně jako dalšími autory (de Campos et al. 2011; Lepri et al. 2006).

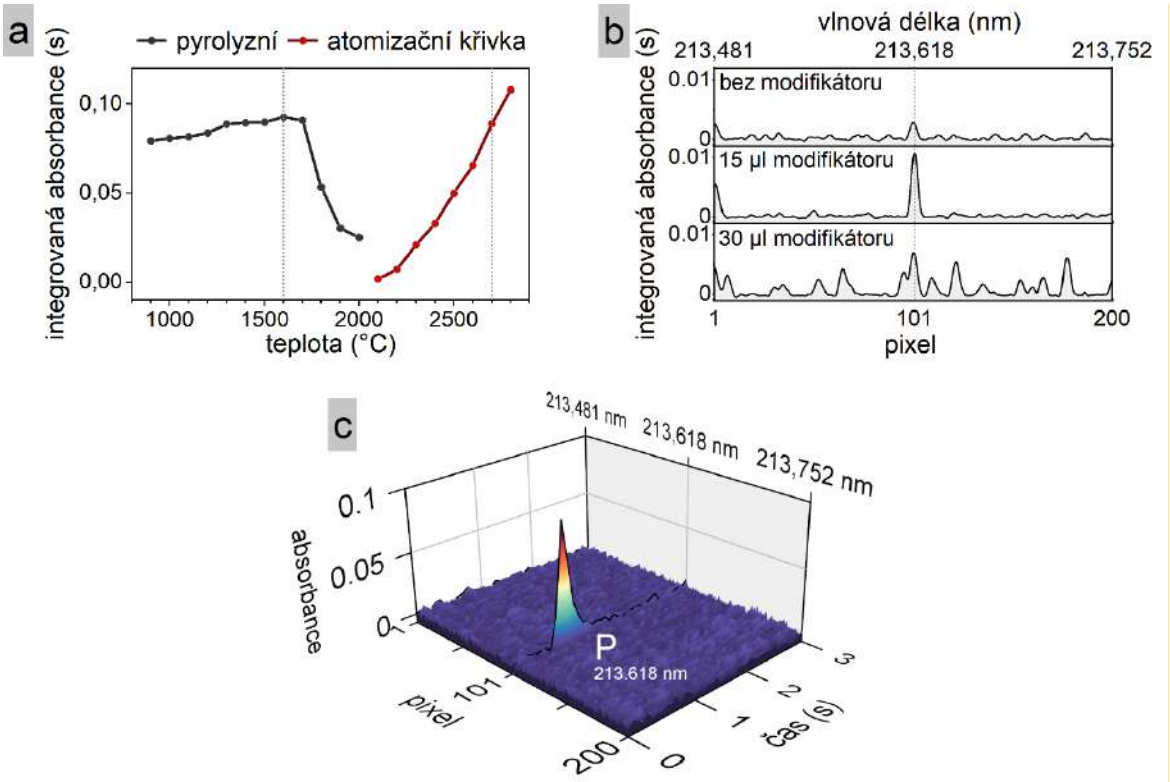

Obrázek 12: a) pyrolyzní a atomizační křivka fosforu, b) spektra ukazující vliv přídavku modifikátoru na spektrální okolí čáry fosforu, c) výsledné absorpční spektrum při stanovení fosforu ve vzorku rostlinného nápoje (obsah 8 mg/l).

Metoda se uplatnila v praxi; byť původně vyvinutá pro již uvedenou studii *Mineral profile of cricket powders, some edible insect species and their implication for gastronomy*, byla adaptována pro mnohé další materiály. V rámci závěrečných studentských prací byla aplikována na vyšší desítky vzorků různých matric vč. rostlinných extraktů. Limit stanovitelnosti je přibližně 1 mg/l, což se prokázalo jako odpovídající v analýze přírodních materiálů. Na základě zkušeností ji lze bez obav doporučit jako alternativu pro tradiční molybdátovanadátovou spektrofotometrickou metodu.

5.4.2. Stanovení vápníku

Jediná metoda této práce vyvinutá pro plamenovou AAS je pro stanovení vápníku. Může až překvapit, kolik pečlivosti je nutné věnovat stanovení tak „běžného“ prvku – pokud má vést k pravdivým výsledkům.

V roce 1958 požádal Alan Walsh svého kolegu J.B. Willise o vyvinutí metody pro stanovení vápníku v krevním séru. Ten věc brzy uzavřel s tím, že pro analýzu vzorků s komplikovanými matricemi nepostačuje teplota plamene svítiplyn–vzduch, ale bude nutné přejít na plamen o vyšší

teplotě. Plamen acetylen-vzduch se stal novým standardem (a stále jím je). Ani jeho teplota však nestačí k úplnému osvobození vápníku od tvorby stabilních fosfátů a hlinitanů. Vyšší množství těchto doprovodných prvků ve vzorku tak vede k potlačení signálu. Interferenci částečně omezuje uvolňovací činidlo na bázi lanthanu.

Až vysokoteplotní plamen acetylen – oxid dusný tento problém řeší zcela – byť za cenu ionizace části analytu. Tuto ionizaci je nutné potlačit tzv. *ionizačními pufry* (přídavkem snadněji ionizovatelného prvku, který posunuje elektronovou rovnováhu v plameni, např. cesia). Dalším neduhem plamene acetylen – oxid dusný je jeho vlastní intenzivní emise. Právě v blízkosti analytické čáry vápníku 422,673 nm se nachází výrazný emisní pás radikálu CN^- (Welz and Sperling 1999). Jeho maximum však leží nanometr od analytické čáry, což je v HR-CS velmi bezpečná vzdálenost. V LS-AAS bylo nutné vymezení úzké vstupní štěrbiny monochromátoru.

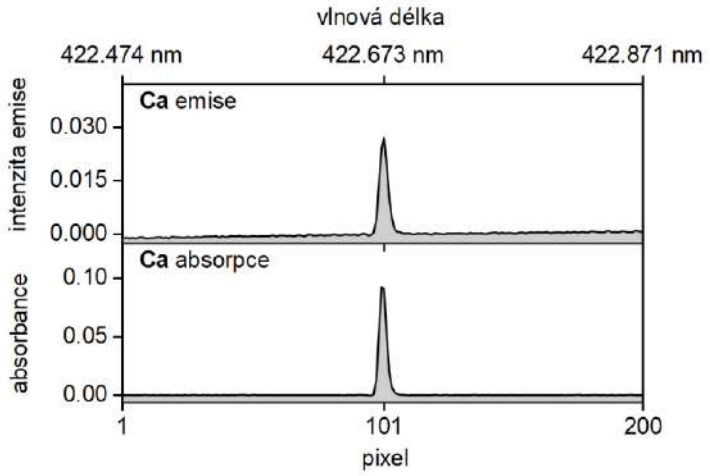

Obrázek 13: Porovnání emisního a absorpčního spektra při měření vápníku v plameni acetylen – oxid dusný (vzorek: referenční materiál čajových lístků – mineralizát)

Vápník lze v plameni acetylen – oxid dusný měřit s dostatečnou citlivostí i na základě jeho atomové *emise* (F-AES). Porovnány byly oba přístupy, oba plameny a různá přídavná činidla. Ze spekter na obrázku 13 je patrné, že lepší signál poskytuje absorpční měření; je intenzivní a nezatížený šumem. Naopak, při měření emise se poněkud ztrácí výhoda HR-CS AAS – tzn. potlačení šumu způsobeného vlastním vyzařováním plamene díky řádově intenzivnějšímu záření výbojky. (Další zřejmou výhodou F-AES bylo, že laboratořím umožňovala měřit i prvky, pro které nevlastnily lampy, kterýžto argument s univerzálním zdrojem záření také odpadá.)

Výsledná metoda je tedy založená na měření absorpce a pracuje s použitím cesia jakožto ionizačního pufru a navíc přídavkem 5-sulfosalicylové kyseliny. Díky tomu je robustní vzhledem

k chemickým interferencím a díky HR-CS není zatížena spektrálními interferencemi – ani těmi z plamene.

Tato metoda byla rozvíjena a uplatnila se v závěrečných pracích studentů: ***Vybrané mikroprvky v rastlinných náhradách mäsa*** (Mgr. Mária Dávidová, diplomová práce obhájena 2024, školitel) a ***Olejnatá semena jako zdroje vápníku*** (Dominika Michaličková, bakalářská práce obhájena 2023, školitel) a ***Vápník v potravinách určených pro vegany a vegetariány*** (Lucie Nováková, diplomová práce obhájena 2023, konzultant). Na základě těchto závěrečných prací nedávno vznikla metodická studie *Essential and toxic elements (Ca, Cd, Fe, P, Pb, and Zn) in plant-based dairy alternatives assessed using HR-CS AAS*, která je aktuálně v recenzním řízení.

5.4.3. Generování těkavých sloučenin v kombinaci s HR-CS AAS

Některé těžko stanovitelné prvky se v AAS s výhodou analyzují pomocí generování jejich těkavých sloučenin. Jde zejména o hydridotvorné prvky As, Bi, Ge, Pb, Sb, Se, Sn a Te. Ve formě své monoatomické páry se stanovuje rtuť.

Detekci arsenu na základě jeho hydridu arsanu AsH_3 využívala už Marshova zkouška (Marsh 1836). V AAS se techniky generování těkavých hydridů (*hydride generation*, HG) a studených par rtuti (*cold vapor*, CV) uplatňují od konce šedesátých let (Holak 1969; Hatch and Ott 1968). Běžné stanovení uvedených prvků atomizací v plameni nebo grafitové kyvetě totiž často nepostačuje citlivostí. Převedení na těkavou formu se ukázalo jako výhodné řešení; analyt je efektivně oddělen od matrice a s vysokou účinností zaveden do atomizátoru. Díky tomu se dosahuje vynikajících detekčních limitů a osvobození od mnohých interferencí. Vzhledem k často stopovým obsahům uvedených prvků je tento přístup velmi populární.

Tak například matrice rostlinných i živočišných vzorků (a to i po kvalitní mineralizaci) významně komplikují stanovení stopových množství arsenu a selenu. Ani s výkonnou korekcí pozadí v HR-CS ET-AAS není reálné dosáhnout citlivosti srovnatelné s metodou generování těkavých sloučenin. Jde proto o dva prvky nejčastěji měřené pomocí hydridové techniky. Rozdíl v citlivosti při analýze reálných vzorků mezi ET-AAS a HG AAS činí několik řádů (Shaltout et al. 2020).

Tvorba těkavé sloučeniny se provádí chemicky (reakcí s $NaBH_4$), elektrochemicky (redukcí analytu stejnosměrným proudem), nebo fotochemicky (pomocí radikálové reakce iniciované působením UV záření na přidané organické kyseliny).

Vzniklé těkavé sloučeniny jsou odděleny od kapalné fáze v separátoru fází a vedeny do atomizátoru. Nejčastějším atomizátorem je vyhřívaná křemenná trubice. Techniku lze spárovat také s grafitovou kyvetou, kde dochází k *in-situ* kolekci hydridů na grafitu a následně pak

k atomizaci – detekční limity této techniky se dostávají hluboko pod µg/l (Schlemmer et al. 1999; Welz and Sperling 1999; Shaltout et al. 2011). Všechny způsoby generování těkavých sloučenin jsou kompatibilní i s HR-CS spektrometry.

Vysokorozlišovací spektrometr zde slouží spíše jako prvkově-selektivní detektor. Riziko interferencí je v těchto metodách nízké a pokročilé možnosti korekce pozadí proto nenabývají takového významu. Výhodná je však intenzivní emise Xe lampy, vedoucí k vysokému poměru signálu k šumu. Využitelné je také rozšiřování dynamického rozsahu metodou WSA.

Metoda generování těkavého hydridu arsenu (AsH_3) ve spojení s detekcí HR-CS spektrometrem (HG HR-CS AAS) byla vyvinuta pro analýzu cyanobakteriálních povlaků z antarktických jezer během práce na studii ***Toxic metals in cyanobacterial mat of Big Lachman Lake, James Ross Island, Antarctica*** (příloha II). Čtveřice obzvlášť toxických prvků As, Cd, Hg a Pb byla monitorována v oblasti ostrova Jamese Rosse, kde leží česká vědecká stanice Johanna Gregora Mendela. Arsen byl redukován v průtokovém FIA systému (*flow injection analysis*) pomocí $NaBH_4$ a vzniklý hydrid veden do křemenného atomizátoru vyhřívaného na 1000 °C. Tímto způsobem bylo dosaženo limitu detekce 0,14 mg/kg. V povrchových sedimentech vykazovaly sledované prvky jen nízké obsahy, což je běžné pro daný region. Kvůli nízkému obsahu organického uhlíku zde svrchní pokryv zadržuje prvky jen slabě. Naopak, kumulace toxických prvků byla pozorována v cyanobakteriálních povlacích na dnech jezer. Tyto povlaky tak mohou indikovat vstup prvků do tohoto ekosystému, který je převážně skrze mokrou a suchou atmosférickou depozici.

Technika generování těkavých sloučenin selenu ve spojení s HR-CS AAS pak byla rozvíjena ve studii ***UV-photochemical vapor generation coupled to hydride generation AAS in the study of dietary intake of Se, Hg, Cd, and Pb from fish*** (příloha IV). Zkoumaným materiálem byla tedy rybí svalovina. Těkavé formy selenu byly generovány fotochemicky v přítomnosti kyseliny octové. Výstup z UV fotoreaktoru byl online napojen na generátor hydridů a dále veden do křemenné kyvety v optické ose spektrometru (UV-PVG HG HR-CS AAS). Pro tyto účely vytvořený fotoreaktor umožnil stanovení selenu s detekčním limitem 0,007 mg/kg.

Je zde nutné zmínit, že v případě stanovení selenu (a také rtuti) hraje významnou roli kvalita rozkladu vzorku. Organokovové sloučeniny selenu jsou velice stabilní a jejich přítomnost by vedla k neúplnému výtěžku. Je proto nezbytný dokonalý rozklad vzorku. V tomto případě byl aplikován vysokotlaký rozklad za teploty 250 °C. Je však nutné vyvážit podmínky rozkladu a omezit množství přidané HNO_3. Jelikož oxidující kyselina vede k oxidaci selenu na šestimocnou formu, která odolává redukci; je nutné ji předredukovat na čtyřmocnou formu.

V případě rtuti, jakožto extrémně těkavého prvku, je nutné zamezit ztrátám během rozkladu. Rtuť byla proto měřena metodou studených par (CV HR-CS AAS) ihned po ukončení mineralizace. Rtuť ze vzorku byla v proudu nosné kyseliny HCl vyredukována přídavkem $NaBH_4$. Studené páry byly vedeny do křemenné kyvety HR-CS spektrometru a absorbance měřena na vlnové délce 253,652 nm.

Metody byly aplikovány na vzorky rybího masa – analyzováno bylo 45 vzorků dostupných v tržní síti. Ve spolupráci s nutričními terapeuty byla hodnocena závažnost expozice těhotných a kojících žen rtutí z konzumace ryb. Na základě stanovených obsahů rtuti a míře konzumace ryb zjištěné frekvenčním dotazníkem žádná ze 180 respondentek nepřekračovala tolerovatelný týdenní příjem. Toxický účinek rtuti částečně kompenzuje právě selen, a to zejména při molárním poměru vůči rtuti větším než 1:1. Z tohoto pohledu se výhodně jevily sardinky a makrely.

6. Závěr

Environmentální elementární analýza je náročná disciplína, kladoucí vysoké nároky na přístrojovou techniku i samotné provedení. Zájmové prvky se v prostředí často vyskytují v nízkých koncentracích, zatímco rušivé složky je svým obsahem násobně převyšují. Význam obsahu jednotlivých prvků nelze posuzovat individuálně, je nutné jej zasazovat do kontextu. Analytická metodika proto musí být citlivá, robustní a mnohostranná.

Nově vyvinuté analytické metody představené v této práci dokládají, že HR-CS AAS má mezi technikami využívanými pro analýzu přírodních materiálů pevnou pozici. Vzhledem k tomu, že vůči technikám založeným na ICP vykazuje stále některé výhody (nízké pořizovací i provozní náklady, malou spotřebu vzorku, nebo schopnost měřit prvky jako např. fluor), lze směle očekávat, že směry se budou nadále rozvíjet bok po boku. Je na výrobcích i uživatelích, zdali tuto analytickou techniku udrží plodnou i do budoucna. Do jisté míry to vyžaduje prolomení konzervatismu, ke kterému vedly desítky let rutinního používání klasické AAS. Nové možnosti je však nutné převést do běžné praxe, tedy inkorporovat do snadno aplikovatelných metod. Právě to bylo cílem této habilitační práce – rozvinout nové možnosti HR-CS v environmentální analýze.

Jedním z nejvýraznějších omezení, znevýhodňující AAS v konkurenčním prostředí moderních analytických technik, je schopnost měřit vždy pouze jeden prvek. Práce popisuje aspekty víceprvkových metod v HR-CS AAS a představuje několik praktických aplikací, cílících na současné stanovení zájmových prvků v rostlinných materiálech a potravinách. Tak například zhodnocení míry kontaminace prostředí umožňuje současné stanovení toxického olova spolu se vztažnými nemobilními prvky hliníkem a železem. Vzhledem k tomu, že variabilita těchto prvků v rostlinách je vysoká, je třeba detekovat stopové a zároveň i velmi vysoké koncentrace. Proto práce popisuje i inovativní způsob rozšíření dynamického rozsahu; kombinací současného měření více spektrálních čar a různého způsobu odečítání signálu. Takto se podařilo překonat další tradiční neduh AAS a pracovní rozsah rozšířit ze 2 až 3 na více než 4 řády. Jak se ukázalo, pro hladký průběh monitoringu antarktické suchozemské flóry to byl nezbytný předpoklad.

Podobných metod je zde popsáno několik. Všechny již byly prověřeny v praxi a přinesly nové poznatky o výskytu a dynamice potenciálně toxických prvků. Metody jsou snadno adaptovatelné v dalších laboratořích. Jejich účelem je sloužit pro další výzkum přírodního a vnitřního prostředí a k zajištění bezpečnosti potravinářských surovin.

7. Použitá literatura

ALKEMADE, C. T. J. and J. M. W. MILATZ, 1955. A double-beam method of spectral selection with flames. *Applied Scientific Research*. **4**(1), 289–299. ISSN 0003-6994. doi:10.1007/bf02316494

ARAUJO, Rennan G. O., Fabíola VIGNOLA, Ivan N. B. CASTILHO, Bernhard WELZ, Maria Goreti R. VALE, Patricia SMICHOWSKI, Sérgio L. C. FERREIRA and Helmut BECKER-ROSS, 2013. Determination of silver in airborne particulate matter collected on glass fiber filters using high-resolution continuum source graphite furnace atomic absorption spectrometry and direct solid sampling. *Microchemical journal, devoted to the application of microtechniques in all branches of science*. **109**, 36–40. ISSN 0026-265X. doi:10.1016/j.microc.2012.05.009

BACON, Jeffrey R., Owen T. BUTLER, Warren R. L. CAIRNS, Olga CAVOURA, Jennifer M. COOK, Christine M. DAVIDSON and Regina MERTZ-KRAUS, 2024. Atomic spectrometry update – a review of advances in environmental analysis. *Journal of analytical atomic spectrometry*. **39**(1), 11–65. ISSN 0267-9477. doi:10.1039/D3JA90044D

BARGAGLI, Roberto, 2008. Environmental contamination in Antarctic ecosystems. *The Science of the total environment*. **400**(1–3), 212–226. ISSN 0048-9697. doi:10.1016/j.scitotenv.2008.06.062

BECHLIN, Marcos André, Felipe Manfroi FORTUNATO, Ricardo Moutinho DA SILVA, Edilene Cristina FERREIRA and José Anchieta GOMES NETO, 2014. A simple and fast method for assessment of the nitrogen–phosphorus–potassium rating of fertilizers using high-resolution continuum source atomic and molecular absorption spectrometry. *Spectrochimica acta. Part B: Atomic spectroscopy*. **101**, 240–244. ISSN 0584-8547. doi:10.1016/j.sab.2014.09.012

BECKER-ROSS, H., S. FLOREK, U. HEITMANN, HUANG, M. OKRUSS and B. RADZIUK, 2006. Continuum source atomic absorption spectrometry and detector technology: A historical perspective. *Spectrochimica acta. Part B: Atomic spectroscopy*. **61**(9), 1015–1030. ISSN 0584-8547. doi:10.1016/j.sab.2006.09.016

BECKER-ROSS, H., S. FLOREK, U. HEITMANN and R. WEISSE, 1996. Influence of the spectral bandwith of the spectrometer on the sensitivity using continuum source AAS. *Fresenius' journal of analytical chemistry*. **355**(3), 300–303. ISSN 0937-0633. doi:10.1007/s0021663550300

BECKER-ROSS, Helmut, Stefan FLOREK and Uwe HEITMANN, 2000. Observation, identification and correction of structured molecular background by means of continuum source AAS—determination of selenium and arsenic in human urine. *Journal of analytical atomic spectrometry*. **15**(2), 137–141. ISSN 0267-9477. doi:10.1039/A903571K

BORGES, Aline R., Emilene M. BECKER, Luciane L. FRANÇOIS, Alexandre DE JESUS, Maria Goreti R. VALE, Bernhard WELZ, Morgana B. DESSUY and Jailson B. DE ANDRADE, 2014. Investigation of spectral interferences in the determination of lead in fertilizers and limestone samples using high-resolution continuum source graphite furnace atomic absorption spectrometry. *Spectrochimica acta. Part B: Atomic spectroscopy*. **101**, 213–219. ISSN 0584-8547. doi:10.1016/j.sab.2014.08.040

BUSTOS, Daniel E., Juan A. TORO, Marisol BRICEÑO and Ricardo E. RIVAS, 2022. Use of slow atomization ramp in high resolution continuum source graphite furnace atomic absorption

spectrometry for the simultaneous determination of Cd and Ni in slurry powdered chocolate samples. *Talanta*. 123547. ISSN 0039-9140. doi:10.1016/j.talanta.2022.123547

COMNAP SECRETARIAT, 2017. *Antarctic Station Catalogue*. COMNAP Secretariat. ISBN 9780473404093.

COUFALÍK, Pavel, Ondřej ZVĚŘINA, Lukáš KRMÍČEK, Richard POKORNÝ and Josef KOMÁREK, 2015. Ultra-trace analysis of Hg in alkaline lavas and regolith from James Ross Island. *Antarctic science / Blackwell Scientific Publications*. **27**(03), 281–290. ISSN 0954-1020. doi:10.1017/S0954102014000819

DE ANDRADE, Rodolpho M., Jefferson S. DE GOIS, Isabela Maia TOALDO, Diego Barros BATISTA, Aderval S. LUNA and Daniel L. G. BORGES, 2017. Direct Determination of Trace Elements in Meat Samples via High-Resolution Graphite Furnace Atomic Absorption Spectrometry. *Food analytical methods*. **10**(5), 1209–1215. ISSN 1936-9751. doi:10.1007/s12161-016-0659-3

DE CAMPOS, Reinaldo Calixto, Carolina Lyrio T. CORREIA, Flavia VIEIRA, Tatiana D. SAINT'PIERRE, Ana Cristina OLIVEIRA and Rodrigo GONÇALVES, 2011. Direct determination of P in biodiesel by high-resolution continuum source graphite furnace atomic absorption spectrometry. *Spectrochimica acta. Part B: Atomic spectroscopy*. **66**(5), 352–355. ISSN 0584-8547. doi:10.1016/j.sab.2011.05.003

DOS SANTOS, Lisia M. G., Rennan G. O. ARAUJO, Bernhard WELZ, Silvana DO, C. JACOB, Maria GORETI, R. VALE and Helmut BECKER-ROSS, 2009. Simultaneous determination of Cd and Fe in grain products using direct solid sampling and high-resolution continuum source electrothermal atomic absorption spectrometry. *Talanta*. **78**, 577–583. ISSN 0039-9140. doi:10.1016/j.talanta.2008.12.006

DOUVRIS, Chris, Trey VAUGHAN, Derek BUSSAN, Georgios BARTZAS and Robert THOMAS, 2023. How ICP-OES changed the face of trace element analysis: Review of the global application landscape. *The Science of the total environment*. **905**, 167242. ISSN 0048-9697. doi:10.1016/j.scitotenv.2023.167242

FERNÁNDEZ-LÓPEZ, Laura, Beatriz GÓMEZ-NIETO, Mª Jesús GISMERA, Mª Teresa SEVILLA and Jesús R. PROCOPIO, 2018. Direct determination of copper and zinc in alcoholic and non-alcoholic drinks using high-resolution continuum source flame atomic absorption spectrometry and internal standardization. *Spectrochimica acta. Part B: Atomic spectroscopy*. **147**, 21–27. ISSN 0584-8547. doi:10.1016/j.sab.2018.05.016

FERREIRA, Sergio L. C., Jucelino B. DA SILVA, Ivanice Ferreira DOS SANTOS, Olivia M. C. DE OLIVEIRA, Victor CERDA and Antonio F. S. QUEIROZ, 2022. Use of pollution indices and ecological risk in the assessment of contamination from chemical elements in soils and sediments – Practical aspects. *Trends in Environmental Analytical Chemistry*. **35**, e00169. ISSN 2214-1588. doi:10.1016/j.teac.2022.e00169

GÓMEZ-NIETO, Beatriz, Ma Jesús GISMERA, Ma Teresa SEVILLA and Jesús R. PROCOPIO, 2015. Fast sequential multi-element determination of major and minor elements in environmental samples and drinking waters by high-resolution continuum source flame atomic absorption spectrometry. *Analytica chimica acta*. **854**, 13–19. ISSN 0003-2670. doi:10.1016/j.aca.2014.10.051

GÓMEZ-NIETO, Beatriz, Carmen ISABEL-CABRERA, María Jesús GISMERA, María Teresa SEVILLA, Jesús R. PROCOPIO and María Isabel SÁNCHEZ DE ROJAS, 2023. An environmentally friendly approach for the characterization of construction materials: determination of trace, minor, and major elements by slurry sampling high-resolution

continuum source graphite furnace atomic absorption spectrometry. *Analytical Methods*. **15**(9), 1105–1115. ISSN 1759-9679. doi:10.1039/d2ay02036j

HATCH, W. Ronald and Welland L. OTT, 1968. Determination of submicrogram quantities of mercury by atomic absorption spectrophotometry. *Analytical chemistry*. **40**(14), 2085–2087. ISSN 0003-2700. doi:10.1021/ac50158a025

HEITMANN, Uwe, Bernhard WELZ, Daniel L. G. BORGES and Fábio G. LEPRI, 2007. Feasibility of peak volume, side pixel and multiple peak registration in high-resolution continuum source atomic absorption spectrometry. *Spectrochimica acta. Part B: Atomic spectroscopy*. **62**(11), 1222–1230. ISSN 0584-8547. doi:10.1016/j.sab.2007.10.011

HESSE, Stefan, Thomas RISTAU and Jürgen W. EINAX, 2015. Chemical vapor generation by coupling high-pressure liquid flow injection to high-resolution continuum source hydride generation atomic absorption spectrometry for determination of arsenic. *Microchemical journal, devoted to the application of microtechniques in all branches of science*. **123**, 42–50. ISSN 0026-265X. doi:10.1016/j.microc.2015.04.023

HOLAK, Walter, 1969. Gas-sampling technique for arsenic determination by atomic absorption spectrophotometry. *Analytical chemistry*. **41**(12), 1712–1713. ISSN 0003-2700. doi:10.1021/ac60281a025

HOSSAIN, Mobarok, Dipti KARMAKAR, Syeda Nurunnesa BEGUM, Syed Yakub ALI and Pulak Kumar PATRA, 2021. Recent trends in the analysis of trace elements in the field of environmental research: A review. *Microchemical journal, devoted to the application of microtechniques in all branches of science*. **165**, 106086. ISSN 0026-265X. doi:10.1016/j.microc.2021.106086

IAATO, 2020. IAATO (International Association of Antarctica Tour Operators). *IAATO Data and Statistics* [cit.. 2024-02-22]. https://iaato.org/information-resources/data-statistics/

KELIHER, Peter N. and Charles C. WOHLERS, 1974. High resolution atomic absorption spectrometry using an echelle grating monochromator. *Analytical chemistry*. **46**(6), 682–687. ISSN 0003-2700. doi:10.1021/ac60342a011

KOIRTYOHANN, S. R., 1991. A history of atomic absorption spectroscopy from an academic perspective. *Analytical chemistry*. **63**(21), 1024A-1031A. ISSN 0003-2700. doi:10.1021/ac00021a001

LEPRI, Fábio G., Morgana B. DESSUY, Maria Goreti R. VALE, Daniel L. G. BORGES, Bernhard WELZ and Uwe HEITMANN, 2006. Investigation of chemical modifiers for phosphorus in a graphite furnace using high-resolution continuum source atomic absorption spectrometry. *Spectrochimica acta. Part B: Atomic spectroscopy*. **61**(8), 934–944. ISSN 0584-8547. doi:10.1016/j.sab.2006.08.001

L'VOV, B. V., 2005. Fifty years of atomic absorption spectrometry. *Journal of Analytical Chemistry*. **60**(4), 382–392. ISSN 1061-9348. doi:10.1007/s10809-005-0103-0

MACHADO, Raquel C., Daniel F. ANDRADE, Diego V. BABOS, Jeyne P. CASTRO, Vinicius C. COSTA, Marco Aurelio SPERANÇA, José Augusto GARCIA, Raimundo R. GAMELA and Edenir R. PEREIRA-FILHO, 2020. Solid sampling: advantages and challenges for chemical element determination—a critical review. *Journal of analytical atomic spectrometry*. **35**(1), 54–77. ISSN 0267-9477. doi:10.1039/C9JA00306A

MARSH, James, 1836. Method of separating small quantities of arsenic from substances with which it may have been mixed. *Journal of the Franklin Institute*. **22**(5), 338–343. ISSN 0016-0032. doi:10.1016/s0016-0032(36)90946-8

MARSHALL, John, Barbara J. OTTAWAY, John M. OTTAWAY and David LITTLEJOHN, 1986. Continuum-source atomic absorption spectrometry — new lamps for old? *Analytica chimica acta*. **180**, 357–371. ISSN 0003-2670. doi:10.1016/0003-2670(86)80018-6

MCCONNELL, J. R., O. J. MASELLI, M. SIGL, P. VALLELONGA, T. NEUMANN, H. ANSCHÜTZ, R. C. BALES, M. A. J. CURRAN, S. B. DAS, R. EDWARDS, S. KIPFSTUHL, L. LAYMAN and E. R. THOMAS, 2014. Antarctic-wide array of high-resolution ice core records reveals pervasive lead pollution began in 1889 and persists today. *Scientific reports*. **4**, 5848. ISSN 2045-2322. doi:10.1038/srep05848

NIU, Yuanyuan, Fang WANG, Songmin LIU and Wenjie ZHANG, 2021. Source analysis of heavy metal elements of PM2.5 in canteen in a university in winter. *Atmospheric environment*. **244**, 117879. ISSN 0004-6981. doi:10.1016/j.atmosenv.2020.117879

OTRUBA, V., J. JAMBOR, J. KOMÁREK, J. HORÁK and L. SOMMER, 1978. Simple mode of zeeman splitting of absorption lines in atomic absorption spectrometry. *Analytica chimica acta*. **101**(2), 367–374. ISSN 0003-2670. doi:10.1016/S0003-2670(01)93371-9

OZBEK, Nil, 2019. Simultaneous determination of Co, Fe, Ni and K with HR CS GFAAS. *Microchemical journal, devoted to the application of microtechniques in all branches of science*. **145**, 1066–1069. ISSN 0026-265X. doi:10.1016/j.microc.2018.12.002

PASIAS, Ioannis N., Nikolaos I. ROUSIS, Aikaterini K. PSOMA and Nikolaos S. THOMAIDIS, 2021. Simultaneous or Sequential Multi-element Graphite Furnace Atomic Absorption Spectrometry Techniques: Advances Within the Last 20 Years. *Atomic Spectroscopy*. **42(6)**. doi:10.46770/AS.202.707

PATRIARCA, Marina, Nicola BARLOW, Alan CROSS, Sarah HILL, Anna ROBSON and Julian TYSON, 2023. Atomic spectrometry update: review of advances in the analysis of clinical and biological materials, foods and beverages. *Journal of analytical atomic spectrometry*. **38**(3), 496–577. ISSN 0267-9477. doi:10.1039/D3JA90008H

POMAROLLI, Luiza Carolina, Márcia Andréia Mesquita Silva DA VEIGA, Martín RESANO and Flávio Venâncio NAKADI, 2020. Understanding polyatomic interference in the determination of phosphorus via PO molecules using high-resolution continuum source graphite furnace molecular absorption spectrometry with direct solid analysis. *Journal of analytical atomic spectrometry*. **35**(10), 2305–2314. ISSN 0267-9477. doi:10.1039/D0JA00254B

RASMUSSEN, Pat E., Christine LEVESQUE, Marc CHÉNIER, H. David GARDNER, Heather JONES-OTAZO and Sanya PETROVIC, 2013. Canadian House Dust Study: population-based concentrations, loads and loading rates of arsenic, cadmium, chromium, copper, nickel, lead, and zinc inside urban homes. *The Science of the total environment*. **443**, 520–529. ISSN 0048-9697. doi:10.1016/j.scitotenv.2012.11.003

RESANO, M., E. GARCÍA-RUIZ, M. ARAMENDÍA and M. A. BELARRA, 2019. Quo vadis high-resolution continuum source atomic/molecular absorption spectrometry? *Journal of analytical atomic spectrometry*. **34**(1), 59–80. ISSN 0267-9477. doi:10.1039/C8JA00256H

RESANO, Martín, Eduardo BOLEA-FERNÁNDEZ, Engracia MOZAS, María R. FLÓREZ, Patricia GRINBERG and Ralph E. STURGEON, 2013. Simultaneous determination of Co, Fe, Ni and Pb in carbon nanotubes by means of solid sampling high-resolution continuum source

graphite furnace atomic absorption spectrometry. *Journal of analytical atomic spectrometry*. **28**(5), 657–665. ISSN 0267-9477. doi:10.1039/C3JA30377B

RESANO, Martín, Jorge BRICEÑO and Miguel A. BELARRA, 2009. Direct determination of phosphorus in biological samples using a solid sampling-high resolution-continuum source electrothermal spectrometer: comparison of atomic and molecular absorption spectrometry. *Journal of analytical atomic spectrometry*. **24**(10), 1343. ISSN 0267-9477. doi:10.1039/b907937h

SCHLEMMER, G. and M. PETEK, 2000. Optimization of a class 100 clean room cabinet for electrothermal atomization AAS. *Atomic Spectroscopy*. **21**(1), 1–4. doi:10.46770/AS.2000.01.001

SCHLEMMER, Gerhard, Bernard RADZIUK, Birkhäuser VERLAG, Or Gerhard SCHLEMMER and Or Bernard RADZIUK, 1999. *Analytical Graphite Furnace Atomic Absorption Spectrometry A Laboratory Guide*. Birkhäuser Verlag. ISBN 9783034875783.

SHAH, Nasrullah, Muhammad Balal ARAIN and Mustafa SOYLAK, 2020. Chapter 2 - Historical background: milestones in the field of development of analytical instrumentation. In: Mustafa SOYLAK and Erkan YILMAZ, eds. *New Generation Green Solvents for Separation and Preconcentration of Organic and Inorganic Species*. Elsevier, p. 45–73. ISBN 9780128185698. doi:10.1016/B978-0-12-818569-8.00002-4

SHALTOUT, Abdallah A., Jamel BOUSLIMI and Hatem BESBES, 2020. The challenges of Se quantification in bean samples using line and continuum sources atomic absorption spectrometry. *Food chemistry*. **328**, 127124. ISSN 0308-8146. doi:10.1016/j.foodchem.2020.127124

SHALTOUT, Abdallah A., Ivan N. B. CASTILHO, Bernhard WELZ, Eduardo CARASEK, Irland B. Gonzaga MARTENS, Andreas MARTENS and Silvia M. F. COZZOLINO, 2011. Method development and optimization for the determination of selenium in bean and soil samples using hydride generation electrothermal atomic absorption spectrometry. *Talanta*. **85**(3), 1350–1356. ISSN 0039-9140. doi:10.1016/j.talanta.2011.06.015

SLAVIN, W., D. C. MANNING and G. R. CARNRICK, 1981. The stabilized temperature platform furnace. *Atomic Spectroscopy*. **2**(5), 137–145.

SMITH, S. B. and G. M. HIEFTJE, 1983. A New Background-Correction Method for Atomic Absorption Spectrometry. *Applied spectroscopy*. **37**(5), 419–424. ISSN 0003-7028. doi:10.1366/0003702834634893

ŠTOLL, Ivan, 1996. Jan Marek Marci z Lanškrouna. *Vesmír*. **75**(523) [cit.. 2024-01-30]. https://vesmir.cz/cz/casopis/archiv-casopisu/1996/cislo-9/jan-marek-marci-z-lanskrouna.html

THE EUROPEAN COMMISSION, 2023. *Commission Regulation (EU) 2023/915 on maximum levels for certain contaminants in food*. 2023. [cit.. 2024-02-13]. https://eur-lex.europa.eu/legal-content/en/TXT/?uri=CELEX%3A32023R0915

VAN DER VIJGH, W. J., 1991. Clinical pharmacokinetics of carboplatin. *Clinical pharmacokinetics*. **21**(4), 242–261. ISSN 0312-5963. doi:10.2165/00003088-199121040-00002

WALSH, Alan, 1974. Atomic absorption spectroscopy. Stagnant or pregnant. *Analytical chemistry*. **46**(8), 698A – 708a. ISSN 0003-2700. doi:10.1021/ac60344a052

WALSH, Alan, 1999. The development of the atomic absorption spectrophotometer. *Spectrochimica acta. Part B: Atomic spectroscopy*. **54**(14), 1943–1952. ISSN 0584-8547. doi:10.1016/S0584-8547(99)00171-8

WELZ, Bernhard, Helmut BECKER-ROSS, Stefan FLOREK and Uwe HEITMANN, 2005. *High-Resolution Continuum Source AAS: The Better Way to Do Atomic Absorption Spectrometry*. Weinheim ; [Great Britain]: John Wiley & Sons. ISBN 9783527307364.

WELZ, Bernhard, Lísia M. G. dos SANTOS, Rennan G. O. ARAUJO, Silvana do C. JACOB, Maria Goreti R. VALE, Michael OKRUSS and Helmut BECKER-ROSS, 2010a. Unusual calibration curves observed for iron using high-resolution continuum source graphite furnace atomic absorption spectrometry. *Spectrochimica acta. Part B: Atomic spectroscopy*. **65**(3), 258–262. ISSN 0584-8547. doi:10.1016/J.SAB.2010.01.007

WELZ, Bernhard and Michael SPERLING, 1999. *Atomic Absorption Spectrometry, Third edition*. Wiley. ISBN: 978-3-527-28571-6

WELZ, Bernhard and Michael SPERLING, 2008. *Atomic Absorption Spectrometry*. John Wiley & Sons. ISBN 9783527611683.

WELZ, Bernhard, Maria Goreti R. VALE, Stefan FLOREK, Michael OKRUSS, Mao-Dong HUANG and Helmut BECKER-ROSS, 2010b. High-resolution Continuum Source Atomic Absorption Spectrometry-Theory and Applications. In: *Encyclopedia of Analytical Chemistry*. John Wiley & Sons, Ltd, p. 1–34. ISBN 9780470027318. doi:10.1002/9780470027318.a9124

WILLIS, J. B., 1965. Nitrous Oxide – Acetylene Flame in Atomic Absorption Spectroscopy. *Nature*. **207**(4998), 715–716. ISSN 0028-0836. doi:10.1038/207715a0

WILLIS, J. B., 1997. The development of the nitrous oxide-acetylene flame for atomic absorption spectroscopy — a personal account. *Spectrochimica acta. Part B: Atomic spectroscopy*. **52**(6), 667–674. ISSN 0584-8547. doi:10.1016/S0584-8547(97)00009-8

ZVĚŘINA, Ondřej, Pavel COUFALÍK, Miloš BARTÁK, Michal PETROV and Josef KOMÁREK, 2018. The contents and distributions of cadmium, mercury, and lead in Usnea antarctica lichens from Solorina Valley, James Ross Island (Antarctica). *Environmental monitoring and assessment*. **190**(1). ISSN 0167-6369. doi:10.1007/s10661-017-6397-1

ZVĚŘINA, Ondřej, Kamil LÁSKA, Rostislav ČERVENKA, Jan KUTA, Pavel COUFALÍK and Josef KOMÁREK, 2014. Analysis of mercury and other heavy metals accumulated in lichen Usnea antarctica from James Ross Island, Antarctica. *Environmental monitoring and assessment*. **186**(12), 9089–9100. ISSN 0167-6369. doi:10.1007/s10661-014-4068-z

8. Přílohy

I. **Zvěřina, O**; Brůhová, L; Coufalík, P; Stringer, CD; Rieger, J; Goessler, W, 2024. *Multi-element analysis (Pb, Al, Fe) of Antarctic flora using HR-CS ETAAS with an extended working range.* SPECTROCHIMICA ACTA PART B-ATOMIC SPECTROSCOPY. 10.1016/j.sab.2024.106979

II. Coufalík, P; Vašinka, M; Krmíček, L; Ševčík, R; **Zvěřina, O**; Brůhová, L; Komárek, J, 2024. *Toxic metals in cyanobacterial mat of Big Lachman Lake, James Ross Island, Antarctica.* ENVIRONMENTAL MONITORING AND ASSESSMENT. 10.1007/s10661-023-12224-3

III. **Zvěřina, O**; Vychytilová, M; Rieger, J; Goessler, W, 2023. *Fast and simultaneous determination of zinc and iron using HR-CS GF-AAS in vegetables and plant material.* SPECTROCHIMICA ACTA PART B-ATOMIC SPECTROSCOPY. 10.1016/j.sab.2023.106616

IV. Coufalík, P; **Zvěřina, O**; Sádovská, K; Komárek, J, 2023. *UV-photochemical vapor generation coupled to hydride generation AAS in the study of dietary intake of Se, Hg, Cd, and Pb from fish.* JOURNAL OF FOOD COMPOSITION AND ANALYSIS. 10.1016/j.jfca.2023.105668

V. Kosečková, P; **Zvěřina, O** ✉; Pechová, M; Krulíková, M; Duborská, E; Borkovcová, M, 2022. *Mineral profile of cricket powders, some edible insect species and their implication for gastronomy.* JOURNAL OF FOOD COMPOSITION AND ANALYSIS. 10.1016/j.jfca.2021.104340

VI. **Zvěřina, O**; Venclíček, O; Kuta, J; Coufalík, P; Hagarová, I; Brat, K, 2021. *A simple dilute-and-shoot procedure for the determination of platinum in human pleural effusions using HR-CS GF-AAS.* JOURNAL OF TRACE ELEMENTS IN MEDICINE AND BIOLOGY. 10.1016/j.jtemb.2021.126869

VII. Brtnický, M; Pecina, V; Galiová, MV; Prokeš, L; **Zvěřina, O**; Juřička, D; Klimánek, M; Kynický, J, 2020. *The impact of tourism on extremely visited volcanic island: Link between environmental pollution and transportation modes.* CHEMOSPHERE. 10.1016/j.chemosphere.2020.126118

VIII. **Zvěřina, O**; Coufalík, P; Šimůnek, J; Kachlík, P; Chlupová, R; Pavelková, J, 2020. *Inorganic pollutants in the indoor environment of the Moravian Library: assessment of Cd, Pb, Cu, and Zn in total suspended particles and dust using HR-CS GF-AAS.* ENVIRONMENTAL MONITORING AND ASSESSMENT. 10.1007/s10661-020-08748-7

IX. **Zvěřina, O**; Kuta, J; Coufalík, P; Kosečková, P; Komárek, J, 2019. *Simultaneous determination of cadmium and iron in different kinds of cereal flakes using high-resolution continuum source atomic absorption spectrometry.* FOOD CHEMISTRY. 10.1016/j.foodchem.2019.125084

Spectrochimica Acta Part B: Atomic Spectroscopy 218 (2024) 106979

Contents lists available at ScienceDirect

Spectrochimica Acta Part B: Atomic Spectroscopy

journal homepage: www.elsevier.com/locate/sab

Analytical note

Multi-element analysis (Pb, Al, Fe) of Antarctic flora using HR-CS ETAAS with an extended working range

Ondřej Zvěřina [a,*], Lenka Brůhová [a], Pavel Coufalík [b], Christopher D. Stringer [c], Jaqueline Rieger [d], Walter Goessler [d]

[a] Masaryk University, Department of Public Health, Kamenice 5, 625 00 Brno, Czech Republic
[b] Institute of Analytical Chemistry of the Czech Academy of Sciences, Veveří 97, 60200 Brno, Czech Republic
[c] School of Geography and water@leeds, University of Leeds, Woodhouse Lane, Leeds, West Yorkshire LS2 9JT, UK
[d] University of Graz, Institute of Chemistry, Universitaetsplatz 1, 8010 Graz, Austria

ARTICLE INFO

Keywords:
Simultaneous multi-element analysis
HR-CS ETAAS
Antarctic flora analysis
Biomonitoring
Antarctica

ABSTRACT

This paper introduces a new method for the simultaneous determination of lead, aluminum, and iron in plant samples using high-resolution continuum source electrothermal atomic absorption spectrometry (HR-CS ETAAS). The method is suitable for covering a wide range of concentrations for all three elements, by utilizing two spectral lines for Al and employing the wavelength-selected absorbance (WSA) approach, which combines the reading of absorbance signals at both the central and wing parts of the spectral lines. The method was validated against certified reference materials and was then applied in a large-scale analysis of Antarctic flora collected from Nelson Island in the South Shetland Islands, Antarctica. The method was found to be a useful biomonitoring tool for assessing Pb pollution in various plant materials, including lichens, mosses, grass and mushrooms, while Al and Fe contents may serve as normalizing elements in calculations of environmental indices. The observed Pb levels in lichens (median content 0.19 mg Pb/kg) were lower than those reported in other Antarctic regions. These findings indicate that the Stansbury Peninsula on Nelson Island is relatively unaffected by local pollution, compared to other Antarctic regions, and that the data might serve as an example of background levels in the South Shetland Islands.

1. Introduction

Lead is a global contaminant of particular concern due to its high ecosystem-disrupting potential, and is readily transported over long distances, even reaching remote areas like Antarctica [1]. Over the past 130 years, an estimated 660 tons of Pb have been deposited over the continent through long-range atmospheric transport [2]. Additionally, local pollution comes from anthropogenic activities such as the operation of scientific stations and tourism [1,3]. Such activities are mostly localized close to the coast, where most of the terrestrial floral and faunal diversity is concentrated [3,4]. In particular, cryptogams like lichens and mosses, widespread across Antarctica, act as sensitive bioindicators, reflecting local environmental conditions [1,3,5]. A common approach to assessing Pb contamination in bioindicators is to normalize Pb levels to naturally occurring, less mobile elements such as Al and Fe, which act as reference elements due to their stable environmental concentrations.

The elemental analysis of plant materials, including cryptogams, is typically performed using various spectroscopic techniques such as atomic absorption spectrometry with both flame and electrothermal atomization (FAAS and ETAAS), and also methods based on inductively coupled plasma with either optical emission (ICP-OES) or mass spectrometry (ICP-MS) [6].

While ETAAS is a well-established and sensitive technique for the elemental analysis of environmental samples, it suffers from limitations such as single-element determination and a limited working range. However, commercially available high-resolution continuum source (HR-CS) AA spectrometers have introduced features to overcome these limitations, as they allow for detailed monitoring of the selected spectral line and its immediate surroundings.

Measuring elements of interest one by one is a significant limitation of AAS, especially for time-consuming methods like ETAAS. However, HR-CS AAS instruments monitor not only the analytical line itself, but also its immediate surroundings. Any other spectral line close enough to

* Corresponding author.
E-mail address: zverina@med.muni.cz (O. Zvěřina).

https://doi.org/10.1016/j.sab.2024.106979
Received 22 February 2024; Received in revised form 21 June 2024; Accepted 23 June 2024
Available online 24 June 2024

fit into this detection window (approximately 0.2 nm) can be monitored simultaneously. This capability has allowed for the simultaneous analysis of up to four elements in some HR-CS ETAAS applications [7–9] and reviews on multielemental methods indicate a high interest in the benefits of such a feature [10–12]. Previously, a method for the simultaneous analysis of Pb and other elements was described, using Pb's secondary line at 283.306 nm, which is surrounded by secondary lines of Co, Fe, and Ni [8]. Multielemental methods employing the primary line of Pb at 217.001 nm have so far been based on a sequential approach [13,14]. These techniques require cooling of the furnace and realigning of the monochromator between the two separate atomization steps; therefore, time-savings are not as significant as in the case of a truly simultaneous determination.

In ecological studies, measuring Pb concentrations with high sensitivity is crucial, as Pb is typically found in trace amounts. On the other hand, Al and Fe are usually present in substantially higher and varying amounts, for which measurement a wide working range is required. In this regard, HR-CS offers useful tools for extending the dynamic range, which has traditionally been limited in line-source AAS to about two orders of magnitude [15,16]. The dynamic range can be extended in either of the two following ways:

- by using a wavelength-selected absorbance (WSA) approach, which can adjust the sensitivity by reading the signal either at the center of the absorption line or at its wings. In practice, this is achieved by using various pixels to register the absorbance signal. The signal registered by these side-pixels grows linearly in a wide concentration range [17]. Such sensitivity attenuation has already been used in a number of studies, e.g. [18–21]; however, this was only to reduce the signal intensity. In our study, it was undertaken to extend the methods' working range by preparing a series of calibration curves based on the different pixel combinations.
- by using less sensitive spectral lines. In line-source AAS, the use of secondary lines is not very common, mainly because they 1) exhibit a poor signal-to-noise ratio, and 2) are not well studied in terms of potential spectral interferences. The above reasons become invalid with the use of a continuum source (which provides a similar emission intensity for all lines) and high-resolution monochromator (which makes any spectral interference obvious) [21]. Moreover, in the case where multiple lines of the same element fit in the detector window, these having different sensitivity, they can be used to cover different concentration ranges. For instance, such a use of the Ni triplet in the vicinity of 234.6 nm was described in a review by Resano [11], covering a concentration range of more than three orders of magnitude. Similarly, near the primary Pb line at 217.001 nm, two Al lines occur with significantly different sensitivities. These Al lines can be utilized in an analogous approach to expand the measurable Al concentration range.

Both above-mentioned approaches can also be effectively combined, most notably for Al, where the two spectral lines and also the WSA approach can be used to extend the dynamic range of the measurement.

The main objective of this work was the development of a method for assessing environmental lead (Pb) contamination using HR-CS ETAAS, enabling the simultaneous co-determination of the reference elements aluminum (Al) and iron (Fe). The study aimed to develop a routine method involving multi-calibration based on WSA and multi-line evaluation, as well as the use of a simultaneous multi element method for assessing Pb contamination at trace levels. To the best of our knowledge, no routine method including these features has been described so far. A deeper insight into the contamination of the Antarctic flora of Nelson Island is the further contribution of this work.

2. Materials and methods

2.1. Samples of terrestrial flora from Nelson Island

The samples for this work originated from Nelson Island, South Shetland Islands, Antarctica (Fig. 1). Nelson Island is adjacent to King George Island, where most research stations are located, and experiences minimal human activity due to the absence of permanent settlements. Thus, it offers a relatively pristine environment compared to other areas in the region with higher tourist and scientific traffic. The local terrestrial flora is represented by lichens, mosses, grass, and mushrooms.

Samples were collected from the Rip Point oasis, Stansbury Peninsula, located in the northern part of the island. We established 28 sampling sites, each encompassing a circular area with a diameter of approximately 20 m to ensure comprehensive spatial coverage and representative sampling. At each site, we collected representative samples of lichens, mosses, mushrooms, and grass, whenever present. All collected samples were stored in PE plastic bags and kept frozen until analysis.

Samples of lichens included fruticose species prevalent in the area, namely *Usnea antarctica* ($n = 27$), *Usnea aurantiaco-atra* ($n = 23$), and *Ramalina terebrata* ($n = 4$). Moss samples included mainly the locally-dominant specie *Sanionia uncinata* ($n = 15$) followed by *Polytrichum* sp. ($n = 3$) and *Bryum pseudotriquetrum* (n = 3) and their mixtures ($n = 8$). Five samples of grass were all *Deschampsia antarctica* and the mushroom samples consisted of *Arrhenia antarctica* ($n = 6$) and one sample of *Arrhenia* cf. *lilacinicolor*.

2.2. Sample treatment and mineralization

In the laboratory, the samples underwent a series of preparation steps. First, they were subjected to a double wash with ultrapure water (18.2 MΩ cm) to remove any soil particles. Subsequently, the samples were dried for 48 h at 35 °C in a laboratory oven. To achieve a consistent texture, the samples were milled using an IKA A11 stainless-steel mill (IKA, Germany). However, due to the robustness of lichen thalli, an additional grinding step was necessary. The lichens were finely ground using a Pulverisette 7 planetary mill with silicon nitride grinding balls (Fritsch GmbH, Germany), resulting in a uniformly homogenized fine-grained material.

An UltraWAVE high-pressure microwave mineralizer (Milestone, Italy) was used for the decomposition of samples. The traceCLEAN cleaning system (Milestone, Italy) was used for the decontamination of quartz mineralization tubes. The decomposition of samples was carried out in a clean laboratory (class 100). Sub-boiled distilled HNO_3 (MES 2000, Gerber Instruments AG, Switzerland) was used for the mineralization of samples. The mineralized samples were further diluted by deionized water with a specific electrical conductivity of 0.055 μS/cm (Ultra Clear, Evoqua Water Technologies, USA).

200 mg samples of lichens, mosses, and grass (to the nearest 0.1 mg) were weighed into the quartz mineralization tubes; only 50 mg mushroom samples were used due to the scarcity of the material. The samples were digested in 3 mL of concentrated HNO_3. Decomposition was carried out according to a temperature program with a maximum mineralization temperature of 250 °C for 15 min. After cooling, the samples were transferred into PP tubes (Roth, USA) and topped up with deionized water to a volume of 10 mL (5 mL in the case of mushroom samples). White undissolved residues were observed in a few moss and grass samples. These residues were centrifuged to the bottom of the sample tubes, and the clear supernatant solution was used for the analysis.

Four certified reference materials (CRMs) were used to verify the accuracy of metal determinations: BCR-482 Lichen (IRMM, Belgium), NIST 1570a Spinach (NIST, USA), INCT-TL-1 Tea Leaves (INCT, Poland) and Metranal AN-BM02 Green Tea (ANALYTIKA, Czech Republic). CRMs were mineralized in triplicates using the same procedure as the

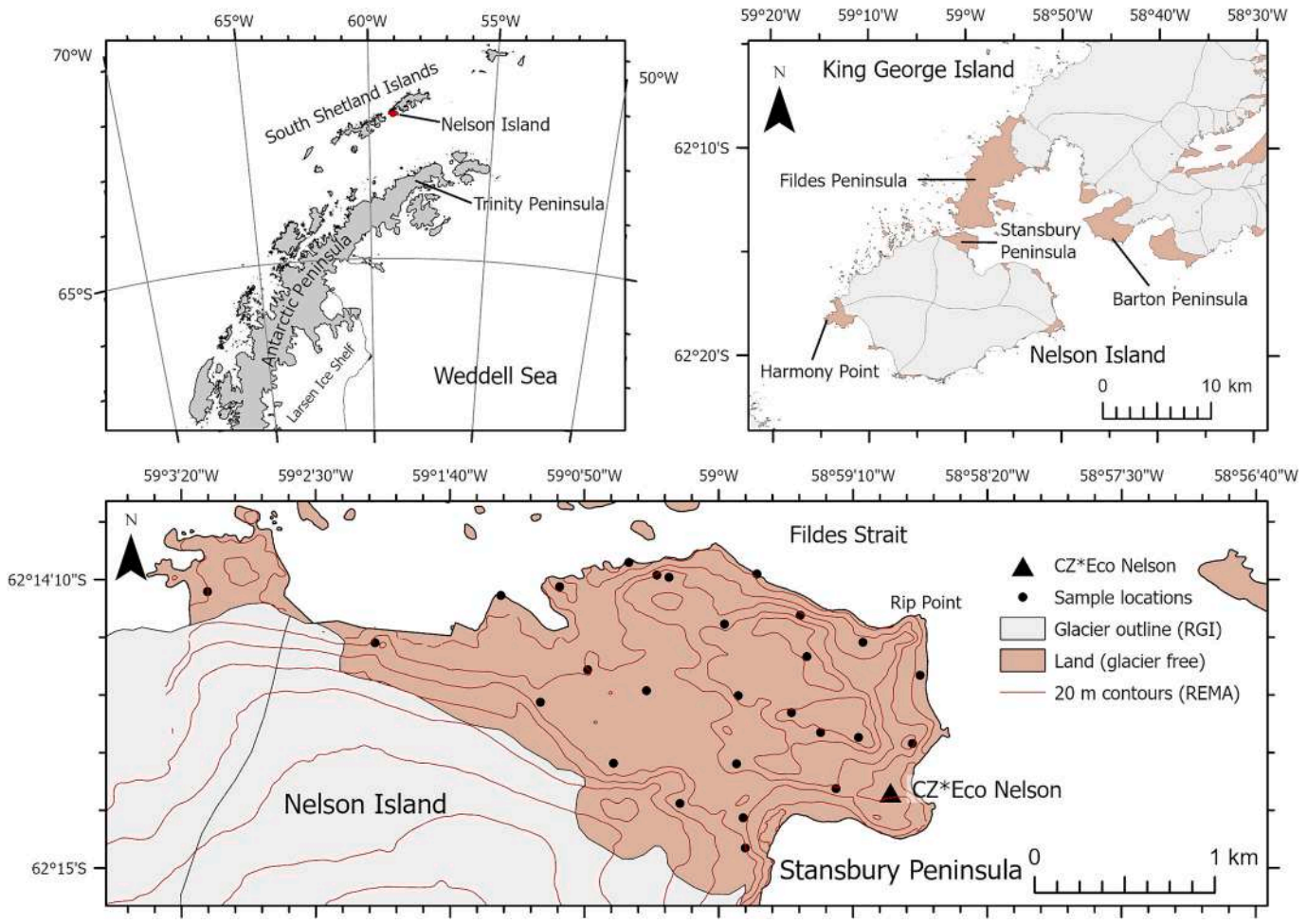

Fig. 1. Map of Nelson Island and sampling locations.

samples. Also, a total digestion of the CRMs was carried out for a trueness study purpose, using a mixture of 3 mL HNO_3 and 0.250 μL HF (Analpure grade, 48%, Analytika, Czech Republic) for the digestion.

2.3. Method for the simultaneous determination of Pb, Al, and Fe

A ContrAA 800G (Analytik Jena, Germany) high-resolution continuum source spectrometer was used for all analyses, this equipped with a Xe short-arc lamp as a continuum light source combined with a high-resolution double-Echelle monochromator and charge-coupled device detector. Graphite tubes with a PIN-platform were utilized for the analysis.

For the analysis, a 10 μL sample was injected into the furnace together with 15 μL of Pd/$Mg(NO_3)_2$ modifier (consisting of Pd 1 g/L and $Mg(NO_3)_2$ 0.6 g/L). The modifier not only prevents Pb losses during pyrolysis but also improves the shape of the Al peaks and reduces spectral interference from phosphorus monoxide. In samples with especially high phosphorus content, remaining molecular absorption bands were further minimized by the least squares background correction (see chapter 3.4. Handling the spectral interferences). The optimized temperature program is presented in Table 1, which is further discussed in the section 3.2. Developing a temperature program. The total duration of the program was 85 s. During the atomization step, the signals of adjacent spectral lines of Pb, Fe and two Al lines were recorded simultaneously using various combinations of detector pixels (see chapter 3.1. Spectral line selection). This approach allows considerable extension of the working range (see chapter 3.3. Method performance and working range). The wide working range allows for the batch analysis of sets of diverse samples, eliminating the need for individual dilutions. The need for operator intervention is thus also minimized. This capability was demonstrated by analyzing a set of 95 real plant materials with widely-varying elemental concentrations.

Table 1
Temperature program for the simultaneous determination of Pb, Al, and Fe using HR-CS ETAAS.

Step	Temperature (°C)	Ramp (°C/s)	Hold (s)	Argon flow (L/min)	Read
Drying	130	10	7	2	
Pyrolysis	900	300	10	2	
Atomization	2500	1500	4	stop	active
Cleaning	2600	100	2	2	

3. Results and discussion

3.1. Spectral line selection

In the immediate vicinity of the primary Pb resonance line at 217.001 nm, there are secondary lines for Al and Fe:

- Al 216.883 nm, with a sensitivity of 5.6% (with respect to primary line of the element),
- Al 216.984 nm, 0.19% sensitivity,
- Fe 217.130 nm, 0.33% sensitivity.

While the Pb line exhibits the highest possible sensitivity for this element, which is crucial for its detection at trace levels, the secondary lines for Al and Fe are less sensitive. However, the reduced sensitivity of the Al and Fe lines corresponds to the generally high contents of Al and Fe in the samples. Because of the presence of two Al lines with significantly different sensitivities, they can be effectively employed to extend the working range of Al determination.

At the relatively low atomization temperatures during normal Pb measurement, neither Al nor Fe volatilizes. However, when an adequate atomization temperature is applied, all four lines become observable in the detection window. An illustrative spectrum obtained during the analysis of a digested lichen sample is presented in Fig. 2.

3.2. Developing a temperature program

The initial drying step was optimized through the observation of the process via the instrument's camera, ensuring smooth drying with no spattering. It is important to note that when adopting this method, the drying program might require optimization for different spectrometer models and specific instrument conditions, such as the flow rate of the protective gas.

In the simultaneous determination of elements in ETAAS, the pyrolysis temperature is limited by the most volatile element, while the atomization temperature is defined by the most refractory element to be determined (in this work, Pb and Al, respectively). Due to the Pd/Mg $(NO_3)_2$ modifier, Pb remained stable up to 1300 °C during pyrolysis. However, as there was no significant nonspecific background absorbance from the matrix, a pyrolysis temperature of 900 °C was chosen.

An atomization temperature of 2500 °C was necessary to achieve a good peak profile for Al, the most refractory element analyzed. This temperature was slightly higher than optimal for Pb, leading to a decrease in the Pb signal (the integrated absorbance was lower by approximately 30%) mainly due to the rapid expansion of the atom cloud (see Fig. 3). Despite the sensitivity (defined as the slope of the calibration curve) might be affected for volatile elements during multielement analyses at high temperature, it is known that the resulting narrower peaks can partially compensate for this. Narrower peaks allow for a shorter integration time, leading to an improved signal-to-noise ratio [15]. To take advantage of this phenomenon, the Pb signal integration time was shortened to only the first 2 s of the atomization step. The resulting limit of quantification was sufficient with respect to the actual concentration in the real samples (see the next chapter).

Also, the simultaneous determination of elements with substantially different volatilities can be performed using multi-step atomization,

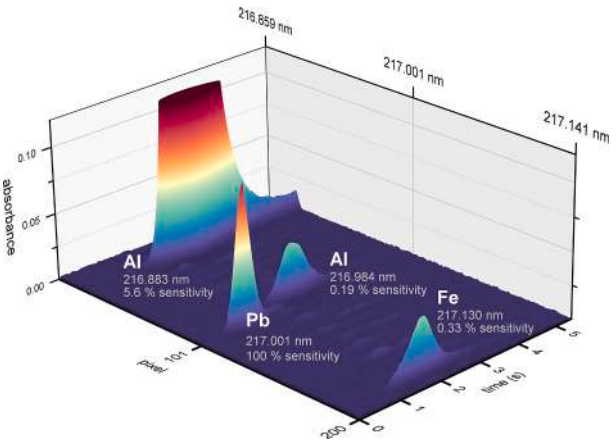

Fig. 2. Wavelength- and time-resolved absorption spectrum from the analysis of a lichen digest (Pb 20 µg/L, Al 7 mg/L, Fe 4 mg/L) using the proposed method. Wavelengths and relative sensitivities of the four monitored spectral lines are indicated.

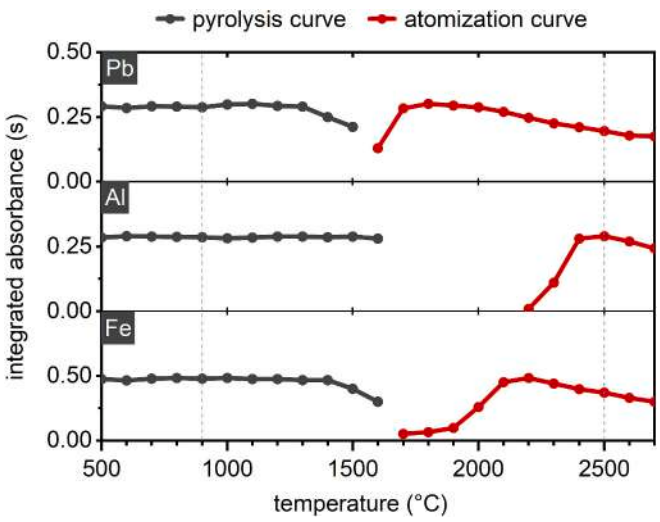

Fig. 3. Atomization and pyrolysis curves for Pb, Al, and Fe, obtained with a proposed method for a lichen sample digest.

leading to the atomization of each element under optimal conditions [22–24]. However, this approach was not feasible in this case. Our experiments revealed that separate Pb atomization resulted in a partial loss of Fe, as it becomes volatile at temperatures exceeding 1700 °C (as can be seen in Fig. 3:).

3.3. Method performance and working range

Our goal was to develop a method that can be routinely used to analyze large sample sets without the need for repeated dilutions or manual recalculation of the results. To achieve a wide working range, calibration curves were constructed using a combination of signals from the two spectral lines (in the case of Al) and also the central and wing portions of the spectral lines, employing the WSA approach. As a result, a series of consecutive calibration curves was employed for each element, as illustrated in Fig. 4. The parameters of these curves are summarized in Table 2.

3.4. Lead

With the default setting, i.e. absorbance readings were obtained from the central pixel and the two adjacent pixels (CP ± 1), the calibration plot for the Pb_a line exhibited linearity from the limit of quantification (LOQ) to 50 µg/L. For concentrations exceeding 50 µg/L, the WSA approach was employed, specifically by recording the signal from pixels 105 and 106, which lie at the wing of the Pb line. This approach yielded a second linear calibration function (the Pb_b line), extending the dynamic range up to 500 µg/L.

3.5. Aluminum

Fig. 4 shows excellent linearity for the calibration plots of all three Al lines. The most sensitive Al line at 216.883 nm (Al_a) is suitable for measuring concentrations from 0.02 to up to 5 mg/L, while the less sensitive line at 216.984 nm (Al_b) provides a follow-up linear calibration line up to 100 mg/L. By employing the WSA approach, the working range of Al_c is extended to up to 500 mg/L. This utilization of the available lines, with their sensitivities differing by a factor of approximately 30, expands the working range to more than four orders of magnitude. This wide working range was found to be necessary for directly analyzing the Al concentrations in the digests during the project.

On completion of the analysis, the control software reports values measured at each of the three lines (Al_a, Al_b, and Al_c). However, the

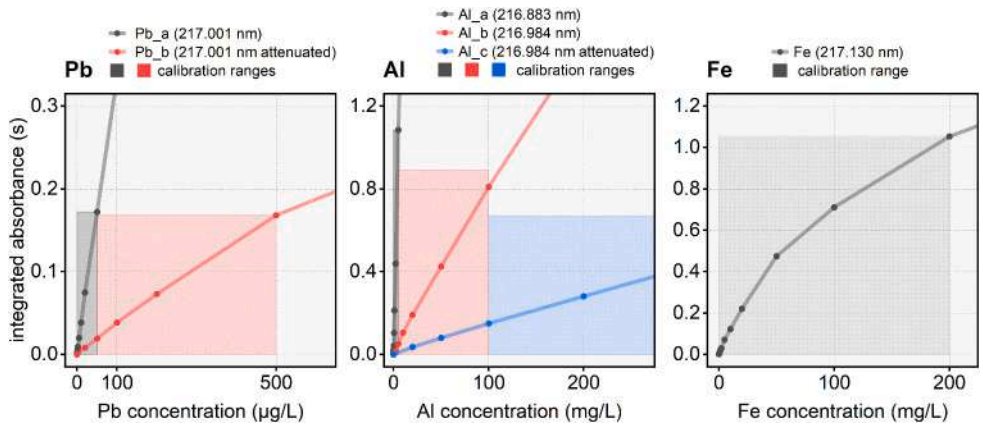

Fig. 4. Calibration plots for Pb, Al, and Fe. Aqueous calibration solutions matching the nitric acid content of the samples (3 mL concentrated HNO_3 in 10 mL final volume) were used to generate these plots using the proposed method. The individual calibration ranges are indicated.

Table 2
Analytical characteristics of the spectral lines investigated based on the detector pixels used and parameters of resulting calibration functions.

line (name)	wavelength (nm)	pixels	characteristic mass m_0 (ng)	LOD (µg/L)[a]	LOQ (µg/L)[a]	working range (µg/L)	calibration function	coefficient of determination R^2
Pb_a	217.001	100 + 101 + 102 (CP ± 1)	0.013	0.3	1	1–50	linear	0.9992
Pb_b	217.001	105 + 106 (attenuated[b])	0.13	4	13	13–500	linear	0.9978
Al_a	216.883	21 + 22 + 23 (CP ± 1)	0.2	6	20	20–5000	linear	0.9999
Al_b	216.984	91 + 92 + 93 (CP ± 1)	5.4	600	2000	2000–100,000	linear	0.9982
Al_c	216.984	89 + 95 (attenuated[b])	32	2000	7000	7000–500,000	linear	0.9992
Fe	217.130	191 + 192 + 193 (CP ± 1)	3–8	360	1200	1200–200,000	nonlinear rational	0.9989

[a] The limits of detection (LOD) and quantification (LOQ) were calculated as three and ten times the standard deviation of the blank solution (nitric acid diluted to the same extent as in the samples) measurement, divided by the slope of the calibration curve, respectively.
[b] attenuation of the signal involves using pixels further away from the peak maximum, measuring the absorbance at the wings of the analytical line.

software lacks the ability to automatically select the optimal line according to the linear ranges of the individual calibrations and the actual concentration of Al. To address this, a simple formula is applied during post-processing of the data in a spreadsheet application. This formula selects the line appropriate for the actual concentration, defined by the upper limits of the individual calibration ranges. The generalized formula is:

Al = IF (Al_a < 6000 µg/L THEN Al_a;
IF Al_b < 100,000 µg/L THEN Al_b;
ELSE Al_c)

In other words, the most sensitive line (Al_a) is chosen if its measured value falls within its calibration range (i.e., below 6000 µg/L). If Al_a exceeds its upper limit, the formula checks the less sensitive line (Al_b) for saturation (below 100,000 µg/L). If both Al_a and Al_b exceed their upper limits, the least sensitive line (Al_c) is chosen. This approach ensures that measurements stay within the reliable linear range of the chosen calibration curve.

Measuring Al concentrations as high as hundreds of milligrams per liter becomes possible and convenient using ETAAS. Although it may seem that aluminum concentrations higher than about 1 mg/L can be measured on flame AAS, such analysis requires a high-temperature acetylene/nitrous oxide flame not available in every laboratory equipped with AAS, and, more importantly, the information on its content is already accessible during Pb measurement with very little effort.

3.6. Iron

In contrast to Al, the calibration plot for Fe displayed significant nonlinearity across the tested concentration range. Linear dependence with an R^2 exceeding 0.995 was only observed up to 10 mg/L. Neither using side pixels nor the central pixel alone resulted in a better linearity. Therefore, a non-linear calibration described by a rational function $y = (a + bx)/(1 + cx)$ with a coefficient of determination of 0.9989 was employed (Table 2.)

Unusual behavior of Fe calibration plots for secondary Fe lines was already observed by Welz et al. [21], who reported a multi-slope response with distinct linear segments. However, a definitive conclusion regarding the presence or absence of these segments in our data might require a wider concentration range or additional investigation. Factors including the atomization temperature and instrumental parameters (e.g. instrument width $\Delta\lambda_{instr}$ which was 1.4 pm per pixel in this case) and atomic line properties such as width and hyperfine structure can influence the calibration plot shape [17,25–27]. Further investigation with a wider concentration range or exploration of different instrumental settings could provide more insights into this aspect.

3.7. Carry-over effects

Carry-over (memory effect) was assessed by measuring blank samples directly following the highest calibration standard (500 mg/L for Al and Fe, 500 µg/L for Pb). Our experiments exhibited minimal carryover for Al, Fe, and Pb. The first blank measurements showed memory effects of 1.5% for Al, 2.4% for Fe, and < 0.05% for Pb. The second blank measurement further reduced carryover to 0.5% for Al, 0.8% for Fe, and < 0.02% for Pb. If the samples to be analyzed are expected to vary

widely in concentrations, enabling "controlled cleaning" after high-concentration samples is recommended. Alternatively, prolonging the cleaning step might be considered.

3.8. Handling the spectral interferences

The spectral region around the Pb resonance line is significantly affected by absorption bands of phosphorus monoxide (PO) molecules, as shown in Fig. 5. These bands interfere with analytical lines, especially in samples with high levels of phosphorus. This interference was most pronounced in the samples of mushrooms, as it is known that they generally accumulate phosphorus in their bodies to a large extent [28]. To effectively minimize this interference, two complementary approaches were employed:

- The suppression of PO molecule formation by the addition of Pd/Mg $(NO_3)_2$ modifier
- The correction of the structured background using least square background correction (LSBC)

The behavior of P in a graphite furnace has been extensively studied with HR-CS AAS in the last few decades. According to current knowledge, the balance between the atomization of P and its vaporization in the form of PO molecules is highly dependent on the addition of a modifier. Modifiers based on Pd, but also other metals such as Ir, W, and Ru, proved to favor the formation of atomic P instead of PO vaporization [29–32]. The relative intensity of PO bands is also highly dependent on the temperature of the atomizer [31]. However, it was not possible to separate PO molecules in the time-resolved spectra because they form at temperatures similar to the atomization temperatures of the analytes. Fig. 5 shows the spectrum of a mushroom sample affected by strong interference. Dosing 10 µL of sample with 20 µL of a Pd/Mg$(NO_3)_2$ modifier reduced the interfering PO background by 50% compared to the addition of only 2 µL of the modifier. Little difference was observed between the addition of 2 and 5 µL and, similarly, between 15 and 20 µL. This indicates that the effective ratio between sample and modifier should be at least 1:1.5.

In most cases, the addition of 15 µL of the modifier suppressed PO interferences effectively. As an additional step for samples exhibiting exceptionally high phosphorus content, like the one presented in Fig. 5, LSBC was employed. In such cases, the residual structured background was eliminated by subtracting the reference spectrum of a pure phosphate (Fig. 5b) from the samples signal through LSBC using instrument's software. The result was a clear, interference-free spectrum (the black line in Fig. 5c).

3.9. Trueness assessment using CRMs

The contents of elements determined in CRMs using the method's novel multi-line approach for an extended working range are listed in Table 3. Each value is labeled according to the used line. The concentrations of all samples, including CRMs, were determined against standard solutions with an HNO_3 content matching that used for sample preparation.

For Pb, the determined contents in CRMs exhibited a slight negative bias compared to the certified values (bias ranging from −11 to −7%). This might be attributed to incomplete digestion of silicate matrices when hydrofluoric acid was omitted, resulting in a small non-dissolved residue. Conversely, digestion with a mixture of HNO_3 and HF led to a complete digestion with no observable residue. In this case, the bias for Pb, Al, and Fe improved, ranging from −5 to +7%, 8 to 12%, and − 4 to +5%, respectively.

However, even when HNO_3 alone was used, no significant difference was detected between the measured contents of the elements and their certified values according to Student's *t*-test at a 95% confidence interval. Therefore, the method demonstrated the capacity to provide true results for complex matrices, as evidenced by the good agreement between the measured and certified element contents in various CRMs.

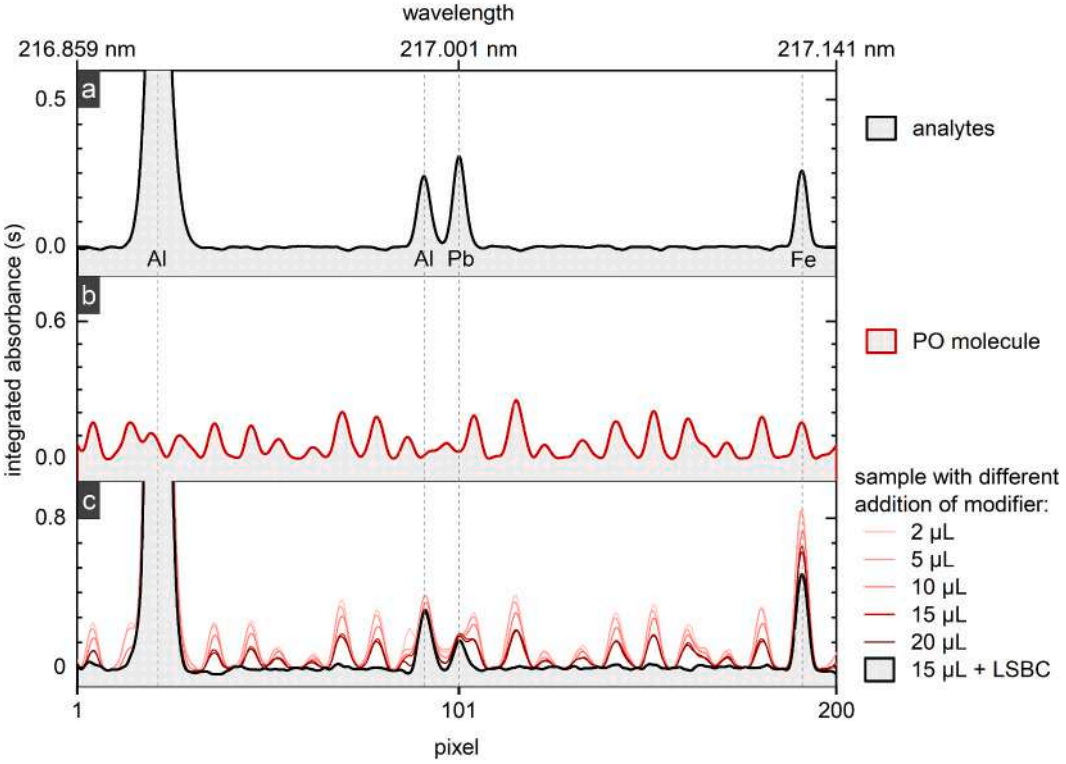

Fig. 5. Wavelength-resolved spectra obtained by measuring a) a simple solution of the analytes, b) ammonium phosphate solution (reference spectrum of PO molecules), and, c) a mushroom sample with strong interference arising from PO molecules, with different additions of Pd/Mg$(NO_3)_2$ modifier and correction using LSBC.

Table 3
Determined levels of Pb, Al, and Fe in certified reference materials. Values are expressed as mean ± standard deviation (mg/kg dry weight, $n = 3$) and bias (percentual difference between found and certified value).

element	value	reference material			
		BCR-482 Lichen	INCT-TL-1 Tea leaves	NIST 1570a Spinach leaves	AN-BM02 Green tea
Pb	certified	40.9 ± 1.4	1.78 ± 0.24	0.2[a]	1.54 ± 0.09
	HNO_3 digestion	37.9 ± 1.0[c] (−7%)	1.59 ± 0.2[b] (−11%)	0.19 ± 0.01[b] (−5%)	1.43 ± 0.1[b] (−7%)
	HNO_3/HF digestion	38.9 ± 3.5[c] (−5%)	1.80 ± 0.1[b] (1%)	0.21 ± 0.02[b] (7%)	1.51 ± 0.1[b] (−2%)
Al	certified	1103 ± 24	2290 ± 280	310 ± 15	1700 ± 60
	HNO_3 digestion	1060 ± 90[e] (−4%)	2160 ± 220[e] (−6%)	278 ± 14[d] (−10%)	1760 ± 100[e] (4%)
	HNO_3/HF digestion	1105 ± 69[e] (0%)	2288 ± 227[e] (0%)	323 ± 25[d] (4%)	1573 ± 135[e] (−8%)
Fe	certified	804±160[a]	432[a]	–	216 ± 15
	HNO_3 digestion	777 ± 32 (−3%)	479 ± 27 (11%)	245 ± 13	220 ± 21 (2%)
	HNO_3/HF digestion	799 ± 73 (2%)	414 ± 41 (−4%)	263 ± 14	227 ± 19 (5%)

[a] indicative values [b, c, d, e] determined using lines: b) Pb_a; c) Pb_b; d) Al_a; e) Al_b.

3.10. Pb, Al, and Fe in terrestrial Antarctic flora of Nelson Island

The contents of investigated elements in the samples of Antarctic flora are summarized in Fig. 6. In terms of Pb median contents in mg/kg, groups were sorted as follows: grass (0.34) > moss (0.28) > lichens (0.19) > mushrooms (0.13). The highest content of Pb was, however, observed in a sample of moss (1.5 mg/kg) and mosses as a group contained significantly more Pb than lichens and mushrooms (Mann-Whitney test, $p < 0.001$).

Whilst the Pb content in mosses is consistent with data from similar studies conducted in non-polluted areas across the Antarctic (Table 4), levels found in the lichens on Nelson Island are among the lowest ever reported in the Antarctic. Historically, the sampling area on Nelson Island has experienced very little local pollution, as there is only a small human presence due to the lack of large-scale research facilities. As a result, these values may indicate the relative background level in this region.

Lead contents in *U. antarctica* (median 0.199 mg Pb/kg) and *U. aurantiaco-atra* (median 0.183 mg Pb/kg) were statistically similar (according to Mann-Whitney test). The similarity of both lichen species in terms of metal accumulation patterns has already been observed [33]. The four samples of the lichen *Ramalina terebrata*, on the other hand, exhibited a median value of 0.086 mg Pb/kg, which is significantly less than the two *Usnea* species. *R. terebrata* was found only at a few sites adjacent to the sea, heavily exposed to sea spray.

Some of the first data on Pb in *U. antarctica* were reported back in 1991 from King George Island, South Shetland Islands. In the study, using the PIXE technique, the authors observed Pb levels in lichens growing in the vicinity of Arctowski Station to be as high as 12 mg/kg, while only 2 mg/kg were detected in areas further away from the station [34]. Although analytical methods have evolved substantially since these pioneer studies were published (e.g. recent studies have shown ICP-MS to be the analytical method of choice), recently published values have remained consistent. Levels of Pb reported for *U. aurantiaco-atra* growing in the vicinity of the nearby Korean research station at King George Island were up to 8.36 mg/kg (even 13 mg/kg observed in a single thalli), while lichens growing at least 1 km from the station contained only ca. 1 mg/kg, indicating local anthropogenic pollution [35].

A recent study at background sites on King George Island reported Pb contents in the lichens *U. aurantiaco-atra* and *U. antarctica* of 0.51 ± 0.25 and 0.27 ± 0.11 mg/kg (mean ± SD), respectively, which are only slightly higher than our means for the same lichens (0.23 ± 0.1 and 0.24 ± 0.1 mg/kg, respectively). The study reported Pb contents in *Deschampsia antarctica* grass of 0.79 ± 0.47 mg/kg, exceeding our mean value of 0.43 ± 0.4 mg/kg. However, the limited number of samples analyzed in that study (2 and 3 samples of the respective lichens and 3 samples of grass), limits the representativeness of its findings.

In contrast to the gradually expanding knowledge on the elemental composition of cryptogams at various sites across the Antarctic, little data has been reported on the composition of Antarctic mushrooms. Although there is a sparsity of macrofungi in the Antarctic, observations on them have been steadily increasing in recent decades [36]. It is also expected that increasing temperatures together with more intense human activity will allow further colonization of the Antarctic by more fungal populations [37,38]. However, no data is yet available on their elemental composition. Similarly, only very limited data is available on the elemental composition of vascular plants, with the hair grass *Deschampsia antarctica* being one of only two native species [38–41]. Such a scarcity of comparative values makes it difficult to assess the current burden on the Antarctic ecosystem.

Regarding the Al and Fe contents in the samples, both elements correlated tightly (Pearson's $r = 0.97$, $p < 0.001$). Such strong correlation between Al and Fe, along with other lithophile elements, has been documented in some previous studies (e.g. [35,42,43] listed in Table 4). This finding aligns with the fact that both elements are non-mobile, originating mainly from local bedrock weathering instead of human

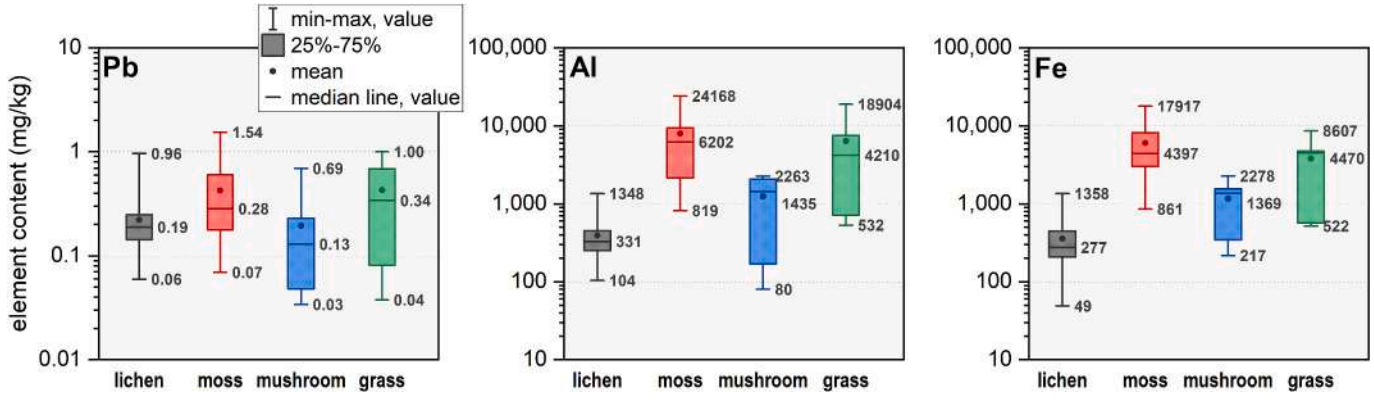

Fig. 6. Boxplots summarizing the contents of Pb, Al, and Fe in lichens, mosses, mushrooms, and grass (mg/kg dry weight). Median, minimum, and maximum values are given (note the logarithmic scale).

Table 4
Selected references for the studied elements across the Antarctic (expressed on a dry mass basis, chronological order).

Study site	Plant material	Pb (mg/kg)	Al (mg/kg)	Fe (mg/kg)	Analytical method	Reference
King George Island, South Shetland Islands	lichens *U. antarctica*	2–12	–	170–414	PIXE	[34]
25 de Mayo Island, South Shetland Islands	lichens (*U. antarctica* and U. aurantiaco-atra)	<LOD–2.76	–	263–1365	FAAS	[33]
Edmonson point, Victoria Land	moss (*Pottia heimii, B. argenteum, B. pseudo-triquetrum and Ceratodon purpureus*)	0.3–1.4	1700–3700	3500–7100	ETAAS, ICP-OES	[44]
King George Island, South Shetland Islands	lichen (*Usnea* spp.)	–	–	139	FAAS	[40]
	moss (*Bryum* spp. and *Polytrichum* spp.)	–	–	3040–4348		
	grass (*Deshampsia antarctica*)	–	–	610		
King George Island, South Shetland Islands	lichens (*U. aurantiaco-atra*)	0.77–8.36	182–426	273–490	ICP-MS	[35]
King George Island, South Shetland Islands	lichens (various species)	ca. 0.4 [a]	–	ca. 550 [a]	FAAS, ETAAS	[45]
	moss (various species)	ca. 2.8 [a]	–	ca. 3750 [a]		
	grass (*D. antarctica* and *C. quitensis*)	ca. 2.4 [a]	–	ca. 2600 [a]		
James Ross Island, Brandy Bay, the northern Antarctic Peninsula	lichens (*U. antarctica*)	0.9–3	1800–6400	–	ICP-MS	[42]
Terra Nova Bay	moss (unspecified)	0.12–1.4	–	2480–13,400	ICP-MS, ICP-OES	[46]
James Ross Island, Solorina Valley, the northern Antarctic Peninsula	lichens (*U. antarctica*)	0.99–2.51	–	–	ETAAS	[5]
Larseman Hills, East Antarctica	lichens (foliose *Umbilicaria* sp. and crustose *Buellia* sp.	0.28–1.9	400–10,800	300–18,700	ICP-MS, ICP-OES	[43]
	moss (different genera)	0.65–1.49	1800–11,600	2900–13,800		
King George Island, South Shetland Islands	lichens: a) *U. aurantiaco-atra,* b) *U. antarctica*	a) 0.51 ± 0.25 b) 0.27 ± 0.11	a) 373 ± 191 b) 630 ± 355	a) 395 ± 226 b) 739 ± 500	ICP-MS	[41]
	Moss (*Ceratodon purpureus, Politrichastrum alpinum, Schistidium antarctici*)	0.41–0.84	2903–10,310	2140–8165		
	Grass (*D. antarctica*)	0.79 ± 0.47	8625 ± 7174	9618 ± 7818		
Nelson Island, South Shetland Islands	lichens	0.06–0.96	104–1348	49–1358	HR-CS ETAAS	this study
	moss	0.07–1.54	819–24,168	861–17,917		
	mushroom	0.03–0.69	80–2263	217–2278		
	grass	0.04–1.00	532–18,904	522–8607		

[a] the values were retrieved from the graph.

activities, and thus, they both often serve as reference elements for, for example, enrichment factor calculations in ecological studies. Both elements were least abundant in the lichen samples, indicating low contents of captured mineral particles such as soil and dust in the thalli. Their highest content, in contrast, was observed in moss, likely due to its complex three-dimensional structure, which is prone to entrapping dust and soil particles. This is consistent with studies which analyzed both fruticose lichens and mosses (i.e. [40,41]), and also apparent from comparison with other reported data listed in Table 4. This highlights the significance of proper sample cleaning procedures to differentiate between element uptake by the organism and captured exogenous material accumulated on the upper surface of the thallus. Most listed studies (including this one) removed excess soil particles using tweezers and/or washing with deionized water. Nevertheless, according to the presence of undissolved residue in some digests of moss and grass, even a careful cleaning procedure may not be sufficient to remove all mineral particles. Thus, also in the grass, the Al and Fe contents displayed a wide range, similar to the values recently reported from King George Island [41]. Similarly, within the grass samples, both elements exhibited a strong positive correlation (Pearson's correlation coefficient = 0.95, *p*-value <0.05). This finding may suggest a similar uptake mechanism, despite the known differences in mineral acquisition strategy among these organisms. Lichens and mosses primarily rely on passive methods like surface absorption and dust capture, while grasses have a well-developed root system for active nutrient uptake. Mushrooms often benefit from mycorrhizal associations with plant roots. However, the current lack of data on the elemental composition of Antarctic mushrooms hinders a comprehensive understanding of the element accumulation patterns in these representatives of Antarctic flora and their potential as biomonitors of environmental conditions.

3.11. Enrichment of Pb in the flora

To evaluate the enrichment of Pb in the samples, the enrichment factor for Pb (EF_{Pb}) was calculated according to the method described by [47]. The formula is $EF_{Pb} = (c_{Pb}/c_{Al})_{sample}/(c_{Pb}/c_{Al})_{background}$, where c_{Pb} represents the content of Pb and c_{Al} represents the content of the reference element in the sample and in the background. Both Al and Fe are commonly used as reference elements for normalizing pollutant contents and enrichment. As the contents of the two metals correlated closely, so did the corresponding enrichment factors calculated on the basis of either Al or Fe as the reference elements (Pearson correlation coefficient 0.9 with p-value <0.05). Eventually, Al was chosen, as it has often been suggested as a suitable reference element in studying cryptogams such as lichens and mosses [47–49]. As its background level, the average concentration in the Earth's crust was obtained from the work of Yaroshevsky [50].

The medians of EF_{Pb} were as follows: lichens 2.8 > mushrooms 0.5 > grass 0.4 > moss 0.3.

According to EF categories, lichens exhibited only minor enrichment while mushrooms, grass and moss exhibited no enrichment [49]. It is important to acknowledge the limitations of EFs, with one of the most significant being the difficulty of completely removing trapped mineral particles from samples. As a consequence, the presence of more soil or dust particles in the samples tends to decrease EF values [51]. This is probably the reason for the lower EF_{Pb} observed for mosses than for lichens.

Despite their limitations, EFs for Pb still provide some valuable insights: given the relative ease of obtaining clean lichen together with their ability to accumulate airborne contaminants, lichens present a suitable material for bioindicative purposes, owing to their relatively

high and consistent Pb–Al ratio, particularly evident for the dominant lichen species, *U. antarctica* and *U. aurantiaco-atr*a.

4. Conclusion

We present here a novel analytical method based on HR-CS ETAAS suitable for assessing the Pb contamination of plant material. The co-determination of Al and Fe as reference elements allows for the calculation of ecological risk indices. The method utilizes the highly-sensitive resonance Pb line at 217.001 nm, ensuring detection of the typically trace levels of this contaminant in environmental samples. Importantly, it also achieves a wide working range (e.g., four orders of magnitude for Al), eliminating the need for sample re-dilution and re-measurement for environmental samples with varying metal contents. Broadening of the working range was achieved by combining the use of spectral lines with different sensitivities and also by measuring absorbance at multiple points within each spectral line. This is a significant advantage considering the traditionally limited dynamic range of AAS compared to techniques like ICP-MS or ICP-OES. While developed for the analysis of Antarctic terrestrial flora, the method is generally applicable to environmental research studies involving various sample types.

Using the method, a large set of Antarctic floral samples, including lichens, mosses, mushrooms, and grass, was analyzed. In fact, the achieved working range proved necessary for analyzing these diverse samples without dilution steps. This also translates into less time required for operator intervention during analysis. According to the results, relatively low Pb contamination of the Nelson Island ecosystem was observed compared to data reported from the region. On the basis of enrichment factors, the analyzed fruticose lichens such as *U. antarctica* and *U. aurantiaco-atra* provide the most relevant information on the degree of contamination. In contrast, the other popular bioindicators, mosses, appear to be more influenced by trapped dust due to their structure. Apart from lichens and mosses, samples of substantially less-studied Antarctic mushrooms and grass were also subjected to the same analysis. In fact, the analysis of mushrooms presented the most significant challenge due to interference arising from their high phosphorus contents. However, using a combination of an excess of modifier and the LSBC model, the interference was suppressed, allowing data on Pb contents in these species to be reported for the first time.

Advanced methods, such as the one presented here, not only broaden the variety of routine techniques applicable for specific purposes, but also emphasize the demand for HR-CS AAS to develop into a truly multi-elemental technique. The successful application of multiple spectral lines for single element calibration demonstrates a promising approach for extending the dynamic range of both existing and also future AAS instruments that will be capable of wider spectral region monitoring.

CRediT authorship contribution statement

Ondřej Zvěřina: Writing – original draft, Visualization, Supervision, Investigation, Formal analysis, Data curation, Conceptualization. **Lenka Brůhová:** Investigation. **Pavel Coufalík:** Writing – original draft, Methodology, Investigation. **Christopher D. Stringer:** Writing – original draft, Investigation. **Jaqueline Rieger:** Investigation. **Walter Goessler:** Writing – original draft, Supervision.

Declaration of competing interest

The authors declare that they have no known competing financial interests or personal relationships that could have appeared to influence the work reported in this paper.

Data availability

Data will be made available on request.

Acknowledgement

This work was supported by funding from AKTION Austria–Czech Republic, project 96p6. The authors are also grateful for the support of Masaryk University (projects MUNI/A/2022/1366 and MUNI/A/1623/2023). The involvement of PC was funded by the Institute of Analytical Chemistry of the CAS under the Institutional Research Plan RVO: 68081715. CDS was in receipt of a PhD studentship from the Leeds-York-Hull Natural Environment Research Council (NERC) Doctoral Training Partnership (DTP) Panorama [NE/S007458/1]. Fieldwork was supported by the Czech Antarctic Foundation.

References

[1] R. Bargagli, Environmental contamination in Antarctic ecosystems, Sci. Total Environ. 400 (2008) 212–226.
[2] J.R. McConnell, O.J. Maselli, M. Sigl, P. Vallelonga, T. Neumann, H. Anschütz, R. C. Bales, M.A.J. Curran, S.B. Das, R. Edwards, S. Kipfstuhl, L. Layman, E. R. Thomas, Antarctic-wide array of high-resolution ice core records reveals pervasive lead pollution began in 1889 and persists today, Sci. Rep. 4 (2014) 5848.
[3] W.-L. Chu, N.-L. Dang, Y.-Y. Kok, K.-S. Ivan Yap, S.-M. Phang, P. Convey, Heavy metal pollution in Antarctica and its potential impacts on algae, Polar Sci. 20 (2019) 75–83.
[4] R. Bargagli, E. Rota, Environmental contamination and climate change in Antarctic ecosystems: an updated overview, environmental science, Advances 3 (2024) 543–560.
[5] O. Zvěřina, P. Coufalík, M. Barták, M. Petrov, J. Komárek, The contents and distributions of cadmium, mercury, and lead in Usnea antarctica lichens from Solorina Valley, James Ross island (Antarctica), Environ. Monit. Assess. 190 (2018), https://doi.org/10.1007/s10661-017-6397-1.
[6] M. Hossain, D. Karmakar, S.N. Begum, S.Y. Ali, P.K. Patra, Recent trends in the analysis of trace elements in the field of environmental research: a review, Microchem. J. 165 (2021) 106086.
[7] N. Ozbek, Simultaneous determination of co, Fe, Ni and K with HR CS GFAAS, Microchem. J. 145 (2019) 1066–1069.
[8] M. Resano, E. Bolea-Fernández, E. Mozas, M.R. Flórez, P. Grinberg, R.E. Sturgeon, Simultaneous determination of co, Fe, Ni and Pb in carbon nanotubes by means of solid sampling high-resolution continuum source graphite furnace atomic absorption spectrometry, J. Anal. At. Spectrom. 28 (2013) 657–665.
[9] F. Rovasi Adolfo, P. Cícero do Nascimento, L. Brudi, D. Bohrer, L. Machado de Carvalho, Simultaneous determination of Ba, Co, Fe, and Ni in nuts by high-resolution continuum source atomic absorption spectrometry after extraction induced by solid-oil-water emulsion breaking, Food Chem. 345 (2021) 128766.
[10] I.N. Pasias, N.I. Rousis, A.K. Psoma, N.S. Thomaidis, Simultaneous or sequential multi-element graphite furnace atomic absorption spectrometry techniques: advances within the last 20 years, At. Spectrosc. 42 (6) (2021), https://doi.org/10.46770/AS.202.707.
[11] M. Resano, L. Rello, M. Flórez, M.A. Belarra, On the possibilities of high-resolution continuum source graphite furnace atomic absorption spectrometry for the simultaneous or sequential monitoring of multiple atomic lines, Spectrochim. Acta part B, At. Spectrosc. 66 (2011) 321–328.
[12] M. Resano, M.R. Flórez, E. García-Ruiz, High-resolution continuum source atomic absorption spectrometry for the simultaneous or sequential monitoring of multiple lines. A critical review of current possibilities, Spectrochim. Acta part B, At. Spectrosc. 88 (2013) 85–97.
[13] A.C.M. Aleluia, F.A. de Santana, G.C. Brandao, S.L.C. Ferreira, Sequential determination of cadmium and lead in organic pharmaceutical formulations using high-resolution continuum source graphite furnace atomic absorption spectrometry, Microchem. J. 130 (2017) 157–161.
[14] J.S. Almeida, O.C.C.O. Souza, L.S.G. Teixeira, Determination of Pb, cu and Fe in ethanol fuel samples by high-resolution continuum source electrothermal atomic absorption spectrometry by exploring a combination of sequential and simultaneous strategies, Microchem. J. 137 (2018) 22–26.
[15] G. Schlemmer, B. Radziuk, B. Verlag, O.G. Schlemmer, O.B. Radziuk, Analytical Graphite Furnace Atomic Absorption Spectrometry a Laboratory Guide, Birkhäuser Verlag, 1999.
[16] B. Gómez-Nieto, M.J. Gismera, M.T. Sevilla, J.R. Procopio, Fast sequential multi-element determination of major and minor elements in environmental samples and drinking waters by high-resolution continuum source flame atomic absorption spectrometry, Anal. Chim. Acta 854 (2015) 13–19.
[17] U. Heitmann, B. Welz, D.L.G. Borges, F.G. Lepri, Feasibility of peak volume, side pixel and multiple peak registration in high-resolution continuum source atomic absorption spectrometry, Spectrochim, Acta part B At. Spectrosc. 62 (2007) 1222–1230.
[18] L. Fernández-López, B. Gómez-Nieto, M.J. Gismera, M.T. Sevilla, J.R. Procopio, Direct determination of copper and zinc in alcoholic and non-alcoholic drinks using high-resolution continuum source flame atomic absorption spectrometry and internal standardization, Spectrochim. Acta part B, At. Spectrosc. 147 (2018) 21–27.
[19] S. Hesse, T. Ristau, J.W. Einax, Chemical vapor generation by coupling high-pressure liquid flow injection to high-resolution continuum source hydride

generation atomic absorption spectrometry for determination of arsenic, Microchem. J. 123 (2015) 42–50.
[20] M.A. Bechlin, F.M. Fortunato, R.M. da Silva, E.C. Ferreira, J.A. Gomes Neto, A simple and fast method for assessment of the nitrogen–phosphorus–potassium rating of fertilizers using high-resolution continuum source atomic and molecular absorption spectrometry, Spectrochim, Acta part B At. Spectrosc. 101 (2014) 240–244.
[21] B. Welz, L.M.G. dos Santos, R.G.O. Araujo, S.C. do Jacob, M.G.R. Vale, M. Okruss, H. Becker-Ross, Unusual calibration curves observed for iron using high-resolution continuum source graphite furnace atomic absorption spectrometry, Spectrochim, Acta part B At. Spectrosc. 65 (2010) 258–262.
[22] O. Zvěřina, J. Kuta, P. Coufalík, P. Kosečková, J. Komárek, Simultaneous determination of cadmium and iron in different kinds of cereal flakes using high-resolution continuum source atomic absorption spectrometry, Food Chem. 298 (2019) 125084.
[23] L.M.G. dos Santos, B. Welz, R.G.O. Araujo, S. do C. Jacob, M.G.R. Vale, A. Martens, I.B. Gonzaga Martens, H. Becker-Ross, Simultaneous determination of cd and Fe in beans and soil of different regions of Brazil using high-resolution continuum source graphite furnace atomic absorption spectrometry and direct solid sampling, J. Agric. Food Chem. 57 (2009) 10089–10094.
[24] M. Resano, E. García-Ruiz, High-resolution continuum source graphite furnace atomic absorption spectrometry: is it as good as it sounds? A critical review, Anal. Bioanal. Chem. 399 (2011) 323–330, https://doi.org/10.1007/s00216-010-4105-x.
[25] D.N. Wichems, R.E. Fields, J.M. Harnly, Characterization of hyperbolic calibration curves for continuum source atomic absorption spectrometry with array detection, J. Anal. At. Spectrom. 13 (1998) 1277–1284.
[26] B. Welz, H. Becker-Ross, S. Florek, U. Heitmann, High-Resolution Continuum Source AAS: The Better Way to Do Atomic Absorption Spectrometry, John Wiley & Sons, Weinheim; [Great Britain], 2005.
[27] Z. Kowalewska, J. Pilarczyk, Ł. Gościniak, Spectral aspects of the determination of Si in organic and aqueous solutions using high-resolution continuum source or line source flame atomic absorption spectrometry, Spectrochim, Acta part B At. Spectrosc. 120 (2016) 45–56.
[28] P. Kalač, Chemical composition and nutritional value of European species of wild growing mushrooms: a review, Food Chem. 113 (2009) 9–16.
[29] F.G. Lepri, M.B. Dessuy, M.G.R. Vale, D.L.G. Borges, B. Welz, U. Heitmann, Investigation of chemical modifiers for phosphorus in a graphite furnace using high-resolution continuum source atomic absorption spectrometry, Spectrochim, Acta part B At. Spectrosc. 61 (2006) 934–944.
[30] L.C. Pomarolli, M.A.M.S. da Veiga, M. Resano, F.V. Nakadi, Understanding polyatomic interference in the determination of phosphorus via PO molecules using high-resolution continuum source graphite furnace molecular absorption spectrometry with direct solid analysis, J. Anal. At. Spectrom. 35 (2020) 2305–2314.
[31] M. Resano, J. Briceño, M.A. Belarra, Direct determination of phosphorus in biological samples using a solid sampling-high resolution-continuum source electrothermal spectrometer: comparison of atomic and molecular absorption spectrometry, J. Anal. At. Spectrom. 24 (2009) 1343.
[32] R.C. de Campos, C.L.T. Correia, F. Vieira, T.D. Saint'Pierre, A.C. Oliveira, R. Gonçalves, Direct determination of P in biodiesel by high-resolution continuum source graphite furnace atomic absorption spectrometry, Spectrochim. Acta part B, At. Spectrosc. 66 (2011) 352–355.
[33] A. Poblet, S. Andrade, M. Scagliola, C. Vodopivez, A. Curtosi, A. Pucci, J. Marcovecchio, The use of epilithic Antarctic lichens (Usnea aurantiacoatra and U. Antartica) to determine deposition patterns of heavy metals in the Shetland Islands, Antarctica, Sci. Total Environ. 207 (1997) 187–194.
[34] M. Olech, Preliminary observations on the content of heavy metals in thalli of Usnea antarctica Du Rietz (Lichenes) in the vicinity of the H Arctowski, Polish Antarctic Station, Polish Polar Reports 12 (1991) 129–131.
[35] H.S. Lim, M.J. Han, D.C. Seo, J.H. Kim, J.I. Lee, H. Park, J.-S. Hur, Y.H. Cheong, J. S. Heo, H.I. Yoon, J.-S. Cho, Heavy metal concentrations in the fruticose lichen usnea aurantiacoatra from King George Island, South Shetland Islands, West Antarctica, Hanguk Ungyong Saengmyong Hwahakhoe Chi 52 (2009) 503–508.
[36] G. Palfner, J. Binimelis-Salazar, S.T. Alarcón, G. Torres-Mellado, G. Gallegos, F. Pea-Cortés, A. Casanova-Katny, Do new records of macrofungi indicate warming of their habitats in terrestrial Antarctic ecosystems? Czech Polar Rep. 10 (2020) 281–296.
[37] P.D. Bridge, B.M. Spooner, Non-lichenized Antarctic fungi: transient visitors or members of a cryptic ecosystem? Fungal Ecol. 5 (2012) 381–394.
[38] J. Singh, R.P. Singh, R. Khare, Influence of climate change on Antarctic flora, Polar Sci. 18 (2018) 94–101.
[39] J. Tapia, M. Molina-Montenegro, C. Sandoval, N. Rivas, J. Espinoza, S. Basualto, P. Fierro, L. Vargas-Chacoff, Human activity in Antarctica: effects on metallic trace elements (MTEs) in plants and soils, Plants 10 (2021), https://doi.org/10.3390/plants10122593.
[40] I.R. dos Santos, E.V. Silva-Filho, C. Schaefer, S. Maria Sella, C.A. Silva, V. Gomes, M.J.A.C.R. de Passos, P. Van Ngan, Baseline mercury and zinc concentrations in terrestrial and coastal organisms of Admiralty Bay, Antarctica, Environ. Pollut. 140 (2006) 304–311.
[41] A.R. Reindl, L. Wolska, A.I. Piotrowicz-Cieślak, D. Saniewska, J. Bołałek, M. Saniewski, The impact of global climate changes on trace and rare earth elements mobilization in emerging periglacial terrains: insights from western shore of Admiralty Bay (King George Island, Antarctic), Sci. Total Environ. 926 (2024) 171540.
[42] O. Zvěřina, K. Láska, R. Červenka, J. Kuta, P. Coufalík, J. Komárek, Analysis of mercury and other heavy metals accumulated in lichen Usnea antarctica from James Ross island, Antarctica, Environ. Monit. Assess. 186 (2014) 9089–9100.
[43] S. Bhakta, T.K. Rout, D. Karmakar, C. Pawar, P.K. Padhy, Trace elements and their potential risk assessment on polar ecosystem of Larsemann Hills, East Antarctica, Polar Sci. 31 (2022) 100788.
[44] R. Bargagli, J.C. Sanchez-Hernandez, L. Martella, F. Monaci, Mercury, cadmium and lead accumulation in Antarctic mosses growing along nutrient and moisture gradients, Polar Biol. 19 (1998) 316–322.
[45] B. Wojtuń, K. Kolon, A. Samecka-Cymerman, M. Jasion, A.J. Kempers, A survey of metal concentrations in higher plants, mosses, and lichens collected on King George Island in 1988, Polar Biol. 36 (2013) 913–918.
[46] I. Zelano, M. Malandrino, A. Giacomino, S. Buoso, E. Conca, Y. Sivry, M. Benedetti, O. Abollino, Element variability in lacustrine systems of Terra Nova Bay (Antarctica) and concentration evolution in surface waters, Chemosphere 180 (2017) 343–355.
[47] R. Bargagli, The elemental composition of vegetation and the possible incidence of soil contamination of samples, Sci. Total Environ. 176 (1995) 121–128.
[48] L. Gandois, Y. Agnan, S. Leblond, N. Séjalon-Delmas, G. Le Roux, A. Probst, Use of geochemical signatures, including rare earth elements, in mosses and lichens to assess spatial integration and the influence of forest environment, Atmos. Environ. 95 (2014) 96–104.
[49] M. Aničić Urošević, G. Vuković, P. Vasić, T. Jakšić, D. Nikolić, S. Škrivanj, A. Popović, Environmental implication indices from elemental characterisations of collocated topsoil and moss samples, Ecol. Indic. 90 (2018) 529–539.
[50] A.A. Yaroshevsky, Abundances of chemical elements in the Earth's crust, Geochem. Int. 44 (2006) 48–55.
[51] C. Reimann, P. de Caritat, Intrinsic flaws of element enrichment factors (EFs) in environmental geochemistry, Environ. Sci. Technol. 34 (2000) 5084–5091.

Environ Monit Assess (2024) 196:43
https://doi.org/10.1007/s10661-023-12224-3

RESEARCH

Toxic metals in cyanobacterial mat of Big Lachman Lake, James Ross Island, Antarctica

Pavel Coufalík · Martin Vašinka · Lukáš Krmíček · Radek Ševčík · Ondřej Zvěřina · Lenka Brůhová · Josef Komárek

Received: 6 September 2023 / Accepted: 7 December 2023 / Published online: 16 December 2023

Abstract The northern part of James Ross Island is the largest deglaciated area in the Antarctic Peninsula region with a unique ecosystem created during the Late Glacial. This research aims to evaluate the degree of contamination of the locality with toxic metals (As, Hg, Cd, and Pb) through bioindicators in the aquatic environment—colonies of cyanobacteria and algae. For this purpose, bottom lake sediments of Big Lachman Lake were studied for contents of Fe, As, Hg, Cd, Pb, Cr, Co, Ni, Cu, and Zn, as well as samples of cyanobacterial mat, in which Fe, As, Hg, Cd, and Pb were determined. Metal contents were determined by means of inductively coupled plasma optical emission spectrometry and atomic absorption spectrometry. The contents of metals in sediments did not differ from the usual values in the area of the Antarctic Peninsula. The bioaccumulation of metals in cyanobacterial mat was evaluated by calculating enrichment factors (the calculation to Fe as a reference element). According to this method, moderate pollution of Big Lachman Lake was confirmed for Hg and Cd.

Keywords Heavy metal contamination · Lake · Sediment · Cyanobacterium · Antarctic Peninsula · Antarctica

Highlights
- Cyanobacterial mats and lake sediments of James Ross Island were analyzed.
- Hg and Cd bioaccumulate in benthic cyanobacterial mats of Big Lachman Lake.
- Moderate pollution of the lake with Hg and Cd was indicated by enrichment factors.

P. Coufalík (✉)
Institute of Analytical Chemistry of the Czech Academy of Sciences, Veveří 97, 60200 Brno, Czech Republic
e-mail: coufalik@iach.cz

M. Vašinka
Agrovyzkum Rapotin Ltd., Výzkumníků 267, 788 13 Vikýřovice, Czech Republic

L. Krmíček
Institute of Geology of the Czech Academy of Sciences, Rozvojová 269, 165 02 Prague 6, Czech Republic

L. Krmíček
Institute of Geotechnics, Faculty of Civil Engineering, Brno University of Technology, Veveří 95, 602 00 Brno, Czech Republic

R. Ševčík
Institute of Theoretical and Applied Mechanics of the Czech Academy of Sciences, Centre Telč, Prosecká 809/76, 190 00 Prague 9, Czech Republic

O. Zvěřina
Department of Public Health, Faculty of Medicine, Masaryk University, Kamenice 5, 62500 Brno, Czech Republic

L. Brůhová · J. Komárek
Department of Chemistry, Faculty of Science, Masaryk University, Kotlářská 2, 61137 Brno, Czech Republic

Introduction

The input of contaminants from southern hemisphere countries into the Antarctic region (Bargagli, 2005, 2008) is largely limited by the Antarctic Circumpolar Current and the circumpolar cyclonic vortex. However, the transport of persistent organic pollutants and metals does occur (Szopińska et al., 2019; Szumińska et al., 2018), which is obvious in the high concentrations of Hg and Cd found in marine organisms (Bargagli, 2008). Hg and Pb also reach Antarctica by long-range transport in the atmosphere (Cortizas et al., 2014; Santos et al., 2005; Wang et al., 2023). Elemental mercury (the main Hg form in the atmosphere) accumulates in the polar regions, which serves as "cold traps" (Bargagli, 2005), through repeated evaporation and condensation known as the "grasshopper effect" (Szumińska et al., 2018). An increase in Pb concentrations in Antarctica is related to anthropogenic emissions from industry and the use of leaded gasoline (Yin et al., 2006). The enrichment of Cr, Cu, Ni, Pb, and V in aerosol samples relative to both bedrock and seawater was observed in the Antarctic Peninsula (Bargagli, 2008). Higher concentrations of As, Cd, and Zn have been determined in Antarctic snow and ice, which probably result from non-ferrous metal smelting in South America, Southern Africa, and Australia (Pacyna & Pacyna, 2001; Szumińska et al., 2018; Yin et al., 2006). Except for long-range transported pollutants (such as the already mentioned metals or persistent organic substances), anthropogenic contamination is generally linked to local human activity (Bargagli, 2005; Cortizas et al., 2014; Nędzarek et al., 2014; Potapowicz et al., 2020; Ribeiro et al., 2011). Extreme concentrations of toxic metals have been found in soils heavily contaminated by anthropogenic activity around polar stations in the Antarctic Peninsula (Guerra et al., 2011). Lake sediments represent a historical archive of the development of atmospheric metal concentrations (Bargagli, 2005). In depth profiles of lake sediment from Nelson Island (South Shetland Islands), anthropogenic Pb contamination has been observed since the beginning of the industrial revolution (Yin et al., 2006). Nevertheless, determination of the contents of organic pollutants, trace metals, and fly ash particles in Antarctic lake sediments indicate much less contamination of the south polar region compared to the northern hemisphere (Cortizas et al., 2014). The determination of metals in depth profiles of lake sediment from Livingston Island (South Shetland Islands) did not show elevated Pb, Cu, or Zn contents that would be of anthropogenic origin (Cortizas et al., 2014).

The environments of freshwater lakes, surface streams, and wetlands are abundantly populated by colonies of cyanobacteria and algae, which form an important biotic component of the Antarctic ecosystem (Bargagli, 2005). Thus, cyanobacterial mats are varied communities, which are vertically stratified, with morphology, structure, and color given by the composition of phototrophic organisms, and also by incorporated inorganic material. In general, cyanobacteria interact with metals by adsorption and absorption and metabolize them; they can also change their ligands, thus, their toxicity (Webster-Brown & Webster, 2007). The question is to what extent a possible bioaccumulation of metals in cyanobacterial mat is determined by abiotic processes and to what extent by their physiological activity. However, active metabolism of trace metals in cyanobacteria can be observed by preferential trace metal enrichment (Webster-Brown & Webster, 2007). The monitoring of these cyanobacterial mats as bioindicators is much more advantageous than the sampling of snow or aerosol, due to the extreme variability of the dry and wet deposition of pollutants in time and space (Bargagli, 2005), and the extremely low concentrations of metals in Antarctic snow (Szumińska et al., 2021).

James Ross Island (JRI) has, for many decades, been the object of study of Czech polar expeditions to the Johann Gregor Mendel Czech Antarctic Station. According to our research so far, there is an increased deposition of mercury from the atmosphere. Does this effect also occur with other metals? How is it possible to observe atmospheric deposition of metals at such low concentration levels in snowfall? Is the use of biomonitors suitable for these purposes? In which parts of the ecosystem can contamination be observed? These questions led us to carry out this study, which should make this topic more visible. This study aimed to determine the extent of the contamination of this area by toxic metals through the use of bioindicators such as colonies of microorganisms in shallow coastal lakes, and lake sediment samples. The problem of contamination from remote areas should be at the center of research for polar stations in the Antarctic Peninsula region.

Materials and methods

Locality and collection of samples

James Ross Island (64°10′S, 57°45′W), situated on the east side of the Antarctic Peninsula, is the largest island in the Weddell Sea (Fig. 1). The bedrock consists mostly of local (James Ross Island Volcanic Group) basalts (typically 90–95%); the rest is formed by Cretaceous sandstones, siltstones, shales, and conglomerates (Košler et al., 2009; Nývlt et al., 2011; Vašinka et al., 2020). The Ulu Peninsula (JRI) has been permanently deglaciated since ice sheet retreat during the Late Glacial (Nedbalová et al., 2013; Nývlt et al., 2011). The northern part of the Ulu Peninsula and Cape Lachman is formed by the Mendel Formation—a Late Miocene (5.9–5.4 Ma) sedimentary sequence (Nývlt et al., 2011), which also forms the bedrock of the studied lakes. The limnology, physical, and chemical characteristics of the Big Lachman Lake were described by Nedbalová et al. (2013). A detailed description of this locality is given, for example, in Vašinka et al. (2020). The area of shallow coastal lakes on Cape Lachman as well as a large part of the area covering the Mendel Formation are covered by shallow wetlands fed by water from melting snow, which are the habitat of numerous colonies of cyanobacteria and algae (Coufalík et al., 2016; Skácelová et al., 2013). The high water temperature and high nutrient content in Big Lachman Lake (Coufalík et al., 2016; Nedbalová et al., 2013) are the main factors in the development of cyanobacterial mat after the beginning of the polar spring.

Two depth profiles of bottom lake sediments were collected in the area covering the Mendel Formation—from the Big Lachman Lake (63°47′50.6″S, 57°48′30.7″W) and the temporary unnamed lake (63°48′31.4″S, 57°52′33.1″W). Sediment profiles were collected using a polypropylene (PP) sediment probe. The sediment profile from Big Lachman Lake

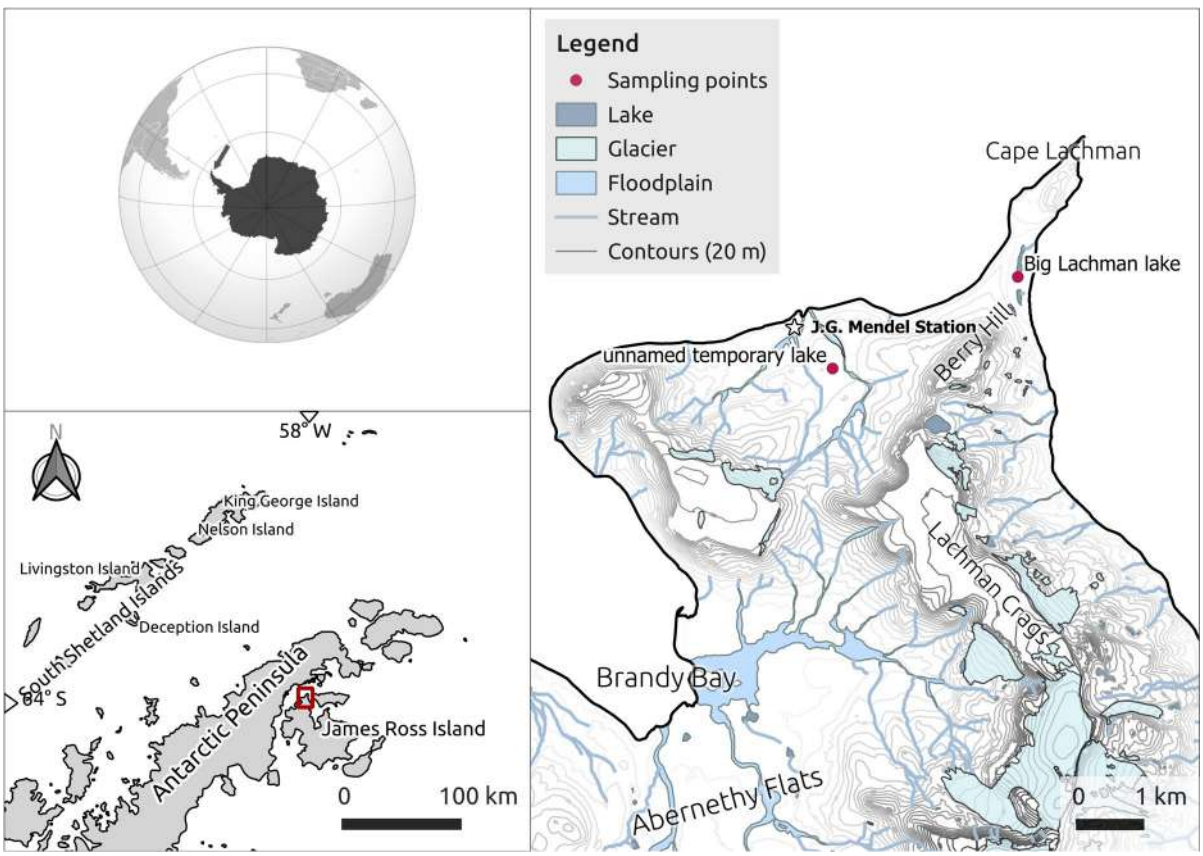

Fig. 1 Location and sampling sites (modified map of CGS, 2009)

was divided into 6 subsamples (L1A-L1F, 0–12 cm), the profile from the temporary lake into 7 subsamples (L2A-L2G, 0–14 cm). Big Lachman Lake was selected for the collection of six samples of cyanobacterial mat. The samples of cyanobacterial mat were collected into PP vials together with the lake water. All samples were stored and transported in a refrigerated box at 4 °C.

Preparation of analytical samples

Lake sediment samples were dried in a clean bench at laboratory temperature. Subsequently, the samples were homogenized using a Pulverisette 7 mill (Fritsch, Germany). The pseudo-total contents of selected heavy metals were determined after wet decomposition using aqua regia according to the widely used ISO 11466 (1995). Samples with weights of 3 g were placed into 250-mL Erlenmeyer flasks equipped with reflux condensers, and 30 mL of aqua regia was added. The flasks were left to stand for 16 h and then boiled for 2 h in an open system. After cooling, the mineralizates were carefully decanted and diluted to a volume of 100 mL. The total weight of collected samples was sufficient only for two analyses. The accuracy of the method was verified by applying the same procedure to Metranal 1 quality control material (Analytika, Czech Republic). The analysis of QCM Metranal 1 was performed in four parallel decompositions. Six experimental blanks were prepared using the same procedure.

Samples of cyanobacterial mat were lyophilized using a Maxi Dry Lyo lyophilizer (Heto-Holten, Denmark) for 72 h. The lyophilized samples were homogenized in an agate mortar. The samples were then decomposed by microwave pressure decomposition using an UltraWAVE mineralizer (Milestone, Italy) at a temperature of 250 °C. A total of 200 mg of sample was decomposed using 2 mL of subboiling HNO_3 and then diluted to 10 mL with deionized water. Due to the limited mass of the Antarctic samples, two parallel decompositions were always performed. (The rest of the material was used for the determination of total Hg directly from the solid material—three parallel analyses.) The six experimental blanks were processed together with samples as well as the following certified reference materials (CRMs) to verify the accuracy and precision of metal determinations: BCR-482 Lichen (IRMM, Belgium), IAEA-336 Lichen (IAEA, Austria), INCT-TL-1 Tea Leaves (INCT, Poland), and Metranal AN-BM02 Green Tea (ANALYTIKA, Czech Republic).

Instrumentation and analytical methods

The content of total (TC) and total organic (TOC) carbon in sediments was determined using a Vario TOC cube analyser (Elementar, Germany). Samples weighing 50 mg were packed into Ag-foil. For the determination of TOC, the samples in Ag-foil were treated with 0.5 mL of 1 mol/L HCl followed by 30 min of drying.

The determination of Hg in samples of lake sediments and cyanobacterial mat was performed directly from solid homogenized samples using an AMA-254 mercury analyzer (Altec, Czech Republic).

The determination of pseudo-total contents of As, Pb, Cr, Co, Ni, Cu, and Zn in aqua regia mineralizates of lake sediments and QCM Metranal 1 was performed by means of inductively coupled plasma optical emission spectrometry (ICP-OES) using a Spectroblue (Spectro, Germany).

A ContrAA 300 atomic absorption spectrometer (Analytik Jena, Germany) with an HS 60 modular hydride generator (Analytik Jena, Germany) was used to determine As in Antarctic cyanobacterial mat and CRMs by means of the hydride generation method (HR-CS HGAAS).

The ContrAA 300 spectrometer was also used to determine Fe in all Antarctic samples by means of the flame technique using a high-resolution continuum source flame atomic absorption spectrometry (HR-CS FAAS).

An AAnalyst 600 atomic absorption spectrometer (Perkin-Elmer, USA) was used for the determination of Cd and Pb in mineralized samples of mat and CRMs. (A pre-mixed $PO_4^{3-}/Mg(NO_3)_2$ matrix modifier was used for these measurements.) Cd in lake sediment samples was determined using this technique (graphite furnace atomic absorption spectrometry, GFAAS).

The contents of metals in sediments and cyanobacterial mats were calculated as the average of two parallel analyses of homogenized samples. The determination of Hg was performed directly from solid samples in six (sediments) or three (mats) parallel analyses. The limit of detection (LOD) and the limit of quantification (LOQ) were calculated, respectively,

as three times and ten times the standard deviation of the experimental blank for the respective method—i.e., the determination of As, Pb, Cr, Co, Ni, Cu, and Zn in blank decompositions in aqua regia using ICP-OES, the determination of Cd in blank decompositions in aqua regia using GFAAS, the determination of Fe in blank decompositions in aqua regia using HR-CS FAAS, the determination of Fe in blank decompositions in nitric acid using HR-CS FAAS, the determination of Cd and Pb in blank decompositions in nitric acid using GFAAS, the determination of As in blank decompositions in nitric acid using HR-CS HGAAS, and the blank determination of Hg using the AMA-254 analyzer.

Enrichment factors (EFs) related to the contents of elements in the Earth's crust were calculated to assess anthropogenic contamination (Guerra et al., 2011; Navas et al., 2008; Santos et al., 2005). The formula for calculating EF is "$EF = (c_n/c_{ref})/(B_n/B_{ref})$", where "c" are the concentrations in samples, "B" are the average concentrations in the Earth's crust, "n" is related to determined element, and "ref" is related to reference element. The contents of elements in the upper crust were obtained from the work of Rudnick and Gao (2014). For the calculation of EF, Fe was chosen as the reference element (Navas et al., 2008; Santos et al., 2005). The Fe contents determined in sediment mineralizates corresponded to the Fe contents determined directly from the solid material by means of X-ray fluorescence spectrometry (unpublished results). EFs were calculated for samples of cyanobacterial mat both from the average contents of elements in the Earth's crust (Rudnick & Gao, 2014) and from the average contents in sediments of the L1 profile.

Results and discussion

Trace metals in lake sediments

The pseudo-total metal contents in the depth profile of the Big Lachman Lake (Fig. 2, L1 profile) were determined as well as the contents in the reference location—the temporary unnamed lake (Fig. 2, L2 profile), both located on the bedrock formed by the Mendel Formation (Nývlt et al., 2011; Vašinka et al., 2020). The LODs and LOQs of all elements are shown along with the QCM Metranal 1 analysis in Table 1.

Differences in metal contents between the L1 and L2 profiles were observed for As, Hg, Cr, and Ni. Co and Cu contents differed twofold. Pb and Zn contents were similar in both sediment profiles (Fig. 2). Changes in contents as a function of the depth of the subsample are shown in Fig. 2. Big Lachman Lake is a shallow coastal lake fed by melting snow (Kňažková et al., 2021; Nedbalová et al., 2013); it has a slightly alkaline pH and high conductivity, which is supported by a high concentration of Na^+, K^+, Mg^{2+}, and Cl^- (Nedbalová et al., 2013). A relatively high TOC content (about 2.5%) compared to regolith (Coufalík et al., 2015) was determined in the L1 profile in spite of the area not being colonized by seabirds, and in spite of its generally poor macrofauna. In contrast, the temporary unnamed lake (L2 profile) exhibited a very low TOC content (0.3–0.6%), which was comparable to the TOC content of the JRI regolith (about 0.4%) (Coufalík et al., 2015). In addition to the high TOC content in Big Lachman Lake sediments, the high content (about 20%) of clay mineral montmorillonite can also increase the retention of metals originating from meltwater from snow patches (Vašinka et al., 2020).

The determined metal contents in sediments were generally comparable (Table 2) to total metal contents in soils (As, Cr, Cu, Ni, Pb, Zn) in other parts of the Ulu Peninsula of the JRI (Vlček et al., 2017) as well as in soils of the South Shetland Islands (Nędzarek et al., 2014; Potapowicz et al., 2020; Santos et al., 2005). A whole-rock analysis was performed in a previous study of Big Lachman Lake sediments (Vašinka et al., 2020). The contents of Pb and Cr were twice as high (using the total decomposition including silicates) as the pseudo-total contents determined in this study; the contents of Co, Cu, Ni, and Zn were of a comparable order. Volcanic rock samples from JRI showed Pb enrichment relative to primitive mantle composition (Košler et al., 2009). The Pb content in Big Lachman Lake sediments was higher compared to basalts from the bedrock (Vašinka et al., 2020). Conversely, the contents of Cr, Co, and Ni in lake sediments were lower than in basalts (Košler et al., 2009).

In general, the metal contents of Big Lachman Lake sediments are determined by the chemical balance between sediment particles and the water

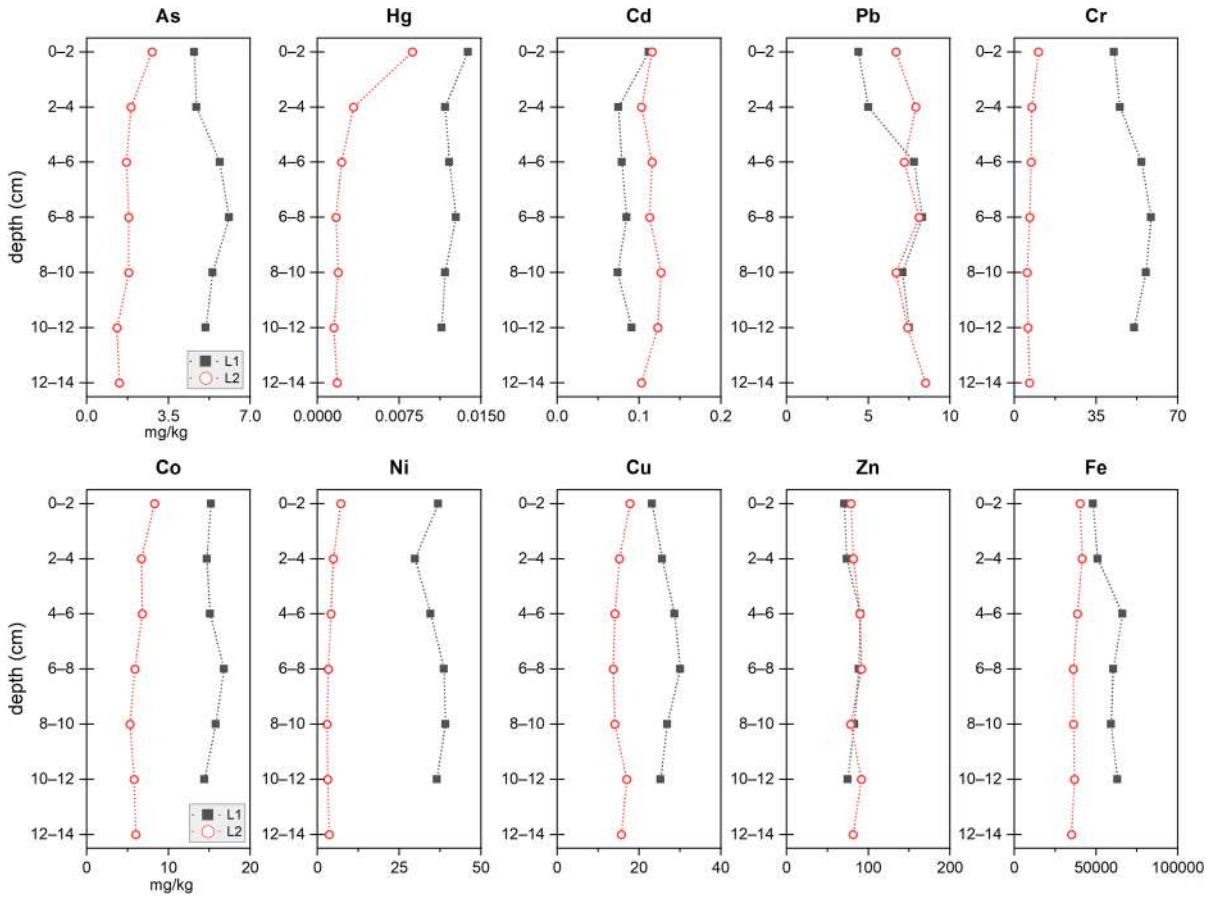

Fig. 2 Depth profiles of the elements in samples of lake sediments

Table 1 Contents of Fe (%) and trace metals (mg/kg) in Metranal 1 quality control material

Sample	Fe[a] (%)	As[b]	Hg[c]	Cd[d]	Pb[b]	Cr[b]	Co[b]	Ni[b]	Cu[b]	Zn[b]
$Met.1_{det}$	2.31 ± 0.10	21.1 ± 1.2	1.57 ± 0.04	2.78 ± 0.02	64.5 ± 3.6	72 ± 4	10.0 ± 0.4	29.4 ± 1.2	72.0 ± 0.6	372 ± 4
$Met.1_{cert}$	2.55 ± 0.27	24.1 ± 3.2	1.55 ± 0.14	2.66 ± 0.54	82.4 ± 16.4	93 ± 14	12.5 ± 1.5	35.4 ± 5	91.2 ± 8	465 ± 64
LOD	0.00002	0.14	0.0001	0.006	0.14	0.10	0.05	0.04	0.13	1.0
LOQ	0.00007	0.47	0.0003	0.020	0.46	0.32	0.16	0.12	0.42	3.2

[a]Contents determined using HR-CS FAAS

[b]Contents determined using ICP-OES

[c]Contents determined using AMA-254 analyser

[d]Contents determined using GFAAS

column, which is significantly influenced by water temperature, water level fluctuations, the inflow of water from melting snow, the accumulation of deposited aerosol particles and their transport, and the long-term accumulation of the fine fraction of particulate material subject to chemical weathering (Vašinka et al., 2020). The average contents of the monitored metals in the lake sediments of Big Lachman Lake corresponded approximately to the estimated contents in the upper continental crust (Rudnick & Gao,

Table 2 Reported ranges of element contents (mg/kg) in sediments and soils

Location, author	TC (%)	TOC (%)	Fe (%)	As	Hg	Cd	Pb	Cr	Co	Ni	Cu	Zn
James Ross Island (this study)	0.3–2.9	0.3–2.9	4.0–6.6	1.3–6.1	0.002–0.014	0.074–0.127	4.4–8.5	5.5–58.6	5.3–16.8	2.9–39.1	13.7–30.1	70.7–91.8
James Ross Island (Vlček et al., 2017)	-	-	-	8–20	-	-	4–15	10–161	-	4–86	11–40	53–87
James Ross Island (Vašinka et al., 2020)	0.06–5.8	-	2.5–4.8	-	-	-	13–16.5	69–103	13.6–32.8	33–87	10.2–30.2	56.6–96.3
King George Island (Potapowicz et al., 2020)	-	0.8–6.6	2.8–5.0	3.2–15.9	-	< 0.38	1.6–22.1	6.6–21.9	8.1–23.5	6.3–19.1	83.9–195	62.9–1176
King George Island (Santos et al., 2005)	-	-	6.2	-	-	-	11.5	40	-	5.1	44	52
King George Island (Vlček et al., 2017)	-	-	-	13	-	-	4	17	-	8	160	78
Livingston Island (Vlček et al., 2017)	-	-	-	12	-	-	9	55	-	22	23	70
Deception Island (Vlček et al., 2017)	-	-	-	10–11	-	-	4–19	2–51	-	3–25	28–86	74–99

2014). The calculated EFs for metals in the L1 profile were as follows: 0.74 for As, 0.17 for Hg, 0.66 for Cd, 0.26 for Pb, 0.38 for Cr, 0.61 for Co, 0.52 for Ni, 0.65 for Cu, and 0.81 for Zn.

Bioaccumulation of As, Hg, Cd, and Pb in cyanobacterial mat

Figure 3 presents the determined contents of As, Hg, Cd, and Pb in cyanobacterial mat. Analytical procedures for the determination of As, Hg, Cd, and Pb in mineralizates were verified by CRMs analysis (Table 3). The contents of all determined elements in reference materials corresponded with declared values. No significant differences (Student's t test; p values < 0.05) were found between observed and certified contents.

Comparing metal contents in mat and sediment samples of the L1 profile, an accumulation of Hg was evident. The calculation of bioaccumulation of metals is recommended according to the ratios of trace elements to the reference element, Fe (Webster-Brown & Webster, 2007), due to the impossibility of separating biotic and abiotic components of the mat. EFs related to average metal contents in lake sediment were slightly higher than those according to average crustal composition; the values were as follows: 1.05 for As, 2.41 for Hg, 2.82 for Cd, and 0.53 for Pb. According to the scale devised by Guerra et al. (2011), these EFs signified a moderate level of pollution by Hg and Cd. The high Hg accumulation (26–309 µg/kg) in cyanobacterial mat was observed in our previous study for this location and a high proportion (up to 75%) of methylmercury was found (Coufalík et al., 2018). The total contents of Hg determined in mat samples collected from Big Lachman Lake (Fig. 3) ranged between 21 and 59 µg/kg. Hg contents are often correlated with organic matter (Wang et al., 2023), which is a major factor in Hg accumulation in lakes (Bargagli et al., 2007). Higher metal contents were found in mat than in sediments in a similar study from East Antarctica (Webster-Brown & Webster, 2007); however, after the evaluation of metal contents in relation to Fe, this bioaccumulation was not confirmed.

The calculated EFs in biota for Hg and Cd may indicate a higher deposition of both metals in the studied locality. In a previous study (Coufalík et al., 2016), the effect of sea spray on the elemental composition of cyanobacterial mat was not confirmed.

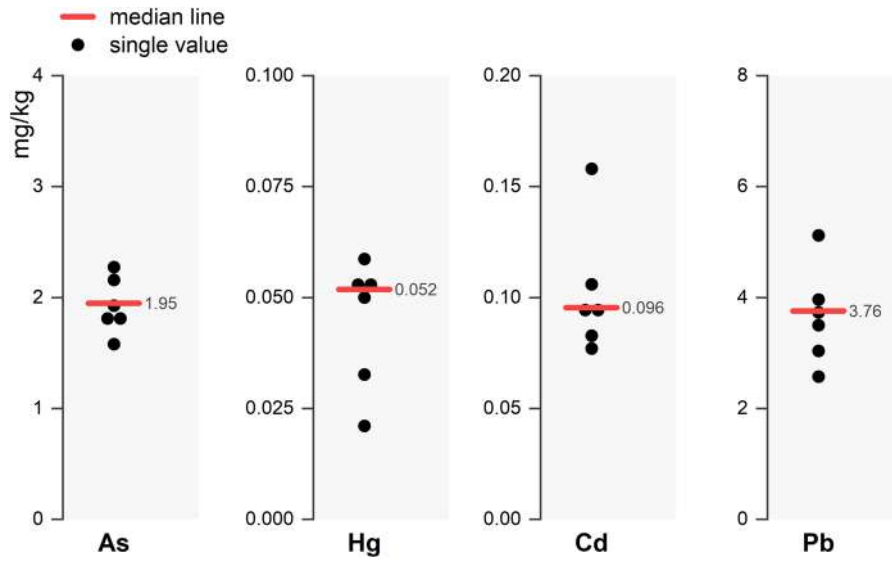

Fig. 3 Contents of As, Hg, Cd, and Pb (mg/kg) in samples of cyanobacterial mat

Table 3 Contents of Fe (%) and As, Hg, Cd, and Pb (mg/kg) in certified reference materials

Sample	Fe[a] (%)	As[b]	Hg[c]	Cd[d]	Pb[d]
$BCR\text{-}482_{det}$		0.81 ± 0.06	0.479 ± 0.008	0.545 ± 0.008	40.7 ± 0.9
$BCR\text{-}482_{cert}$	-	0.85 ± 0.07	0.48 ± 0.02	0.56 ± 0.02	40.9 ± 1.4
$IAEA\text{-}336_{det}$	0.0400 ± 0.0015	0.70 ± 0.07	0.165 ± 0.006	0.101 ± 0.003	4.39 ± 0.13
$IAEA\text{-}336_{cert}$	0.043 ± 0.005	0.63 ± 0.08	0.20 ± 0.04	0.117 ± 0.017	4.9 ± 0.6
$INCT\text{-}TL\text{-}1_{det}$	0.0420 ± 0.0020	0.123 ± 0.007	0.0055 ± 0.0002	0.026 ± 0.001	1.74 ± 0.04
$INCT\text{-}TL\text{-}1_{cert}$	0.0432	0.106 ± 0.021	0.005 ± 0.0007	0.030 ± 0.004	1.78 ± 0.24
$AN\text{-}BM02_{det}$	0.0210 ± 0.0010	0.146 ± 0.009	0.0138 ± 0.0005	0.072 ± 0.001	1.47 ± 0.05
$AN\text{-}BM02_{cert}$	0.0216 ± 0.0015	0.156 ± 0.012	0.014 ± 0.002	0.075 ± 0.004	1.54 ± 0.09
LOD	0.00003	0.001	0.0001	0.003	0.009
LOQ	0.00009	0.003	0.0003	0.011	0.029

[a]Contents determined using HR-CS FAAS

[b]Contents determined using HR-CS HGAAS

[c]Contents determined using AMA-254 analyser

[d]Contents determined using GFAAS

-Value is not certified

Atmospheric deposition can be considered as the main source of Hg in the local ecosystem (Coufalík et al., 2018). The Lachman Cape area was also investigated in terms of wind flows and the accumulation of aerosol particles (Kavan et al., 2020; Kňažková et al., 2021). A high deposition rate for aerosol particles was confirmed on James Ross Island; the source of particles are local rocks and also long-range transport in the upper layers of the atmosphere (Kavan et al., 2020). The origin of these particles can be traced to Patagonia and South America in general (Kavan et al., 2020, and citations within). Snow together with aerosol particles are deposited on the surface, on the leeward sides of the Berry Hill volcanic mesa. The accumulation of snow in snow patches on Cape Lachman reaches several meters and fine particle enrichment was observed as a thin layer on the snow surface. A large proportion of these particles is subsequently deposited in Big Lachman Lake (Kňažková et al., 2021). Thus, the source of Hg and

Cd contamination in the studied locality could be long-range transport.

Conclusions

The area to the east of the Antarctic Peninsula is seemingly more protected of pollutants than maritime Antarctica, which is contaminated by the long-range transport from industrial areas of the southern hemisphere. According to the metal contents determined in the sediments and cyanobacterial mat of Big Lachman Lake, the accumulation of both Hg and Cd in the mat was observed. The cyanobacterial mat appears to be a suitable biomonitor for the pollution of Antarctic surface water. Accumulation in the mat can be a consequence of the high mobility of both metals in the ecosystem, as well as the physiological activity of microorganisms. Due to the generally low contents of Hg and Cd in lake sediments, the input of these metals can be expected from the atmosphere together with snowfall, which is the main source of surface water in this locality. In general, increased deposition of Hg and Cd from the atmosphere in the Antarctic Peninsula region could also increase the toxic burden on the marine animal food chain.

Acknowledgements The authors are grateful to the J.G. Mendel Czech Antarctic Station for allowing them use of its facilities.

Author contribution Pavel Coufalík: conceptualization, methodology, validation, investigation, resources, writing—original draft, funding acquisition; Martin Vašinka: investigation, funding acquisition; Lukáš Krmíček: conceptualization, validation, funding acquisition; Radek Ševčík: validation, investigation, resources, data curation, funding acquisition; Ondřej Zvěřina: formal analysis, resources, data curation, funding acquisition; Lenka Brůhová: investigation; Josef Komárek: methodology, resources, funding acquisition.

Funding The authors gratefully acknowledge the financial support they have received from various grants and institutions: The work of Pavel Coufalík was supported by the Institute of Analytical Chemistry of the CAS under the Institutional Research Plan RVO: 68081715. The work of Martin Vašinka was supported by the Ministry of Agriculture of the Czech Republic, institutional support MZE-RO1223. The work of Lukáš Krmíček was supported by the Institute of Geology of the CAS under the Institutional Research Plan RVO: 67985831. The work of Radek Ševčík was supported by the Institute of Theoretical and Applied Mechanics of the CAS under the Institutional Research Plan RVO: 68378297. The work of Ondřej Zvěřina was supported by the MUNI/A/1366/2022 research program of Masaryk University. The work of Josef Komárek was supported by the MUNI/A/1298/2022 research program of Masaryk University.

Data availability The dataset used in this study is available from the corresponding author on the request.

Declarations

Ethic approval All authors have read, understood, and have complied as applicable with the statement on "Ethical responsibilities of Authors" as found in the instructions for authors.

Consent to participate The authors consent to participate in this research and writing of the manuscript.

Consent for publication The authors consent to publish this manuscript.

Competing interests The authors declare no competing interests.

References

Bargagli, R. (2005). *Antarctic ecosystems. Environmental contamination, climatic change, and human impact* (p. 395). Springer-Verlag.

Bargagli, R., Monaci, F., & Bucci, C. (2007). Environmental biogeochemistry of mercury in Antarctic ecosystems. *Soil Biology & Biochemistry, 39*, 352–360.

Bargagli, R. (2008). Environmental contamination in Antarctic ecosystems. *Science of the Total Environment, 400*, 212–226.

Cortizas, A. M., Muñiz, I. R., Taboada, T., Toro, M., Granados, I., Giralt, S., & Pla-Rabés, S. (2014). Factors controlling the geochemical composition of Limnopolar Lake sediments (Byers Peninsula, Livingston Island, South Shetland Island, Antarctica) during the last ca. 1600 years. *Solid Earth, 5*, 651–663.

Coufalík, P., Zvěřina, O., Krmíček, L., Pokorný, R., & Komárek, J. (2015). Ultra-trace analysis of Hg in alkaline lavas and regolith from James Ross Island. *Antarctic Science, 27*(3), 281–290.

Coufalík, P., Prochazková, P., Zvěřina, O., Trnková, K., Skácelová, K., Nývlt, D., & Komárek, J. (2016). Freshwater mineral nitrogen and essential elements in autotrophs in James Ross Island, West Antarctica. *Polish Polar Research, 37*(4), 477–491.

Coufalík, P., Meszarosová, N., Coufalíková, K., Zvěřina, O., & Komárek, J. (2018). Determination of methylmercury in cryptogams by means of GC-AFS using enzymatic hydrolysis. *Microchemical Journal, 140*, 8–13.

Czech Geological Survey. (2009). James Ross Island – northern part. Topographical map, 1:25000. Prague: Czech Geological Survey.

Guerra, M. B. B., Schaefer, C. E. G. R., de Freitas Rosa, P., Simas, F. N. B., Pereira, T. T. C., & Pereira-Filho, E. R. (2011). Heavy metals contamination in century-old man-made technosols of Hope Bay, Antarctic Peninsula. *Water, Air, & Soil Pollution, 222*, 91–102.

ISO 11466 (1995). Soil quality — Extraction of trace elements soluble in aqua regia (p. 6). Geneva: International Organization of Standardization.

Kavan, J., Nývlt, D., Láska, K., Engel, Z., & Kňažková, M. (2020). High-latitude dust deposition in snow on the glaciers of James Ross Island, Antarctica. *Earth Surface Processes and Landforms, 45*, 1569–1578.

Kňažková, M., Nývlt, D., & Hrbáček, F. (2021). Slope processes connected with snow patches in semi-arid ice-free areas of James Ross Island, Antarctic Peninsula. *Geomorphology, 373*, 107479.

Košler, J., Magna, T., Mlčoch, B., Mixa, P., Nývlt, D., & Holub, F. V. (2009). Combined Sr, Nd, Pb and Li isotope geochemistry of alkaline lavas from northern James Ross Island (Antarctic Peninsula) and implications for back-arc magma formation. *Chemical Geology, 258*, 207–218.

Navas, A., López-Martínez, J., Casas, J., Machín, J., Durán, J. J., Serrano, E., José-Antonio Cuchi, J. A., & Mink, S. (2008). Soil characteristics on varying lithological substrates in the South Shetland Islands, maritime Antarctica. *Geoderma, 144*, 123–139.

Nedbalová, L., Nývlt, D., Kopáček, J., Šobr, M., & Elster, J. (2013). Freshwater lakes of Ulu Peninsula (James Ross Island, NE Antarctic Peninsula): Origin, geomorphology and physical and chemical limnology. *Antarctic Science, 25*(3), 358–372.

Nędzarek, A., Tórz, A., & Drost, A. (2014). Selected elements in surface waters of Antarctica and their relations with the natural environment. *Polar Research, 33*, 21417.

Nývlt, D., Košler, J., Mlčoch, B., Mixa, P., Lisá, L., Bubík, M., & Hendriks, B. W. H. (2011). The Mendel Formation: Evidence for Late Miocene climatic cyclicity at the northern tip of the Antarctic Peninsula. *Palaeogeography, Palaeoclimatology, Palaeoecology, 299*, 363–384.

Pacyna, J. M., & Pacyna, E. G. (2001). An assessment of global and regional emissions of trace metals to the atmosphere from anthropogenic sources worldwide. *Environmental Reviews, 9*, 269–298.

Potapowicz, J., Szumińska, D., Szopińska, M., Bialik, R. J., Machowiak, K., Chmiel, S., & Polkowska, Ż. (2020). Seashore sediment and water chemistry at the Admiralty Bay (King George Island, Maritime Antarctica) – geochemical analysis and correlations between the concentrations of chemical species. *Marine Pollution Bulletin, 152*, 110888.

Ribeiro, A. P., Figueira, R. C. L., Martins, C. C., Silva, C. R. A., França, E. J., Bícego, M. C., Mahiques, M. M., & Montone, R. C. (2011). Arsenic and trace metal contents in sediment profiles from the Admiralty Bay, King George Island, Antarctica. *Marine Pollution Bulletin, 62*, 192–196.

Rudnick, R. L., & Gao, S. (2014). Composition of the continental crust. In H. Holland & K. Turekian (Eds.), *Treatise on geochemistry.* Elsevier.

Santos, I. R., Silva-Filho, E. V., Schaefer, C. E. G. R., Albuquerque-Filho, M. R., & Campos, L. S. (2005). Heavy metal contamination in coastal sediments and soils near the Brazilian Antarctic Station, King George Island. *Marine Pollution Bulletin, 50*, 185–194.

Skácelová, K., Barták, M., Coufalík, P., Nývlt, D., & Trnková, K. (2013). Biodiversity of freshwater algae and cyanobacteria on deglaciated northern part of James Ross Island, Antarctica. A preliminary study. *Czech Polar Reports, 3*(2), 93–106.

Szopińska, M., Szumińska, D., Bialik, R. J., Dymerski, T., Rosenberg, E., & Polkowska, Ż. (2019). Determination of polycyclic aromatic hydrocarbons (PAHs) and other organic pollutants in freshwaters on the western shore of Admiralty Bay (King George Island, Maritime Antarctica). *Environmental Science and Pollution Research, 26*, 18143–18161.

Szumińska, D., Czapiewski, S., Szopińska, M., & Polkowska, Ż. (2018). Analysis of air mass back trajectories with present and historical volcanic activity and anthropogenic compounds to infer pollution sources in the South Shetland Islands (Antarctica). *Bulletin of Geography, 15*, 111–137.

Szumińska, D., Potapowicz, J., Szopińska, M., Czapiewski, S., Falk, U., Frankowski, M., & Polkowska, Ż. (2021). Sources and composition of chemical pollution in Maritime Antarctica (King George Island), part 2: Organic and inorganic chemicals in snow cover at the Warszawa Icefield. *Science of the Total Environment, 796*, 149054.

Vašinka, M., Krmíček, L., Všianský, D., Hrbáček, F., & Nývlt, D. (2020). Chemical weathering in Antarctica: An example of igneous rock particles in Big Lachman Lake sediments, James Ross Island. *Environmental Earth Sciences, 79*(8), 186–199.

Vlček, V., Juřička, D., & Míková, J. (2017). Heavy metal concentration in selected soils and sediments of Livingston Island, Deception Island, King George Island, James Ross Island (Antarctica). *Czech Polar Reports, 7*(1), 18–33.

Wang, Y., Shi, G., Wang, D., Zhao, Q., Jiang, S., Li, Y., Wang, D., Li, C., Chen, Z., & Bargagli, R. (2023). Relationships between concentrations of mercury and organic carbon in soils allow the identification of Antarctic ice-free areas with enhanced deposition of the metal. *CATENA, 220*, 106718.

Webster-Brown, J. G., & Webster, K. S. (2007). Trace metals in cyanobacterial mats, phytoplankton and sediments of the Lake Vanda region, Antarctica. *Antarctic Science, 19*(3), 311–319.

Yin, X., Liu, X., Sun, L., Zhu, R., Xie, Z., & Wang, Y. (2006). A 1500-year record of lead, copper, arsenic, cadmium, zinc level in Antarctic seal hairs and sediments. *Science of the Total Environment, 371*, 252–257.

Spectrochimica Acta Part B: Atomic Spectroscopy 201 (2023) 106616

Contents lists available at ScienceDirect

Spectrochimica Acta Part B: Atomic Spectroscopy

journal homepage: www.elsevier.com/locate/sab

Fast and simultaneous determination of zinc and iron using HR-CS GF-AAS in vegetables and plant material

Ondřej Zvěřina [a,*], Monika Vychytilová [a], Jaqueline Rieger [b], Walter Goessler [b]

[a] Masaryk University, Department of Public Health, Kamenice 5, 625 00 Brno, Czechia
[b] University of Graz, Institute of Chemistry, Universitaetsplatz 1, 8010 Graz, Austria

ARTICLE INFO

Keywords:
High-resolution continuum source graphite furnace atomic absorption spectrometry
Iron
Zinc
Simultaneous determination

ABSTRACT

Due to the high nutritional importance of zinc and iron, accurate methods for their determination in foodstuffs are required. Here, we present a routine-ready method for their co-determination by means of high-resolution continuum source graphite-furnace atomic absorption spectrometry. As the technique allows for monitoring a narrow spectral interval, adjacent secondary lines of Zn (307.588 nm) and Fe (307.572 nm) can be measured simultaneously in a single firing. The analysis is therefore fast (under 2 min) and its sensitivity corresponds to common concentrations of the elements in foodstuffs. The accuracy of the method was verified by means of reference materials and also by comparison with an independent technique. Analysis of a large set of vegetable samples proved the applicability of the method in a routine laboratory setting. The vegetables for analysis were obtained from both markets and local gardeners. The results indicate higher contents of zinc and iron in homegrown vegetables compared to store-bought ones.

1. Introduction

As the most often deficient elements in human diet, iron and zinc have stayed in the spotlight of dietitians. Their content in the foodstuffs is an important nutritional parameter and thus fast and accurate methods for their determination are required.

In most foodstuffs, both iron and zinc occur at the levels ranging from milligrams to tens of milligrams per kilogram. They are usually determined after wet digestion of the solid samples with atomic spectrometric-based methods such as flame or graphite furnace atomic absorption spectrometry (F-AAS and GF-AAS), inductively coupled plasma with optical emission (ICP-OES) or mass spectrometry (ICP-MS). An alternative approach is direct solid sample analysis, often combined with GF-AAS (SS-GF AAS).

When it comes to determination of Fe and Zn, traditional GF-AAS is not the first-choice method. Detection limits for both elements are in the sub-μg L^{-1} range, which actually hinders the analysis, as these elements are critical with regard to contamination from solvents, containers and also laboratory air [1]. The fluctuation of the blank is therefore the main limiting factor [1,2]. Using alternate wavelength is a common approach to decrease this oversensitivity. A problem in this regard is with Zn, which has only one alternate spectral line of a very low sensitivity. However, the introduction of commercially available high-resolution continuum source (HR-CS) spectrometers made GF-AAS much more suitable for measuring high concentrations [3,4]. As the emission of Xe-lamp is intensive over the spectrum, sensitivity of secondary lines is only affected by their absorption and thus, they offer improved analytical usability [5].

Moreover, as the detection window in commercially available HR-CS instruments covers a spectral range of 0.2–1 nm, two (or even more) spectral lines can be measured simultaneously. This opens the possibility to multielemental analysis which doubles the efficiency in terms of running time and costs [6,7]. Although the number of HR-CS instruments in laboratories is increasing, the advantages that this technique has brought are not always exploited.

Here, we present a routine-ready method for simultaneous determination of Zn and Fe using HR-CS GF-AAS. Due to use of less-sensitive spectral lines, its linear range is suitable for direct analysis of digested foodstuffs. The method is fast and simple, does not require any chemical modifier and can be easily adopted in any lab.

* Corresponding author.
E-mail address: zverina@med.muni.cz (O. Zvěřina).

https://doi.org/10.1016/j.sab.2023.106616
Received 21 October 2022; Received in revised form 9 January 2023; Accepted 10 January 2023
Available online 13 January 2023

Table 1
Optimized temperature program for simultaneous determination of Zn and Fe using HR-CS GF-AAS.

Step	Temperature (°C)	Ramp (°C/s)	Hold (s)	Argon flow (L min^{-1})
Drying	120	10	12	2
Pyrolysis	500	100	10	2
Gas adaptation	500	0	5	–
Zn atomization	1550	1500	4	–
Fe atomization	2500	1500	4	–
Cleaning	2500	0	3	4

2. Experimental

2.1. Instrumentation

A high-resolution continuum source spectrometer ContrAA 800G (Analytik Jena, Germany) equipped with a graphite furnace with PIN-platform tubes was used for the analyses. The source of a continuum light is a Xe short-arc lamp combined with a high-resolution double-Echelle monochromator and charge-coupled device detector.

As a comparative technique, ICP-MS was used (Agilent 7900, Agilent Technologies). While both methods are well established for trace element determination, ICP-MS offers several advantages over GF-AAS, such as greater sensitivity and dynamic range and reduced matrix interferences. However, the instrumentation and running costs of ICP-MS are substantially higher.

2.2. Samples and their treatment

Samples of vegetables (n = 106) were obtained from both local markets and also from local gardeners and mushroom pickers. In a laboratory, all the samples were homogenized using A-10 laboratory mill (IKA Germany). About 2 g of fresh material (weighed to 0.1 mg) were then mixed with 5 mL of HNO_3 and 1 mL of H_2O_2 (of analpure and p.a. + purity, respectively, both obtained from Analytika, Czech republic) and digested by means of microwave assisted acid digestion using Multiwave Go plus digestion system (Anton Paar, Austria). The acid digests were then diluted up to 15 mL with ultrapure water (with specific resistivity of 18.2 MΩ cm^{-1}).

Moreover, an additional set of 20 digests of various vegetables samples (carrots, lettuces, mushrooms, and potatoes) was measured with both HR-CS GF-AAS method and ICP-MS for quality control. Whilst using the developed method, the digests were measured directly, for ICP-MS analysis the solutions were diluted ten times.

To check the trueness of the method, a set of 3 reference materials was processed the same way as the real samples and the results were compared with the certified concentrations. The reference materials included: Spinach Leaves (NIST 1570a), Green algae (Metranal 8), and Lichen (BCR-482). The weights of 250 mg of reference materials (roughly corresponding to 2 g of fresh material) were digested in triplicates and brought to a final volume of 15 mL.

2.3. A method for co-determination of Fe and Zn

Using a proposed method, both Fe and Zn were simultaneously determined using conventional HR-CS GF-AAS in a single firing. As the concentration of the elements in typical foodstuff digests is relatively high (ranging from hundreds of μg L^{-1} to units of mg/L), secondary lines at 307 nm were selected. The intensity of selected lines is relatively low, but also the background noise is negligible in the given spectral region.

The temperature program (in Table 1) was optimized to be as fast as possible while maintaining optimal conditions for atomization of both elements due to two-stage atomization (see chapter Temperature program optimization). The duration of the temperature program is 88 s. Entire procedure including sample injection and furnace cooling takes 2 min. Each sample was measured three times and the median value was used.

Obtained peaks (see Fig. 1) were nicely shaped and well distinguished from the background. The peaks are separated not only spatially (16 pm is enough for a clear separation in HR-CS AAS) but also in time.

3. Results and discussion

3.1. Line selection: two possible combinations

In contrast to Fe, which has >500 absorption lines, Zn has only two useful analytical lines. Both those lines have adjacent Fe lines that fit into the narrow detection window of the instrument. So, the possible combinations are:

- primary resonance line of Zn at 213.857 nm (100% sensitivity) & secondary line of Fe at 213.970 nm, with a relative sensitivity of 0.83% (compared to the most intensive absorption line of the element – in case of Fe at 248.327 nm)

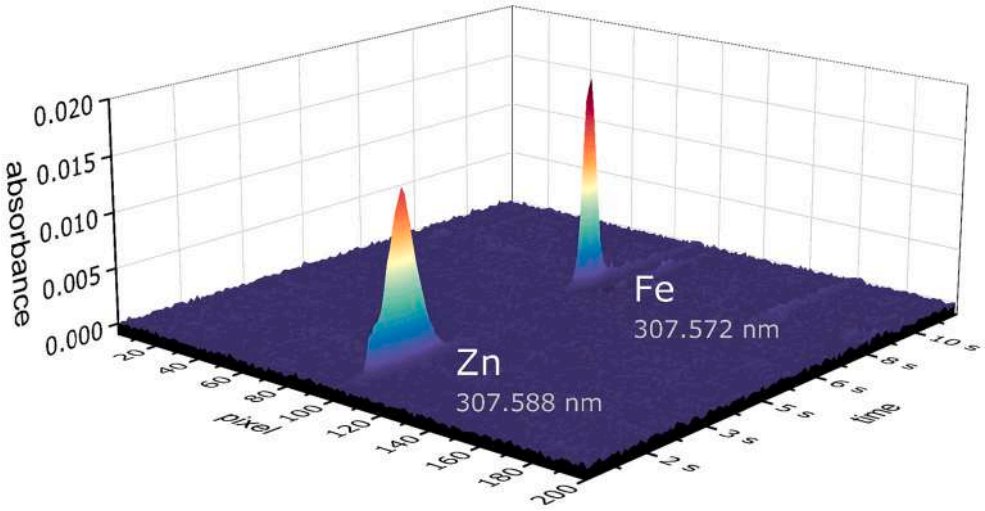

Fig. 1. A time- and wavelength-resolved absorption spectrum (analysis of a lettuce digest containing ~1 mg/ L Zn and ~ 3 mg/ L Fe).

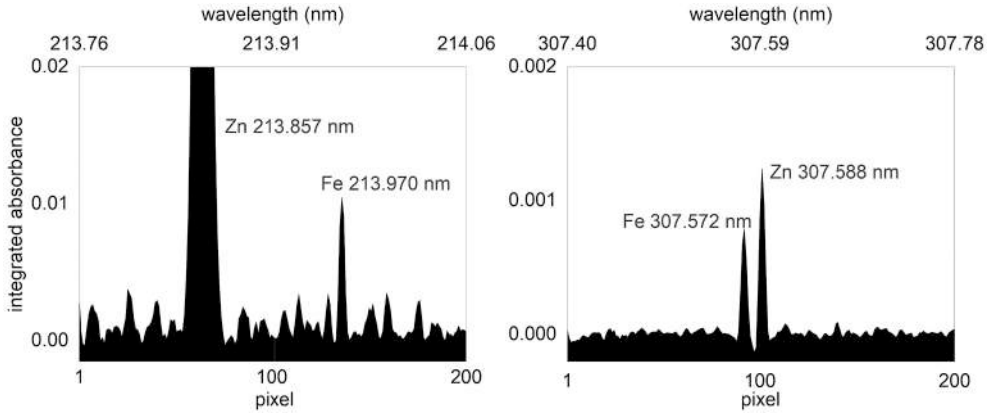

Fig. 2. Absorption spectrum of the same sample (digest of lettuce) recorded at spectral region of a primary Zn line at 213 nm (left) and a secondary line at 307 nm (right).

- secondary line of Zn at 307.588 nm, with 0.02% relative sensitivity & secondary line of Fe at 307.572 nm, with 0.043% relative sensitivity

The experiments have shown that the latter combination of less sensitive lines is far more suitable for their simultaneous determination in the vegetable samples. Three reasons led to the choice:

First, Because of the extreme sensitivity of the Zn primary line, the signal has to be attenuated for measuring concentrations higher than a few μg L^{-1}. This can be done by reading the signal at the line wings [8]. However, presence of the extremely strong Zn line affects the baseline position, which in turn affects reading of the relatively weak Fe line.

Second, the background noise observed in the spectral region of 307 nm was much lower compared to that at 213 nm (Fig. 2), improving the signal-to-noise ratio. Being expressed as the standard deviation of the signal recorded at pixels not involved in analytes measurement, the noise was about twenty-times lower. The NO absorption bands (arising from HNO_3 used for the digestion) are one of the main culprits of deteriorating the background baseline at 213 nm [3,9].

Third, the primary Zn line has a direct overlap with another Fe line (213.859 nm, 0.17% sensitivity), which would have to be corrected by the background correction system or omitted from signal integration as Fe atomizes later than Zn. However, as with possible correction of NO bands, this would make the method less robust.

For the reasons mentioned above, analytical lines at a region of 307 nm are preferred.

3.2. Temperature program optimization

Temperature program, in particular the pyrolysis and atomization temperature, has to reflect the thermal behavior of the analyte. A key factor in optimizing the program for the two elements selected was that zinc is a much more volatile element than iron. This difference in volatility allowed the atomization to be split into two separate steps, and thus, achieving optimal atomization conditions for both elements. Where possible, splitting the atomization into separated steps for each element is preferred because it yields the best possible performance for the multi-elemental methods [7]. In addition, this allows for better temporal separation of the signals of individual elements and integration of only the relevant time region of the recorded spectrum (see Reading the signal chapter).

For Zn, the pyrolysis temperature of 500 °C was set as no significant background absorption was observed during the analysis of any of the samples investigated. Hence, there was also no need to use a matrix modifier, which allowed for a faster analysis. Atomization at temperatures around 1350 °C provided the highest signal, however, led to a formation of double peaks, which may compromise reproducibility and repeatability of the measurement. Atomization at higher temperature

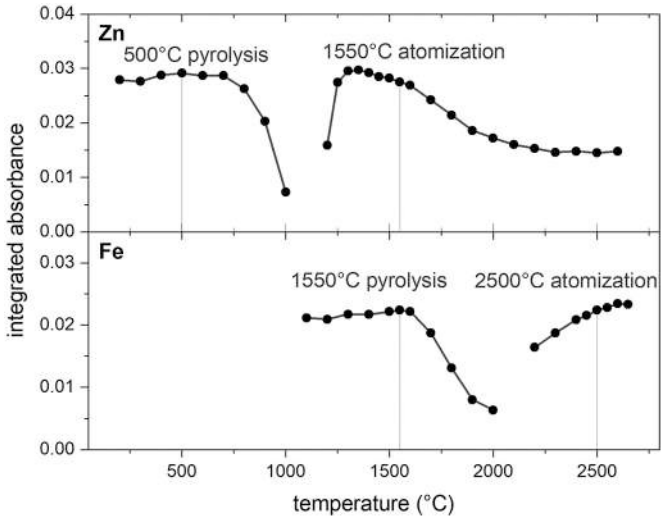

Fig. 3. Pyrolysis and atomization curves for Zn and Fe.

provided nicely shaped peaks with a better repeatability. Improving a signal-to-noise ratio by raising the atomization temperature 100–200 °C higher than the maximum is generally recommended for volatile elements [10]. Therefore, the transient signal was the reason for selecting a temperature of 1550 °C.

As can be seen in Fig. 3, 1550 °C as an Zn atomization temperature was in fact just suitable pyrolysis temperature for analysis of Fe. During the atomization, Fe pronounced symmetrical peaks at all the investigated temperatures. Therefore, the atomization temperature of 2500 °C was chosen as a compromise between sufficient sensitivity and saving the graphite tube life-time.

The resulting time- and wavelength-resolved spectrum can be seen in Fig. 1.

3.3. Reading the signal

Signal integration was limited to 0–3.5 s for Zn and 5–8 s for Fe. This setting reduces the integration of non-useful noise before and after the analytical signal and thus improves the signal-to-noise ratio.

In this way, the two lines are not only separated spatially (different wavelengths), but also temporally (different time intervals). As a result, there is no overlap of the lines even in the case of a significant excess of one of the elements. Selectivity was checked by measuring 1000 μg L^{-1} solutions of each element in the presence of 10- and 100-fold excess of the other. In neither case was the measurement affected.

Table 2
Figures of merit.

Parameter	Zn	Fe
LOD	0.02 mg/L	0.05 mg/L
LOQ	0.06 mg/L	0.2 mg/L
working range	0.06–5 mg/L	0.2–10 mg/L
R-squared	0.9999	0.9997
repeatability (intra-day, n = 5)*	3.1%	4.5%
reproducibility (inter-day, $n = 5$)*	9.0%	8.9%

* A precision expressed as a relative standard deviation (RSD) of replicated measurement of a digest of NIST 1570a (repeatability) and the RSD of measurements conducted in five consecutive days (reproducibility).

3.4. Characteristic concentration: the effect of the number of pixels

In HR-CS spectrometry, the sensitivity depends also on the number of pixels involved in the signal integration. According to the number of used pixels (central pixel [CP] only, CP ± 1, CP ± 2, and, CP ± 3 pixels), the characteristic concentrations were as follows: for Zn, 400, 150, 125, and 125 μg L^{-1} and, for Fe, 1700, 650, 500, and, 500 μg L^{-1}, respectively. It follows that the integration of >5 pixels (CP ± 2) did not improve the characteristic concentration as the range already covered the entire profile of the lines. Therefore, reading of 5 pixels, i.e. CP ± 2, was selected to obtain the highest possible signal. With this setting, the characteristic concentration was 125 μg L^{-1} for Zn and 500 for Fe μg L^{-1}.

3.5. Comparison with similar methods

Compared to the conventional GF-AAS measurement, the proposed method offers several advantages:

- time effective (twice against the measuring element by element),
- cost effective (saving cuvette life, argon, electricity),
- less prone to contamination from ambient air (fluctuation of blank hinders measurement of Zn and Fe at primary lines)

To our best knowledge, there is currently only one paper on simultaneous determination of Zn and Fe using HR-CS GFAAS. For analysis of samples of dried blood spots using solid sampling, the authors used a compromise temperature program with a single atomization temperature of 2400 °C [3]. During the optimization of the method, the authors examined only the temperature range from 1800 °C. Thus, their range did not cover the maximum absorbance and showed only a descending part of the curve. From the atomization curves in Fig. 3 it is obvious that use of a single atomization step at the temperature ideal for Fe leads to a reduction in Zn signal by about 50% (mainly due to diffusion effect).

The other authors measured Fe and Zn in water sequentially [9]. Sequential approach, in contrast to the simultaneous measurement, involves realignment of the monochromator between the first and second atomization step. This approach allowed authors to measure both elements using their primary lines, which was necessary given the mission of the study. However, in our experience, realignment of the monochromator during the atomization process may not be that straightforward and control software is not well prepared for such operation and thus it is not suitable for routine use.

Table 4
Contents of zinc and iron in vegetables and mushrooms (mg kg^{-1} ± standard deviation).

Samples	Zn	Fe
Carrots (homegrown, $n = 30$)	2.9 ± 1.1	2.9 ± 1.5
Carrots (market, $n = 18$)	1.8 ± 0.5	2.1 ± 0.9
Lettuce (homegrown, $n = 37$)	3.8 ± 1.7	6.9 ± 3.2
Lettuce (market, $n = 15$)	2.8 ± 1.2	6.7 ± 2.5
Mushrooms (wild, $n = 6$)	12.1 ± 4.3	5.3 ± 2.8

3.6. Validation: figures of merit, trueness checking

Performance of the method (Table 2) is given by the use of secondary lines and its purpose – to be used for routine analysis of food.

Compared to the nominal sensitivity of GF-AAS, limits of detection and quantification (LOD and LOQ) for both Fe and Zn are substantially reduced. This reduction in sensitivity reflects the low intensity of the selected absorption lines (0.02% for Zn and 0.043% for Fe). The resulting working range approximately corresponds to that of F-AAS (including HR-CS F-AAS), which typically spans from tenths to single units of ppm for both elements [11–13].

At first glance, concentrations at ppm levels may seem relatively high for GF-AAS as the method traditionally used for trace analysis. However, such concentrations are commonly measured in multi-elemental determinations, where secondary spectral lines are widely used [7]. Thus, HR-CS GF-AAS is nowadays commonly used even for determinations that have traditionally been performed by F-AAS. Similarly, detection limits ranging from 1 to 2 mg Fe kg^{-1} (dry weight) were reported for direct solid sample analysis of plant material (using HR-CS SS-GF AAS), when Fe was measured using its secondary line in a simultaneous determination [14,15].

The working range of the method (Table 2) matches the actual elements' concentration in typical digests of food. Relatively narrow calibration ranges (usually 2–3 orders of magnitude) are usual in AAS. For comparison, the working ranges of ICP-based techniques are substantially wider, reaching from 6 orders of magnitude for ICP-OES to up to 9 orders of magnitude for ICP-MS [16]. However, HR-CS AAS has brought some capabilities for extending the limited dynamic range. For example, in the case of need for measuring even higher concentrations, the range may be further extended by measuring the signal at line wings [8], or by injecting a reduced volume of a sample.

Contents of Zn and Fe determined in reference materials corresponded with declared values (Table 3). No statistically significant differences were observed using Student's *t*-test at 95% confidence level. The trueness ranged between 92 and 103%. The matrices of the reference materials used included spinach, lichen, and algae. (See Table 4.)

To ensure that even real-sample matrices do not affect the measurement by interferences, the results obtained for a set of vegetables (carrots, lettuces, mushrooms, potatoes, altogether $n = 20$) were compared to those obtained by ICP-MS as an independent technique. The results agreed closely with correlation coefficients of $r > 0.99$ and no significant difference between the two methods was observed using paired *t*-test.

The results were plotted using Bland-Altman plot, which is a convenient approach for comparison of methods. In contrast to basic

Table 3
Determined levels of Zn and Fe in reference materials (values in mg kg^{-1} ± standard deviation ($n = 3$), corrected to a dry mass at 105 °C).

Reference material	Zn			Fe		
	Found	Certified	Trueness[a]	Found	Certified	Trueness[a]
NIST 1570a Spinach leaves	85.1 ± 5.2	82.3 ± 3.9	103%	259 ± 17	–	–
Metranal 8 Green algae	35.1 ± 0.5	38 ± 3	92%	287 ± 10	290 ± 20	99%
BCR-482 Lichen	102 ± 9	100.6 ± 2.2	101%	751 ± 16	804 ± 160[b]	93%

[a] Expressed as a ratio between the mean measured content and mean reference value *100.
[b] Indicative value.

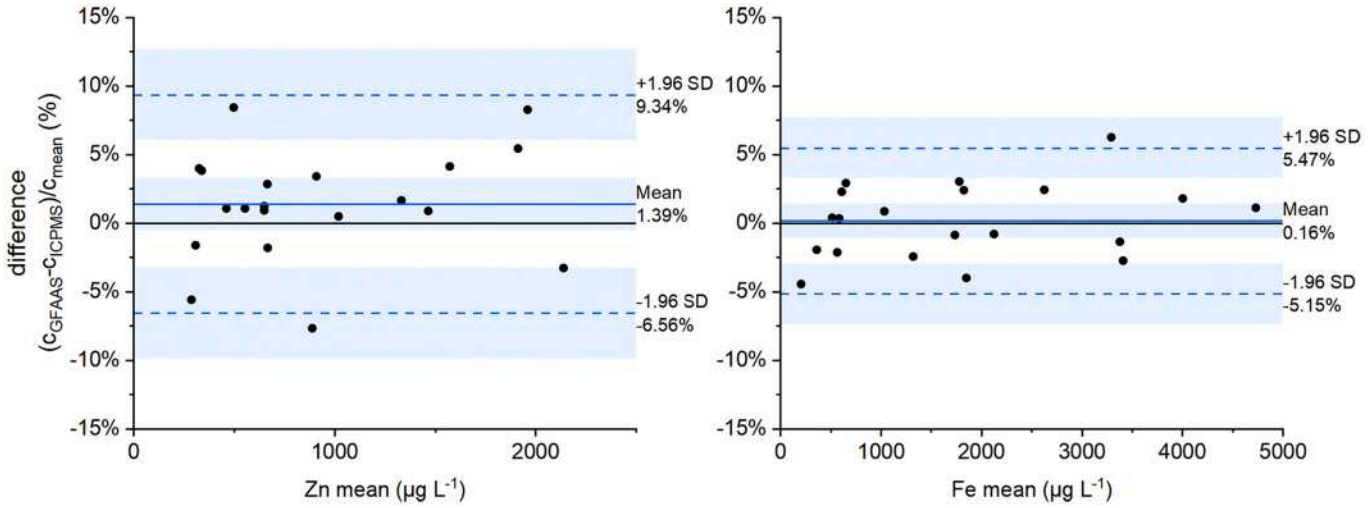

Fig. 4. A Bland-Altman comparison of the results obtained by HR-CS GF-AAS and ICP-MS. The difference between methods (*y*-axis) is plotted against the average value obtained using both methods (*x*-axis). The marked lines approximately define 95% confidence intervals as mean ± 1.96 standard deviation (SD).

comparison using correlation coefficient, it is not influenced by the range of the values and readily detects instrument bias [17]. As can be seen in Fig. 4, the values obtained by both techniques agreed sufficiently closely. The method biases (1.4 and 0.2% for Zn and Fe, respectively) were very small. Even though the precision is somewhat lower in the case of Zn, most of the results still fall between confidence interval ± 1.96*standard deviation.

3.7. Zn and Fe in vegetable and mushroom samples

We used the method for a routine analysis of vegetables (carrots, lettuce) and mushrooms (including *Chanterellus*, *Boletus*, and *Amanita rubescens*), altogether 106 samples. The samples were obtained from local gardeners and mushroom pickers in Czech cities Brno and Letohrad and also from local markets.

As for the vegetables, the lettuce samples were significantly richer in both elements compared to carrots. Mean levels of elements were consistently higher for homegrown vegetables, however, the differences were statistically significant only for carrots (*t*-test, significance level 0.05).

4. Conclusions

The advantages that HR-CS has brought to the GF-AAS include multi-element analysis and also the ability to handle higher concentrations. Here, the two advantages are combined in a method useful for co-measuring iron and zinc at mg L^{-1} levels, for example in vegetables and other food samples. The sensitivity is similar to flame AAS, however, the method provides the benefits of graphite furnace such as low sample consumption (20 µL for the analysis), ease of automation and operation and a possibility of introducing samples with more complex matrices.

CRediT authorship contribution statement

Ondřej Zvěřina: Conceptualization, Methodology, Investigation, Writing – original draft. **Monika Vychytilová:** Investigation, Resources. **Jaqueline Rieger:** Investigation, Validation. **Walter Goessler:** Methodology, Writing – review & editing, Supervision.

Declaration of Competing Interest

The authors declare that they have no known competing financial interests or personal relationships that could have appeared to influence the work reported in this paper.

Data availability

Data will be made available on request.

Acknowledgement

Authors thank the Ministry of Education, Youth and Sports for supporting this research (project 8J21AT006) and also Masaryk University (projects MUNI/C/0063/2022 and MUNI/A/1366/2022).

References

[1] G. Schlemmer, M. Petek, Optimization of a class 100 clean room cabinet for electrothermal atomization AAS, At. Spectrosc. 21 (2000) 1–4.
[2] Z. Polgári, Z. Ajtony, P. Kregsamer, C. Streli, V.G. Mihucz, A. Réti, B. Budai, J. Kralovánszky, N. Szoboszlai, G. Záray, Microanalytical method development for Fe, Cu and Zn determination in colorectal cancer cells, Talanta. 85 (2011) 1959–1965.
[3] A.L. Vieira, E.C. Ferreira, S.R. Oliveira, F. Barbosa, J.A.G. Neto, Simultaneous determination of Fe and Zn in dried blood spot by HR-CS GF AAS using solid sampling, Microchem. J. 160 (2021), 105637.
[4] B. Welz, L.M.G. dos Santos, R.G.O. Araujo, S.C. do Jacob, M.G.R. Vale, M. Okruss, H. Becker-Ross, Unusual calibration curves observed for iron using high-resolution continuum source graphite furnace atomic absorption spectrometry, Spectrochim, Acta Part B At. Spectrosc. 65 (2010) 258–262.
[5] G. Ring, J. O'Mullane, A. O'Riordan, A. Furey, Trace metal determination as it relates to metallosis of orthopaedic implants: evolution and current status, Clin. Biochem. 49 (2016) 617–635.
[6] S.L.C. Ferreira, M.A. Bezerra, A.S. Santos, W.N.L. dos Santos, C.G. Novaes, O.M. C. de Oliveira, M.L. Oliveira, R.L. Garcia, Atomic absorption spectrometry – a multi element technique, Trends Anal. Chem. 100 (2018) 1–6.
[7] I.N. Pasias, N.I. Rousis, A.K. Psoma, N.S. Thomaidis, Simultaneous or sequential multi-element graphite furnace atomic absorption spectrometry techniques: advances within the last 20 years, At. Spectrosc. (2021), https://doi.org/10.46770/AS.2021.707.
[8] O. Zvěřina, P. Coufalík, J. Šimůnek, P. Kachlík, R. Chlupová, J. Pavelková, Inorganic pollutants in the indoor environment of the Moravian library: assessment of Cd, Pb, Cu, and Zn in total suspended particles and dust using HR-CS GF-AAS, Environ. Monit. Assess. 192 (2020) 771.
[9] M. Krawczyk, M. Jeszka-Skowron, H. Matusiewicz, Sequential multi-element determination of iron and zinc in water samples by high-resolution continuum source graphite furnace atomic absorption spectrometry after column solid-phase extraction onto multiwalled carbon nanotubes, Microchem. J. 117 (2014) 138–143.
[10] B. Welz, M.G.R. Vale, Atomic absorption spectrometry and related techniques, in: G. Nelu, R. Sonia (Eds.), Ewing's Analytical Instrumentation Handbook, Fourth Edition, 2018.
[11] S.N.P. Souza, C.C. Nascentes, L.M. Costa, Validation of a microwave-assisted digestion procedure of pâté samples using diluted HNO 3 for Fe and Zn determination by FS FAAS, Anal. Methods 5 (2013) 6411–6415.
[12] O. Acar, A. Tunçeli, A.R. Türker, Comparison of wet and microwave digestion methods for the determination of copper, Iron and Zinc in some food samples by FAAS, Food Anal. Methods 9 (2016) 3201–3208.

[13] E. Zambrzycka-Szelewa, E. Nalewajko-Sieliwoniuk, M. Zaremba, A. Bajguz, B. Godlewska-Żyłkiewicz, The mineral profile of polish beers by fast sequential multielement HR CS FAAS analysis and its correlation with Total phenolic content and antioxidant activity by Chemometric methods, Molecules. 25 (2020), https://doi.org/10.3390/molecules25153402.

[14] M. Pozzatti, F.V. Nakadi, M.G.R. Vale, B. Welz, Simultaneous determination of nickel and iron in vegetables of Solanaceae family using high-resolution continuum source graphite furnace atomic absorption spectrometry and direct solid sample analysis, Microchem. J. 133 (2017) 162–167.

[15] F.R. Adolfo, P.C. do Nascimento, G.C. Leal, D. Bohrer, C. Viana, L.M. de Carvalho, Simultaneous determination of Fe and Ni in guarana (*Paullinia cupana* Kunth) by HR-CS GF AAS: comparison of direct solid analysis and wet acid digestion procedures, J. Food Compos. Anal. 88 (2020), 103459.

[16] S. Suzanne Nielsen, Food Analysis, Springer International Publishing, 2017.

[17] C. Sobin, N. Parisi, T. Schaub, E. de la Riva, A bland-Altman comparison of the Lead care® system and inductively coupled plasma mass spectrometry for detecting low-level lead in child whole blood samples, J. Med. Toxicol. 7 (2011) 24–32.

Journal of Food Composition and Analysis 124 (2023) 105668

Contents lists available at ScienceDirect

Journal of Food Composition and Analysis

journal homepage: www.elsevier.com/locate/jfca

UV-photochemical vapor generation coupled to hydride generation AAS in the study of dietary intake of Se, Hg, Cd, and Pb from fish

Pavel Coufalík [a,*], Ondřej Zvěřina [b], Kateřina Sádovská [b], Josef Komárek [c]

[a] Institute of Analytical Chemistry of the Czech Academy of Sciences, Veveří 97, 60200 Brno, Czech Republic
[b] Department of Public Health, Faculty of Medicine, Masaryk University, Kamenice 5, 62500 Brno, Czech Republic
[c] Department of Chemistry, Faculty of Science, Masaryk University, Kotlářská 2, 61137 Brno, Czech Republic

ARTICLE INFO

Keywords:
Selenium
Trace element
Dietary intake
Pregnancy
Fish
AAS

ABSTRACT

The consumption of fish by pregnant and lactating women is at the center of attention both from the point of view of ensuring healthy nutrition for fetal and neonatal development, and from the toxicological point of view. This research included a questionnaire survey on the frequency of fish consumption and the particular fish species consumed by 180 pregnant and lactating women in the Czech Republic, as well as the determination of Se, Hg, Cd, and Pb in the most commonly consumed species available on the Czech market. For this purpose, an analytical method for the determination of total selenium in biological samples using UV-photochemical vapor generation coupled to hydride generation atomic absorption spectrometry (UV-PVG-HG-AAS) was developed. This unique UV-photoreactor enables accurate and precise determination of Se with a detection limit of 0.007 mg/kg. Fish consumption by female respondents was generally low compared to the EU average. The determined Se contents in samples indicate a low intake of Se from fish in the Czech Republic; one third of the samples had Se contents below the detection limit. The highest Se contents were observed in the species *Scomber scombrus*, *Sander lucioperca*, and *Thunnus albacares*. The Hg content in fish samples did not exceed the EU maximum permissible values for mercury and methylmercury. The Tolerable Weekly Intake (TWI), which is 1.3 μg/kg of body weight per week, was not exceeded by any of the respondents. The maximum permissible value for Cd given by the European Commission was exceeded in the case of one sample of *Scomber scombrus*. Most of the samples had Cd content below the detection limit (0.002 mg/kg). The content of Pb in the analyzed samples was below the detection limit (0.013 mg/kg).

1. Introduction

Pregnant and lactating women are recommended to consume fish because of the omega-3 fatty acids – eicosapentaenoic acid (EPA) and docosahexaenoic acid (DHA), iodine, selenium, and other substances necessary for the proper development of the fetus and infant. However, fish can also contain mercury and other trace elements with toxic effects on human health (Mukherjee et al., 2023), to which the developing fetus and small children are especially sensitive. Exposure to mercury can lead to damage of the nervous system, kidneys and other systems (U.S. Department of Health and Human Services HHS (1999)). The contamination of the aquatic ecosystem with mercury, and its biotransformation and subsequent bioaccumulation in the food chain has an important impact on aquatic animals and human health (Jinadasa et al., 2021; Mukherjee et al., 2023; de Almeida Rodrigues et al., 2019). Maximum permissible values of Hg and methylmercury (MeHg) in fish and shellfish vary considerably between countries (Jinadasa et al., 2021; de Almeida Rodrigues et al., 2019). The Food and Agriculture Organization of the United Nations (FAO) sets the maximum permissible value of Hg in fish intended for human consumption at 0.5 mg/kg in fish muscle (except for Japan, where the limit is lower) for most fish species, except for a list of specific predatory species, such as sharks, swordfish, tuna, pike, catfish, and eel, where the limit is 1.0 mg/kg. The levels of contaminants in fish above these levels are not recommended for consumption. In order to protect public health, these maximum permissible values of Hg in fish were subsequently adopted by the European Union – Commission Regulation EC No, 1881/2006 2006. The maximum permissible value for Cd in fish muscle for human consumption set by the European Commission is 0.05 mg/kg, with the exception of certain species such as tuna and sardine, for which the limit is 0.10 mg/kg (wet

* Corresponding author.
E-mail address: coufalik@iach.cz (P. Coufalík).

https://doi.org/10.1016/j.jfca.2023.105668
Received 22 May 2023; Received in revised form 27 August 2023; Accepted 3 September 2023
Available online 9 September 2023

weight in all cases mentioned here) (Commission Regulation EC No, 1881/2006 2006). The maximum permissible value of Pb in fish muscle set by the European Commission is 0.30 mg/kg (Commission Regulation EC No, 1881/2006 2006). In order to protect the consumer from the adverse effects of MeHg, a so-called Tolerable Weekly Intake (TWI) of 1.3 μg/kg of body weight per week was established by the European Food Safety Authority (EFSA). A TWI of 4 μg/kg of body weight per week was set by EFSA for inorganic Hg species (EFSA, 2012).

Swordfish, shark, marlin, ray, and large freshwater predatory fish (e.g. pikeperch, pike, asp) often have high Hg contents (EFSA, 2014), i.e. fish species that represent the final link of the food chain. The toxic effect of Hg depends mainly on its form (Spiller, 2018). MeHg is an irreversible inhibitor of selenoenzymes, which protect endocrine and nervous tissues from oxidative damage (Ralston and Raymond, 2010). The affinity of MeHg to Se is many orders of magnitude higher than the affinity of MeHg to the thiol group; thus, mercury-induced selenium deficiency inhibits the regeneration of selenoproteins (Spiller, 2018). Hg bioaccumulation in fish also depends on the concentration of Se in the ecosystem (Ralston and Raymond, 2010). Freshwater fish are often low in Se; in contrast, the consumption of marine fish rich in Se (organic forms of selenium) can largely eliminate the toxic effects of MeHg (Grgec et al., 2020; Ralston and Raymond, 2010). Several animal studies have shown that a Se:Hg molar ratio ≥ 1 can provide protection against Hg by forming Hg-Se complexes. In addition, dietary selenium reduces the rate of Hg absorption in the intestinal tract (Jinadasa et al., 2021; Spiller, 2018.).

Atomic absorption spectrometry (AAS) is commonly used to determine Hg or Se in environmental matrices (Mukherjee et al., 2023). Since graphite furnace atomic absorption spectrometry (GF-AAS) has a low sensitivity for Hg and is prone to volatilization losses for both Hg and Se, cold vapor atomic absorption spectrometry (CV-AAS) is used for Hg determination in most cases. (The decrease in the detection limit (LOD) and the elimination of spectral interferences are the main reasons for the generation of volatile forms of analytes.) Hydride generation atomic absorption spectrometry (HG-AAS) is used to determine Se forms rather than total contents. In fact, the direct reduction of Se(VI) to selenium hydride cannot be carried out; pre-reduction to the tetravalent form is necessary. The pre-reduction of Se(VI) to Se(IV) by HCl (at increased temperature) is commonly used, and alternative methods enabling the generation of volatile selenium forms have also been invented (Brindle and Emilia Lugowska, 1997; Rubio et al., 1997; Rybínová et al., 2016a; Sturgeon, 2017). Generally, volatile species of hydride-forming elements and transition metals are generated by a reducing agent in the chemical vapor generation (CVG) method (a common procedure for HG-AAS), while the reducing agent is usually omitted in the UV photochemical vapor generation (UV-PVG) method (Leonori and Sturgeon, 2019; Rybínová et al., 2016a; Rybínová et al., 2016b; Sturgeon, 2017). Various types of reactors have been developed to generate volatile forms of selenium; they are made of polytetrafluoroethylene (PTFE) or quartz capillary in the base (Rybínová et al., 2016a, refs. incl.). Reactors for on-line flow injection analysis are based on sample heating by means of convection (Stripeikis et al., 2000) and microwave radiation (Stripeikis et al., 2000, refs. incl.); the next principle is the use of UV-photochemical reaction – precisely the UV-PVG method (Sturgeon, 2017; Vilanó et al., 1998) used in this research. The yield of UV-PVG depends on the form of the analyte, the photochemical agent, temperature, the duration of the irradiation, and the total energy absorbed by the sample (radiant flux versus the geometric arrangement of the photoreactor, the thickness of the sample layer, or the thickness of the capillary wall) (Rybínová et al., 2016a). A thin sample layer is required for efficient UV-PVG generation (Sturgeon and Grinberg, 2012). Formic and acetic acid are the most commonly used photochemical reagents for Se determination using UV-PVG (Campanella et al., 2016; Rybínová et al., 2016b; Takatani et al., 2007). The photolytic splitting of organic acids takes place under the action of UV radiation (Takatani et al., 2007), and, subsequently, the photoreduction of Se(VI) probably takes place due to the action of emerging radicals (García et al., 2006). Signal suppression occurs in the presence of nitrate and nitrite during UV-PVG (Sturgeon, 2017); HNO_3 and H_2O_2 prevent the determination of selenium owing to the oxidation of Se(IV) to Se(VI) (Brindle and Emilia Lugowska, 1997; Campanella et al., 2016; Rybínová et al., 2016b).

The questions outlined in this research were: What is the intake of selenium from fish among pregnant Czech women? What is the intake of toxic elements (Hg, Cd, Pb) from fish available from local food stores? What is the awareness of the benefits and risks of eating fish? What is the weekly Hg intake in this selected group of the population? The important goal of this work was the development of an analytical method for the determination of total selenium in biological samples using the UV-PVG technique coupled to hydride generation atomic absorption spectrometry (UV-PVG-HG-AAS), which would be quantitative, fast, and compatible with common commercial instrumentation for HG-AAS. Such a method was needed to assess the intake of selenium from fish consumed by pregnant and lactating women. The developed method enabled the parallel determination of trace concentrations of Se and Hg using the same analytical technique – that is, with the coupling of the UV-photoreactor for selenium, and its disconnection for mercury.

2. Materials and methods

2.1. Design of the study

This study was carried out to assess the intake of four elements (Hg, Se, Cd, Pb) from fish consumed by pregnant and lactating women in the Czech Republic. The data on fish consumption were obtained from a food frequency questionnaire completed by 180 respondents. On the basis of the results, the most frequently consumed fish species available on the Czech market were selected, and the contents of Se, Hg, Cd, and Pb were subsequently determined in these species. A unique method for the determination of selenium in biological samples was devised as part of the investigation.

2.2. Reagents and certified reference materials

Sub-boiling distilled HNO_3 was used to decompose the samples. The determination of metals was carried out by three techniques of AAS. $NaBH_4$ (p.a., Hg $\leq$ 0.1 mg/kg, Se $\leq$ 2 mg/kg, Merck, Germany), NaOH (Suprapur, Hg $\leq$ 0.01 mg/kg, Merck, Germany), and HCl (Suprapur, 30%, Hg, Pb, Cd $\leq$ 0.005 mg/kg, Merck, Germany) were used for the determination of Hg by CV-AAS; CH_3COOH (Suprapur, 96%, Merck, Germany) was additionally used for Se determination by the UV-PVG-HG-AAS method. $Mg(NO_3)_2$. 6 H_2O (Suprapur, 99.99%, Pb, Cd $\leq$ 0.005 mg/kg, Merck, Germany) and $NH_4H_2PO_4$ (Suprapur, 99.99%, Pb, Cd $\leq$ 0.005 mg/kg, Merck, Germany) were used for the determination of Cd and Pb by GF-AAS. The Se, Hg, Cd, and Pb standards for AAS (1000 $\pm$ 4 mg/L in 2% HNO_3, Sigma-Aldrich, Switzerland) were used for the calibration. To verify the accuracy of the determination of elements, the certified reference material ERM-CE278k "Mussel tissue" (IRMM, Belgium) was used.

2.3. Digestion of samples

The most frequently consumed fish species (see Table 5) were selected for this study according to the results of a questionnaire survey of pregnant and lactating women (180 respondents). Samples were purchased in Brno (Czech Republic) at local food stores and also in fish shops.

Samples of chilled, frozen, and canned fish (45 in total) were homogenized using an IKA A11 analytical mill (IKA, Germany). 0.25 g of homogenized sample was used for the analysis. Samples were decomposed in 3 mL HNO_3 by microwave digestion using an UltraWAVE mineralizer (Milestone, Italy) at a temperature of 250 °C. Mineralizates were diluted with deionized water (Ultra Clear, Evoqua Water

Technologies) to a volume of 10 mL directly in quartz tubes. In addition, three parallel weights of the certified reference material of lyophilized mussel (ERM – CE278k) and six experimental blanks were processed.

All operations with samples were performed in a clean laboratory in a clean bench (class 100). The traceCLEAN cleaning system (Milestone, Italy) was used for the decontamination of quartz mineralization tubes.

2.4. Instrumentation

A new UV-photoreactor was developed for the determination of selenium, enabling online coupling with commercial instrumentation for HG-AAS. The UV-photoreactor consists of a low-pressure mercury discharge lamp with a power of 4 W (Philips 4 W/UV-C), which is tightly wrapped by 6 m of thin-walled PTFE capillary with an inner diameter of 0.55 mm. The internal volume is 1.4 mL, which allows exposure of the entire aliquot of the sample used for one analysis. The sample is loaded into the reactor inlet; the outlet of the reactor is connected to the hydride generator.

A ContrAA 300 at. absorption spectrometer (Analytik Jena GmbH, Germany) with a HS 60 modular hydride generator (Analytik Jena GmbH, Germany) was used to determine Se and Hg concentrations in the samples. For Hg determination, the standard quartz atomizer (Analytik Jena GmbH, Germany) was replaced by a quartz atomizer of length 16 cm and inner diameter 7 mm closed with quartz windows (Perkin-Elmer, USA) to increase the sensitivity of Hg determination. Instrumental settings (HS 60 modular, Analytik Jena) for the determination of Se and Hg are shown in Table 1.

The determination of Cd and Pb in the samples was performed using an AAnalyst 600 at. absorption spectrometer (Perkin-Elmer, USA) with hollow cathode lamps (Lumina, Perkin-Elmer, USA) at a wavelength of 228.8 nm for Cd (4 mA; 0.7 nm spectral bandpass), and 283.3 nm for Pb (10 mA; 0.7 nm spectral bandpass).

2.5. Analytical procedures

First, Hg was determined directly from the mineralizates in quartz tubes using the CV-AAS technique, which avoids possible Hg contamination or loss. 3% HCl was used as the carrier solution. The reducing agent was 0.3% $NaBH_4$ in 0.1% NaOH, which was prepared daily. Calibration was performed by the calibration curve method using calibration solutions prepared from the Hg standard for AAS. Instrumental settings are listed in Table 1.

The following procedure was developed for Se determination by UV-PVG-HG-AAS. The sample was diluted in a PP test tube in the ratio of 2 mL of sample + 9.75 mL of 3% HCl + 0.25 mL of 96% CH_3COOH, and then shaken. This solution was loaded through the UV-photoreactor into the hydride generator according to the parameters in Table 1. (Load time as well as other times were relatively long due to the length and small inner diameter of the photoreactor capillary.) The volume of solution for one measurement corresponded to the inner volume of the photoreactor capillary (1.4 mL). For the determination of both Se and Hg, 3 replicates and 1 pre-run were performed. (When the sample was continuously loaded into the UV-photoreactor for Se determination, the exposure time was unified after the pre-run.) Again, the carrier solution was 3% HCl and the reducing agent was 0.3% $NaBH_4$ in 0.1% NaOH. Calibration solutions prepared from the Se standard for AAS were diluted using the same procedure for real samples.

Cd and Pb were determined from the remaining volumes of undiluted samples by means of GF-AAS. The temperature programs for Cd and Pb determination using the graphite furnace are shown in Table 2. An injection volume of 20 μL of sample and 10 μL of the matrix modifier ($NH_4H_2PO_4/Mg(NO_3)_2$) were injected for both analytes; thus, the resulting amount of matrix modifier was 50 μg PO_4^{3-} + 3 μg $Mg(NO_3)_2$ per atomization. Calibration for both elements was performed using standard additions of Cd and Pb standards for AAS to real samples (to exclude matrix effects).

The determinations of Hg, Se, Cd, and Pb in CRM ERM-CE278k and experimental blanks were carried out by the same analytical procedures.

2.6. Analytical figures of merit

The linearity of the Se, Hg, Cd, and Pb determinations was monitored within the calibration ranges shown in Table 3. The intraday and interday (three days) precision was monitored using the calibration solutions for all analytes. The interday precision of Se determination was observed over six days using the calibration solutions and CRM ERM-CE278k. The accuracy of the method developed for Se determination as well as the accuracy of the determination of Hg, Cd, and Pb were verified using CRM ERM-CE278k. The second method of verifying the accuracy of Se determination was the use of standard additions to real samples with Se contents below the detection limit, and, subsequently, the recoveries of spiked samples were calculated. The indicative values of limits of detection (LOD) and limits of quantification (LOQ) for all elements were calculated from measurements of the six experimental blanks. The LOD was determined as three times the standard deviation of the blank; the LOQ was determined as ten times the standard deviation of the blank.

3. Results and discussion

3.1. Method developed for total selenium determination

As already mentioned in the introduction, the main problem in the determination of total Se by HG-AAS is the generation of volatile forms only from Se(IV) and not from Se(VI). The developed UV-photoreactor aims at the the pre-reduction of Se(VI) to Se(IV). The suggested design does not differ from other photoreactors (e.g. García et al., 2006; Guo et al., 2003; Vilanó et al., 1998; Rubio et al., 1997; Rybínová et al., 2016b). However, there are three important differences – the large surface of the solution exposed to UV radiation, the low power of the discharge lamp, and, the use of a suitable photochemical agent at an optimal concentration. This work does not aim to clarify the mechanism of Se(VI) photoreduction at low radiant flux in the UV region. However, the photoreduction of Se(VI) to Se(IV) is described in the literature as

Table 1
Instrumental settings for determination of Se and Hg (HS 60 modular, Analytik Jena).

	Se	Hg
Wavelength	196.0267	253.6519
Mode	Hydride (cont.)	Hg without enrich. (cont.)
Cell temp.	900 °C	150 °C
Gas flow	6 L/h	6 L/h (31 L/h, FBR mode)
Pump speed level	2	1
Load time	40 s	15 s
AZ wait time	60 s	10 s
Reaction time	40 s	15 s
Wash time 1	40 s	20 s
Wash time 2	-	10 s (31 L/h)
Read time	80 s	45 s

Table 2
Temperature programs for Cd and Pb determination by GF-AAS (Analyst 600, PerkinElmer).

Step	Temperature (°C) / Ramp (°C/s) / Hold (s)	
	Cd	Pb
Drying 1	110/1/30	110/1/30
Drying 2	130/15/30	130/15/30
Pyrolysis	500/20/20	800/20/20
Atomization	1600/0/3	1600/0/3
Cleaning	2450/1/2	2450/1/2

Table 3
Analytical performance characteristics.

Element	Calibration range (μg/L)	Slope	Correlation coefficient (R^2)	LOD (μg/kg)	LOQ (μg/kg)
Se[a]	0.25–4	0.4682	0.9994	7	23
Hg[b]	0.1–4	0.3516	0.9987	3	9
Cd[c]	0.2–2	0.0852	0.9996	2	8
Pb[c]	5–50	0.0031	0.9992	13	44

[a] UV-PVG-HG-AAS, [b] CV-AAS, [c] GF-AAS

producing a transient state that can be re-oxidized to Se(VI) by high radiant power (Vilanó and Rubio, 1999). In our set-up, the low power of the mercury discharge lamp (4 W) in combination with the large area of the sample exposed to UV radiation (6 m of thin-walled PTFE capillary with an inner diameter of 0.55 mm) proved to be sufficient for such reduction in the case of an optimized solution composition. However, the length of the reactor loop proposed here is limiting for the acquisition of reproducible measurements due to the considerable resistance to the flow of the solution through the narrow cross-section of the capillary, which is connected on-line to the hydride generator.

The resulting dilution ratio of the sample in our method is 2 mL of mineralizate, 9.75 mL of 3% HCl, and 0.25 mL of 96% CH_3COOH. However, the dilution ratio depends on the resulting concentration of HNO_3 in the mineralizate, i.e. also on the process of sample digestion. (Losses of HNO_3 during digestion also depend on the type of pressure microwave mineralizer.) The high-concentrated HCl typically used for sample dilution interferes with Se determination. In fact, Se(IV) is oxidized to Se(VI) by chlorine at laboratory temperature (Brindle and Emilia Lugowska, 1997; Stripeikis et al., 2000). In our method, the sample can be diluted by 3% HCl, and it is necessary to optimize the amount of CH_3COOH against the ratio of HNO_3:HCl (for use in other laboratories with different instrumentation and sample mineralization procedures). ($(CH_3)_2Se$ is generated by UV radiation in the presence of acetic acid (Guo et al., 2003; D'Ulivo et al., 2011).) Under these conditions, sample exposure in the reactor for longer than 1 min enables reproducible measurements with a maximum deviation of up to 5% (verified by CRM ERM-CE278k).

3.2. Analytical parameters of Se, Hg, Cd, and Pb determination

According to least square analysis, the obtained calibration curves showed great linearity (Table 3), with a coefficient of determination (R^2) of around 0.999. The precision of determinations was observed for calibration standards at metal concentrations in the middle of the calibration curves – 2 μg/L Se, 2 μg/L Hg, 1 μg/L Cd, and 25 μg/L Pb. Relative standard deviations (RSDs) for these measurements were 6.74%, 4.96%, 3.19%, and 4.42%, respectively. The RSD of Se determination was 5.32% according to the analysis of CRM ERM-CE278k over six days. Table 4 lists the contents of elements determined in CRM ERM-CE278k. According to t-test, the determined contents were not significantly different from certified values at a 95% confidence interval. The recovery of spiked samples using the Se standard was 96.5 ± 7.2%. The LODs and LOQs of elements are shown in Table 3. The LOD achieved here for the determination of total selenium is comparable to the LODs for Se (mostly in the form of Se(IV)) published by other authors (Nováková et al., 2017; Rybínová et al., 2016b, refs. incl.).

Table 4
The accuracy of quantifications of Se, Hg, Cd, Pb (mg/kg±SD).

	Se	Hg	Cd	Pb
CRM ERM-CE278k				
Determined content	1.49 ± 0.04	0.078 ± 0.007	0.320 ± 0.027	2.07 ± 0.04
Certified content	1.62 ± 0.12	0.071 ± 0.007	0.336 ± 0.025	2.18 ± 0.18

3.3. Determination of Se, Hg, Cd, and Pb in fish samples

As mentioned in chapter 2.5., Hg and Se were determined using the techniques of CV-AAS and UV-PVG-HG-AAS. Table 5 shows the ranges of the contents of Hg and Se determined in analyzed fish samples. The highest Hg contents were determined for the species *Xiphias gladius*, *Thunnus albacares*, and *Sander lucioperca*; the lowest values were observed for *Pangasius hypophthalmus*. None of the analysed samples exceeded the maximum permissible value of Hg set by the European Commission in Commission Regulation EC No, 1881/2006 2006. (Of the exceptions for which a higher permissible value is allowed, tuna and swordfish were analyzed.) This limit was not exceeded either in fish from breeding localities in the Czech Republic (e.g. Kenšová et al., 2012; Sehonova et al., 2022). Generally, the quality of the fish available on the Czech market, including canned fish (Kral et al., 2017), is generally good in terms of Hg content. The Se content was below the LOD (0.007 mg/kg) in 13 samples. *Scomber scombrus*, *Sander lucioperca*, and *Thunnus albacares* had the highest Se contents. All *Oncorhynchus mykiss* and *Clarias gariepinus* samples had Se contents below the LOD. The Se contents were higher in marine fish than in freshwater fish. Overall, the determined contents of Se in our fish samples was relatively low compared to other studies (EFSA, 2014; Grgec et al., 2020). A molar ratio of Se:Hg ≥ 1 may provide protection against the toxic effects of Hg (Jinadasa et al., 2021; Spiller, 2018). The ratio of Se:Hg ≥ 1 was found in 58% of fish samples; the highest Se:Hg ratios were determined for samples of *Sardina pilchardus*, *Thunnus albacares*, and *Scomber scombrus*.

The contents of Cd and Pb were also determined in all fish samples. The Pb content was below the LOD (0.013 mg/kg) in all cases. A Cd content above LOQ (0.008 mg/kg) was observed in eight fish samples – seven samples of canned fish and one fresh swordfish sample. The highest Cd content of 0.128 mg/kg was found in *Scomber scombrus* (0.022 mg/kg in the second sample of this specie). Thus, the highest Cd content determined in canned *Scomber scombrus* exceeded the maximum permissible value given by the European Commission (Commission Regulation EC No, 1881/2006 2006). The Cd contents in the other samples were as follows: *Xiphias gladius* – 0.052 mg/kg; *Sardina*

Table 5
Contents of Se and Hg in fish samples (mg/kg).

Species	N	Se	Se ($\bar{x}$ ± SD)	Hg	Hg ($\bar{x}$ ± SD)
Salmo salar	6	0.010–0.083	0.030 ± 0.030	0.016–0.038	0.023 ± 0.007
Thunnus albacares	5	0.140–0.239	0.185 ± 0.038	0.016–0.269	0.098 ± 0.094
Pollachius virens	5	0.017–0.108	0.048 ± 0.032	0.021–0.140	0.063 ± 0.040
Oncorhynchus mykiss	5	<LOD		0.008–0.019	0.016 ± 0.004
Sander lucioperca	4	0.008–0.245	0.080 ± 0.096	0.049–0.200	0.099 ± 0.060
Sardina pilchardus	4	0.045–0.121	0.069 ± 0.031	0.005–0.038	0.015 ± 0.013
Clarias gariepinus	3	<LOD		0.003–0.006	0.004 ± 0.001
Scomber scombrus	3	0.096–0.255	0.169 ± 0.066	0.032–0.064	0.046 ± 0.013
Pangasius hypophthalmus	3	<LOD–0.007		<LOD –0.005	
Cyprinus carpio	3	0.013–0.047	0.030 ± 0.017	0.008–0.044	0.020 ± 0.017
Clupea harengus	2	0.013–0.027	0.020 ± 0.007	0.029–0.127	0.078 ± 0.049
Xiphias gladius	1	0.136		0.929	
Sprattus sprattus	1	0.071		0.018	

N – number of samples

pilchardus – 0.031 mg/kg, 0.028 mg/kg, and 0.022 mg/kg; *Sprattus sprattus* 0.014 mg/kg; *Thunnus albacares* – 0.012 mg/kg.

3.4. Summary of food questionnaire survey and assessment of mercury intake

The average fish consumption was 149 g per week (4–1082 g per week); the median of fish consumption amounted to 105 g per week. The average fish consumption of respondents was 7.5 kg per year which was higher than the average fish consumption in the Czech Republic of 4–6 kg per year per inhabitant reported by the Czech Statistical Office (2021). Even so, fish consumption was lower than the recommendations of both national and European authorities. The recommended consumption of 1–4 fish portions per week according to the European Food Safety Authority (EFSA) (EFSA, 2014) or 1–2 portions per week according to the National Institute of Public Health (NIPH) of the Czech Republic was met by less than half of the respondents (42%). Only 5% of women consumed fish 3–4 times a week. Only 22% of respondents increased their fish consumption during pregnancy, while 25% of respondents decreased their intake. During breastfeeding, 30% of respondents increased their fish intake, while 8% of them decreased their fish intake. Marine fish were preferred among respondents (80% of consumption). Respondents most often bought chilled fish instead of frozen and canned fish.

Nutritional knowledge about fish consumption during pregnancy and breastfeeding was also monitored in the questionnaire survey. According to the respondents, fish were considered a good source of omega-3 fatty acids (93% of respondents), a high-quality source of protein (48%), and good sources of iodine (33%), vitamin B12 (10%), iron (10%), and zinc (4%), while only 3% of interviewed women considered fish a source of selenium. When asked how often pregnant women should consume fish according to the recommendation (i.e. 1–2 portions per week according to NIPH), 73% of respondents answered at least once a week. A further 5% of women thought that pregnant women should eat fish at least three times a week. In contrast, 19% of participants thought that fish should be consumed by pregnant women only 1–2 times a month, and 3% of respondents thought that fish should not be consumed at all during pregnancy.

On the basis of the questionnaire survey on the frequency of fish consumption and fish species consumed by pregnant and lactating women and the chemical analysis of fish samples, an estimate of the average weekly intake of Hg from fish was determined at 0.125 μg/kg of body weight, which did not exceed for any of the respondents the Tolerable Weekly Intake for MeHg of 1.3 μg/kg of body weight determined by the EFSA (EFSA, 2012). The calculation was made for a weight of 70 kg. For this calculation, the mercury determined in our study was considered to be MeHg, although MeHg only accounts for the majority of total Hg content (EFSA, 2012; Kenšová et al., 2012). This approach is also used by the NIPH CZ. The median of Hg weekly intake was 0.079 μg/kg; the maximum Hg weekly intake was 1.217 μg/kg. Only two respondents exceeded the average Tolerable Weekly Intake of Hg from fish in the worst-case scenario, where all the fish consumed had the highest determined content of Hg in the analysed samples.

4. Conclusions

The exposure of pregnant and lactating women to mercury through the consumption of contaminated fish deserves attention, especially if fish consumption in this population group is high. This study aimed to assess mercury intake among the investigated population on the basis of a questionnaire survey and the chemical analysis of fish commonly available on the market in the Czech Republic. Our findings show that the respondents did not exceed the Tolerable Weekly Intake for methylmercury (1.3 μg/kg of body weight), which indicates the safety of fish on the Czech market in this regard. However, total fish consumption among our respondents was lower than recommended, and the estimated average weekly intake of Hg of 0.125 μg/kg of body weight did not include the contribution of other foods that may represent other sources of Hg to which the respondents may be exposed. Among other trace elements, cadmium was detected in some samples; lead was below the detection limit.

In this research, a unique UV-photoreactor was designed enabling the generation of volatile selenium forms for the quantitative determination of this element. The developed photoreactor used for the UV-PVG-HG-AAS technique enables precise and accurate determinations of total selenium in mineralized biological samples, and, in addition, allows coupling to any commercial hydride generator for AAS instrumentation. The selenium content in the analyzed fish samples was relatively low, which puts even more emphasis on the need for its sufficient intake by pregnant and lactating women in the Czech Republic.

Funding

The research was supported by the Institute of Analytical Chemistry of the CAS under the Institutional Research Plan RVO: 68081715, and under the research programs of Masaryk University – MUNI/A/1402/2021, MUNI/A/1366/2022, and MUNI/A/1298/2022.

CRediT authorship contribution statement

Pavel Coufalík: Conceptualization; Methodology; Validation; Investigation; Resources; Writing – original draft; Funding acquisition. **Ondřej Zvěřina**: Formal analysis; Investigation; Resources; Data curation; Funding acquisition. **Kateřina Sádovská**: Investigation; Data curation. **Josef Komárek**: Resources; Funding acquisition.

Declaration of Competing Interest

The authors declare that they have no known competing financial interests or personal relationships that could have appeared to influence the work reported in this paper.

Data availability

Data will be made available on request.

References

Brindle, I.D., Emilia Lugowska, E., 1997. Investigations into mild conditions for reduction of Se(VI) to Se(IV) and for hydride generation in determination of selenium by direct current plasma atomic emission spektrometry. Spectrochim. Acta B 52, 163–176.

Campanella, B., Menciassi, A., Onor, M., Ferrari, C., Bramanti, E., D'Ulivo, A., 2016. Studies on photochemical vapor generation of selenium with germicidal low power ultraviolet mercury lamp. Spectrochim. Acta B 126, 11–16.

Commission Regulation (EC) No 1881/2006, 2006. Setting maximum levels for certain contaminants in foodstuffs. Off. J. Eur. Union 364, 5–24.

Czech Statistical Office, 2021. Consumption of food, beverages and cigarettes in the Czech Republic in 2011 – 2020. Czech Statistical Office, Prague.

EFSA, 2012. Scientific Opinion on the risk for public health related to the presence of mercury and methylmercury in food (Panel on Contaminants in the Food Chain (CONTAM)). EFSA J. 10 (12), 2985.

EFSA, 2014. Scientific Opinion on health benefits of seafood (fish and shellfish) consumption in relation to health risks associated with exposure to methylmercury (Dietetic Products, Nutrition, and Allergies (NDA)). EFSA J. 12 (7), 3761.

García, M., Figueroa, R., Lavilla, I., Bendicho, C, C., 2006. On-line photoassisted vapour generation implemented in an automated flow-injection/stopped-flow manifold coupled to an atomic detector for determination of selenium. J. Anal. . Spectrom. 21, 582–587.

Grgec, A.S., Kljaković-Gašpić, Z., Orct, T., Tičina, V., Sekovanić, A., Jurasović, J., Piasek, M., 2020. Mercury and selenium in fish from the eastern part of the Adriatic Sea: A risk-benefit assessment in vulnerable population groups. Chemosphere 261, 127742.

Guo, X., Sturgeon, R.E., Mester, Z., Gardner, G.J., 2003. UV vapor generation for determination of selenium by heated quartz tube atomic absorption spektrometry. Anal. Chem. 75, 2092–2099.

Jinadasa, B.K.K.K., Jayasinghe, G.D.T.M., Pohl, P., Fowler, S.W., 2021. Mitigating the impact of mercury contaminants in fish and other seafood – A review. Mar. Pollut. Bull. 171, 112710.

Kenšová, R., Kružíková, K., Svobodová, Z., 2012. Mercury speciation and safety of fish from important fishing locations in the Czech Republic. Czech J. Food Sci. 30 (3), 276–284.
Kral, T., Blahova, J., Sedlackova, L., Kalina, J., Svobodova, Z., 2017. Mercury in canned fish from local markets in the Czech Republic. Food Addit. Contam. Part B Surveill. 10 (2), 149–154.
Leonori, D., Sturgeon, R.E., 2019. A unified approach to mechanistic aspects of photochemical vapor generation. J. Anal. . Spectrom. 34, 636–654.
Mukherjee, A.G., Renu, K., Gopalakrishnan, A.V., Veeraraghavan, V.P., Vinayagam, S., Paz-Montelongo, S., Dey, A., Vellingiri, B., George, A., Madhyastha, H., Ganesan, R., 2023. Heavy metal and metalloid contamination in food and emerging technologies for its detection. Sustainability 15, 1195.
Nováková, E., Linhart, O., Červený, V., Rychlovský, P., Hraníček, J., 2017. Flow injection determination of Se in dieatry supplements using TiO_2 mediated ultraviolet-photochemical volatile species generation. Spectrochim. Acta B 134, 98–104.
Ralston, N.V.C., Raymond, L.J., 2010. Dietary selenium's protective effects against methylmercury toxicity. Toxicology 278, 112–123.
de Almeida Rodrigues, P., Ferrari, R.G., dos Santos, L.N., Conte Junior, C.A., 2019. Mercury in aquatic fauna contamination: a systematic review on its dynamics and potential health risks. J. Environ. Sci. 84, 205–218.
Rubio, R., Padró, A., Rauret, G., 1997. Photoreduction-hydride generation: a new on-line system for the determination of selenate and selenite. Anal. Chim. Acta 353, 91–97.
Rybínová, M., Musil, S., Červený, V., Vobecký, M., Petr Rychlovský, P., 2016a. UV-photochemical vapor generation of selenium for atomic absorption spectrometry: Optimization and ^{75}Se radiotracer efficiency study. Spectrochim. Acta B 123, 134–142.
Rybínová, M., Červený, V., Hraníček, J., Rychlovský, P., 2016b. UV-photochemical vapor generation with quartz furnace Atomic absorption spectrometry for simple and sensitive determination of selenium in dietary supplements. Microchem. J. 124, 584–593.
Sehonova, P., Harustiakova, D., Mikula, P., Medkova, D., Malacova, K., Svobodova, Z., 2022. Do the total mercury concentrations detected in fish from Czech ponds represent a risk for consumers? Sci. Rep. 12, 553.
Spiller, H.A., 2018. Rethinking mercury: the role of selenium in the pathophysiology of mercury toxicity. Clin. Toxicol. 56 (5), 313–326.
Stripeikis, J., Costa, P., Tudino, M., Osvaldo Troccoli, O., 2000. Flow injection-hydride generation atomic absorption spectrometric determination of Se(VI) and Se(IV): utility of a conventionally heated water bath for the on-line reduction of Se(VI). Anal. Chim. Acta 408, 191–197.
Sturgeon, R.E., Grinberg, P., 2012. Some speculations on the mechanisms of photochemical vapor generation. J. Anal. . Spectrom. 27, 222–231.
Sturgeon, R.E., 2017. Photochemical vapor generation: a radical approach to analyte introduction for atomic spektrometry. J. Anal. . Spectrom. 32, 2319–2340.
Takatani, T., Fitzgerald, N., Galbraith, J.M., 2007. Proposed reaction mechanisms for selenium UV photolysis vapor generation by computational methods. Anal. Bioanal. Chem. 388, 859–862.
D'Ulivo, A., Dědina, J., Mester, Z., Sturgeon, R.E., Wang, Q., Welz, B., 2011. Mechanisms of chemical generation of volatile hydrides for trace element determination (IUPAC Technical Report). Pure Appl. Chem. 83 (6), 1283–1340.
U.S. Department of Health and Human Services (HHS), 1999. Toxicological Profile for Mercury, Agency for Toxic Substances and Disease Registry, Atlanta.
Vilanó, M., Padró, A., Rubio, R., Raureta, G., 1998. Organic and inorganic selenium speciation using high-performance liquid chromatography with UV irradiation and hydride generation – quartz cell atomic absorption spectrometric detection. J. Chromatogr. A 819, 211–220.
Vilanó, M., Rubio, R., 1999. Liquid chromatography – UV irradiation – hydride generation – atomic fluorescence spectrometry for selenium speciation. J. Anal. . Spectrom. 15, 177–180.

Journal of Food Composition and Analysis 107 (2022) 104340

Contents lists available at ScienceDirect

Journal of Food Composition and Analysis

journal homepage: www.elsevier.com/locate/jfca

Original Research Article

Mineral profile of cricket powders, some edible insect species and their implication for gastronomy

Pavlína Kosečková [a], Ondřej Zvěřina [a,*], Marie Pěchová [a], Martina Krulíková [a], Eva Duborská [b], Marie Borkovcová [c]

[a] Department of Public Health, Faculty of Medicine, Masaryk University, Brno, Czech Republic
[b] Institute of Laboratory Research on Geomaterials, Faculty of Natural Sciences, Comenius University in Bratislava, Slovakia
[c] Department of Food Analysis and Chemistry, Faculty of Technology, Tomas Bata University in Zlín, Czech Republic

ARTICLE INFO

Keywords:
Entomophagy
House cricket powder
Edible insect
Trace elements
Potentially toxic elements

ABSTRACT

Entomophagy is proclaimed as a sustainable nutritional strategy due to the high protein content in edible insects. As it turns out, it may also represent an effective tool for increasing dietary intake of nutrients that are frequently deficient. Cricket powder (CP) appears to be the simplest way. The objectives of this work were to determine the contents of fourteen minerals in CPs and in insect species namely, house cricket, yellow mealworm, desert locust, and superworm. To assess these insect species as sources of minerals with respect to the dietary recommended values (DRV) for some minerals, and to determine mineral enrichment level of some recipes with using CP. Samples were analyzed by means of high-resolution continuum source graphite furnace atomic absorption spectrometry and flame atomic absorption/emission spectrometry. These insect species can be considered as a uniform source of Fe. The species of house cricket, yellow mealworm, and desert locust would provide more than the DRV for Zn, Cu, and P. Replacing 10 % of the wheat flour with CP in bread and pasta recipes increases Zn content by 92–107 %. Finally, the low Cd and Pb contents indicate that the consumption of the given insect species presents no risk.

1. Introduction

Despite the fact that using insects as a food has been a feature of human activity since prehistoric times and insects have formed a major part of the human diet for thousands of years, entomophagy is only now becoming an evolving trend in western nutrition and in the food industry (Van Huis et al., 2013). In contrast to some African, Asian and Latin American countries, where the tradition of consuming edible insects has persisted, in Europe and the US, the consumption of insects has been strongly suppressed by cultural preconceptions and eating habits. Nowadays, interest in entomophagy has returned and is growing worldwide. In Europe, the "Novel Food" Regulation of 2018 may have contributed to this trend (Regulation EU, 2018). Since edible insect products, such as cricket flour, began to appear on the market, edible insects have gradually moved from gastronomic experience to a daily diet.

Demand for edible insects in European countries is increasing for several reasons, the main one being a reduction in consumption of meat (e.g. flexitarianism). Edible insects may offer a similar nutritional profile to meat and a lower risk of the transmission of zoonoses such as H1N1 influenza and BSE (Persistence Market Research, 2018). In addition, their breeding seems to offer advantages over the breeding of livestock such as higher feed conversion efficiency, higher production per unit area, and the reduced consumption of water and energy. Furthemore, the breeding of insects for food usually raises fewer ethical concerns (Pimentel et al., 1975; Pimentel, 2004; Paoletti and Dreon, 2005; Steinfeld et al., 2006).

Edible insects are usually appreciated for their relatively high energy content and the quality of their protein with an amino acid profile corresponding well to human nutrition. Edible insects contain between 10 and 35 g of protein per 100 g of fresh weight depending on species and developmental stage, etc. (Bukkens, 1997). At the most positive end of the range, insects may provide even more protein than meat, chicken eggs, or dairy products (Mlček et al., 2014). They also contain an optimal fatty acid profile, rich in monounsaturated and/or polyunsaturated fatty acids (Nowak et al., 2016). Furthermore, the basic

* Corresponding author.
E-mail address: zverina@med.muni.cz (O. Zvěřina).

https://doi.org/10.1016/j.jfca.2021.104340
Received 9 September 2021; Received in revised form 1 December 2021; Accepted 8 December 2021
Available online 10 December 2021

component of insect shells is chitin, a great source of insoluble dietary fiber (Whistler, 1993).

As for micronutrients, Rumpold and Schlüter (2013), compiling 236 nutrient compositions of edible insects, determined 100 g of insect material to be a generally rich source of vitamin B2, B5 and B7. Crickets, grasshoppers, locusts, and beetles were also rich in folic acid.

Edible insects are also interesting for their high contents of particular minerals, including iron (Fe), zinc (Zn), calcium (Ca), potassium (K), sodium (Na), phosphorus (P), manganese (Mn), magnesium (Mg) and copper (Cu), with the potential to achieve the dietary reference value (DRV) for some of them in a 100 g portion (Finke, 2002; Rumpold and Schlüter, 2013; Mlček et al., 2014; Kouřimská and Adámková, 2016). The mineral composition is influenced by many factors such as harvesting season, geographical location, living conditions (whether insects are harvested in the wild or bred on a farm), and feed (Payne et al., 2016a, b).

The bioaccessibility rate of minerals in insects is also the subject of current investigation. During processing (e.g. boiling), interactions between minerals and other substances (such as chitin, proteins and phytochemicals) can occur, which can decrease the bioaccessibility of some minerals (Manditsera et al., 2019). In insects, Fe is found predominantly in non-heme form (ferritin, holoferritin and cytochromes); only some species contain hemoglobin, and no species contain myoglobin (Nichol and Locke, 1999; Bauserman et al., 2016). Some data regarding Fe availability have been reported from *in vitro* experiments. Latunde-Dada et al. (2016) showed that species like grasshopper (*Sphenarium purpurascens*), cricket (*Gryllus bimaculatus*), yellow mealworm (*Tenebrio molitor*), and buffalo worm (*Alphitobius diaperinus*) could be excellent sources of bioavailable Fe. Fe solubility was even significantly higher from the insects than from beef sirloin. Grasshopper, cricket, and mealworms also have significantly higher amounts of available Ca, Cu, Mg, Mn, and Zn than beef.

Despite the benefits resulting from consumption of insects, their acceptance by consumers is highly problematic (Huis 2013). Some people consider insects as primitive, disgusting and inferior food, and reject them because of sensory properties, and fear of it (Caparros Megido et al., 2016; Tan et al., 2016; Hartmann and Siegrist, 2017; Gallen et al., 2019).

Edible insects in crushed form seems to enjoy much higher acceptability (Pascucci, 2013; Menozzi et al., 2017; Sogari et al., 2017; Stoops et al., 2017), especially incorporated into a variety of food products, such as crackers, pasta, baked goods, protein bars, raw bars and cookies. Thus, insect powder (flour) has made its way into the market. Due to its longer shelf life and easier handling, it is also used by consumers at home.

Insect powder is the most frequently made from crushed crickets, specifically the house cricket *(Acheta domesticus)*, which appears to be one of the most promising farm insect species for human consumption because of its nutritional profile and breeding advantages (Collavo et al., 2005; Skotnicka et al., 2021).

The main objective of this study was to assess the contents of 14 minerals (Ca, Cd, Co, Cr, Cu, Fe, K, Mg, Mn, Na, Ni, P, Pb, and Zn) in cricket powders, as well as in bodies of popular insect species available in the Czech Republic, including house cricket *(A. domesticus)*, yellow mealworm *(Tenebrio molitor)*, desert locust *(Schistocerca gregaria)* and superworm *(Zophobas morio)*.

The obtained results deepen our understanding of the nutritional composition of edible insects and their role in human nutrition. The possibility of increasing the dietary intake of frequently deficient elements by including the given insect species into the diet is discussed. Special emphasis is devoted to elements of high nutritional importance such as Fe, Zn, and Ca.

2. Materials and methods

The contents of the tested elements in the samples were determined by means of high-resolution continuum source graphite furnace atomic absorption spectrometry (HR-CS GF-AAS) and flame atomic absorption/emission spectrometry (F-AAS/AES) after microwave digestion of the samples.

2.1. Samples and sample treatment

A total of 14 samples including commercially available cricket powder (n = 3) and farmed insect species: house cricket adult (n = 3), yellow mealworm beetle larvae (n = 3), desert locust adult (n = 2), and superworm larvae (n = 3) were used in this study. The samples were purchased from retail supermarkets and pet shops in the south Moravian region (Czech Republic). Prior to analysis, insects were left to starve for two days, then freeze killed, dried in a hot air oven (105 °C, 12 h), and homogenized. Cricket powders were analyzed as received.

In laboratory, all samples were mineralized using an MLS-1200 Mega microwave digestion system (Milestone, Italy). The 250-mg aliquots of each sample were mixed with 4 mL of nitric acid and 0.5 mL of hydrogen peroxide and then digested. Subsequently, the obtained solutions were diluted to 25 mL with MQ water. To ensure the accuracy of the analysis, four certified reference materials, which cover all the investigated elements (SRM 1570a Spinach leaves, INCT-TL-1 Tea leaves, BCR-482 Lichen, and BCR-191 Brown bread) were digested and analyzed together with the samples.

2.2. Determination of elements in digests

The concentrations of elements in the digests were determined using HR-CS GF-AAS (Cd, Co, Cr, Fe, Ni, P, and Pb), F-AAS (Ca, Cu, Mn, Mg, and Zn) and F-AES (K, Na) using ContrAA 800 G (Analytik Jena, Germany) and Unicam Solaar 939 (Cambridge, UK) spectrometers. Measurement conditions were optimized prior to analysis and trueness of the measurement was checked by means of a set of four abovementioned reference materials. The recoveries obtained were in the range of 90–106 %. See supplementary table S1 for detailed information.

2.3. Statistical analyses

The obtained data were statistically analyzed using “R” Statistical Software version 3.4.1 (R Core Team, 2016). Since the normality of the data within individual sample groups could not be assumed, nonparametric Kruskal-Wallis test was used to compare the investigated groups.

3. Results and discussion

The determined ranges of mineral contents are listed in Table 1 (all results can be found in the supplementary table S2). The values are related to dry weight for the reason that European and American consumers accept insects much more willingly in dried form, e.g. as powders or protein bars (Tan et al., 2015; Hartmann et al., 2018). The utilization of dried insects for food processing offers advantages such as a longer shelf life, enriched nutrient levels, and easier transport and handling (Tančinová et al., 2005). Still, in some African countries insects are commonly consumed fresh, however, direct consumption is neither common nor popular in western countries (Van Huis, 2016; Jideani and Netshiheni, 2017; Mutungi et al., 2019).

3.1. Iron content

Cricket powders exhibited the median Fe content of 6.2 mg/100 g which was higher than any of unprocessed edible insect species investigated. Generally, the production of commercial cricket powder involves removing of legs and wings, which, combined with different quality of feed, may explain the difference in Fe contents between unprocessed crickets and cricket powders (Cricket Flours, 2021). The same applies to the other elements. Nevertheless, both cricket powders and

Table 1
Contents of elements in samples of edible insects (in mg/100 g dry weight).

element	cricket powder (made of *Acheta domesticus*)	house cricket (*A. domesticus*)	mealworm (*Tenebrio molitor*)	desert locust (*Schistocerca gregaria*)	superworm (*Zophobas morio*)
Ca	176–254	176–265	66–142	169–190	80–98
Cd	0.002–0.01	0.004–0.006	0.008–0.014	0.003–0.008	0.002–0.003
Co	0.001–0.009	0.001–0.015	0.002–0.008	0.005–0.009	<0.001–0.001
Cr	0.01–0.039	0.013–0.018	0.008–0.023	0.017–0.045	0.012–0.021
Cu	2.1–2.4	1.8–2.9	2.1–2.4	3.5–7.8	1.2–1.5
Fe	5.6–6.4	4.2–5.1	4.5–5	3.6–5	2.9–4.5
K	287–1245	1075–1154	994–1187	651–1131	627–817
Mg	68.2–120.4	84–125	263–335	69–164	95–127
Mn	4.2–5.8	2.5–2.8	0.5–0.9	0.2–0.6	0.5–0.8
Na	157–418	331–413	159–208	151–216	85–111
Ni	0.019–0.064	0.05–0.061	0.046–0.077	0.026–0.103	0.028–0.151
P	989–1233	741–896	798–1054	569–894	410–658
Pb	0.006–0.019	0.01–0.014	0.004–0.01	0.01–0.015	0.002–0.004
Zn	25.4–26.3	16–16.9	11.2–14.1	12.6–17.2	7.9–9.1

examined insect species exhibit richer source of Fe than most of common cereals, grains and flours (Zvěřina et al., 2019; Ertl and Goessler, 2018).

Fe contents in unprocessed edible insects did not significantly differ between the four species (Kruskal-Wallis, $p = 0.3$). This finding allows the individual investigated insect species to be considered as a uniform source of Fe.

In comparison with available data, the contents of Fe observed in house cricket (4.2–5.1 mg/100 g) were slightly lower than those reported by Rumpold and Schlüter (2013) for the same species (6.27–19.68 mg/100 g). The difference may be attributed to the use of different feed (Rumpold and Schlüter, 2013; Finke, 2015a,2015b). The contents of Fe in yellow mealworm and superworm were consistent with the above-mentioned review.

When compared to values published by Zielinska et al. (2015), the iron contents observed here are slightly higher for yellow mealworm (4.5–5.0 vs. 3.29 ± 015 mg/100 g) but lower for desert locust (3.6–5.0 vs 8.38 ± 0.34 mg/100 g). The reason for these different values may be due to the different feeds used.

Some insect species are known to have very high Fe contents; however, such species are not common in this region. For example, *Oecophylla smaragdina* contains 109 mg Fe/100 g in dry weight (Rumpold and Schlüter, 2013) and the termites in Kenya contains 332 mg Fe/100 g. Very high Fe content was reported for the cricket species from Kenya, which contained 1562 mg/100 g (Ramos-Elorduy et al., 1997)

3.2. Zinc content

Zn content was the highest in cricket powders with median value of 25.5 mg/100 g. In unprocessed edible insect species, the highest Zn content (16.9 mg/100 g) was observed in house cricket, while the lowest amount (7.9 mg/100 g,) was found in superworm. Other authors found very similar amounts of Zn to our values in the same insect species (7.29–18.64 mg/100 g in dry weight) (Rumpold and Schlüter, 2013; Zielińska et al., 2015). The study of Rumpold and Schlüter (2013) shows that nymphs of domestic cricket (29.69 mg Zn/100 g in dry weight, measured in one sample) can be an even better source of Zn than adults (15.91–18.64 mg/100 g in dry weight). In our work, only adults of house cricket were used, which are commonly processed for the production of cricket powder.

Zn deficiency occurs in human populations globally, with pregnant women and children under 5 being at the highest risk (Balei et al. 2015). It seems that the cricket powder can greatly promote an adequate dietary supply of Zn. It contains much more Zn than cereals (Ertl and Goessler, 2018). Among the species of edible insects, there are even Zn-richer species than the cricket. Such is the case of locust species *Sphenarium histrio* living in Mexico, which contains 78 mg/100 g in dry weight (Rumpold and Schlüter, 2013).

3.3. Calcium content

In addition to Fe and Zn, Ca is also an element whose intake is often inadequate in the diet. Its median content in cricket powders was 186 mg/100 g. Measured values of 208 and 180 mg/100 g in house cricket and desert locust, respectively, are in good agreement with reported general Ca contents in the insects (Rumpold and Schlüter, 2013; Latunde-Dada et al., 2016). On the other hand, yellow mealworm beetle and superworm contained about half that amount. Unlike Fe, the content of Ca varied significantly between individual species. Therefore, the degree to which diet can be enriched with Ca through the inclusion of insects depends highly on the chosen species. It was shown that Ca contents in insects can be increased by up to 20 times through the use of Ca- fortified food. However, the apparent increase was composed of residues in the digestive tract rather than Ca incorporated in the insects' body (Finke, 2004). This might be an explanation for some of the very high Ca contents reported such as 1290 mg/100 g for house cricket (Barker et al., 1998). To eliminate this distortion, insects in this work were left without feed for two days before analysis.

Despite the fact that Ca contents determined here are similar to those reported by studies that proposed insects as an alternative source of Ca, the nutritive significance of such levels is disputable (see chapter Meeting DRV by a single serving of edible insects).

3.4. Potentially toxic elements

The safety of entomophagy is an area which requires extensive research due to the great potential of the practical use of edible insects in the food industry. A risk may arise from the presence of heavy metals due to their ability to accumulate in the insect tissues (Murefu et al., 2019). Recently, elevated levels of Cd, Cu, Mn, Ni, Pb, and Zn have been observed in some edible insects (Handley et al., 2007; Banjo et al., 2010; Greenfield et al., 2014).

Our data showed that the maximum Cd and Pb contents were 0.014 and 0.019 mg/100 g, respectively. The maximum permitted levels of Cd and Pb in insects has not been officially determined; nevertheless, the contents observed in this work are far below the limits suggested for crustaceans, which are anatomically similar (0.05 mg/100 g). The maximum permitted levels of heavy metals are usually given for foods in fresh weight. Since contents in dry weight that are presented in our study are lower than the recommended values in fresh weight of crustaceans, we can assume that no insect species investigated in our work pose a risk with respect to levels of Cd or Pb contamination (Commission Regulation, 2006). The maximum detected levels of Pb in insects also do not exceed the limits of Pb for cereals and cereal products (0.02 mg/100 g) (EFSA (European Food Safety Authority), 2019).

3.5. Nutritional significance of a single serving of edible insects in the context of DRV

In this section, content of particularly important elements determined in the samples is compared to that in foodstuffs considered as their good sources. Contents of minerals in the foodstuffs used for comparison were obtained from USDA database (2019). Furthermore, to illustrate the significance of the assessed edible insects as sources of minerals, the amounts of minerals provided in a single portion of dried insect are compared to DRV (Dietary Recommended Values) in Table 2. The DRV indicates a daily amount of a nutrient needed to maintain health in an otherwise healthy individual. A portion size of 100 g was chosen since the standard serving size for edible insects has not yet been proposed, and this size portion is also standard on food labels.

Food items such as red meat and offal are considered to be some of the best sources of Fe (EFSA (European Food Safety Authority), 2015b) with only 36 g of goose liver or 2 large-sized portions of raw beef (550 g) providing the DRV. The DRV for Fe may be also achieved by consuming the unrealistic amount of 20 egg yolks (provided 1 egg yolk weighs 20 g), 1.5 kg of broccoli, or approximately 240 g of insects such as house cricket, yellow mealworm beetle, and desert locust, or 344 g of superworm.

Foods that contain relatively high amounts of Zn are meat, egg yolks, grains, and legumes (EFSA (European Food Safety Authority), 2014). As little as about 57 g of house cricket, or 65 g of yellow mealworm beetle or desert locust can provide the DRV compared to 200 g of beef, 20 egg yolks, and approximately 290 g raw lentils or wheat whole-grain flour.

According to some studies (Adámková et al., 2014), edible insects can be as good a source of Ca as milk; however, to drink 3 glasses of milk may be an easier way of meeting the DRV for Ca than eating 555 g of desert locust, or approximately 1.1 kg of yellow mealworm beetle or superworm. The DRV for Ca can be achieved also by 2 full handfuls of poppy seeds, 140 g of gouda cheese, or approximately 2 kg of broccoli.

For effective Ca absorption in the body, it is also important to ensure an adequate Ca to P ratio, which should be from 1.4:1 to 1.9:1 (EFSA (European Food Safety Authority), 2015a). None of our insect samples achieved this ratio. The measured content of P in house cricket and desert locust was four times greater than the respective content of Ca. In superworm it was five times greater, and in samples of yellow mealworm beetles it was as much as eleven times greater. Since other authors also report a low ratio of calcium to phosphorus in insects (Rumpold and Schlüter, 2013; Tang et al., 2019), we can infer that calcium in the given insects is difficult to absorb effectively.

In contrast, we found that the intake of Cu, P, and Zn from a 100-g portion of some insect species can even exceed the DRV for these elements.

3.6. Implication of cricket powder for gastronomy

Cricket powder can be used in same way as an ordinary flour, and its properties (medium brown color, and slightly nut- to cereal-like taste and aroma) allow it to be added to meals and foods without being notices by consumers (Barton et al., 2020).

On the other hand, in terms of nutritional composition it is a fundamentally different ingredient. In addition to a more favorable ratio of macronutrients (high amount of protein at the expense of carbohydrates, high dietary fiber, and fat content, especially unsaturated, see Montowska et al., 2019), it also contains a richer mineral profile. In comparison with wheat flour, cricket powder contains much more Fe (6.2 vs 3.86 mg/100 g), Zn (25.5 vs. 3.24 mg/100 g), and Ca (186 vs. 38 mg/100 g), also Mn (4.3 vs. 3.56 mg/100 g), K (384 vs. 376 mg/100 g), Cu (2.3 vs. 0.45 mg/100 g), Na (174 vs. 3 mg/100 g), and P (1097 vs. 376 mg/100 g), only content of Mg is lower (79.2 vs. 136 mg/100 g) (median of determined contents vs.USDA (U.S. Department of Agriculture), 2019).

Cricket powder is also gluten-free which makes it suitable for people with celiac disease or gluten allergy (Pauter et al., 2018; Kowalczewski et al., 2019). However, the absence of gluten results in slightly different dough properties and requires some practice to learn how to bake with the cricket powder – especially if it is added in large quantities.

Cricket powder may be combined with cereal flours and, thus is used as a partial replacement of common types of flour in various cereal products (muffins, bread, pasta, cookies etc.) to increase their nutritional profile, which is highly desirable. The added proportion of cricket powder in the range of 2–15 % is the most frequently used in the scientific studies (Pauter et al., 2018; Duda et al., 2019; González et al., 2019; Biró et al., 2020).

To demonstrate the nutritional consequences, in this work, cricket powder was used as a 10 % flour replacement in recipes for pasta and bread, and as a 50 % replacement in the pancake recipe (Fig. 1).

- Pasta recipe (90 g flour, 10 g cricket powder, 1 egg, olive oil and salt) for 1 portion
- Bread recipe (150 g whole-grain flour, 120 g wheat flour, 30 g cricket powder, 1 tsp dried yeast, 1 tsp salt, 1 tsp cumin, 300 mL water)
- Pancake recipe (2 tbsp wheat flour, 2 tbsp cricket powder, 1 medium banana, 1 egg, 60 mL milk) for 1 portion

Of all the minerals, changes of Zn content were the most apparent with an increase ranging from 92 to 386 % in meals. The greatest increase in elements is observed in the pancakes with the highest proportion of cricket powder used: approx. 48 % increase in Ca content, 71 % in Fe and approx. 386 % in Zn (Table 3).

Replacing ten percent of the wheat flour with cricket powder is almost indistinguishable in the final taste of the meal. Yet, this enrichment of a common bread recipe increased Zn content by 92 %, Ca by 44 % and Fe by 15 % (Table 3). It seems that one third of the DRV for Zn may be achieved by a portion of pancakes.

Table 2
Contribution of a 100-g serving of dried edible insect per day to the DRV of some essential elements.

Element	DRV*		Percentage of DRV provided by a 100 g serving of dried edible insects			
	AI (mg/day)	PRI (mg/day)	house cricket (*Acheta domesticus*)	yellow mealworm (*Tenebrio molitor*)	desert locust (*Schistocerca gregaria*)	superworm (*Zophobas morio*)
Ca	–	1000	18–27	7–14	17–19	8–10
Cu	1.6	–	113–181	131–150	219–488	75–94
Fe	–	11	38–46	41–45	33–45	26–41
K	3500	–	31–33	28–31	19–32	18–23
Mg	350	–	24–36	17–96	20–47	27–32
Na	2000	–	17–21	8–11	8–11	5–6
P	550	–	135–163	145–192	104–163	75–120
Zn	–	9.4	170–180	119–150	134–183	84–97

* DRV in mg per adult male, obtained from EFSA's DRVs. The Adequate Intake (AI) was used for Cu, Mg, Na, K, and P. The Population Reference Intake (PRI) was used for Fe, Zn, and Ca (EFSA (European Food Safety Authority), 2019).

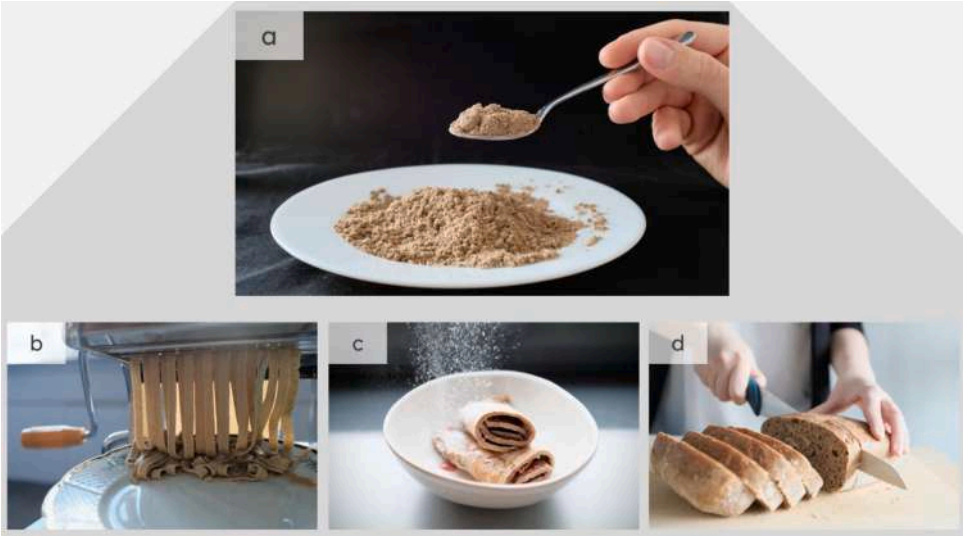

Fig. 1. Cricket flour (a) and the examples of recipes with its addition: b) a pasta, c) pancakes, d) a bread.

Table 3
Changes in the mineral profile of the meals caused by replacing part of the wheat flour in the recipe with cricket powder.

Meal (and portion of wheat flour replaced with cricket powder)	Changes in the contents of minerals in food (mg/100 g) with the addition of cricket powder		
	Fe	Zn	Ca
Pasta (10 %)	1.3 → 1.6	1.4 → 2.9	31.3 → 42.6
Bread (10 %)	3.3 → 3.8	2.5 → 4.8	38.8 → 56.0
Pancakes (50 %)	0.7 → 1.2	0.7 → 3.4	41.7 → 61.9

4. Conclusion

Including edible insects and derived products (e.g., cricket powder) in the human diet can increase dietary variety. Much is known about their high protein content, but also worth noting is their mineral content. Cricket powder can be a simple means of improving the mineral profile of meals, including those plant based. Besides vegetarian diet, it can promote adequate nutrition in people with high nutritional requirements, such as adolescent girls, pregnant women, seniors, and malnourished patients with chronic diseases. The bioavailability of minerals is, however, still in need of investigation if edible insects are to be assessed as reliable sources of such minerals.

Data availability

No data was used for the research described in the article.
Data will be made available on request.

Funding information

The work was funded by Masaryk University (project MUNI/A/1608/2020).

Author statement

Pavlína Kosečková – methodology, writing – original draft, data curation, visualization
Ondřej Zvěřina – methodology, validation, formal analysis, supervision
Marie Pěchová – methodology, writing – original draft
Martina Krulíková – methodology
Eva Duborská – writing – original draft
Marie Borkovcová – conceptualization, methodology, resources.

Declaration of Competing Interest

The authors declare no conflict of interest.

Appendix A. Supplementary data

Supplementary material related to this article can be found, in the online version, at doi:https://doi.org/10.1016/j.jfca.2021.104340.

References

Adámková, A., Kouřimská, L., Borkovcová, M., Mlček, J., Bednářová, M., 2014. Calcium in edible insects and its use in human nutrition. Potravinárstvo 8 (1), 233–238. https://doi.org/10.5219/366.
Banjo, A.D., Lawal, O.A., Fasunwon, B.T., Alimi, G.O., 2010. Alkali and heavy metal contaminants of some selected edible arthropods in South Western Nigeria. Am. Eurasian J. Toxicol. Sci. 2 (1), 25–29.
Barker, D., Fitzpatrick, M.P., Dierenfeld, E.S., 1998. Nutrient composition of selected whole invertebrates. Zoo Biol. 17 (2), 123–134. https://doi.org/10.1002/(SICI)1098-2361(1998)17:2<123. AID-ZOO7>3.0.CO;2-B.
Barton, A., Richardson, C.D., McSweeney, M.B., 2020. Consumer attitudes toward entomophagy before and after evaluating cricket *(Acheta domesticus)*-based protein powders. J. Food Sci. 85 (3), 781–788. https://doi.org/10.1111/1750-3841.15043.
Bauserman, M., Lokangaka, A., Kodondi, K.-K., Gado, J., et al., 2016. Caterpillar cereal as a potential complementary feeding product for infants and young children: nutritional content and acceptability. Matern. Child Nutr. 11, 214–220. https://doi.org/10.1111/mcn.12037.
Biró, B., Sipos, M.A., Kovács, A., Badak-Kerti, K., Pásztor-Huszár, K., Gere, A., 2020. Cricket-enriched oat biscuit: technological analysis and sensory evaluation. Foods 9 (11). https://doi.org/10.3390/foods9111561.
Bukkens, S.G., 1997. The nutritional value of edible insects. Ecol. Food Nutr. 36, 287–319. https://doi.org/10.1080/03670244.1997.9991521.
Caparros Megido, R., Gierts, C., Blecker, C., Brostaux, Y., Haubruge, É., Alabi, T., Francis, F., 2016. Consumer acceptance of insect-based alternative meat products in Western countries. Food Qual. Prefer. 52, 237–243. https://doi.org/10.1016/j.foodqual.2016.05.004.
Collavo, A., Glew, R.H., Huang, Y.-S., Chuang, L.T., Bosse, R., Paoletti, M.G., 2005. Housekricket Smallscale Farming in Ecological Implications of Minilivestock: Potential of Insects, Rodents, Frogs and Snails. View Project. Sci. Publ. Enfield, USA. 515–540.
Commission Regulation, 2006. Commission Regulation (EC) No 1881/2006 of 19 December 2006 setting maximum levels for certain contaminants in foodstuffs. Off. J. Eur. Union. L 364/5.
Cricket Flours, 2021. How to Make Cricket Flour (accessed 07 July 2021). https://www.cricketflours.com/how-to-make-cricket-flour/.

Duda, A., Adamczak, J., Chełmińska, P., Juszkiewicz, J., Kowalczewski, P., 2019. Quality and Nutritional/Textural properties of durum wheat pasta enriched with cricket powder. Foods. 8 (2), 46. https://doi.org/10.3390/foods8020046.

EFSA (European Food Safety Authority), 2014. Scientific Opinion on Dietary Reference Values for Zinc. https://doi.org/10.2903/j.efsa.2014.3844 (accessed 14 November 2020).

EFSA (European Food Safety Authority), 2015a. Scientific Opinion on Dietary Reference Values for Phosphorus. https://doi.org/10.2903/j.efsa.2015.4185 (accessed 14 November 2020).

EFSA (European Food Safety Authority), 2015b. Scientific Opinion on Dietary Reference Values for Iron. https://doi.org/10.2903/j.efsa.2015.4254 (accessed 14 November 2020).

EFSA (European Food Safety Authority), 2019. DRV Finder. https://www.efsa.europa.eu/en/interactive-pages/drvs?fp%C5%99eklada%C4%8Dlid=IwAR1Bp%C5%99eklVHFPPqOdkRDw9uKvvEGCnIi6KHhBAO7mNvhM-BqR5yQ0v5h4dFO7Oc.

Ertl, K., Goessler, W., 2018. Grains, whole flour, white flour, and some final goods: an elemental comparison. Eur. Food Res. Technol. 244, 2065–2075. https://doi.org/10.1007/s00217-018-3117-1.

Finke, M.D., 2002. Complete nutrient composition of commercially raised invertebrates used as food for insectivores. Zoo Biol. 21, 269–285. https://doi.org/10.1002/zoo.10031.

Finke, M.D., 2004. Nutrient content of insects. In: Capinera, J.L. (Ed.), Encyclopedia of Entomology. Kluwer Academic, pp. 1563–1575.

Finke, M.D., 2015a. Complete nutrient content of four species of commercially available feeder insects fed enhanced diets during growth. Zoo Biol. 34 (6), 554–564. https://doi.org/10.1002/zoo.21246.

Finke, M.D., Rojo, S., Roos, N., et al., 2015b. The European Food Safety Authority scientific opinion on a risk profile related to production and consumption of insects as food and feed. J. Insects Food Feed. 1 (4), 245–247. https://doi.org/10.3920/JIFF2015.x006.

Gallen, C., Pantin-Sohier, G., Peyrat-Guillard, D., 2019. Cognitive acceptance mechanisms of discontinuous food innovations: the case of insects in France. Rech. Appl. En Mark. 34 (1), 48–73. https://doi.org/10.1177/2051570718791785.

González, C.M., Garzón, R., Roselli, C.M., 2019. Insects as ingredients for bakery goods. A comparison study of *H. Illucens, A. domestica* and *T. Molitor* flours. IFSET. 51. Innovations in Food Science and Technology at the Spanish National Research Council (CSIC), pp. 205–210. https://doi.org/10.1016/j.ifset.2018.03.021.

Greenfield, R., Akala, N., Van Der Bank, F.H., 2014. Heavy metal concentrations in two populations of Mopane worms (*Imbrasia belina*) in the Kruger National Park pose a potential human health risk. Bull. Environ. Contam. Toxicol. 93, 316–321. https://doi.org/10.1007/s00128-014-1324-4.

Handley, M.A., Hall, C., Sanford, E., et al., 2007. Globalization, binational communities, and imported food risks: results of an outbreak investigation of lead poisoning in Monterey County. California. Am J Public Health. 97 (5), 900–906. https://doi.org/10.2105/AJPH.2005.074138.

Hartmann, C., Siegrist, M., 2017. Consumer perception and behaviour regarding sustainable protein consumption: a systematic review. Trends Food Sci. Technol. 61, 11–25. https://doi.org/10.1016/j.tifs.2016.12.006.

Hartmann, C., Ruby, M.B., Schmidt, P., Siegrist, M., 2018. Brave, health-conscious, and environmentally friendly: positive impressions of insect food product consumers. Food Qual. Prefer. 68, 64–71. https://doi.org/10.1016/j.foodqual.2018.02.001.

Jideani, A.I.O., Netshiheni, R.K., 2017. NetshiheniSelected edible insects and their products in traditional medicine, food and pharmaceutical industries in Africa: utilisation and prospects. In: Mikkola, H. (Ed.), Future Foods. IntechOpen.

Kouřimská, L., Adámková, A., 2016. Review article: nutritional and sensory quality of edible insects. NFSJ. 4, 22–26. https://doi.org/10.1016/j.nfs.2016.07.001.

Kowalczewski, P., Walkowiak, L.K., Masewicz, L., Bartczak, O., Lewandowicz, J., Kubiak, P., Baranowska, H.M., 2019. Gluten-free bread with cricket powder—mechanical properties and molecular water dynamics in dough and ready product. Foods 8 (7). https://doi.org/10.3390/foods8070240.

Latunde-Dada, G.O., Yang, W., Aviles, M.V., 2016. In vitro Iron availability from insects and sirloin beef. J. Agric. Food Chem. 64 (44), 8420–8424. https://doi.org/10.1021/acs.jafc.6b03286.

Manditsera, F.A., Luning, P.A., Fogliano, V., Lakemond, C.M.M., 2019. Effect of domestic cooking methods on protein digestibility and mineral bioaccessibility of wild harvested adult edible insects. Food Res. Int. 121, 404–411. https://doi.org/10.1016/j.foodres.2019.03.052.

Menozzi, D., Sogari, G., Veneziani, M., Simoni, E., Mora, C., 2017. Eating novel foods: an application of the Theory of Planned Behaviour to predict the consumption of an insect-based product. Food Qual. Prefer. 59, 27–34. https://doi.org/10.1016/j.foodqual.2017.02.001.

Mlček, J., Rop, O., Borkovcová, M., Bednářová, M., 2014. A comprehensive look at the possibilities of edible insects as food in Europe–a review. Pol J. Food Nutr. Sci. 64 (3), 147–157. https://doi.org/10.2478/v10222-012-0099-8.

Montowska, M., Kowalczewski, P.Ł., Rybicka, I., Fornal, E., 2019. Nutritional value, protein and peptide composition of edible cricket powders. Food Chem. 289, 130–138. https://doi.org/10.1016/j.foodchem.2019.03.062.

Murefu, T.R., Macheka, L., Musundire, R., Manditsera, F.A., 2019. Safety of wild harvested and reared edible insects: A review. Food Control 101, 209–224. https://doi.org/10.1016/j.foodcont.2019.03.003.

Mutungi, C., Irungu, F.G., Nduko, J., Mutua, F., Affognon, H., Nakimbugwe, D., Ekesi, S., Fiaboe, K.K.M., 2019. Postharvest processes of edible insects in Africa: a review of processing methods, and the implications for nutrition, safety and new products development. Crit. Rev. Food Sci. Nutr. 59 (2), 276–298. https://doi.org/10.1080/10408398.2017.1365330.

Nichol, H., Locke, M., 1999. Secreted ferritin subunits are of two kinds in insects molecular cloning of cDNAs encoding two major subunits of secreted ferritin from Calpodes ethlius. Insect Biochem. Mol. Biol. 29 (11), 999–1013. https://doi.org/10.1016/s0965-1748(99)00076-4.

Nowak, V., Persijn, D., Rittenschober, D., Charrondiere, U.R., 2016. Review of food composition data for edible insects. Food Chem. 193, 39–46. https://doi.org/10.1016/j.foodchem.2014.10.114.

Paoletti, M.G., Dreon, A.L., 2005. Minilivestock, environment, sustainability, and local knowledge disappearance. In: Paoletti, M.G. (Ed.), Ecological Implications of Minilivestock. Potential of Insects, Rodents, Frogs and Snails. Science Publishers Inc., Enfield, pp. 1–18.

Pascucci, S., 2013. Information Bias condemning radical food innovators? The case of insect-based products in the Netherlands. IFAMA 16 (3), 1–16 (accessed 07 July 2021). https://www.ifama.org/resources/Documents/v16i3/Pascucci-Magistris.pdf.

Pauter, P., Różańska, M., Wiza, P., Dworczak, S., Grobelna, N., Sarbak, P., KowalczewskI, P., 2018. Effects of the replacement of wheat flour with cricket powder on the characteristics of muffins. Inst. Food Technol. Plant Origin 17 (3), 227–233. https://doi.org/10.17306/J.AFS.2018.0570.

Payne, C.L.R., Scarborough, P., Rayner, M., Nonaka, K., 2016a. Are edible insects more or less' healthy' than commonly consumed meats? A comparison using two nutrient profiling models developed to combat over- and undernutrition. Eur. J. Clin. Nutr. 70 (3), 285–291. https://doi.org/10.1038/ejcn.2015.149.

Payne, C.L.R., Nonaka, K., Scarborough, P., Rayner, M., 2016b. A systematic review of nutrient composition data available for twelve commercially available edible insects, and comparison with reference values. Trends Food Sci. Technol. 47, 69–77. https://doi.org/10.1016/j.tifs.2015.10.012.

Persistence Market Research, 2018. Edible Insects Market: Global Analysis, Size, Share, Value, Demand, Market Growth by 2024. https://www.persistencemarketresearch.com/market-research/edible-insects-market.asp.

Pimentel, D., 2004. Livestock production and energy use. In: Cleveland, C.J. (Ed.), Ed.), Encyclopedia of Energy. Elsevier Science, pp. 671–676.

Pimentel, D., Dritschilo, W., Krummel, J., Kutzman, J., 1975. Energy and land constraints in food protein production. Science 190 (42), 754–761. https://doi.org/10.1126/science.190.4216.754.

R Core Team, 2016. R: A Language and Environment for Statistical Computing. Vienna, Austria. Available online at: https://www.R-project.org/ (accessed 7 March 2020).

Ramos-Elorduy, J., Moreno, J.M.P., Prado, E.E., et al., 1997. Nutritional value of edible insects from the state of Oaxaca. Mexico. J Food Compost Anal. 10 (2), 142–157. https://doi.org/10.1006/jfca.1997.0530.

Regulation (EU), 2018. Commission Implementing Regulation (EU) 2018/1023 of 23 July 2018 correcting Implementing Regulation (EU) 2017/2470 establishing the Union list of novel foods. Off. J. Eur. Union, L 187, 1–133.

Rumpold, B.A., Schlüter, O.K., 2013. Nutritional composition and safety aspects of edible insects. Mol. Nutr. Food Res. 57 (5), 802–823. https://doi.org/10.1002/mnfr.201200735.

Skotnicka, M., Karwowska, K., Kłobukowski, F., Borkowska, A., Pieszko, M., 2021. Possibilities of the Development of Edible Insect-Based Foods in Europe. Foods. https://doi.org/10(4)10.3390/foods10040766.

Sogari, G., Menozzi, D., Mora, C., 2017. Exploring young foodies' knowledge and attitude regarding entomophagy:a qualitative study in Italy. Int. J. Gastron. Food Sci. 7, 16–19. https://doi.org/10.1016/j.ijgfs.2016.12.002.

Steinfeld, H., Gerber, P., Wassenaar, T., Castel, et al., 2006. Livestock's Long Shadow, Environmental Issues and Options. FAO, Rome, Italy. Available online at: http://www.fao.org/3/a0701e/a0701e00.pdf (accessed 10 November 2020).

Stoops, J., Vandeweyer, D., Crauwels, S., Verreth, C., Boeckx, H., Van Der Borght, M., Claes, J., Lievens, B., Van Campenhout, L., 2017. Minced meat-like products from mealworm larvae *(Tenebrio molitor and Alphitobius diaperinus)*: microbial dynamics during production and storage. IFSET 41, 1–9. https://doi.org/10.1016/j.ifset.2017.02.001.

Tan, H.S.G., Fischer, A.R.H., Tinchan, P., Stieger, M., Steenbekkers, L.P.A., Van Trijp, H.C.M., 2015. Insects as food: exploring cultural exposure and individual experience as determinants of acceptance. Food Qual. Prefer. 42, 78–89. https://doi.org/10.1016/j.foodqual.2015.01.013.

Tan, H.S.G., Fischer, A.R.H., Van Trijp, H.C.M., Stieger, M., 2016. Tasty but nasty? Exploring the role of sensory-liking and food appropriateness in the willingness to eat unusual novel foods like insects. Food Qual. Prefer. 48, 293–302. https://doi.org/10.1016/j.foodqual.2015.11.001.

Tančinová, D., Maková, J., Felsöciová, S., Kačániová, M., Kmeť, V., 2005. Mikrobiológia Potravín, First ed.SLovenská Poľnohospodárska Univerzita, Nitra.

Tang, C., Yang, D., Liao, H., et al., 2019. Edible insects as a food source: a review. Food Prod Process and Nutr. 1 (8) https://doi.org/10.1186/s43014-019-0008-1.

USDA (U.S. Department of Agriculture), 2019. FoodData Central Search Results (accessed 18 November 2020). https://fdc.nal.usda.gov/index.html.

Van Huis, A., 2016. Edible insects are the future? Proc. Nutr. Soc. 75 (3), 294–305. https://doi.org/10.1017/S0029665116000069.

Van Huis, A., Van Itterbeeck, J., Klunder, H., Mertens, et al., 2013. Edible Insects: Future Prospects for Food and Feed Security. FAO Forestry paper 171, Rome, Italy. . Available online at: http://www.fao.org/3/i3253e/i3253e.pdf (accessed 10 November 2020).

Whistler, R.L., 1993. Chitin. In: Whistler, R.L., Bemiller, J.N. (Eds.), Industrial Gums: Polysaccharides and Their Derivatives. Academic Press, pp. 601–604.

Zielińska, E., Baraniak, B., Karaś, M., Jakubczyk, A., Rybczyńska, A.K., 2015. Selected species of edible insects as a source of nutrient composition. Food Res. Int. 77, 460–466. https://doi.org/10.1016/j.foodres.2015.09.008.

Zvěřina, O., Kuta, J., Coufalík, P., Kosečková, P., Komárek, J., 2019. Simultaneous determination of cadmium and iron in different kinds of cereal flakes using high-

resolution continuum source atomic absorption spectrometry. Food Chem. 298 https://doi.org/10.1016/j.foodchem.2019.125084.

Journal of Trace Elements in Medicine and Biology 68 (2021) 126869

Contents lists available at ScienceDirect

Journal of Trace Elements in Medicine and Biology

journal homepage: www.elsevier.com/locate/jtemb

A simple dilute-and-shoot procedure for the determination of platinum in human pleural effusions using HR-CS GF-AAS

Ondřej Zvěřina [a,*,1], Ondřej Venclíček [b,1], Jan Kuta [c], Pavel Coufalík [d], Ingrid Hagarová [e], Kristián Brat [b]

[a] Department of Public Health, Faculty of Medicine, Masaryk University, Kamenice 5, 625 00, Brno, Czech Republic
[b] Department of Respiratory Diseases, University Hospital Brno and Faculty of Medicine, Masaryk University, Jihlavská 20, 625 00, Brno, Czech Republic
[c] Research Centre for Toxic Compounds in the Environment (RECETOX), Faculty of Science, Masaryk University, Kamenice 5, 625 00, Brno, Czech Republic
[d] Institute of Analytical Chemistry of the Czech Academy of Sciences, Veveří 97, 602 00, Brno, Czech Republic
[e] Institute of Laboratory Research on Geomaterials, Faculty of Natural Sciences, Comenius University in Bratislava, Slovakia

ARTICLE INFO

Keywords:
Lung cancer
Platinum
Pleural effusion
HR-CS GF-AAS

ABSTRACT

Background: High-resolution continuum source AAS is an emerging technique for the determination of trace elements in clinical analysis. We aimed to develop a method for the direct determination of platinum (Pt) in pleural effusions that could deepen the understanding of the dynamics of intrapleural Pt concentration during cytostatic therapy.

Materials and methods: Samples were collected by thoracic drainage from five patients with lung cancer undergoing platinum based chemotherapy. A simple dilute-and-shoot method for Pt determination in the pleural effusions was developed. Ashing of the sample in an oxygen flow in a graphite tube allowed for direct analysis without prior mineralization. The trueness of the method was verified using an independent technique (ICP-MS). As platinum derivatives are only active in its free form (not bound to proteins), Pt in samples was further divided into free and protein-bound forms by means of ultrafiltration.

Results: Using the proposed method, Pt contents (free and total) were determined in samples collected at different times after the intravenous application of the Pt derivative. The concentration of total Pt reached values of up to 5,000 μg/L and different patterns of its dynamics in intrapleural fluid were observed.

Conclusions: The developed method enables the fast and simple determination of Pt in biological fluids. It may be applied on a large scale to improve the understanding of Pt dynamics during cytostatic therapy, and also to determine the optimal timing of both thoracic drainage and administration of systemic chemotherapy.

1. Introduction

High-resolution continuum source atomic absorption spectrometry (HR-CS AAS) has brought significant improvements and new possibilities with respect to the determination of trace elements in biological materials. The importance of this accurate and sensitive analytical method is growing, especially in the case of the analysis of medical samples and microsamples. In this work, this method was adapted to determine the concentration of platinum (Pt) in pleural effusions from lung cancer patients.

Lung cancer is the most common form of cancer worldwide (with the exception of skin cancers) with high incidence and mortality. In 2018, more than two million new cases were reported worldwide [1], claiming 1,761,007 lives [2]. In the Czech Republic, >6,500 new cases of lung cancer were reported in 2016 [3]. This project focused on lung cancer patients presenting with a significant pleural effusion that required thoracic drainage.

Pleural effusion is an accumulation of a pathological amount of fluid in the pleural cavity [4]. The quantity is not precisely defined, we consider pleural effusion to be any amount of fluid that is visible in the pleural cavity using a CT, X-ray or ultrasound of the chest. The occurrence of pleural effusion in patients with lung cancer ranges between 7 and 23 % [5]. Malignant pleural effusion most frequently occurs in patients with lung cancer of adenocarcinoma histology, followed by

* Corresponding author at: Department of Public Health, Masaryk University, Kamenice 5, 625 00, Brno, Czech Republic.
E-mail address: zverina@med.muni.cz (O. Zvěřina).
[1] The authors contributed equally to this work.

https://doi.org/10.1016/j.jtemb.2021.126869
Received 7 June 2021; Received in revised form 21 September 2021; Accepted 24 September 2021
Available online 28 September 2021
0946-672X/

patients with small-cell lung cancer [5]. Significant pleural effusion presents by dyspnoea and it is often necessary to manage it by thoracic drainage [6].

In such cases, it is possible to determine the concentrations of Pt derivatives in pleural effusion samples, collected from the chest drain at specific time points after the intravenous application of Pt-based cytostatic therapy.

Only a few papers addressed this topic previously, mostly reporting on the concentration of Pt in the pleural effusion after its intrapleural administration [7], or the concentration of Pt directly in the tumor tissue [8].

The clinical importance of the pleural dynamics of Pt concentration, particularly of its effective free fraction (i.e. protein-unbound), lies in the possibility of timing systemic chemotherapy within the management of pleural effusion. Both cisplatin (cis-DDP) and carboplatin (CBDCA) are irreversibly bound to proteins, however, the protein binding of CBDCA is lower [9]. The question is whether the concentration of free Pt in the pleural effusion may directly affect the metastases of the pleura (in the sense of local therapy) and whether it would be advantageous to leave a certain amount of pleural effusion, containing the active Pt (a volume tolerable by the patient), intentionally in situ to maintain the effect of Pt on the pleural metastases, rather than attempting to completely evacuate the pleural cavity.

The clinical aim of the investigation should therefore be to find the optimal timing of both thoracic drainage and the administration of systemic chemotherapy. Analysis of pleural effusion samples collected regularly during the platinum-based chemotherapy may provide clinically relevant information about the time course of Pt concentration. However, there is a limited number of patients in need of both chest drainage and platinum-based chemotherapy at the same time, therefore obtaining the samples itself is complicated.

Since the measurement of Pt concentrations in biological fluids may be not so straightforward, new methods of laboratory testing are desired. Graphite furnace atomic absorption spectrometry (GF-AAS) is among the methods traditionally used for the determination of Pt in clinical samples [10,11] together with inductively coupled plasma-mass spectrometry, adsorptive voltammetry, and neutron activation analysis [12,13]. A modern version of GF-AAS equipped with a high-resolution continuum source (HR-CS) instrument has brought numerous improvements to the technique [14–16] and HR-CS GF-AAS is now gradually being put into practice. For the analysis of clinical samples, the salient feature of the technique is background correction carried out mathematically using HR spectra, which allows the handling of higher nonspecific absorbance than classical approaches like deuterium or Zeeman background corrections [14]. This feature is particularly useful when analyzing complex biological matrices such as pleural effusions.

Our main goal was to develop a simple dilute-and-shoot method for the direct determination of Pt using HR-CS GF-AAS despite the fact that pleural effusions represent a complicated matrix containing substantial amounts of proteins. The second aim was to fractionate Pt contained in the pleural effusions into free and protein-bound forms by means of ultrafiltration using a 20 kDa cut-off.

To our best knowledge, HR-CS GF-AAS method for a direct determination of Pt in biological fluids without a prior sample mineralization has not yet been described in the literature. In addition, we explored the possibility of modulating signal intensity by using secondary spectral lines of Pt which also opens up an attractive opportunity of the simultaneous co-determination of iron in a single run.

2. Experimental

2.1. Experimental setup

The experimental scheme was designed to develop, test, and validate the analytical procedure for Pt determination using HR-CS GF-AAS. For the determination of total Pt content, diluted samples were dosed into the graphite tube and ashed in the oxygen flow prior to atomization. Free Pt was determined after its ultrafiltration (the filtrate was directly dosed into the tube).

The trueness of Pt measurement was evaluated by an independent determination of Pt using inductively coupled plasma-mass spectrometry (ICP-MS).

Protein content in an aliquot of the sample was determined by means of the bicinchoninic acid method (BCA) followed by UV–vis detection.

2.2. HR-CS GF-AAS instrumentation

A ContrAA 800 G high-resolution continuum source atomic absorption spectrometer (Analytik Jena, Germany) was used for all performed measurements. The spectrometer is equipped with a transversely heated graphite furnace and a 300 W xenon short-arc lamp, operating in hot-spot mode, combined with a high-resolution echelle double monochromator and CCD array detector.

The determination of Pt in pleural effusions was performed on both the primary atomic line of 265.945 nm (using three pixel integration and also signal attenuation, i.e. the signal was read at the wings of the line – *see* Section 2.6. *Pt determination by HR-CS GF-AAS*) and the less sensitive secondary lines 306.471 nm and 292.979 nm for a possible reduction of excessive signals.

2.3. Reagents and standards

A solution of Triton X-100 surfactant (Merck, Germany) was used for the dilution of samples. Pt standard (Analytika Ltd., Czech Republic) and HNO_3 (Analpure, Analytika Ltd., Czech Republic) were used to prepare calibration solutions. BCA protein assay kit (Pierce, USA) was used to determine the total protein content in samples.

2.4. Samples of pleural effusion

In this research, samples were taken from patients with lung cancer. The study was approved by the Ethics Committee of the University Hospital Brno on November 13th, 2019; approval code/number: 02-131119. Pleural effusion samples were collected from three patients undergoing cisplatin-based and two patients undergoing carboplatin-based chemotherapy. The time intervals after the intravenous application of the platinum derivative were set at 1, 3, 6, 12 and 24 h after the infusion. In two cases, incomplete sets of samples were obtained due to technical difficulties (e.g., obturation of the chest tube). Samples (19 altogether) in polypropylene vials were immediately frozen and stored at −18 °C until analysis.

2.5. Preparation of analytical samples

Prior to analysis, the samples were thawed at laboratory temperature and filtered through 0.22 μm Spin-X centrifuge filter units.

In order to determine the total Pt contents, the samples were diluted with 0.01 % (v/v) Triton X-100 in the ratio of 1 + 3 and also 1 + 9.

Free Pt was determined after ultrafiltration of the pleural effusions using Centrisart I units (Supelco, MWCO 20 kDa). Samples in units were centrifuged using EBA 20 centrifuge (Hettich, Germany) at 1750×g for 90 min. The filtrate was then transferred into a new tube immediately after centrifugation.

A potential loss of the analyte due to adsorption to the ultrafiltration unit was assessed by a mass balance test. The test involved measuring Pt concentration in both permeate and retentate and comparing the combined Pt masses to that in the introduced sample.

2.6. Pt determination by HR-CS GF-AAS

The temperature program for Pt determination using HR-CS GF-AAS was optimized for the determination of Pt contents in pleural effusions

as well as in their ultrafiltrates. First, direct analysis of ultrafiltered samples, undiluted pleural effusions, and decomposed samples was performed. Subsequently, the samples were diluted with Triton X-100 solution in the ratio of 1 + 1, 1 + 2, 1 + 3 and 1 + 9. For the development of the atomization program, the Pt standard solution (acidified with HNO_3) and the sample of pleural effusion diluted with Triton X-100 solution in the ratio of 1 + 9 were used.

Calibration was performed using both external calibration against aqueous solutions and also using standard additions to four samples of pleural effusions, including an ultrafiltrated sample.

The signal was measured at the resonance line of Pt (265.945 nm) at the central pixel plus the adjacent ones (CP ± 1). To explore the possibilities of reducing signal intensity (e.g. for extension of the linear range) the signal was also measured on the wings of the atomic line (with weak attenuation, ±2 pixels), and also using selected secondary lines of Pt (306.471 nm and 292.979 nm).

Pt determination was performed using a temperature program that included oxygen ashing (Table 1). Atomization from a graphite platform was performed for a sample volume of 20 μL for all measurements.

The experimental limit of detection (LOD) and quantification (LOQ) were calculated as three and ten times the standard deviation, respectively, where standard deviation was obtained from ten measurements of an experimental blank (a control sample of pleural effusion with no detectable Pt concentration).

2.7. Comparative ICP-MS measurement

The reference determination of Pt contents was performed using an inductively coupled plasma mass spectrometer (7700x Agilent ICP-MS, Agilent Technologies Inc., Japan) at the Centre for Toxic Compounds in the Environment RECETOX (Brno, Czech Republic). Quantification was based on external calibration (^{194}Pt and ^{195}Pt isotopes) with the correction of signal drift and non-spectral interferences on internal standards (^{185}Re and ^{209}Bi). Samples were 100x diluted with 4 % HCl prior to analysis.

2.8. Determination of protein content

As proteins are the main component of the pleural effusion matrix, their content was determined in a set of 11 samples and their respective ultrafiltrates. The total protein contents were quantified using Pierce BCA Protein Assay kit (Thermo Scientific). The analysis was based on the reduction of Cu(II) to Cu(I) followed by selective detection of the cuprous cation using bicinchoninic acid. The absorption of the purple-colored reaction product was then detected by UV–vis at 562 nm using a Specord 50 plus UV–vis spectrophotometer (Analytik Jena, Germany).

Table 1
Optimized temperature program for Pt determination using oxygen ashing in HR-CS GF-AAS.

no. #	step	temperature (°C)	ramp (°C/s)	hold (s)	gas
1	Drying 1	95	5	5	Ar (2 L/min)
2	Drying 2	110	5	5	Ar (2 L/min)
3	Pyrolysis	350	50	20	Ar (2 L/min)
4	Oxygen ashing	500	20	20	O_2 (2 L/min)
5	Pyrolysis (gas exchange)	500	0	10	Ar (2 L/min)
6	Pyrolysis	1300	300	20	Ar (2 L/min)
7	Gas adaptation	1300	0	5	–
8	Atomization	2350	1500	5	–
9	Cleaning	2500	500	4	Ar (2 L/min)

2.9. Statistical analysis

Statistical calculations were performed and Figs. 2, 4 and 5 generated using R software [17]. Differences between the values obtained by AAS and ICP-MS measurements were compared using *t*-test as well as differences between aqueous and matrix-matched standard solutions prepared for calibration. Values of $P < 0.05$ were considered statistically significant.

3. Results

3.1. Analytical procedure involving oxygen ashing

A high content of organic matter in the pleural effusion represents a considerable complication in the atomization process. The protein content was 34 ± 6 g/L. Residues of such an organic-rich matrix in the atomizer, resulting from the dosing of undiluted pleural effusion, are obvious in Fig. 1. Of the tested dilution ratios of pleural effusion with Triton X-100 solution, the ratio of 1 + 9 proved to be suitable for measurement. Undiluted samples clog the atomizer rapidly, even when oxygen ashing is used. In addition, the dosing of a sample causes uneven spillage of the sample across the platform and reduces the reproducibility of the measurement. Even though ultrafiltration significantly reduced the protein content, samples for free-Pt determination still needed to be treated with oxygen ashing in order to prevent gradual clogging of the tube (see Fig. 1), as they still contained 1.7 ± 1.2 g/L – about half the protein content of the ten-times diluted effusions. The use of oxygen ashing during the pyrolysis step (Table 1) proved to be an effective technique for overcoming this problem and allowed the determination of Pt in all samples. Thus, samples of pleural effusions and their ultrafiltrates do not need to be mineralized prior to analysis.

The optimized temperature program for the atomizer (Table 1) included a gradual increase in the temperature of the drying step due to significant sample foaming. The temperature of oxygen ashing (carbon removal) was set to 500 °C due to the highly corrosive effects of oxygen above this temperature. The next pyrolysis step at 1300 °C served to remove inorganic salts from the sample matrix. Overall, the temperature program including oxygen ashing lasted 164 s.

3.2. Measurement using different Pt lines

The calibration lines obtained using the primary line (CP ± 1 and also using attenuation, i.e. the reading of the signal on the wings of the absorption profile) and secondary lines are presented in Fig. 2. Even when using the most sensitive line, 265.945 nm, the upper end of the working range reaches up to 1,000 μg/L, which is sufficient in most cases.

The correlation coefficients (*r*) were >0.999 for all the calibration curves, including the 5-point calibration ranging from 10 to 40 μg/L (which results in integrated absorbance of approx. 0.03), tested for the samples with very low Pt concentrations (not included in the figure).

In the case of high concentration samples, dilution is a preferred strategy, as a smaller amount of matrix is introduced into the atomizer. However, in some cases (e.g. of spectral interferences), it may be beneficial to use less-sensitive Pt lines. Similar sensitivities and calibration ranges for secondary lines were reported by Eskina et al. who applied HR-CS GF-AAS for determination of Pt in spent-automobile catalysts solutions [18].

It is worth special attention that the use of the Pt line 292.979 nm provides an attractive possibility to co-determine iron in the sample in one run (see the Section 3.3. *Possibility of simultaneous Fe determination*).

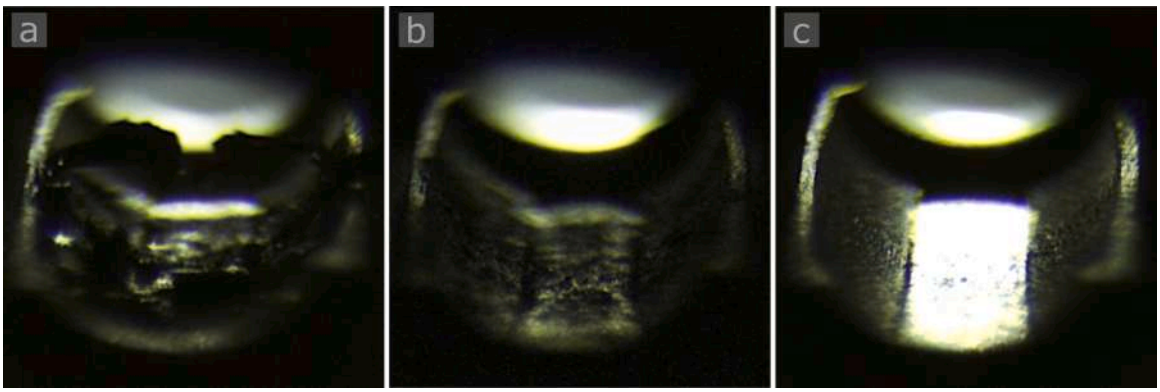

Fig. 1. Tube atomizer after 5 firings of diluted (1 + 3) pleural effusion without oxygen ashing (a), after 30 firings of ultrafiltrate of pleural effusion without oxygen ashing (b), and after 100 firings of diluted (1 + 3) pleural effusion with oxygen ashing (c).

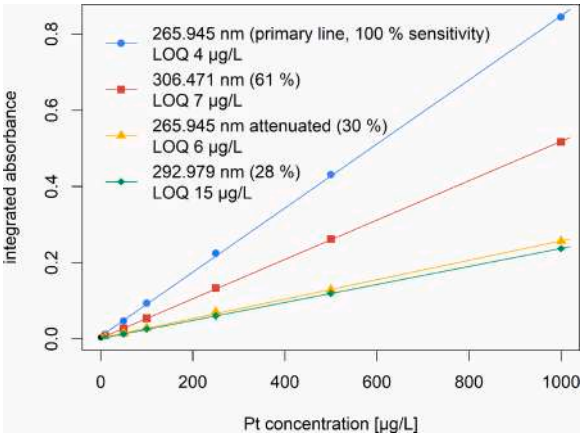

Fig. 2. Calibration using different Pt lines.

3.3. Possibility of simultaneous Fe determination

As can be seen in Fig. 3, there is a secondary iron (Fe) line visible in the vicinity of the Pt line 292.979 nm, which can be used for simultaneous Fe determination. The sensitivity of the 292.901 nm Fe line is 0.56 % (related to the sensitivity of its primary line), which allows Fe determination in concentrations of approx mg/L, i.e. at its usual serum concentration.

3.4. Aqueous vs. matrix-matched calibration

To check the possible influence of the sample matrix on signal intensity, in addition to aqueous standards, sets of matrix-matched calibration solutions were also prepared from pleural effusions not exposed to Pt. The slopes of the calibration functions prepared in pleural effusions diluted in the ratios of 1 + 3 and 1 + 9, and also in ultrafiltrated sample were in agreement with the slope of the calibration curve determined using aqueous Pt standards (t-test 95 %, R-squared in all cases >0.9995). This allowed straightforward calibration with aqueous standards.

3.5. Comparing HR-CS GF-AAS method with ICP-MS

As there is no suitable certified reference material with a similar matrix and Pt content available, the trueness of the method was checked by comparing the obtained results with a reference measurement by ICP-MS.

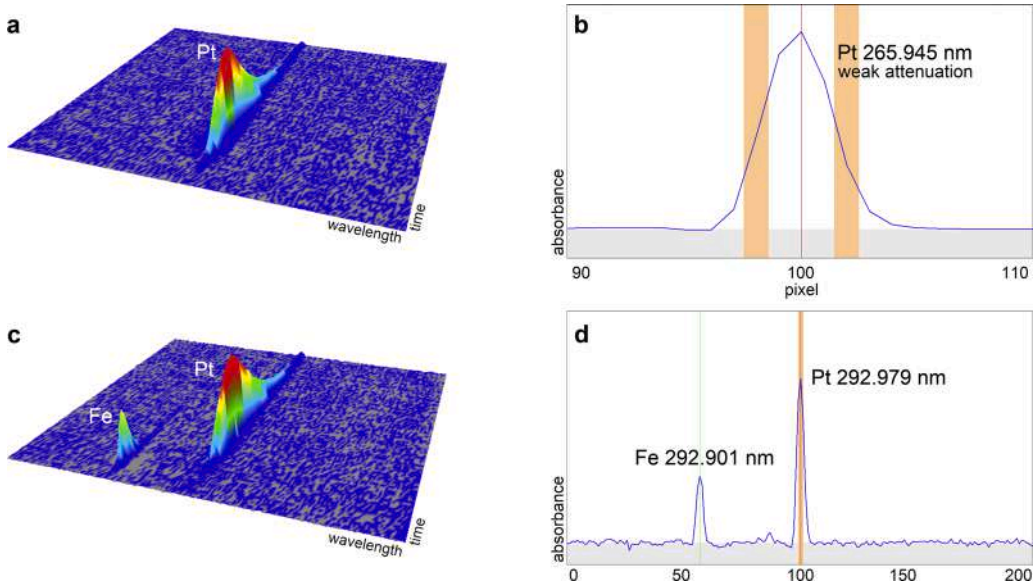

Fig. 3. Signals of diluted pleural effusion measurement: Pt at primary line 265.945 nm (a) and signal reading with weak attenuation (b), and Fe line 292.901 nm in vicinity of Pt line 292.979 nm (c, d).

A test set of pleural effusions and their ultrafiltrates (14 samples altogether with Pt concentration from 5 to 690 μg/L) was analyzed by both methods and no significant differences between the obtained results were observed (paired *t*-test, p = 0.9). A visual comparison of the results of both the methods is given in Fig. 4.

4. Discussion and conclusion

The aim of this work was to describe a new analytical method and its usability for analyses of Pt concentrations in high-protein-content biological samples (in our case pleural fluid). Using the proposed method, Pt concentrations were determined in a test set of 50 samples (comprising 25 samples of pleural fluids and 25 ultrafiltered aliquots).

4.1. Sensitivity of the method

When measured at the primary Pt line (265.945 nm), LOD and LOQ were 1 and 4 μg/L, respectively (Fig. 2). Sensitivity of the presented method in terms of LOQ is therefore slightly higher than that reported for classic line-source GF-AAS (e.g. 12 μg/L in urine or 21 μg/L in blood plasma [11,16]) and more than order of magnitude higher when compared to flame HR-CS AAS (180 μg/L [16],).

4.2. Determining the contents of free- and total Pt in pleural effusions

Total Pt contents reached values of up to 5,000 μg/L, a value which, due to dilution, was still within the calibration range, even when measuring at the most sensitive Pt-line at 265.945 nm. For samples with a particularly high Pt content, the sensitivity can be reduced not only by dilution, but also by using secondary lines. In particular, the use of the 292.979 nm Pt line may be beneficial due to the possibility of the simultaneous co-determination of Fe, whilst the sensitivity of 28 % is still satisfactory for the determination of total Pt.

Protein-unbound Pt occurred at levels ranging from tens of μg/L to up to 2,500 μg/L. The former concentrations were still easily measurable due to the fact that such filtered samples do not require to be further diluted, as the protein content is already reduced by the ultrafiltration. The latter had to be diluted or injected into the tube in a reduced volume in order to be measured using the primary Pt line.

According to the mass study test, there was no loss of Pt during ultrafiltration, as the sum of Pt masses in the filtrate and retentate was 96.1–103.9 % compared to the originally introduced sample (n = 6).

4.3. Clinical relevance of Pt determination in pleural effusions

From a clinical point of view, it is currently impossible to draw meaningful and reliable scientific conclusions concerning the analyzed samples from the pive patients participating in this study. Therefore, we comment on this aspect only briefly.

In a healthy person, the pleural space contains only a small amount of fluid, this enabling physiological lung motion. The fluid is produced in the parietal pleura and reabsorbed by the parietal pleura lymphatics. The estimated pleural fluid turnover is about 0.15 mL/kg/h [19]. An effusion occurs in the case of an imbalance between the production and reabsorption of the pleural fluid, e.g., in cases of malignancy.

We observed two different patterns of pleural fluid Pt dynamics, these exhibiting considerable variability with respect to the results. Patients 1-3 exhibited the pattern of a gradual increase in total Pt concentration over the 24 -h (or 12 -h) sampling period. The concentration of free (protein-unbound) Pt in the pleural effusion peaked 6−12 h after the intravenous administration of the drug and then decreased. It appears that a larger proportion of Pt entered the pleural space bound to plasmatic proteins during production of the effusion by the parietal pleura.

In patients 1-3, who underwent cisplatin-based chemotherapy, the daily fluid production was rather limited, not exceeding a few hundreds of mL per day. In contrast, the results for patients 4 and 5, who underwent carboplatin-based chemotherapy, differed from the pattern observed for patients 1-3. In these patients, the platinum concentration peaked immediately after the intravenous administration of the drug and then followed a clear and steady downward trend, however, there is a difference even between CBDCA patients – patient 5 showed higher concentration of total Pt than patient 4, while a major proportion of the initial total Pt was constituted by free Pt, the fraction of protein-bound Pt subsequently increasing during the 24 h sampling period. We speculate that in this patient the pleural concentration of platinum directly followed the intravenous administration of the drug because of the extreme permeability of the parietal pleura. To support this thesis, we further evaluated the clinical data on this patient. The patient had a very severe metastatic cancer involving the pleura and an extensive daily production of pleural fluid of up to 2,500 mL per day. Only a few days after platinum chemotherapy treatment, the daily volumes of pleural fluid production decreased to a minimum and the chest drains could be removed. The patient responded well to the treatment and a reduction in the mass of the tumor was documented. It appears that the excessive Pt concentrations in the pleural fluid following the course of chemotherapy facilitated this significant response to treatment. We speculate that if

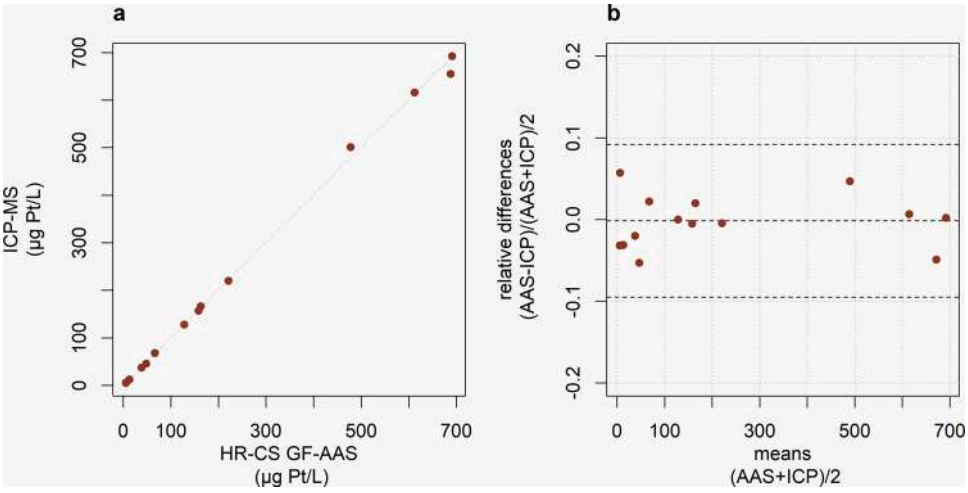

Fig. 4. Comparison of the results obtained by the developed method (HR-CS GF-AAS) and ICP-MS visualized using: a) an XY-plot, and b) a Bland-Altman-Plot showing relative differences between the two methods against the average Pt contents.

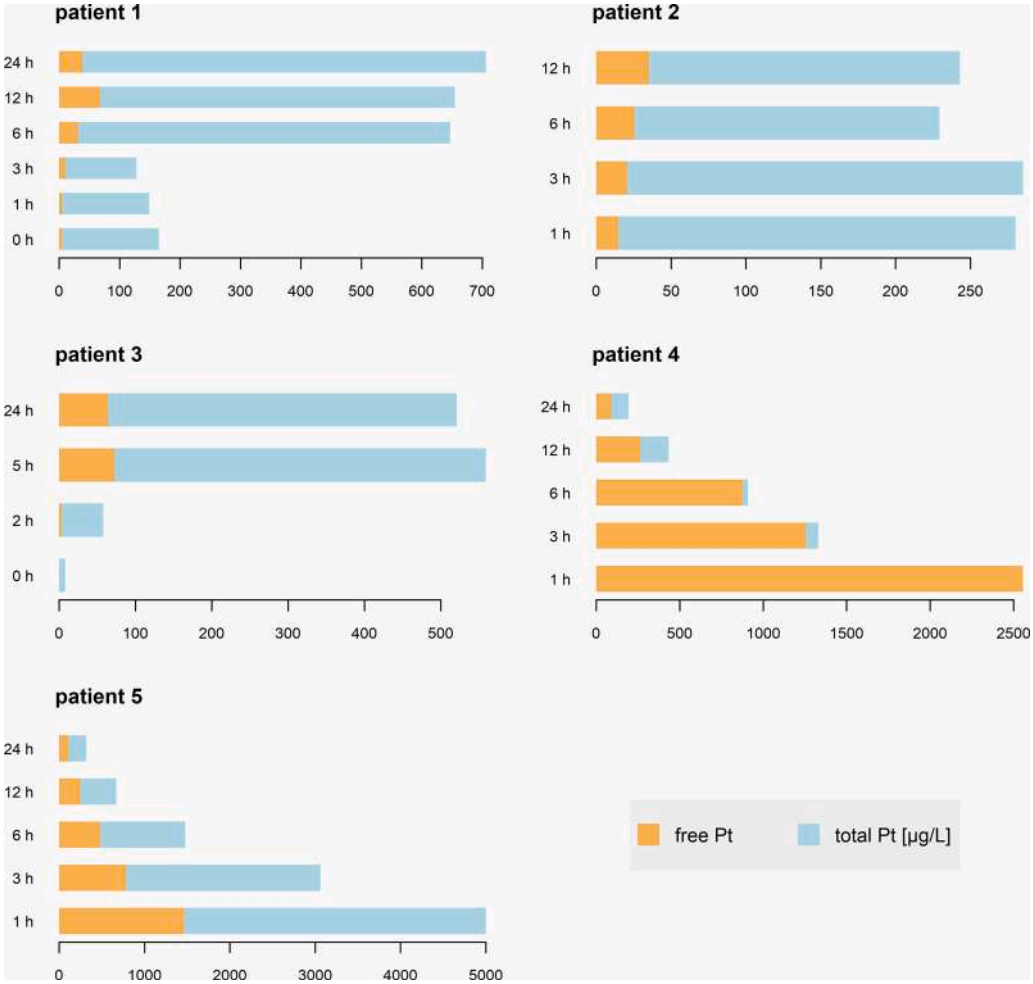

Fig. 5. Total Pt and free Pt in pleural effusions at different times after the intravenous application of the Pt derivative determined by HR-CS GF-AAS.

this hypothesis is correct, a pleural pharmacokinetic concentration curve similar to that of patient 4 might be a good predictor of a positive treatment response in similar patients. Patient 5 also clinically presented with massive pleural effusion and similarly to patient 4, responded well to the treatment. In case of patient 5, the concentration of total Pt was much higher than in patient 4. The question is, whether the differences between patients 1-3 and 4-5 are caused by the speed of production of the effusion, slightly different pharmacokinetics of cis-DDP/CBDCA, or both. The number of patients is still low to draw definite conclusions and further investigation is needed.

Author statement

Ondřej Zvěřina: Conceptualization; Investigation; Visualization; Supervision; Writing - original draft. **Ondřej Venclíček**: Conceptualization; Investigation; Methodology; Writing - original draft. **Jan Kuta**: Investigation; Writing- Reviewing and Editing. **Pavel Coufalík**: Conceptualization; Writing - original draft. **Ingrid Hagarová**: Writing-Reviewing and Editing. **Kristián Brat**: Investigation; Methodology; Writing- Reviewing and Editing, Supervision

Declaration of Competing Interest

There are no conflicts of interest.

Acknowledgements

Authors thanks to Research Infrastructure RECETOX RI (No LM2018121) financed by the Ministry of Education, Youth and Sports, and Operational Programme Research, Development and Innovation - project CETOCOEN EXCELLENCE (No CZ.02.1.01/0.0/0.0/17_043/0009632) for supportive background; Masaryk University (project MUNI/A/1608/2020); and the Ministry of Health of the Czech Republic (MH CZ-DRO FNBr 65269705). The involvement of Pavel Coufalík was supported by the Institute of Analytical Chemistry of the CAS under the Institutional Research Plan RVO: 68081715. We also thank Martin Pěkný for consulting with us throughout the project.

References

[1] S.G. Spiro, G.A. Silvestri, One hundred years of lung cancer, Am. J. Respir. Crit. Care Med. 172 (09) (2005) 523–529, https://doi.org/10.1164/rccm.200504-531OE.
[2] World Health Organisation, Cancer Facts Sheets: Lung Cancer (n.d.). https://gco.iarc.fr/today/data/factsheets/cancers/15-Lung-fact-sheet.pdf (Accessed April 1, 2020), 2021.
[3] Institute of Health Information and Statistics of the Czech Republic, Cancer Incidence in the Czech Republic, Novotvary, 2016 (n.d.). https://www.uzis.cz/sites/default/files/knihovna/novotvary2016.pdf (Accessed February 8, 2021).
[4] B. Jany, T. Welte, Pleural effusion in adults-etiology, diagnosis, and treatment, Arztebl. Int. 116 (2019) 377–386, https://doi.org/10.3238/arztebl.2019.0377.
[5] W.W. Johnston, The malignant pleural effusion. A review of cytopathologic diagnoses of 584 specimens from 472 consecutive patients, Cancer 56 (1985) 905–909, https://doi.org/10.1002/1097-0142(19850815)56:4<905::aid-cncr2820560435>3.0.co;2-u.
[6] A.O. Clive, H.E. Jones, R. Bhatnagar, N.J. Preston, N. Maskell, Interventions for the management of malignant pleural effusions: a network meta-analysis, Cochrane Database Syst. Rev. (2016), https://doi.org/10.1002/14651858.CD010529.pub2.
[7] Kyushu Yamaguchi Thoracic Oncology Group, T. Seto, S. Ushijima, H. Yamamoto, K. Ito, J. Araki, Y. Inoue, H. Semba, Y. Ichinose, Intrapleural hypotonic cisplatin treatment for malignant pleural effusion in 80 patients with non-small-cell lung

cancer: a multi-institutional phase II trial, Br. J. Cancer 95 (9) (2006) 717–721, https://doi.org/10.1038/sj.bjc.6603319.
[8] V. Laszlo, T. Klikovits, A. Tisza, M. Bonta, M. Hoda, W. Berger, M. Grusch, W. Klepetko, B. Hegedus, A. Limbeck, B. Dome, P2.06-21 low intratumoral platinum concentration is associated with unfavorable clinical outcome in malignant pleural mesothelioma, J. Thorac. Oncol. 13 (10) (2018) S750, https://doi.org/10.1016/j.jtho.2018.08.1276.
[9] W.J. van der Vijgh, Clinical pharmacokinetics of carboplatin, Clin. Pharmacokinet. 21 (1991) 242–261, https://doi.org/10.2165/00003088-199121040-00002.
[10] W.I. Mortada, M.M. Hassanien, A.A. El-Asmy, Speciation of platinum in blood plasma and urine by micelle-mediated extraction and graphite furnace atomic absorption spectrometry, J. Trace Elem. Med. Biol. 27 (2013) 267–272, https://doi.org/10.1016/j.jtemb.2013.04.004.
[11] I. Hagarová, M. Bujdoš, J. Kubová, P. Matúš, Direct spectrochemical determination of carboplatin species in human blood serum after their chemotherapy application for pharmacokinetic study, Fresenius Environ. Bull. 21 (2012) 343–350.
[12] Z. Yang, X. Hou, B.T. Jones, Determination of platinum in clinical samples, Appl. Spectrosc. Rev. 37 (2002) 57–88, https://doi.org/10.1081/ASR-120004747.
[13] M. Balcerzak, Methods for the determination of platinum group elements in environmental and biological materials: a review, Crit. Rev. Anal. Chem. 41 (07) (2011) 214–235, https://doi.org/10.1080/10408347.2011.588922.
[14] M. Wójciak-Kosior, W. Szwerc, M. Strzemski, Z. Wichłacz, J. Sawicki, R. Kocjan, M. Latalski, I. Sowa, Optimization of high-resolution continuum source graphite furnace atomic absorption spectrometry for direct analysis of selected trace elements in whole blood samples, Talanta 165 (04) (2017) 351–356, https://doi.org/10.1016/j.talanta.2016.12.077.
[15] B. Welz (Ed.), High-Resolution continuum Source AAS: the Better Way to Do Atomic Absorption Spectrometry, Wiley-VCH, Weinheim; [Great Britain], 2005.
[16] A.C. da Costa Jr, M.A. Vieira, A.S. Luna, R.C. de Campos, Determination of platinum originated from antitumoral drugs in human urine by atomic absorption spectrometric methods, Talanta 82 (2010) 1647–1653, https://doi.org/10.1016/j.talanta.2010.07.029.
[17] R Core Team, R: a Language and Environment for Statistical Computing, R Foundation for Statistical Computing, Vienna, Austria, 2020. https://www.R-project.org/.
[18] V.V. Eskina, O.A. Dalnova, D.G. Filatova, V.B. Baranovskaya, Y.A. Karpov, Direct precise determination of Pd, Pt and Rh in spent automobile catalysts solution by high-resolution continuum source graphite furnace atomic absorption spectrometry, Spectrochim. Acta Part B At. Spectrosc. 165 (03) (2020) 105784, https://doi.org/10.1016/j.sab.2020.105784.
[19] G. Miserocchi, Physiology and pathophysiology of pleural fluid turnover, Eur. Respir. J. 10 (1997) 219–225, https://doi.org/10.1183/09031936.97.10010219.

Chemosphere 249 (2020) 126118

Contents lists available at ScienceDirect

Chemosphere

journal homepage: www.elsevier.com/locate/chemosphere

The impact of tourism on extremely visited volcanic island: Link between environmental pollution and transportation modes

Martin Brtnický [a, b], Václav Pecina [a, b], Michaela Vašinová Galiová [a, b, *], Lubomír Prokeš [c, d], Ondřej Zvěřina [e], David Juřička [a], Martin Klimánek [f], Jindřich Kynický [g]

[a] Department of Geology and Pedology, Faculty of Forestry and Wood Technology, Mendel University in Brno, Zemědělská 1, 613 00 Brno, Czech Republic
[b] Institute of Chemistry and Technology of Environmental Protection, Faculty of Chemistry, Brno University of Technology, Purkyňova 118, 61200 Brno, Czech Republic
[c] Department of Chemistry, Faculty of Science, Masaryk University, Kamenice 5, 625 00 Brno, Czech Republic
[d] Department of Physical Electronics, Faculty of Science, Masaryk University, Kotlářská 2, 611 37 Brno, Czech Republic
[e] Department of Public Health, Faculty of Medicine, Masaryk University, Kamenice 5, 625 00 Brno, Czech Republic
[f] Department of Forest Management and Applied Geoinformatics, Faculty of Forestry and Wood Technology, Mendel University in Brno, Zemědělská 3, 613 00 Brno, Czech Republic
[g] Central European Institute of Technology, Brno University of Technology, Purkyňova 656/123, 612 00 Brno, Czech Republic

HIGHLIGHTS

- The anthropogenic contamination by Cu, Cr and Pb has been found out on Santorini.
- The contamination may represent a moderate ecological risk to local ecosystems.
- Airport traffic is a significant source of soil pollution on the island.
- The dominant factor determining HM content of volcanic island soils is parent rock.
- HM monitoring may serve as background for introducing tourist quotas.

GRAPHICAL ABSTRACT

ARTICLE INFO

Article history:
Received 27 November 2019
Received in revised form
10 January 2020
Accepted 3 February 2020
Available online 4 February 2020

Handling Editor: Patryk Oleszczuk

ABSTRACT

The enormous tourism boom raises concern about possible negative environmental impacts worldwide. One of the risks posed by tourism may be heavy metal pollution. On the example of the volcanic island of Santorini, a popular tourist destination, pollution of soils categorized according to the tourism load was monitored. Significant anthropogenic contamination by heavy metals, especially Cu, Cr and Pb, was found out. This contamination may constitute a moderate ecological risk to the island ecosystems. Tourism has been shown to be a significant pollution factor as evidenced by the contaminated soils near the airport. Simultaneously, airport traffic has been proved to be an important emitter of Co, Cr and especially Zn. The comparison with other volcanic islands has shown that on Santorini the content of

* Corresponding author. Institute of Chemistry and Technology of Environmental Protection, Faculty of Chemistry, Brno University of Technology, Purkyňova 118, 61200 Brno, Czech Republic.
E-mail addresses: martin.brtnicky@mendelu.cz (M. Brtnický), vaclav.pecina@mendelu.cz (V. Pecina), galiova@fch.vut.cz (M. Vašinová Galiová), prokes@chemi.muni.cz (L. Prokeš), ondrej.zverina@mail.muni.cz (O. Zvěřina), david.juricka@mendelu.cz (D. Juřička), martin.klimanek@mendelu.cz (M. Klimánek), jindrich.kynicky@ceitec.vutbr.cz (J. Kynický).

https://doi.org/10.1016/j.chemosphere.2020.126118

Keywords:
Overtourism
Santorini
Airport
Traffic
Ecological risk
Destination management

heavy metals in soils is significantly lower, despite frequently higher tourism intensity. On this basis, it can be concluded that in case of volcanic islands the dominant factor determining the content of heavy metals in the soil is the parent rock. Given high and ever-increasing intensity of tourism on the island, it can be assumed that soil contamination will continue to rise rapidly. Therefore, without proper steps reducing tourism, increase in soil degradation, growing negative impacts on local ecosystems as well as on the quality of produced wine can be expected on Santorini.

1. Introduction

Tourism is a source of employment and income for local inhabitants, it can be an important component of regional development and can also contribute, for instance, to the preservation of natural and cultural heritage as a source of finance (Pigram and Wahab, 2005; Buckley, 2011; Azam et al., 2018). However, in case of a disproportionately high influx of tourists, there is so-called overtourism (Oklevik et al., 2019) which has already affected, for example, Barcelona, Amsterdam or Rio de Janeiro (Peeters et al., 2018). Then, unduly high tourism entails a number of negatives, such as environmental pollution, ecosystem degradation, soil erosion and may result even in desertification (Zhong et al., 2011; Azam et al., 2018; Drius et al., 2019). In the context of the tourism boom and global change, its environmental impact is becoming an objective of increasing global interest (Li et al., 2014).

The development of large tourist centres threatens the environment with a number of pollutants. The greatest threat is posed by the construction of new infrastructure and transport (Lukashina et al., 1996; Davenport and Davenport, 2006). Transport, as an emitter of pollutants, is associated with vehicular traffic (Has-Schön et al., 2006; Chen et al., 2010; Ciarkowska, 2018), shipping (Adamo et al., 2005; Ali et al., 2011) and air transport (Ray et al., 2012; Massas et al., 2016). Due to fuel combustion it can have both a local and global impact, in particular through greenhouse gas emissions (Buckley, 2011; Azam et al., 2018).

Pollutants directly associated with tourism can be represented, for instance, by heavy metals (HMs) (Ali et al., 2011; Li et al., 2014; Ciarkowska, 2018). HMs naturally occur in the environment and many of them are biologically significant, but they can be toxic to plants, animals and humus at excessive concentrations (Nagajyoti et al., 2010; Werkenthin et al., 2014). Due to high anthropogenic emissions, they are one of the most serious environmental pollution problems because of their toxicity, persistence and bioaccumulation (Tam and Wong, 2000; Werkenthin et al., 2014). HMs are mainly addressed in urbanized areas where population may be permanently exposed to their harmful effects through inhalation, ingestion or absorption of contaminated soil or dust particles (Al-Khashman, 2004; Cheng et al., 2014) but they are also addressed, for example, in agriculture (Huang et al., 2018; Mirzaei et al., 2019). The accumulation of HMs in agricultural soil can limit the growth of crops due to phytotoxic effects, endanger the health and function of soil organisms and ultimately have a negative impact on food safety and marketability (Nagajyoti et al., 2010; Kabata-Pendias, 2011; Mirzaei et al., 2019).

As tourism grows, traffic intensity increases, leading to a greater risk to HMs emitted to the environment in tourist destinations (Has-Schön et al., 2006; Li et al., 2014). However, specific research studying soil contamination by HMs due to tourism is very sporadic and insufficient in the scientific literature. This topic was only historically and marginally addressed by Lukashina et al. (1996) and newly Ciarkowska (2018) and Memoli et al. (2019). Given the worldwide significant growth in tourism, such studies are necessary to determine the environmental burden.

Santorini is one of the most popular tourist destinations in the world (Delitheou and Georgakopoulou, 2017) and it is visited by up to 2,000,000 visitors per year (Peeters et al., 2018). For the economy of the island, tourism is the mainstay that generates most of the revenue (Jenkins et al., 2015). Other important sectors linked to tourism are agriculture, fisheries, craft, services and construction. Tourism development has resulted in the growth of tourist infrastructure that spans the whole island (Delitheou and Georgakopoulou, 2017). Santorini is increasingly associated with overtourism, high traffic issues and inquiries about possible negative environmental impacts are emerging (Peeters et al., 2018). For this reason, Santorini was chosen as a suitable model location for monitoring the impact of tourism on soil contamination and further evaluations.

The objectives of this study are to find out whether tourism causes significant contamination of soil by HMs and whether monitoring of this contamination can be used as a basis for management decisions on the protection of nature and human health via several steps: (1) to map the current HM content (Cd, Co, Cr, Cu, Ni, Pb and Zn) in the soil of the island; (2) to calculate indices assessing the level of contamination and the environmental risk; (3) to evaluate the impact of tourism on the contamination of soils exposed to a high risk of pollution; (4) to compare the impact of airport and road transport on soil contamination; (5) to compare the levels of HMs in soils with other islands.

2. Materials and methods

2.1. Study area

Santorini (Thera) is known as a complex of islands in the southern Aegean Sea (36°25′N 25°26′E) and is a part of the Cyclades archipelago in Greece. The largest island is Thera with an area of 75.8 km^2 (Economou et al., 2007).

Santorini is a multicentric volcanic field and its current appearance is the result of volcanic activities (Dominey-Howes and Minos-Minopoulos, 2004). The great eruption, which took place approximately 3500 years ago, led to the formation of a layer of volcanic ash and pumice with a depth of 30–40 m. This material forms the parent rock on which the current island soils, classified as regosols (Vavoulidou et al., 2006) or entisols (Moustakas and Georgoulias, 2005) have been developed. These soils are often affected by erosion which is accelerated by hundreds of years of intensive farming and prevailing strong winds (Economou et al., 2007).

On Santorini Island, only about 15,000 inhabitants live permanently but, in the summer, the number of people on the island can rise to more than 500,000 (Jenkins et al., 2015). The main tourist destination is Thera which is equipped with the necessary infrastructure, including the airport and port. With the appearance and growth of tourism, urban areas of the island have grown rapidly since the 1970s (Economou et al., 2007), fishing and farming

villages have turned into seaside resorts (Wadih, 2005). Infrastructure growth saturated with increasing tourism continues, especially in the transport sector (Delitheou and Georgakopoulou, 2017).

Santorini is not only a destination but also a transfer hub from plane to ferry and vice versa for neighbouring islands. The Santorini Airport has served as a civil and military airport since 1972. The ever-increasing tourism is reflected in the increasing number of flights from recent years. While in 1994 there were 6096 flights representing 401,048 passengers carried (Hellenic Civil Aviation Authority (HCAA), 2019), in 2018 there were 20,360 flights with a total of 2,254,926 passengers carried. Eight thousand one hundred fifty-nine international flights which are used almost exclusively by tourists, were carried out and 1,068,022 passengers were transported in 2018 (Santorini Airport, 2019). In addition, Santorini is accompanied by many cruise ships and passenger ones contributing to the growth of tourism on the island (Delitheou and Georgakopoulou, 2017). In 2011, 58% of arrivals were made by air and 42% by sea (Peeters et al., 2018). At the same time, the increasing number of tourists led to increased pressure on the infrastructure on the island and increased traffic (Wadih, 2005).

2.2. Soil sampling

Four categories of sampling sites were created according to the type of traffic pollution and the intensity of road network utilization. Specifically, these ones are: (1) **Airport (AIR)** which includes sites around the perimeter of the airport area where direct impact of intensive air traffic is expected as a result of enormous tourism; (2) **Airoport - Ferry port road (AFR)** which includes points on the road connecting two main transport links providing services from the island and there, with intensive traffic as a result of tourism; 3) **Urban roads (UR)** include sites situated in continuous built up area which can be called in the local conditions urban area, roads are widely used by tourists; 4) **Rural roads (RR)** include places situated in the agricultural landscape, without continuous development and tourism.

The locations of the individual sampling points are indicated in Fig. S1. A total of 65 samples were collected and taken within 1 m of the roadside. One mixed sample was taken as a background from five different sites of the uninhabited island of Nea Kameni, located in the centre of the Santorini complex. All the samples were collected as a mixed sample of surface soil (0–10 cm) formed by mixing five sub-samples from an area of 1 m^2.

2.3. Sample preparation and analysis

The soil samples were dried at room temperature and subsequently sieved through a nylon sieve (mesh size 2 mm). The pH was measured in 1 M KCl (ISO 10390: 2005). Carbon oxidation state (Cox) was determined by oxidation with a chromium-sulphur mixture (ISO 14235: 1998).

The content of HMs (Cd, Co, Cr, Cu, Ni, Pb and Zn) was measured for each soil sample. Decompositions were performed prior to measurements of the samples. The sample solutions were obtained by decomposing 1 g of soil with the addition of 3 ml of concentrated nitric acid and 9 ml of concentrated hydrochloric acid in an ETHOS EASY microwave digestion oven (Milestone, IT). Microwave decomposition was performed using an optimized temperature programme. Step 1: gradual heating of the vessels to 110 °C for 15 min at 1800 W, Step 2: maintaining of the temperature 110 °C for 15 min at 1800 W and Step 3: cooling for the time period of 10 min. Then, the mineralized solutions were transferred to a well-defined volume of 50 ml.

Concentrations of the selected metals in soil digests were determined by means of atomic absorption spectrometry (AAS) with graphite furnace (GFAAS) and flame atomization (F-AAS) technique.

For determination of the elements presented in relatively low concentrations (Cd, Co, Cu, Cr, Ni and Pb), the GFAAS technique was employed using high-resolution continuum source spectrometer (ContrAA 800G, Analytik Jena, Germany). The content of Zn was determined using flame technique (Solaar 939, Cambridge, UK) employing standard conditions (air-acetylene flame). The digests were diluted 1:2 for measurement using graphite furnace and 1:10 for flame technique.

Measurement conditions (Table S1) were optimized prior to analysis and trueness of the measurement was verified by means of a set of three certified reference materials: Metranal 31 (light sandy soil), Metranal 33 (clay loam soil) by Analytika, Czech Republic, and 2709a (San Joaquim Soil) by NIST, USA. All the determined values were in agreement with the certified values at the 95% confidence interval (*t*-test). The relative standard deviation was, in all cases, below 8%.

2.4. Data treatment

The content of HMs in soil is assessed in compliance with the Dutch Soil Guidelines Target Values and Intervention Values (VROM, 2013). This standard is widely used in research studies throughout the world (Chabukdhara and Nema, 2013; Cheng et al., 2014; Brtnický et al., 2019). Soil contamination and pollution severity was assessed by Enrichment factor (EF), Geoaccumulation index (Igeo) a Nemerow pollution index (IPI_N) and Potential ecological risk index (RI) (see Supplementary data).

2.5. Statistical analysis

Data visualization using box plots and PCA were performed using Origin software. The values of the contents of the elements of interest and the calculated indices were subjected to statistical analysis using the R programme (https://cran.r-project.org/). Basic data diagnostics (identification of outliers, test of normality and heteroscedasticity of data and testing of conformity of individual contents with background value) was performed by means of box plots. Due to the significant non-normal distribution of the data, further analysis of the data was performed using non-parametric statistical tests. The effect of outliers was eliminated by using bootstrap, respectively permutation tests. Both the classical and permutation one-sample Wilcoxon test were used to test the compliance with the background value for individual sets (Conover, 1999; Sheskin, 2004; Hollander et al., 2014).

Comparison of sets was performed by different variants of single-factor ANOVA and mutual comparison: *a) Kruskall-Wallis nonparametric test* (including its bootstrap variant), based on ranking of individual values, together with Nemenyi paired comparison methods (Hollander et al., 2014) and methods Dwass-Steel-Critchlow-Fligner (Hollander et al., 2014); Dunn (Sheskin, 2004); and Conover (1999). Adjustment of probability values (p-values) for pairwise comparisons was performed by the methods of Hochberg-Benjamini (false discovery rate, FDR) and Holm which provides less conservative estimates than FDR (Goeman and Solari, 2014). Then, *b) Van der Waerden test* (Conover, 1999; Sheskin, 2004) and *Lu-Smith test* (Lu and Smith, 1979), based on normalized scores with adjusting of p-values Hochberg-Benjamini (FDR) and Holm were also used, *c) Anderson-Darling k-sample test* (Scholz and Stephens, 1987) and *k-sample Baumgartner-Weiss-Schindler test* according to Murakami (2012), based on the comparison of distribution functions, again with adjustment of Hochberg- Benjamini (FDR) and Holm and the last one applied was *d) Permutation k-sample test*

(Anderson, 2001; Basso et al., 2009) with a combination of Hochberg-Benjamini (FDR) and Holm. In all cases the significance level $\alpha = 0.05$ was used.

3. Results and discussion

3.1. Soils of the island

The average pH of the studied soils on the island is 7.6. The difference between categories is minimal and not statistically significant. The average carbon content is 2.1%. It is mostly found in urban soils, where its average value is 3.0%. On the contrary, the least carbon content is in soils at the airport, specifically 1.7%.

The contents of the HMs in the individual soil categories of Santorini are given in Table 1 and Fig. S2. The average values did not exceed the target values which reflect the possible natural contents of the elements in the soil, for none of the elements. Maximum values exceeded them for Cu, Pb and Zn. It was four times for Cu, once for the UR and RR categories and twice for the AIR category. It was exceeded only once in the case of Pb in the AFR category. It was three times in the case of Zn - once in the UR category and twice in the AIR category. Intervention Values were not exceeded for any element which means that there is no presumption of serious threat to human, animal or plant health.

The Cd content of Santorini soils is not listed in Table 1 and the element is omitted from subsequent statistical analysis. The reason is that its content was below the detection limit (0.01 mg/kg) in 94% of the soil samples, indicating its very low content in the parent rock and merely local enrichment, probably of anthropogenic origin.

Background values were exceeded for all the elements, indicating potential anthropogenic contamination. The background values themselves can be described as very low, as is also mentioned by Vavoulidou et al. (2006) and Moustakas and Georgoulias (2005) who report that the local soils have a very small quantity of products of weathering.

A significant increase in the soils of the island compared to the background values is evident especially in the case of Cr, Cu, Pb and Zn, while in the case of Co and Ni it is not so significant. The division of the elements into these two groups was also confirmed by PCA (Fig. S3). On this basis, it can be assumed that Co and Ni in the soils of the island are predominantly of geogenic origin, while Cr, Cu, Pb and Zn originate predominantly from anthropogenic activities. In the case of this tourist destination, these are mainly represented by traffic that emits these elements in large quantities (Chen et al., 2010; Werkenthin et al., 2014; Massas et al., 2016) and may also be hypothetically associated with tourism as the cause of high traffic on the island. The growth of tourism related to increasing traffic intensity and greater risk posed by Pb is also mentioned in the study by Has-Schön et al. (2006). Similarly, Memoli et al. (2019) points to the possible impact of enormous tourist traffic in finding of soil contamination by Cr, Cu, Ni and Pb but the variability in the values reported in the study raises questions rather than clarifies the issue.

Locally, for instance, docks for recreational and fishing boats associated with Cu, Zn, Pb and Cd pollution (Ali et al., 2011) can be also identified as sources of pollution on the coast. In the case of the RR category, agricultural practices involving the application of fertilizers and pesticides in the vineyards may also be a source of pollution. These agents may lead to the increase in Cd, Cr, Cu, Ni, Pb and Zn (Massas et al., 2016; Mirzaei et al., 2019).

3.2. Assessment of soil contamination and its risk

The average values of soil contamination indices (EF, I_{geo}, IPI_N) by the selected HMs within each category are shown in Table S2 and their range is graphically presented in Fig. 1 and Fig. S4.

The EF confirmed the anthropogenic contributions of HMs to soils in all the categories as it exceeded the limit value of 1.0 for all of them. Cu (Fig. 1a) proved to be the most anthropogenically emitted element, with an increase of more than ten times the natural values in all the categories. On the contrary, Ni proved to be the least anthropogenically emitted element.

According to the I_{geo}, the most serious contamination occurred in connection with Cr, Cu and Pb. In the categories AIR, AFR and UR, the soils are moderately to heavily contaminated with Cr. For Cu, the soils of the categories AFR, UR and RR are moderately to heavily contaminated, while the AIR soils are even heavily contaminated. For Pb, the soils of the categories AIR and RR are moderately contaminated, while the soils of the categories UR and AFR are moderately to heavily contaminated. Pb and Cu reached the most extreme values (Fig. 1b).

According to the IPI_N, the soils of the categories AFR, UR and RR are classified into the class safe. The AIR soils are already in the class precaution, mainly due to several extreme values (Fig. 1c) indicating heavy local pollution.

According to the RI (Fig. 1d), soils in the categories AIR (157.1) and AFR (184.5) which fall under the category of moderate ecological risk, may pose a certain risk to biota. A closer focus on the risk posed by the individual HMs (Table S3) shows that ecological risk is mainly represented by Cu and Pb. This is mainly due to local soil pollution by these elements and also to the fact that Cu and Pb are ranked among the most toxic metals for both higher plants and certain microorganisms (Kabata-Pendias, 2011). The content of Cu in the AIR soils represents a considerable potential ecological risk, in other categories only moderate potential ecological risk. Pb

Table 1
Contents (mg/kg) of the HMs in the soils of the island.

		Co	Cr	Cu	Ni	Pb	Zn
Airport (n = 19)	Mean	4.9	10.5	22	5.5	7.5	84
	SD	1.2	4.9	23	1.0	4.7	69
Airport − Ferry port (n = 7)	Mean	3.76	8.2	13.6	7.0	24	58
	SD	0.64	2.9	6.2	1.7	36	26
Urban road (n = 13)	Mean	3.50	9.8	15.8	8.0	8.2	67
	SD	0.85	4.5	11.4	4.3	3.3	40
Rural road (n = 25)	Mean	3.6	7.0	13.4	7.1	7.1	45
	SD	1.5	3.0	8.7	4.3	4.4	19
Santorini soils (n = 64)	Mean	4.0	8.7	16	6.8	9.3	63
	SD	1.4	4.2	15	3.5	13.7	47
Background		1.8	1.1	1.3	4.6	1.3	20
Dutch Soil Guideline	Target Value	9	100	36	35	85	140
	Intervention Value	240	380	190	210	530	720

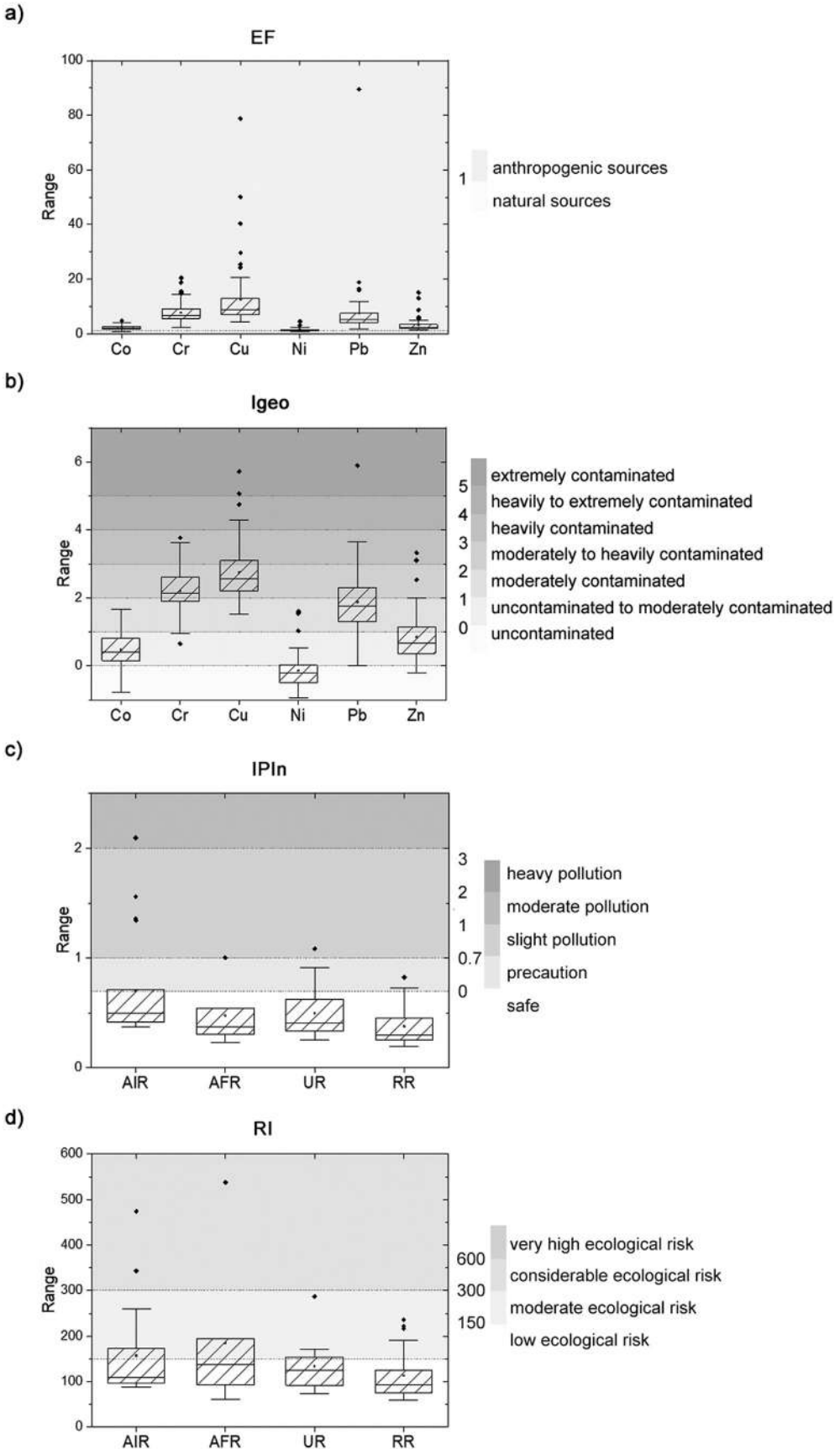

Fig. 1. Pollution and ecological risk indices.

represents a risk only in the AFR category, namely considerable potential ecological risk.

Although the Intervention Value (VROM, 2013) has not been exceeded in any case, which is, among other things, a prerequisite for serious endangering of soil functional properties for humans and other animals and plants, RI points to a potential threat. This is because it considers the adaptation of the ecosystem to natural background values, reflecting the sensitivity of the biological community to HMs (Huang et al., 2018). In the case of sensitive organisms, a significant alteration in natural conditions, in this case represented by anthropogenic contamination, can lead to a number of negative impacts on their health (Fasani et al., 2018). For instance, 2–10 fold increase in the content of HMs, such as Cu and Pb over natural values may lead to 20–40% decrease in soil biological activities (Tyler et al., 1989 in Kabata-Pendias, 2011), thus also in this case the contamination could have a negative impact on soil organisms. This assumption may be related to the findings made on Santorini by Vavoulidou et al. (2006) who states that the surface soils of the island have a general lack of soil fauna and clarification of the reason requires further investigation. Similar conclusions of danger of soil degradation due to tourism are also made by Ciarkowska (2018) in Poland, who associates it with a decrease in enzyme activity.

3.3. *Influence of tourism on soil contamination of the island*

Data visualization using box plots for each HM (not shown) revealed the asymmetry of the distribution, the presence of extreme values, the heteroscedasticity of the data and also the non-normal distribution of all the elements.

Subsequent testing of the compliance of the individual groups (AIR, AFR, UR, and RR) with the background value by Wilcoxon and permutation one-sample test did not indicate statistically significant background compliance for Co, Cr, Cu, Pb and Zn in any of the sets. For Ni, the permutation one-sample test revealed a statistically significant background match with the AFR group, attributed to a small number of measurements (n = 7).

The last step was to compare the individual sets separately for the calculated indices. The results of the application of the various tests are summarized in Table S4–S7. Since the results of statistical processing were not influenced by the choice of the method of adjusting the probability values (Hochberg-Benjamini vs. Holm), they are discussed in summary. The only exception was the application of the permutation k-sample test when testing Igeo in Co (Table S4).

All the tests used indicated a statistically significant mismatch between AIR, AFR, UR and RR at both significance levels 0.05 for both EF and I_{geo} calculated for Co, Cr and Zn (Tables S3 and S4). The methods of mutual comparison divided the sets into two groups.

The values of EF for Co (Table S4) were clearly divided into groups „a" (AIR) vs. „b" consisting of the RR and UR files. The AFR group was integrated into the same group as UR and RR by applying 3 tests (Dwass-Steel-Critchlow-Fligner, Anderson-Darling and Baumgartner-Weiss-Schindle) and at the „ab" group interface after using Nemenyi, Dumn, Conover, Van der Waerden, Lu-Smith and the permutation k-sample test. The ambiguity of the inclusion of AFR is attributed to the low number of samples (n = 7) and the resulting greater confidence interval width. The situation is very similar to Cr (Table S4), where AIR forms a group „a" vs. RR group „b". For most tests used, the AFR and the UR sets are evaluated at the interface of both „ab" groups except for the application of the permutation k-sample test, where all the analysed sets were evaluated as identical. The permutation test is the only one that works with raw data; it does not perform any transformation or exclude outliers, and therefore works with entire sets. From this point of view, this type of the test can be considered the most reliable. The same results were obtained for Zn (Table S4) – AIR (group „a") vs. RR (group „b"). The remaining AFR and UR groups were not unequivocally incorporated and are therefore at the „ab" interface, except for the result of the permutation test. For the other EF of the studied elements (Cu, Ni, and Pb), the tests used did not indicate a statistically significant agreement of the studied sets thus the methods of mutual comparison were not further applied.

Very similar distribution results were obtained in statistical processing of I_{geo} (Table S5). A difference in the application of two methods of adjusting p-values (B–H vs. Holm) after the application of the permutation k-sample test was identified only in I_{geo} of Co. In general, comparing the results of the statistical analysis EF and I_{geo} for all the elements shows that the permutation test at I_{geo} separates individual sets into groups (Co: AIR vs. RR and UR, AFR at the group interfaces or in the group with UR and RR, Cr and Zn: AIR vs. RR, AFR and UR were not clearly integrated).

Similarly, AIR (group „a") and RR (group „b") stand opposite at IPI_N (Table S6) like I_{geo} or EF for Zn. The AFR as well as UR sets were not included in any groups and thus they are on the border of „ab".

Statistical analysis of RI showed statistically significant agreement of the studied sets in all the tests used except for the Baumgartner-Weiss-Schindler test (Table S7). For this reason, the mutual comparison methods were not further applied in these tests. The Baumgartner-Weiss-Schindler test (B–H and Holm) gave the same grouping as IPI_N.

Statistical analysis was applied to determine the contribution of airport and road transport to the level of contamination. In this case, the premise of allocating the AIR set compared to AFR, UR, and RR can be considered to be met for almost all the elements and calculated indices. The samples taken around the perimeter of the airport have always been a separate group indicating the increased content of Co, Cr and Zn due to airport traffic. In the similar research to detect airborne contamination, Ray et al. (2012) state air transport as a possible emitter of Cu, Pb, Zn, Cr and Ni elements. At the same time, however, he adds that their source may also be motor vehicles, as it is difficult to distinguish between these two sources. In another similar study, Massas et al. (2016) links air transport with possible emissions of Zn, Pb and Ni. The consensus is therefore that air transport significantly emits mainly Zn. Nevertheless, further research is needed in this topic.

When evaluating the impact of tourism, it is expected that the AIR, AFR and UR sets will be set aside in comparison with the RR one. The results clearly show that the RR set differs statistically due to the low values of contents and indices of Co, Cr and Zn. Conversely, this is not the case of the AIR set that is also being set aside but with contradictory values of the content and indices. The most complicated set represents the samples collected from the sites on the road connecting two main transport links providing transport from the island and there – AFR. For this set, none of the applied statistical methods demonstrated inclusion in the AIR or RR groups and was evaluated at their interface. This is attributed to the small number of data subjected to statistical processing (n = 7). Thus, the hypothesis cannot be confirmed or refused in the AFR set. The last group to be evaluated is UR. The study of Ciarkowska (2018) mentions the possible pollution of urban soils by Pb, Zn and Cd due to tourism connected mainly with transport. In this case, the inclusion of UR showed statistical compliance with RR or AFR, and in specific cases also with AIR. In terms of the number of tests and results applied, it is likely that there is an agreement with AFR but it is not possible to unambiguously integrate this set and to confirm the impact of tourism statistically. Again, the tested set was relatively small (n = 13). AIR compliance was only detected in EF of Cr and Zn but merely after the application of the permutation k-sample test.

In spite of not entirely clear fulfilment of the initial hypothesis, it can be said that from the point of view of statistical analysis, the influence of tourism has been proved when comparing the results of the sets of two extreme groups, such as airport vs. places situated in the agricultural landscape, without continuous development and significant tourism. However, this is a conclusion that does not consider the level of contamination, only its demonstration. Combined with testing the compliance of the individual sets with the background value, where statistically significant non-compliance was shown, anthropogenic contamination can also be concluded, which was also confirmed by the EF and I_{geo} indices.

The results show that in an area like this, where contamination is still low, the application of statistical methods has been very useful to prove the contamination itself and also the impact of the type of traffic. The same approach should be applied in research studies with a similar topic, even if contamination is at a high level. In such case, the pollutants may already spread to surrounding areas which would normally not be considered problematic. In other words, a high level of contamination can lead to a gradual blurring of the differences between groups and its demonstration should be supported by appropriate statistical approaches. On the other hand, regular inspection of even less polluted tourist areas can prove the increasing effects of individual types of transport. As the mobility of the elements is influenced by a number of factors (Werkenthin et al., 2014), basic data diagnostics, such as monitoring of data distribution, identifying of outliers, testing of normality and heteroscedasticity should be performed on such dynamic systems. Then, all the statistical evaluations must be assessed comprehensively to obtain reliable conclusions, especially regarding the impact on human health, fauna and flora.

The current state of soil contamination of the island may be associated primarily with its development in the context of tourism which began to develop only in the 1970s and transformed fishing villages into tourist resorts (Wadih, 2005). It is therefore the result of fifty years of tourism. But its real dimension can be much larger. Since prevailing strong winds and soil erosion are typical on the island (Vavoulidou et al., 2006; Economou et al., 2007), HMs emitted by traffic can be easily transported off the road and contaminate more distant surroundings. Then, the roadside soils themselves may indicate lower values than would correspond to the level of contamination. A similar phenomenon has been described, for instance, by Chen et al. (2010). On the other hand, their mobility within the soil profile and their current availability for plants may be limited due to the alkaline pH of the island's soils. Further research is necessary in this area.

Given the rapid increase in traffic intensity (Delitheou and Georgakopoulou, 2017; Santorini Airport, 2019) on the island and the overall increase in anthropogenic pressure, soil contamination can be expected to increase rapidly in the future. Subsequent metal accumulation in plants, for example used in agriculture, can reduce their fitness and lead to significant toxic effects (Kabata-Pendias, 2011; Fasani et al., 2018), which may limit the growth of crops and ultimately also negatively affect wholesomeness of the resulting food products and their marketability (Nagajyoti et al., 2010; Mirzaei et al., 2019). This could have negative impacts, for instance, on local wine production. The local wine is of high quality and Santorini is an important wine producing region of the Greece (Vavoulidou et al., 2006).

In addition to contamination, the threat to land resources and agricultural production is represented by erosion associated with construction of tourist infrastructure (Zhong et al., 2011). The anticipated negative impact of increasing soil contamination and degradation may also endanger the ecosystem services of the natural systems of the island which may ultimately lead to tourism damage (Drius et al., 2019).

Santorini is increasingly associated with overtourism and questions about possible negative environmental impacts are emerging (Peeters et al., 2018). The results show that the current situation is unsustainable. It is essential to reduce tourism and introduce tourist quotas which will reduce the rate of increase in contamination and soil degradation. At the same time, it is advisable to continue in soil monitoring, which may lead to the state of better understanding of the HMs mobility in such environment and also better identification of pollution emitters on the example of this locality, which may serve as a model.

3.4. Comparison with other volcanic islands

In comparison with other volcanic islands (Table 2), two things are evident: high variability of HM contents in soils and significant influence of natural conditions. Most islands show markedly higher values for all the HMs, even though their contents are often given merely by geogenic origin and are not directly influenced by anthropogenic activities. Based on these findings, it may be concluded that although tourism can make a significant contribution to soil contamination in volcanic islands, the amount of HMs

Table 2
Average contents of HMs (mg/kg) on tourist attractive volcanic islands.

	Cd	Co	Cr	Cu	Ni	Pb	Zn	Reference**
Réunion (France)	0.2		300	58.0	206		162	1
Santiago (Cape Verde)*	0.2	45.9	135	51.8	137	5.9	83.6	2
Santa Maria (Portugal)*	n.d.	71.2	801	75.4	277	44.0	132	3
São Miguel (Portugal)*	n.d.	3.8	23.0	30.6	12.8	31.4	174	3
La Gomera (Spain)*			2.2	0.3	4.8		2.2	4
El Hierro (Spain)*	1.3	44.2	87.0	43.7	103		85.2	5
Jeju (Korea)*	0.4	77.0	662	49.0	170	44.0	125	6
Hawaii (USA)		66.0		122	294	56.0	282	7
Lesbos (Greece)		43.6	1673	28.9	1379	26.1	80.0	8
Santorini (Greece)	n.d.	4.0	8.7	16.4	6.8	9.3	62.5	This study

* Undisturbed natural soils.
**[1]Doelsch et al. (2006).
[2]Pinto et al. (2015).
[3]Amaral et al. (2006).
[4]Mora et al. (2012).
[5]Mendoza-Grimón et al. (2014).
[6]Ahn and Chon (2010).
[7]Sutherland and Tack (2000).
[8]Kazakou et al.(2010).

emitted by tourism is only a minor enrichment factor on a tourist-attractive volcanic islands globally. The geological bedrock of the island and other natural factors that lead to the majority of soil enrichment are important.

In view of the potential negative impacts on natural ecosystems due to high tourism as an emitter of HMs, primarily islands with a naturally low HM content, whose anthropogenically increased amount may lead to more severe impacts on native biota, which may be more sensitive to higher than natural contents of metals, should be monitored. Conversely, islands with a naturally high HM content and good adaptation of local ecosystems should be primarily monitored for possible health risks to humans. The threat to tourists is negligible in short-term visits but the local population's chronic intake of higher amounts of HMs from the environment can lead to a number of negative health impacts (Chabukdhara and Nema, 2013; Huang et al., 2018; Mirzaei et al., 2019).

4. Conclusions

On the island of Santorini, significant anthropogenic contamination with HMs, especially Cr, Cu and Pb, has been found. This contamination may already represent a moderate ecological risk to local ecosystems.

A significant influence of tourism on contamination of the island has been proved by the example of soil pollution near the airport. Airport traffic has been proved to be an important emitter of Co, Cr and especially Zn.

Compared to other volcanic islands, the detected HM content was mostly significantly lower. On this basis, it can be concluded that in the case of volcanic islands, whether used for tourism or with the potential for tourist use, the dominant factor determining the content of HMs in the soil is the parent rock respectively natural conditions.

Given the increasing intensity of tourism and related activities, it is expected that soil contamination of the island will grow rapidly which may have a negative impact on local ecosystems and, in the future, on the quality of the wine produced. It is therefore essential to reduce tourism by introducing tourist quotas which will reduce the rate of increase in contamination and soil degradation.

Tourism causes significant contamination of soil by HMs. Monitoring of this contamination can be used as a basis for decision making in tourism management and can contribute to the protection of nature and human health as part of fulfilment of environmental challenges within tourism sustainability.

CRediT authorship contribution statement

Martin Brtnický: Conceptualization, Data curation, Investigation, Methodology, Project administration, Resources, Visualization, Funding acquisition, Resources, Supervision, Writing - original draft. **Václav Pecina:** Conceptualization, Data curation, Investigation, Methodology, Project administration, Resources, Visualization, Writing - original draft. **Michaela Vašinová Galiová:** Formal analysis, Project administration, Supervision, Validation, Visualization, Writing - original draft. **Lubomír Prokeš:** Formal analysis, Data curation, Visualization. **Ondřej Zvěřina:** Investigation, Data curation. **David Juřička:** Data curation, Software, Validation, Writing - review & editing. **Martin Klimánek:** Data curation, Software, Validation. **Jindřich Kynický:** Methodology, Project administration, Writing - review & editing.

Acknowledgments

The work was supported by the projects of Ministry of Education, Youth and Sports of the Czech Republic FCH−S-19-5971 and Central European Institute of Technology (CEITEC 2020) LQ1601.

Appendix A. Supplementary data

Supplementary data to this article can be found online at https://doi.org/10.1016/j.chemosphere.2020.126118.

References

Adamo, P., Arienzo, M., Imperato, M., Naimo, D., Nardi, G., Stanzione, D., 2005. Distribution and partition of heavy metals in surface and sub-surface sediments of Naples city port. Chemosphere 61 (6), 800−809. https://doi.org/10.1016/j.chemosphere.2005.04.001.

Ahn, J.S., Chon, C.M., 2010. Geochemical distributions of heavy metals and Cr behavior in natural and cultivated soils of volcanic Jeju island, Korea. Geosystem Engineering 13 (1), 9−20. https://doi.org/10.1080/12269328.2010.10541304.

Santorini Airport, 2019. Air Traffic Statistics. https://www.jtr-airport.gr/en/jtr/air-traffic-statistics/. (Accessed 20 February 2019).

Al-Khashman, O.A., 2004. Heavy metal distribution in dust, street dust and soils from the work place in Karak Industrial Estate, Jordan. Atmos. Environ. 38 (39), 6803−6812. https://doi.org/10.1016/j.atmosenv.2004.09.011.

Ali, A.H.A., Hamed, M.A., El-Azim, H.A., 2011. Heavy metals distribution in the coral reef ecosystems of the Northern Red Sea. Helgol. Mar. Res. 65 (1), 67−80. https://doi.org/10.1007/s10152-010-0202-7.

Amaral, A., Cruz, J.V., Cunha, R.T.D., Rodrigues, A., 2006. Baseline levels of metals in volcanic soils of the Azores (Portugal). *Soil and Sediment Contamination*. Int. J. 15 (2), 123−130. https://doi.org/10.1080/15320380500506255.

Anderson, M.J., 2001. Permutation tests for univariate or multivariate analysis of variance and regression. Can. J. Fish. Aquat. Sci. 58 (3), 626−639. https://doi.org/10.1139/f01-004.

Azam, M., Alam, M.M., Hafeez, M.H., 2018. Effect of tourism on environmental pollution: further evidence from Malaysia, Singapore and Thailand. J. Clean. Prod. 190, 330−338. https://doi.org/10.1016/j.jclepro.2018.04.168.

Basso, D., Pesarin, F., Salmaso, L., Solari, A., 2009. Permutation Tests for Stochastic Ordering and ANOVA: Theory and Applications with R, vol. 194. Springer Science & Business Media.

Brtnický, M., Pecina, V., Hladký, J., Radziemska, M., Koudelková, Z., Klimánek, M., Richtera, L., Adamcová, D., Elbl, J., Vašinová Galiová, M., Baláková, L., 2019. Assessment of phytotoxicity, environmental and health risks of historical urban park soils. Chemosphere 220, 678−686. https://doi.org/10.1016/j.chemosphere.2018.12.188.

Buckley, R., 2011. Tourism and environment. Annu. Rev. Environ. Resour. 36, 397−416. https://doi.org/10.1146/annurev-environ-041210-132637.

Chabukdhara, M., Nema, A.K., 2013. Heavy metals assessment in urban soil around industrial clusters in Ghaziabad, India: probabilistic health risk approach. Ecotoxicol. Environ. Saf. 87, 57−64. https://doi.org/10.1016/j.ecoenv.2012.08.032.

Chen, X., Xia, X., Zhao, Y., Zhang, P., 2010. Heavy metal concentrations in roadside soils and correlation with urban traffic in Beijing, China. J. Hazard Mater. 181 (1−3), 640−646. https://doi.org/10.1016/j.jhazmat.2010.05.060.

Cheng, H., Li, M., Zhao, C., Li, K., Peng, M., Qin, A., Cheng, X., 2014. Overview of trace metals in the urban soil of 31 metropolises in China. J. Geochem. Explor. 139, 31−52. https://doi.org/10.1016/j.gexplo.2013.08.012.

Ciarkowska, K., 2018. Assessment of heavy metal pollution risks and enzyme activity of meadow soils in urban area under tourism load: a case study from Zakopane (Poland). Environ. Sci. Pollut. Control Ser. 25 (14), 13709−13718. https://doi.org/10.1007/s11356-018-1589-y.

Conover, W.J., 1999. Practical Nonparametric Statistics, third ed. Wiley, Hoboken.

Davenport, J., Davenport, J.L., 2006. The impact of tourism and personal leisure transport on coastal environments: a review. Estuar. Coast Shelf Sci. 67 (1−2), 280−292. https://doi.org/10.1016/j.ecss.2005.11.026.

Delitheou, V., Georgakopoulou, S., 2017. The contribution of tourism to local development: the case of the island of Santorini. Journal of Tourism Research 17 (1), 173−184. ISSN 2241−7931.

Doelsch, E., Saint Macary, H., Van de Kerchove, V., 2006. Sources of very high heavy metal content in soils of volcanic island (La Réunion). J. Geochem. Explor. 88 (1−3), 194−197. https://doi.org/10.1016/j.gexplo.2005.08.037.

Dominey-Howes, D., Minos-Minopoulos, D., 2004. Perceptions of hazard and risk on Santorini. J. Volcanol. Geoth. Res. 137 (4), 285−310. https://doi.org/10.1016/j.jvolgeores.2004.06.002.

Drius, M., Bongiorni, L., Depellegrin, D., Menegon, S., Pugnetti, A., Stifter, S., 2019. Tackling challenges for Mediterranean sustainable coastal tourism: an ecosystem service perspective. Sci. Total Environ. 652, 1302−1317. https://doi.org/10.1016/j.scitotenv.2018.10.121.

Economou, A., Skouteri, A., Michopoulos, P., 2007. Soils and land use of Santorini, Greece. In: Arnalds, Ó., Óskarsson, H., Bartoli, F., Buurman, P., Stoops, G., García-Rodeja, E. (Eds.), Soils of Volcanic Regions in Europe. Springer, Berlin, Heidelberg.

Fasani, E., Manara, A., Martini, F., Furini, A., DalCorso, G., 2018. The potential of

genetic engineering of plants for the remediation of soils contaminated with heavy metals. Plant Cell Environ. 41 (5), 1201–1232. https://doi.org/10.1111/pce.12963.
Goeman, J.J., Solari, A., 2014. Multiple hypothesis testing in genomics. Stat. Med. 33 (11), 1946–1978. https://doi.org/10.1002/sim.6082.
Has-Schön, E., Bogut, I., Strelec, I., 2006. Heavy metal profile in five fish species included in human diet, domiciled in the end flow of River Neretva (Croatia). Arch. Environ. Contam. Toxicol. 50 (4), 545–551. https://doi.org/10.1007/s00244-005-0047-2.
Hellenic Civil Aviation Authority (HCAA), 2019. Statistical data of Santorini airport for the period 1994–2017. http://www.ypa.gr/en/our-airports/kratikos-aerolimenas-santorinhs-kasr/. (Accessed 20 February 2019).
Hollander, M., Wolfe, D.A., Chicken, E., 2014. Nonparametric Statistical Methods, third ed. Wiley, Hoboken.
Huang, Y., Chen, Q., Deng, M., Japenga, J., Li, T., Yang, X., He, Z., 2018. Heavy metal pollution and health risk assessment of agricultural soils in a typical peri-urban area in southeast China. J. Environ. Manag. 207, 159–168. https://doi.org/10.1016/j.jenvman.2017.10.072.
ISO 10390, 2005. Soil Quality - Determination of pH, 2nd ed. ISO/TC 190/SC 3 Chemical methods and soil characteristics.
ISO 14235, 1998. Soil quality - Determination of organic carbon by sulfochromic oxidation, 1st ed. ISO/TC 190/SC 3 Chemical methods and soil characteristics.
Jenkins, S.F., Barsotti, S., Hincks, T.K., Neri, A., Phillips, J.C., Sparks, R.S.J., Sheldrake, T., Vougioukalakis, G., 2015. Rapid emergency assessment of ash and gas hazard for future eruptions at Santorini Volcano, Greece. Journal of Applied Volcanology 4 (1), 16. https://doi.org/10.1186/s13617-015-0033-y.
Kabata-Pendias, A., 2011. Trace Elements in Soils and Plants, fourth ed. CRC Press, ISBN 978-1-4200-9368-1.
Kazakou, E., Adamidis, G.C., Baker, A.J., Reeves, R.D., Godino, M., Dimitrakopoulos, P.G., 2010. Species adaptation in serpentine soils in Lesbos Island (Greece): metal hyperaccumulation and tolerance. Plant Soil 332 (1–2), 369–385. https://doi.org/10.1007/s11104-010-0302-9.
Li, G., Yang, X., Liu, Q., Zheng, F., 2014. Destination island effects: a theoretical framework for the environmental impact assessment of human tourism activities. Tourism Management Perspectives 10, 11–18. https://doi.org/10.1016/j.tmp.2013.12.001.
Lu, H.T., Smith, P.J., 1979. Distribution of the normal scores statistic for nonparametric one-way analysis of variance. J. Am. Stat. Assoc. 74 (367), 715–722.
Lukashina, N.S., Amirkhanov, M.M., Anisimov, V.I., Trunev, A., 1996. Tourism and environmental degradation in Sochi, Russia. Ann. Tourism Res. 23 (3), 654–665. https://doi.org/10.1016/0160-7383(95)00086-0.
Massas, I., Ioannou, D., Kalivas, D., Gasparatos, D., 2016. Distribution of heavy metals concentrations in soils around the international Athens airport (Greece). An assessment on preliminary data. Bull. Geol. Soc. Greece 50 (4), 2231–2240. https://doi.org/10.12681/bgsg.14279.
Memoli, V., Esposito, F., Panico, S.C., De Marco, A., Barile, R., Maisto, G., 2019. Evaluation of tourism impact on soil metal accumulation through single and integrated indices. Sci. Total Environ. 682, 685–691. https://doi.org/10.1016/j.scitotenv.2019.05.211.
Mendoza-Grimón, V., Hernández-Moreno, J.M., Martín, J.R., Fernández-Vera, J.R., Palacios-Díaz, M.P., 2014. Trace and major element associations in basaltic ash soils of El Hierro Island. J. Geochem. Explor. 147, 277–282. https://doi.org/10.1016/j.gexplo.2014.06.010.
Mirzaei, M., Marofi, S., Solgi, E., Abbasi, M., Karimi, R., Bakhtyari, H.R.R., 2019. Ecological and health risks of soil and grape heavy metals in long-term fertilized vineyards (Chaharmahal and Bakhtiari province of Iran). Environ. Geochem. Health 1–17. https://doi.org/10.1007/s10653-019-00242-5.
Mora, J.L., Arbelo, C.D., Rodríguez-Rodríguez, A., Notario, J.S., Guerra, J.A., Armas, C.M., 2012. The role of metals in soils and accumulation in the laurel forest of La Gomera (Canary Islands, Spain): preliminary results. Eur. J. Soil Sci. 63 (5), 674–684. https://doi.org/10.1111/j.1365-2389.2012.01444.x.
Moustakas, N.K., Georgoulias, F., 2005. Soils developed on volcanic materials in the island of Thera, Greece. Geoderma 129 (3–4), 125–138. https://doi.org/10.1016/j.geoderma.2004.12.039.
Murakami, H., 2012. Modified Baumgartner statistics for the two-sample and multisample problems: a numerical comparison. J. Stat. Comput. Simulat. 82 (5), 711–728. https://doi.org/10.1080/00949655.2010.551516.
Nagajyoti, P.C., Lee, K.D., Sreekanth, T.V.M., 2010. Heavy metals, occurrence and toxicity for plants: a review. Environ. Chem. Lett. 8 (3), 199–216. https://doi.org/10.1007/s10311-010-0297-8.
Oklevik, O., Gössling, S., Hall, C.M., Steen Jacobsen, J.K., Grøtte, I.P., McCabe, S., 2019. Overtourism, optimisation, and destination performance indicators: a case study of activities in Fjord Norway. J. Sustain. Tourism 1–21. https://doi.org/10.1080/09669582.2018.1533020.
Peeters, P., Gössling, S., Klijs, J., Milano, C., Novelli, M., Dijkmans, C., Eijgelaar, E., Hartman, S., Heslinga, J., Isaac, R., Mitas, O., Moretti, S., Nawijn, J., Papp, B., Postma, A., 2018. Overtourism: Impact and Possible Policy Responses. Research for TRAN Committee. European Parliament, Policy Department for Structural and Cohesion Policies, Brussels.
Pigram, J.J., Wahab, S. (Eds.), 2005. Tourism, Development and Growth: the Challenge of Sustainability. Routledge.
Pinto, M.C., da Silva, E.F., Silva, M.M.V.G., Melo-Gonçalves, P., 2015. Heavy metals of Santiago Island (Cape Verde) top soils: estimated background value maps and environmental risk assessment. J. Afr. Earth Sci. 101, 162–176. https://doi.org/10.1016/j.jafrearsci.2014.09.011.
Ray, S., Khillare, P.S., Kim, K.H., 2012. The effect of aircraft traffic emissions on the soil surface contamination analysis around the international airport in Delhi, India. *Asian Journal of Atmospheric Environment* (AJAE) 6 (2). https://doi.org/10.5572/ajae.2012.6.2.118.
Scholz, F.W., Stephens, M.A., 1987. K-sample anderson–darling tests. J. Am. Stat. Assoc. 82 (399), 918–924. https://doi.org/10.1080/01621459.1987.10478517.
Sheskin, D.J., 2004. Handbook of Parametric and Nonparametric Statistical Procedures, third ed. Chapman & Hall, Boca Raton.
Sutherland, R.A., Tack, F.M., 2000. Metal phase associations in soils from an urban watershed, Honolulu, Hawaii. Sci. Total Environ. 256 (2–3), 103–113. https://doi.org/10.1016/S0048-9697(00)00458-7.
Tam, N.F.Y., Wong, Y.S., 2000. Spatial variation of heavy metals in surface sediments of Hong Kong mangrove swamps. Environ. Pollut. 110 (2), 195–205. https://doi.org/10.1016/S0269-7491(99)00310-3.
Tyler, G., Påhlsson, A.M.B., Bengtsson, G., Bååth, E., Tranvik, L., 1989. Heavy-metal ecology of terrestrial plants, microorganisms and invertebrates. Water Air Soil Pollut. 47 (3–4), 189–215. https://doi.org/10.1007/BF00279327.
Vavoulidou, E., Avramides, E.J., Dimirkou, A., Papadopoulos, P., 2006. Influence of different cultivation practices on the properties of volcanic soils on Santorini Island, Greece. Commun. Soil Sci. Plant Anal. 37 (15–20), 2857–2866.
VROM, 2013. Circular on Target Values and Intervention Values for Soil Remediation. Dutch Ministry of Housing Spatial Planning and Environment (VROM).
Wadih, H.E., 2005. Identifying and Assessing Tourism Impact Factors on Localities and Their Nations: with Illustrations from Santorini. Master Thesis. University of Cincinnati.
Werkenthin, M., Kluge, B., Wessolek, G., 2014. Metals in European roadside soils and soil solution–A review. Environ. Pollut. 189, 98–110. https://doi.org/10.1016/j.envpol.2014.02.025.
Zhong, L., Deng, J., Song, Z., Ding, P., 2011. Research on environmental impacts of tourism in China: progress and prospect. J. Environ. Manag. 92 (11), 2972–2983. https://doi.org/10.1016/j.jenvman.2011.07.011.

Environ Monit Assess (2020) 192: 771
https://doi.org/10.1007/s10661-020-08748-7

Inorganic pollutants in the indoor environment of the Moravian Library: assessment of Cd, Pb, Cu, and Zn in total suspended particles and dust using HR-CS GF-AAS

Ondřej Zvěřina · Pavel Coufalík · Jan Šimůnek · Přemysl Kachlík · Radka Chlupová · Jindra Pavelková

Received: 6 May 2020 / Accepted: 10 November 2020 / Published online: 19 November 2020

Abstract In this study, the occurrence of lead (Pb), cadmium (Cd), copper (Cu), and zinc (Zn) in the environment of the Moravian Library in Brno, the second largest library in Czechia, was in focus. The materials of interest were airborne particles, dust originating from books, and also book pages. Total suspended particles (TSP) were sampled in different areas of the library, including the reading room, the book depository, and an external book warehouse. Samples of dusts were obtained from the book-cleaning system, and, moreover, some pages taken from old books were also analyzed. Samples were microwave-digested and analyzed using graphite furnace high-resolution continuum source AAS (HR-CS GF-AAS). During the analysis, possibilities of the signal intensity modulation of the HR-CS technique were demonstrated and employed in order to determine Zn, an element which is rarely determined by GF-AAS. The median TSP concentrations (in ng/m^3) were as follows: Pb, 4.4; Cd, 0.07; Cu, 2.6; and Zn, 20.9. Such concentrations are safely below allowed limits. Contents of Pb determined in dust samples and book pages were slightly higher (up to 707 and 38 mg/kg, respectively) than the usually reported values. However, none of these results indicate a potential risk to library staff or readers.

Keywords Total suspended particles · Book depository · Heavy metals · Indoor environment · High-resolution continuum source atomic absorption spectrometry

O. Zvěřina (✉) · J. Šimůnek
Department of Public Health, Faculty of Medicine, Masaryk University, Kamenice 5, 625 00 Brno, Czech Republic
e-mail: zverina@med.muni.cz

P. Coufalík
Institute of Analytical Chemistry of the Czech Academy of Sciences, Veveří 97, 602 00 Brno, Czech Republic

P. Kachlík · R. Chlupová · J. Pavelková
Moravian Library in Brno, Kounicova 65a, 601 87 Brno, Czech Republic

Introduction

Both the importance of and interest in the quality of indoor environments have been growing in recent decades (Rasmussen et al. 2013). Amongst the various potential risk factors, settled dust and airborne particles are of special significance as they act as carriers of both organic and inorganic pollutants. Such materials may affect human health via inhalation, skin contact, or unintentional ingestion.

Although environments inside buildings are driven by outdoor conditions, indoor dust usually exhibits higher levels of metal contamination, mainly because of limited rates of air exchange and, in some cases, also because of the presence of locally specific sources (Hassan 2012; Tan et al. 2016), for instance, museum exhibits that had been preserved by heavy metal compounds (Marcotte et al. 2017). The presence of some dust is inevitable in institutions that abound in large collections of books and other items, and it is of a matter of concern about public health that the potential risks of such environments be explored.

Inhalation of suspended particulate pollutants is associated with adverse health effects, particularly provoking respiratory and cardiovascular diseases (WHO 2000; Morawska and Salthammer 2003; Zhang et al. 2020). Upon inhalation, only the fine fraction of particles (< 2.5 μm) is capable of deep lung penetration, whilst larger particles are sequestered in the upper airway and eventually reaches gastrointestinal tract.

Adverse human health outcomes are highly dependent on composition of the particles (Mukhtar and Limbeck 2013; Tan et al. 2016; Zhang et al. 2020). The elemental composition of total suspended particles (TSP) and dust sampled in indoor environments has been investigated in numerous studies, focusing mainly on household dust (e. g. Hassan 2012; Rasmussen et al. 2013; Wu et al. 2019), but also on some working environments (Xue et al. 2012; Niu et al. 2021) including museums (Marcotte et al. 2017) and libraries (Zhao et al. 2019; Mašková et al. 2016). Among the associated inorganic pollutants, lead (Pb), cadmium (Cd), copper (Cu), and zinc (Zn) are the most often investigated elements in indoor dust (Morawska and Salthammer 2003).

This work focuses on the inner environment of the Moravian library in Brno, the second largest library in the Czechia, with over 4 million publications. Pb, Cd, Cu, and Zn contents were analyzed in TSP and in samples of dust and leaves from deposited books. The assessment of potential health risks to library staff as well as the development of an analytical method for metal determination was the main aims.

Materials and methods

As for the investigation of indoor airborne particles, TSP were collected in different areas of the library. (Because the substantial proportion of aerosol in the library environment is expected to be composed of coarse particles originating from mechanical processes, TSP rather than fine particles were sampled.) In addition, samples of dust resulting from the cleaning of books from the library collection were assessed, together with samples of pages taken from a selection of books themselves. All these samples were analyzed for contents of the four metals of interest (Pb, Cd, Cu, and Zn) by means of microwave digestion followed by graphite furnace atomic absorption spectrometry (GF-AAS).

Collection of samples and their preparation

Total suspended particles (TSP) were sampled using a NILU filter system (Norwegian Institute for Air Research, Norway) in different areas of the library (Fig. 1), including the book depository, the reading room, and an external book warehouse. Indoor aerosol was collected for 24 h by filtration through Millipore cellulose nitrate membrane filters with a 1.2 μm pore size at a flow rate of 10 L/min. Using this procedure, particles of sizes ranging from ultra-fine to coarse particles are collected. Five filters were sampled in each area.

Samples of dust and dirt from book covers were obtained from a Depulvera® automatic book cleaning system (Oracle, Italy, Fig. 1). The samples were collected from both the inner fine-dust HEPA filter (this fraction is further called "fine dust") and the container for coarse dirt (called "coarse dust", consisting, e.g., of small pieces of book covers) of a vacuum cleaner connected to the system.

In order to assess the actual composition of books, samples of leaves taken from redundant books stored in the library's depositories were also analyzed. The leaves were taken from books dating from the late nineteenth and early twentieth centuries. Parts of these pages obtained by quartation were milled using an IKA A11 Basic laboratory mill (IKA Werke, Germany); then, aliquots of the homogenised material (Fig. 1) were subjected to digestion.

All of the above-mentioned samples were digested by means of a microwave digestion system (MLS-1200 Mega, Milestone, IT). The membrane filters were digested with 3 ml of nitric acid (Analpure ®, Analytika, Czechia). The clear solutions that were obtained were diluted with MQ water up to a volume of 10 ml. Approximately 200 mg aliquots of dust and book pages were digested with 4 mL of nitric acid. After cooling, the digests were filtered to remove undissolved residues and then diluted with MQ water up to a volume of 20 mL.

To ensure the analytical quality of the results, three certified reference materials were processed together with the samples: BCR-482 Lichen, BCR-191 Brown bread, and INCT-TL-1 Tea leaves. In addition, six procedural blanks were prepared for estimation of the limit of determination (LOD) and quantification (LOQ). In the case of TSP, six non-exposed membrane filters were digested.

Fig. 1 Areas of the library: book depository (1a), reading room (1b), and external book warehouse (1c); book cleaning system (2), and samples of book pages (3)

Determination of Cd, Pb, Cu, and Zn by means of HR-CS GF-AAS

The concentrations of the four selected elements in prepared digests were determined by means of high-resolution continuum source graphite furnace AAS (HR-CS GF-AAS) using a ContrAA 800G spectrometer (Analytik Jena, Germany). The optimized conditions are listed in Table 1.

Whereas the concentrations of Cd in digests ranged from sub-ppb to ppb levels (i.e., within the usual calibration range of GF-AAS), the concentrations of Pb, Cu, and especially of Zn were too high to be measured using their primary lines. Owing to the possibility of HR-CS technique to measure the absorption at any wavelength, following means of signal intensity reduction were employed.

While secondary lines of Pb and Cu with lower intensities were used for the determination of higher concentrations (see Table 1), the only secondary absorption line of Zn (307.590 nm) is of limited significance due to its sensitivity of only 0.02 %. Because of this fact—combined with the enormous sensitivity at the primary line (Zn is the most sensitive element in AAS)—GF-AAS is rarely used for Zn determination. Eventually, in our study, the determination of Zn content was performed by reducing the signal using signal attenuation (see following chapter).

Zn determination using signal attenuation

In contrast to conventional line source AAS, the HR-CS technique enables the sensitivity to be reduced by means of signal attenuation, i.e. it allows signal to be read at the line wings. This approach allowed us to determine the high concentrations of Zn without either a large dilution of samples followed by the demanding analysis of ultra-trace concentrations or even employing a completely different method of analysis (e.g. flame-AAS).

Reading the signal with weak, medium, and strong attenuation resulted in signal reduction by factors of 4, 20, and, 50, respectively. For the determination of Zn in our digests, medium attenuation (i.e., reading at +/- 2 pixels from the central pixel, Fig. 2) was selected, which, combined with the injection of 5 μL of solution, enabled a linear range of calibration up to 100 μg/L Zn (integrated absorbance 0.18, $R^2 = 0.998$).

The procedure was optimized in terms of pyrolysis and atomization temperature (Fig. 2). The presence of $Pd/Mg(NO_3)_2$ modifier prevented the formation of double peaks. Obtained peaks were symmetric and Gaussian shaped with a clean baseline.

As for possible interferences, it should be noted that reading a signal at a different wavelength may be associated with new spectral overlaps. Potentially interfering lines representing iron (213.859 nm) and copper (213.970 nm) are in close proximity to the primary Zn

Table 1 Operating conditions and analytical performance of the determination of Pb, Cd, Cu, and Zn

Parameter	Pb	Cd	Cu	Zn
Analytical line and relative sensitivity	283.306 nm (42 %)	228.802 nm (100 %)	327.396 nm (45 %), 216.509 nm (13 %)	213.857 nm (100 %), medium attenuation (+/-2 px)
Sample volume	20 μL	20 μL	20 μL	5 μL
Modifier	$Pd/Mg(NO_3)_2$	$Pd/Mg(NO_3)_2$	$Pd/Mg(NO_3)_2$	$Pd/Mg(NO_3)_2$
Pyrolysis temp.	800 °C	750 °C	1100 °C	800 °C
Atomization temp.	1900 °C	1250 °C	2100 °C	1400 °C
Procedural LOD (dust and pages) [a]	0.01 mg/kg	0.02 mg/kg	0.02 mg/kg	0.04 mg/kg
Procedural LOQ (dust and pages) [a]	0.04 mg/kg	0.06 mg/kg	0.07 mg/kg	0.1 mg/kg
Procedural LOD (suspended particles) [b]	0.1 ng/m^3	0.01 ng/m^3	0.2 ng/m^3	0.7 ng/m^3
Procedural LOQ (suspended particles) [b]	0.3 ng/m^3	0.02 ng/m^3	0.5 ng/m^3	2.4 ng/m^3
Precision [c]	< 3.9 %	< 4.1 %	< 3.2 %	< 5.9 %
Accuracy (recovery of CRMs)	92–106 %	85–99 %	91–111 %	91–108 %

[a] *Procedural limits of detection/quantification (LOD/LOQ) are calculated as 3 and 10 s/m, respectively, where s is the standard deviation obtained from the analyses of six digestion blanks and m is the slope of calibration graph. Values are expressed in mg/kg of solid sample*

[b] *LOD/LOQ of suspended particles analysis were calculated based on standard deviation of six digestions of non-exposed membrane filters*

[c] *Expressed as the relative standard deviation of five replicated measurements of CRM digests*

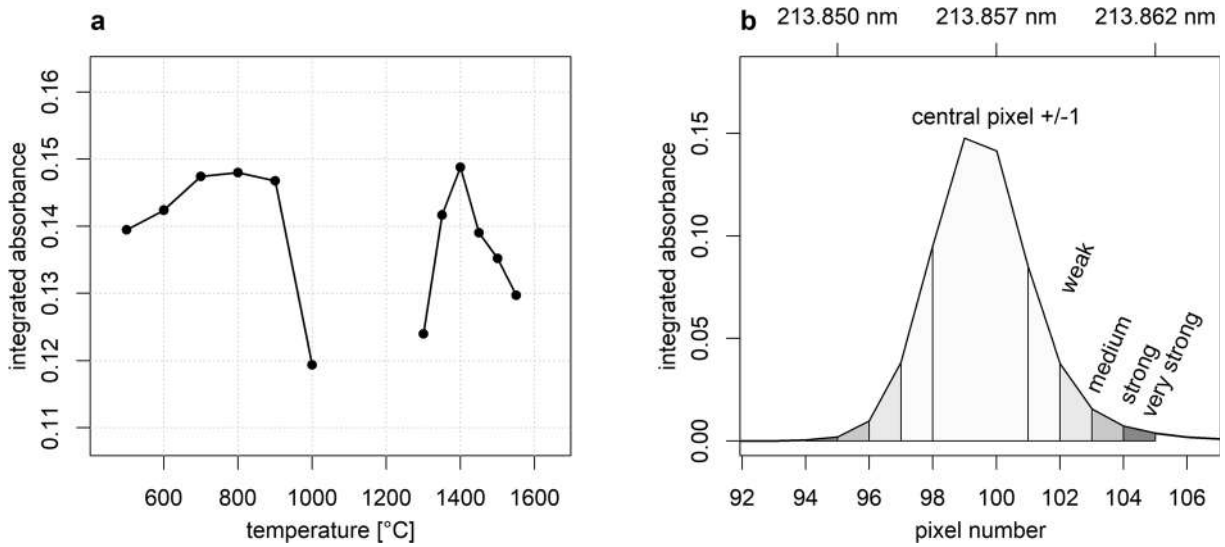

Fig. 2 Pyrolysis and atomization curve for Zn in digests of total suspended particles on a membrane filter with the addition of Pd/$Mg(NO_3)_2$ modifier **a** and a profile of the Zn-absorption line at 213.857 nm with indicated attenuation modes **b**

line (213.857 nm). However, since Fe and Cu are stable at an atomization temperature of 1400 °C, they are not volatilized and, thus, do not interfere under the given measurement conditions.

Data analysis

Statistical analysis of the obtained results was performed using "R" statistical software version 3.4.1 (R Development Core Team 2013). The normality of the data was assessed using the Shapiro-Wilk test; differences in the contents of elements in different kinds of samples were tested using t-test and ANOVA. The significance level was defined as $p < 0.05$.

Results and discussion

Metals in total suspended particles (TSP)

Using the described procedure, the contents of Pb, Cd, Cu, and Zn in TSP samples were determined. Despite the diverse nature of the selected areas of the library, no significant differences in element concentrations between the reading room, the book depository, and the external book warehouse were observed (ANOVA, $p > 0.05$). However, this was mainly the result of the high inter-day variability of the concentrations. Thus, the data from all sampling locations were merged together (see Figure 3, the individual values can be found in Supplementary Table 1). Median concentrations of the investigated elements in TSP decreased in the following order: Zn > Pb > Cu > Cd. Such an order of occurrence is common in indoor TSP and dust (Tan et al. 2016; Wu et al. 2019; Niu et al. 2021). Their absolute concentrations are similar to those reported for household environments in some Chinese cities (Wu et al. 2019) and approx. two to three orders of magnitude lower than reported for some indoor working environments (Xue et al. 2012; Marcotte et al. 2017; Niu et al. 2021) and outdoor environments in urban/industrial areas (Tasić et al. 2017; Zhang et al. 2020). From the comparison of the obtained results with the mentioned studies, the relative cleanliness of the library environment is evident.

Generally, TSP consist of a heterogeneous mixture of particles differing in size and composition. In terms of size, airborne particles range from ultra-fine particles of cca. 1 nm (which corresponds to molecular size and originate mainly from combustion processes) to large particles with diameters of about 100 μm, which result mainly from resuspension and mechanical processes and sediment rapidly due to gravitation (Turner and Colbeck 2008; Bo et al. 2017). The mass ratio of fine particles is usually small due to the typically much higher occurrence of large heavier particles. In library environments, mostly the coarse fraction (larger than 1 μm) is expected as no typical sources of fine particles exist (such as cooking or smoking).

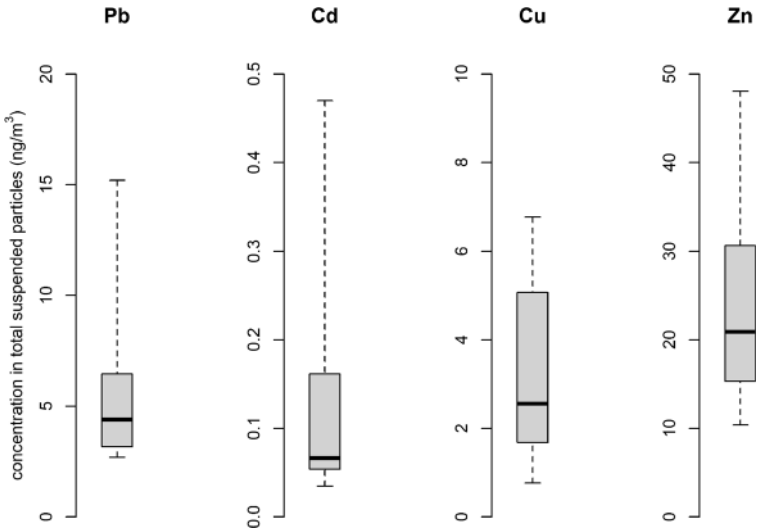

Fig. 3 Concentrations of Pb, Cd, Cu, and Zn in total suspended particles at all three sampling sites

Coarser constituents of TSP have their origin in mechanical processes such as the abrasion of textiles and fittings or, in the case of the library, handling books and magazines. The movement of people was also identified as a source of coarse particles: an increase in particles greater than 1 μm in size was documented during visiting hours at the National Library in Prague (Mašková et al. 2016). Otherwise, in environments with no active sources of suspended particles (the external book warehouse, in our case), the main constituents of TSP may even be particles penetrating from the outdoor environment (Morawska and Salthammer 2003).

Because the TSP fraction sampled here included not only fine particles (i.e., < $PM_{2.5}$) but also particles too large to penetrate the human thorax (WHO 2000), the comparison of our results with studies focused on the composition of PM_{10} (most cases) or with air quality guidelines is problematic. However, according to available data, the usual contribution of PM_{10} to the total suspended particles is known to range between 40 and 80% (WHO 2000; Xue et al. 2012; Tasić et al. 2017). Due to the fact that maximum concentrations of metals in TSP were at least one order of magnitude below WHO guidelines (which are set for Pb and Cd in PM_{10}; WHO Regional Office 2000), the indoor air quality in the Moravian Library can in this regard be considered as safe.

Metals in dust collected from books

The contents of the elements in dust collected from the book cleaning system are plotted in Fig. 4. The contents in both dust fractions followed same order of occurrence as in TSP (Zn > Pb > Cu > Cd). Relatively high Pb contents with a median of 527 and a maximum of 707 mg/kg are of particular note. However, it should be kept in mind that dust obtained only from books presents a very special case and represents only a subtraction of indoor dust, which means that the presented results are of limited comparability with other studies. Nevertheless, the following comparisons reveal recurring trends.

For instance, with respect to data obtained in a large scale Canadian study on household dust performed by Rasmussen et al. (2013), where samples were collected from over a thousand urban homes, our results generally lie within the range published for these household dust samples, except for Cd, which we found at even lower levels than reported in the abovementioned study. Median contents of the other elements in our samples (for fine and coarse dust combined) were close to the 10th percentile for Cu; between the 90th and 95th percentiles for Pb; and finally, between the 98th percentile and the maximum for Zn.

When focusing on Pb, which is a pollutant of special interest in this work due to its role in former letterpress printing process, we can see that its content was higher than values reported in most of the indoor-dust related studies reviewed by Tan et al. (2016), these ranging from 5.8 to 639.1 mg/kg. (The highest levels were observed in areas with heavy traffic and the usage of leaded fuel at that time). Similarly, the contents of Zn found in our study corresponded to the highest reported values, while Cu contents were generally comparable and Cd contents in our samples were lower than reported in most studies included in the review.

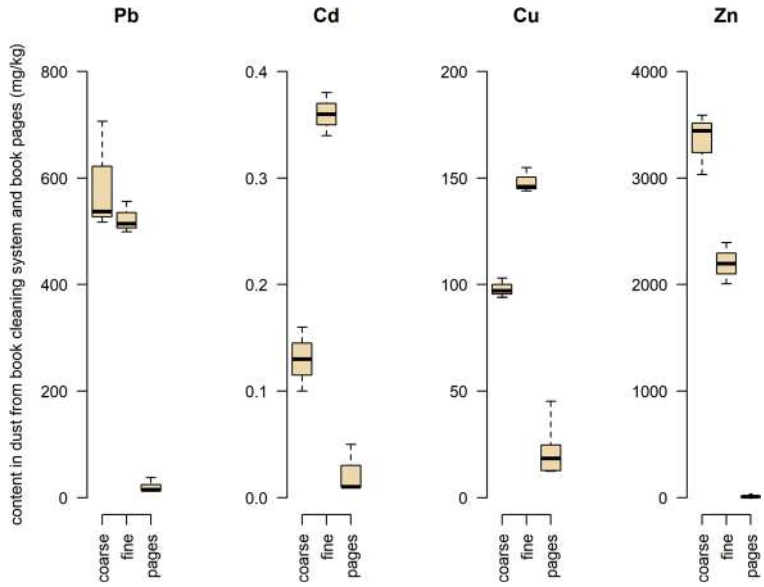

Fig. 4 Contents of Pb, Cd, Cu, and Zn in both coarse and fine dust collected from the book cleaning system and in leaves taken from selected books

The levels of both Pb and Zn were elevated even in comparison with data reported for indoor dust from university libraries in China (Zhao et al. 2019). The contents of Cd and Cu followed, again, a similar trend, i.e., Cd contents in our samples were lower, whilst those of Cu correspond to the reported levels.

From these comparisons with the literature, it is clear that the level of Pb in the studied environment is particularly noteworthy. A former printing technique involving lead-based metal type is expected to be the most important source of Pb in the samples. However, it should be kept in mind that the detected Pb levels are still similar to those usually reported and are far from posing any significant risk. To provide an opposite example, much higher Pb contents were determined in settled dust in an old museum building (over 50 g/kg), with Pb-containing wall paint identified as the likely source (Marcotte et al. 2017).

When considering the differences between the fine and coarse dust fractions separated by the book cleaning system, with the exception of Pb, the contents of metals differed significantly between coarse and fine material (*t* test, $p < 0.05$): higher amounts of Cd and Cu occurred in fine particles whilst contents of Zn were higher in the coarse material. These findings are in agreement with observations by Hassan (2012), who showed how fine particles accumulate heavy metals due to their larger surface. Here, however, this trend did not apply to Pb, which may be explained by its expected origin from the degraded material of book covers themselves rather than from adsorption onto particles from outside sources.

Metals in book pages

The contents of studied metals in leaves taken from books were of different order than those observed in TSP and in both dust fractions: Cu ~ Pb ~ Zn > Cd (Supplementary Table 1). Contents of Pb, Zn, and Cu in pages did not differ significantly (ANOVA, $p > 0.05$). Pb content of up to 37.6 mg/kg most likely results from its presence in type-metal alloys, of which it is the main component (Davis 1973). For example, the maximum determined Pb content of 38 mg/kg determined in a book of weight of 0.5 kg means a total Pb content of 19 mg per this book. Like Pb, Cu has also been used in some alloys for hardening type metal (Ridler 1972).

In general, the determined metal contents are very similar to those reported for modern printed paper (Manso et al. 2011) and also for newspapers (Manso et al. 2007). According to the analysis of newspapers from different years, there has been a decreasing trend in the contents of most metals (Manso et al. 2007). The same trend can be assumed for dust resulting from the degradation of print of different ages.

As can be seen from Fig. 4, the contents of all measured elements in leaves taken from books were substantially lower than in dust collected from the book cleaning system, which may indicate: 1) the tendency of metals to accumulate on the surface of books, which is of greater importance due to the possibility of direct transmission to readers and library staff, 2) that book covers are often decorated in pigments which may be sources of metal contamination, and/or 3) that metals deposited on books have a predominantly exogenic origin.

Conclusions

As people nowadays spend most of their time indoors, the quality of indoor environments is becoming an increasingly important parameter of public health. In terms of the content of the assessed metals (Pb, Cd, Cu, and Zn), the airborne particles suspended in indoor air of the Moravian Library do not pose a health risk. Samples of dust deposited on books in the library collection contain relatively high amounts of Zn and especially of Pb, which distinguishes this material from common household dust. However, none of the observed contents reached potentially toxic levels and, thus, the environment in this regard can be considered as safe for both library staff and visitors. Further research is encouraged in order to obtain more data on the quality of different indoor environments, including specific institutions such as libraries.

Supplementary Information The online version contains supplementary material available at https://doi.org/10.1007/s10661-020-08748-7.

Acknowledgment The work was funded by institutional support for the long term conceptual development of research organization (Moravian Library) by the Czech Ministry of Culture, and by Masaryk University (project MUNI/A/1294/2019). The involvement of Pavel Coufalík was supported by the Institute of Analytical Chemistry of the CAS under the Institutional Research Plan RVO: 68081715.

References

Bo, M., Salizzoni, P., Clerico, M., & Buccolieri, R. (2017). Assessment of indoor-outdoor particulate matter air pollution: a review. *Atmosphere, 8*(12), 136. https://doi.org/10.3390/atmos8080136.

Davis, W. E. (1973). *Emissions study Of industrial sources of lead air pollutants, 1970, EPA contract no. 68-02-0271*. Leawood: W. E. Davis Associates.

Hassan, S. K. M. (2012). Metal concentrations and distribution in the household, stairs and entryway dust of some Egyptian homes. *Atmospheric Environment, 54*, 207–215. https://doi.org/10.1016/j.atmosenv.2012.02.013.

Manso, M., Costa, M., & Carvalho, M. L. (2007). From papyrus to paper: elemental characterization by X-ray fluorescence spectrometry. *Nuclear Instruments and Methods in Physics Research Section A: Accelerators, Spectrometers, Detectors and Associated Equipment, 580*(1), 732–734. https://doi.org/10.1016/j.nima.2007.05.136.

Manso, M., Carvalho, M. L., Queralt, I., Vicini, S., & Princi, E. (2011). investigation of the composition of historical and modern Italian papers by energy dispersive x-ray fluorescence (EDXRF), X-Ray diffraction (XRD), and scanning electron microscopy energy dispersive spectrometry (SEM-EDS). *Applied Spectroscopy, 65*(1), 52–59. https://doi.org/10.1366/10-06105.

Marcotte, S., Estel, L., Minchin, S., Leboucher, S., & Le Meur, S. (2017). Monitoring of lead, arsenic and mercury in the indoor air and settled dust in the Natural History Museum of Rouen (France). *Atmospheric Pollution Research, 8*(3), 483–489. https://doi.org/10.1016/j.apr.2016.12.002.

Mašková, L., Smolík, J., Travnickova, T., Havlica, J., Ondráčková, L., & Ondráček, J. (2016). Contribution of Visitors to the Indoor PM in the National Library in Prague, Czech Republic. *Aerosol and Air Quality Research, 16*(7), 1713–1721. https://doi.org/10.4209/aaqr.2016.01.0044.

Morawska, L., & Salthammer, T. (2003). *Indoor environment airborne particle and settle dust*. https://doi.org/10.1002/9783527610013.

Mukhtar, A., & Limbeck, A. (2013). Recent developments in assessment of bio-accessible trace metal fractions in airborne particulate matter: a review. *Analytica Chimica Acta*Elsevier, *774*, 11–25. https://doi.org/10.1016/j.aca.2013.02.008.

Niu, Y., Wang, F., Liu, S., & Zhang, W. (2021). Source analysis of heavy metal elements of PM2.5 in canteen in a university in winter. *Atmospheric Environment, 244*(April 2020), 117879. https://doi.org/10.1016/j.atmosenv.2020.117879.

Rasmussen, P. E., Levesque, C., Chénier, M., Gardner, H. D., Jones-Otazo, H., & Petrovic, S. (2013). Canadian House Dust Study: Population-based concentrations, loads and loading rates of arsenic, cadmium, chromium, copper, nickel, lead, and zinc inside urban homes. *Science of the Total Environment, 443*, 520–529. https://doi.org/10.1016/j.scitotenv.2012.11.003.

R Development Core Team. (2013). *R: a language and environment for statistical computing*. Vienna: R Foundation for Statistical Computing.

Ridler, V. (1972). *Printing metals*. London: Fry's metals ltd..

Tan, S. Y., Praveena, S. M., Abidin, E. Z., & Cheema, M. S. (2016). A review of heavy metals in indoor dust and its human health-risk implications. *Reviews on Environmental Health, 31*(4), 447–456. https://doi.org/10.1515/reveh-2016-0026.

Tasić, V., Kovačević, R., Maluckov, B., Apostolovski-Trujić, T., Matić, B., Cocić, M., & Šteharnik, M. (2017). The Content of As and Heavy Metals in TSP and PM10 Near Copper Smelter in Bor, Serbia. *Water, Air, & Soil Pollution, 228*(6), 230. https://doi.org/10.1007/s11270-017-3393-6.

Turner, J., & Colbeck, I. (2008). Physical and chemical properties of atmospheric aerosols. In I. Colbeck (Ed.), *Environmental chemistry of aerosols*. Oxford: Blackwell Pub.

WHO. (2000). Guidelines for air quality. Retrieved from https://apps.who.int/iris/handle/10665/66537. Accessed 3 Mar 2020.

WHO Regional Office. (2000). *Air quality guidelines for Europe* (2nd edn.). https://www.euro.who.int/en/publications/abstracts/air-quality-guidelines-for-europe.

Wu, Y., Li, G., Yang, Y., & An, T. (2019). Pollution evaluation and health risk assessment of airborne toxic metals in both indoors and outdoors of the Pearl River Delta, China. *Environmental Research, 179*(July), 108793. https://doi.org/10.1016/j.envres.2019.108793.

Xue, M., Yang, Y., Ruan, J., & Xu, Z. (2012). Assessment of noise and heavy metals (Cr, Cu, Cd, Pb) in the ambience of the production line for recycling waste printed circuit boards. *Environmental Science & Technology, 46*(1), 494–499. https://doi.org/10.1021/es202513b.

Zhang, X., Bai, X., Li, C., Li, T., Wang, R., Zhao, Z., & Norback, D. (2020). Elemental composition of ambient air particles in Taiyuan, China: evaluation of lifetime cancer and non-cancer risks. *Human and Ecological Risk Assessment, 26*(5), 1391–1406. https://doi.org/10.1080/10807039.2019.1579048.

Zhao, X., Lin, L., & Zhang, Y. (2019). Contamination and human health risks of metals in indoor dust from university libraries: a case study from Qingdao, China. *Human and Ecological Risk Assessment: An International Journal*, 1–10. https://doi.org/10.1080/10807039.2019.1697851.

Food Chemistry 298 (2019) 125084

Contents lists available at ScienceDirect

Food Chemistry

journal homepage: www.elsevier.com/locate/foodchem

Analytical Methods

Simultaneous determination of cadmium and iron in different kinds of cereal flakes using high-resolution continuum source atomic absorption spectrometry

Ondřej Zvěřina[a,*], Jan Kuta[b], Pavel Coufalík[c], Pavlína Kosečková[a], Josef Komárek[d]

[a] Department of Public Health, Faculty of Medicine, Masaryk University, Kamenice 5, 625 00 Brno, Czech Republic
[b] Research Centre for Toxic Compounds in the Environment (RECETOX), Faculty of Science, Masaryk University, Kamenice 5, 625 00 Brno, Czech Republic
[c] Institute of Analytical Chemistry of the Czech Academy of Sciences, Veveří 97, 602 00 Brno, Czech Republic
[d] Department of Chemistry, Faculty of Science, Masaryk University, Kotlářská 2, 611 37 Brno, Czech Republic

ARTICLE INFO

Keywords:
Cereals
Cadmium
Iron
Simultaneous determination
HR CS GFAAS

ABSTRACT

A method for simultaneous determination of cadmium and iron in cereal flakes using high-resolution continuum source graphite furnace atomic absorption spectrometry is presented.

Sample digest is introduced into the graphite furnace together with $Pd/Mg(NO_3)_2$ modifier. The primary absorption line of cadmium and adjacent secondary line of iron are used for the determination. Atomization is performed as a two-step process in order to meet ideal conditions for both elements. Interference produced by molecular absorption of PO molecular bands is suppressed by correction model using least squares background correction.

Using the proposed method, levels of cadmium and iron were determined in different kinds of cereal flakes, where both elements are of great interest. Working range (0.01–2 $\mu g\,L^{-1}$ for Cd and 10–500 $\mu g\,L^{-1}$ for Fe) was suitable for the determination of analytes in samples.

The method is fast, robust, and may be routinely used routinely in the analysis of foodstuffs.

1. Introduction

Atomic absorption spectrometry with a graphite furnace (GF AAS) has been one of the most commonly used techniques for trace element determination. In its traditional concept as a line-source AAS technique, the method is most often used for single element analysis. More recently, since the expansion of commercially available high-resolution continuum source (HR CS) spectrometers since 2003 (2007 in the case of the furnace-atomization technique), multielemental analysis has become convenient and reliable even in typical AAS laboratories. The determination of several elements in a single run can significantly shorten the analysis time and even reduce its cost. Nonetheless, several conditions must be fulfilled for such measurement and its optimization may not be straightforward.

Multielemental analysis in HR CS GFAAS is made possible thanks to the combination of a continuum-source short-arc xenon lamp and echelle monochromator with a CCD detector, which allows monitoring not only of the analytical line itself, but also of its spectral neighborhood. Any other line in this spectral interval may also be monitored. The main factor limiting simultaneous analysis, however, is the narrow range of the monitored wavelength, which is about 0.2–0.3 nm in the UV region and where most useful analytical lines are located. The fundamental principles of multielemental analysis in HR CS AAS have already been summed up in a review by Resano, Flórez, and García-Ruiz (2013). Despite limitations arising from the principles of the method, a number of multielemental determinations have been published in the last decade (Ferreira et al., 2018).

In this paper, we present a method for the simultaneous determination of cadmium (Cd) and iron (Fe) in samples of cereal flakes. In fact, dos Santos, Araujo et al. (2009) and dos Santos, Welz et al. (2009) demonstrated the first multielemental use of HR CS GFAAS also in the simultaneous determination of cadmium and iron, employing a prototype spectrometer equipped with solid sampling. The approach was later adapted by Leao, Junior, Brandao, and Ferreira (2016), who extended the method to include the determination of tin. The aim of this work was to develop an easy-to-use analytical method for the simultaneous determination of Cd and Fe in cereal-based foodstuffs, based on the traditional microwave-assisted wet digestion of samples

* Corresponding author.
E-mail address: zverina@med.muni.cz (O. Zvěřina).

https://doi.org/10.1016/j.foodchem.2019.125084
Received 31 January 2019; Received in revised form 12 June 2019; Accepted 25 June 2019
Available online 26 June 2019
0308-8146/

and a commercially available HR CS GFAAS spectrometer.

Both Cd and Fe are very important elements for human health, though in two completely different ways. Fe is an essential element for human life. It is required to make the protein haemoglobin in red blood cells, whose principal function is to transport oxygen from the lungs to the body's cells. The decreased level of haemoglobin in erythrocytes caused by Fe-deficiency anaemia is a worldwide public health problem (Lopez, Cacoub, Macdougall, & Peyrin-Biroulet, 2016). Despite cereals' limited ability to accumulate Fe from soil, together with presence of antinutritional factors (mainly phytate) which hinder its absorption, cereal-based foods present an important dietary source of Fe as they are widely consumed staple foods in many countries (Shahzad, Rouached, & Rakha, 2014; WHO, 1999; EFSA, 2015).

In contrast, Cd is an element offering no beneficial effects on human health. The regular intake of Cd leads to its accumulation and increases the risk of kidney disease, osteoporosis, and developing cancer (Alexander et al., 2009; International Agency for Research on Cancer Monographs, 1993). In the human diet, most Cd comes from agricultural products, as plants accumulate Cd from soils, which may be contaminated by Cd-containing fertilizers or sewage sludge (Alexander et al., 2009). Cereals (especially whole grains) are among the main contributors of dietary Cd intake, primarily because of their high consumption. Different cereal varieties vary in Cd accumulation potential, and therefore, numerous breeding programs aim at reducing the risk related to Cd in human diet (Vergine et al., 2017). In the case of lower body Fe stores, the uptake of Cd from the diet is further enhanced (European Food Safety Authority Scientific Opinion, 2012; Wennberg, Lundh, Nilsson Sommar, & Bergdahl, 2017). For these reasons, the Scientific Panel on Contaminants in the Food Chain (CONTAM) set maximum limits for Cd contents in these foodstuffs (0.10 mg per kilogram of cereal grains excluding wheat and rice, and 0.20 mg per kilogram of wheat and rice grains, wheat bran and wheat germ for direct consumption, and soy beans) (European Food Safety Authority Scientific Opinion, 2012).

In addition to the main objective of developing a reliable method for Cd and Fe determination, a secondary aim was to assess the levels of the two studied metals in different kinds of cereal flakes commonly traded on the Czech market.

2. Experimental

2.1. Samples and sample treatment

In total, 25 packs of various cereal flakes were purchased in local stores. The flakes were of 10 different kinds commonly available in the Czech Republic (coarse and fine oat flakes, spelt, wheat, rye, millet, buckwheat, rice, barley, and amaranth flakes). The products originated mainly from European Union countries, but also from Ukraine, India and China.

About twenty grams of each sample were homogenized using a Pulverisette 7 planetary ball mill (Fritsch GmbH, Germany) for 5 min at 450 RPM. The homogenized material was mineralized using the MLS-1200 Mega microwave digestion system (Milestone, Italy). Three 250-mg aliquots of each sample were mixed with 2.5 mL of nitric acid and 0.5 mL of hydrogen peroxide and digested. The obtained solutions were diluted to a final volume of 25 mL. In the case of the presence of undissolved silicates, the solutions were also filtered.

In addition, sets of six procedural blanks and six mineralizates of BCR-191 Brown bread certified reference material (IRMM, Geel, Belgium) were prepared for quality assurance purposes.

In order to evaluate the influence of HNO_3 concentration on the signal, the residual acidity of digests was determined. Aliquots of digests were titrated with a standardized solution of sodium hydroxide and phenolphthalein as an indicator.

2.2. HR CS GFAAS instrumentation

All measurements were carried out using a ContrAA 800 G high-resolution continuum source atomic absorption spectrometer (Analytik Jena, Germany). The spectrometer is equipped with a Xenon short arc lamp as a continuum source and a high-resolution echelle double monochromator combined with a CCD array detector. The model used was equipped with a transversely heated graphite tube atomizer and an MPE 60 autosampler.

2.3. Analytical lines selection

The primary line of Cd at 228.802 nm and a secondary line of Fe at 228.725 nm of relative sensitivity 0.91% were selected. These lines are located in sufficient proximity and their intensities correspond well with the demands of analysis in terms of required sensitivity. The absorption at both lines was measured using three pixels (the central pixel and the adjacent ones).

2.4. Analytical procedure

For the determination of Cd and Fe in the samples, a 20 µl of digest was introduced into the graphite tube together with 5 µl of Pd/Mg $(NO_3)_2$ modifier. The determination was performed using the 228.802 nm line for Cd and the 228.726 nm line for Fe, these measured simultaneously. The optimized heating program containing the atomization steps is shown in Table 1. The total time of analysis was 152 s (without sample introduction and cooling). The obtained spectra were corrected for interference from PO bands (see chapter Handling interference).

A set of 10 samples were analyzed by means of ICP-MS at the Centre for Toxic Compounds in the Environment RECETOX (Brno, Czech Republic). An Agilent 7700x ICP-MS instrument (Agilent Technologies, Japan) was used for the comparative determination of Cd and Fe in digested samples. Measurement was carried out in He collision mode to suppress potential spectral interferences. Quantification was performed on ^{57}Fe and ^{111}Cd isotopes with correction on ^{72}Ge and ^{115}In internal standards.

3. Results and discussion

3.1. Optimization of temperature program

As Cd and Fe differ significantly in their volatility, the temperature programme has to reflect their thermal behaviour carefully. A sample of oat flake digest with suitable signals for the determined elements was used to develop and optimize the method. A modifier containing 1 g L^{-1} Pd and 0.6 g L^{-1} $Mg(NO_3)_2$ was used for the stabilization of analytes. Fig. 1 shows the pyrolysis and atomization curves for Cd and

Table 1
Temperature program for the simultaneous determination of Cd and Fe.

Step	Temp (°C)	Ramp (°C/s)	Hold (s)	Ar flow (l/min)
Drying 1	80	6	20	2
Drying 2	90	3	15	2
Drying 3	110	5	10	2
Pyrolysis 1	350	50	20	2
Pyrolysis 2	700	300	10	2
Cd atomization	1250	1500	4	0
Fe atomization	2325	2500	5	0
Clean	2550	150	3	2

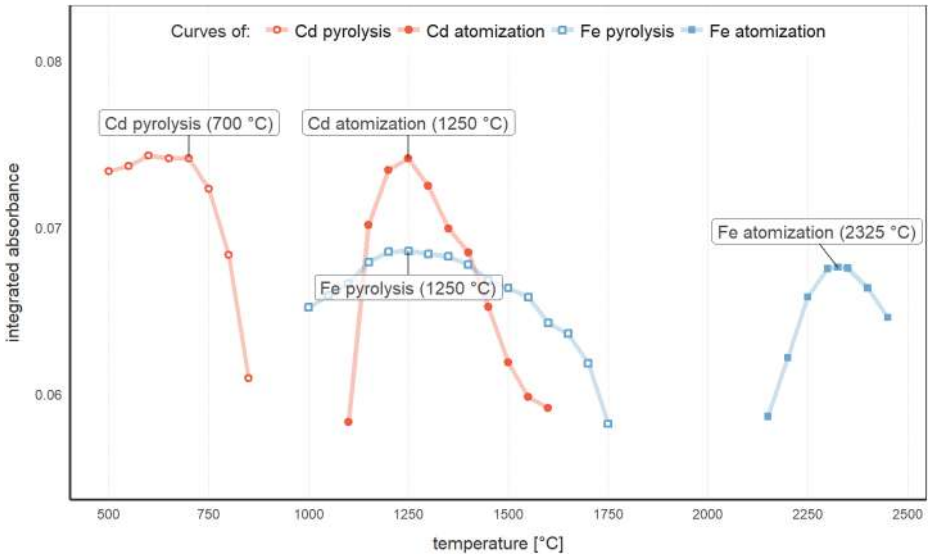

Fig. 1. Atomization and pyrolysis curves for Cd and Fe, obtained by measuring a solution prepared by the acid digestion of oat flakes, and in the presence of Pd/Mg $(NO_3)_2$ modifier.

Fe obtained by injecting 20 µl of oat flake digest together with 5 µl of $Pd/Mg(NO_3)_2$ modifier. The presence of modifier allowed a pyrolysis temperature of 700 °C without any vaporization loss of Cd. The highest signal for Cd was obtained with an atomization temperature of 1250 °C, which was shown to be a suitable temperature for Fe pyrolysis.

By dividing atomization into two steps, a significant improvement in terms of signal intensity and the spatial separation of analytical signals from interference was achieved. Although the analysis can be performed using only one atomization at the Fe atomization temperature of 2325 °C, a 60% increase in the Cd signal was observed when it was measured in optimal conditions, i.e., in a special atomization step at 1250 °C.

In literature, examples of methods based on both single- and multi-step atomizations can be found. The first approach was taken by Leao et al. (2016), who determined Cd, Sn, and Fe in digests of canned foods. A two-step atomization approach was employed in the analysis of grain products, beans, and soil by dos Santos, Araujo et al. (2009) and dos Santos, Welz et al. (2009), who used a prototype high-resolution spectrometer with solid sampling. Using the same prototype, Vignola, Borges, Curtius, Welz, and Becker-Ross (2010) observed an improvement in the Cd signal similar to that reported in this study, during the analysis of sewage sludge employing two atomization steps.

3.2. Handling interference

In addition to improving Cd sensitivity, the two-step atomization approach also allowed the better spatial separation of useful analytical signals from interference produced mostly by the molecular absorption of PO bands. As PO molecules are formed at high temperatures, they do not occur during Cd atomization at 1250 °C. Although it was shown that Pd-based modifier suppresses the formation of PO molecules in favor of atomic phosphorus (Heitmann, Becker-Ross, Florek, Huang, & Okruss, 2006; Lepri et al., 2006; Resano, Briceño, & Belarra, 2009), still, a small level of interference was observed during the second atomization step, this overlapping spectrally with the Fe line. The contribution of PO molecular absorption to the signal varied from sample to sample, but generally accounted for less than 10%. Thanks to the possibilities of least-squares background correction (LSBC), the reference spectrum of PO could be subtracted proportionally from the signal. For this purpose, the reference spectrum of a solution containing 50 µg NaH_2PO_4 was recorded and further subtracted from the signal using LSBC (see Fig. 2).

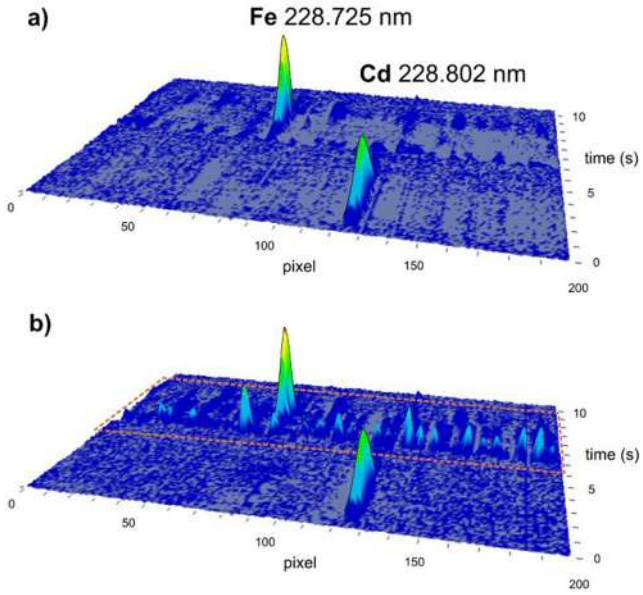

Fig. 2. Spectrum obtained during real sample analysis after (a) and before (b) the masking of interference by background correction.

3.3. Calibration

The calibration was carried out against HNO_3-acidified aqueous standards with a concentration range of 0.05–2 µg L^{-1} Cd and 25–500 µg L^{-1} Fe.

Although the HNO_3 herein used for mineralization causes only mild cuvette corrosion in comparison with highly corrosive acids such as $HClO_4$ or HCl (Rohr, Ortner, Schlemmer, Weinbruch, & Welz, 1999), it is desirable to know its concentration as it forms the main matrix component of the analysed solutions. The concentration of HNO_3 in both reagent and procedural blanks was 1.43 ± 0.01 mol L^{-1}. Residual acidities in sample digests were 1.18 ± 0.03 mol L^{-1}, which means a reduction in the initial acidity by about 20%. Thus, calibration standards were acidified to a similar extent as samples (1 mol L^{-1}). Experiments showed, however, that the slopes of the calibration curves did not differ significantly when using calibration solutions in 0.1-, 1-, and 2 mol L^{-1} HNO_3.

Table 2
Method performance parameters.

Parameter	Cd	Fe
LOD	0.01 µg L^{-1}	0.01 mg L^{-1}
LOD procedural	0.02 µg L^{-1}	0.01 mg L^{-1}
LOD for solid sample[a]	2 µg kg^{-1}	1.4 mg kg^{-1}
LOQ	0.03 µg L^{-1}	0.04 mg L^{-1}
LOQ procedural	0.06 µg L^{-1}	0.05 mg L^{-1}
LOQ for solid sample[a]	6 µg kg^{-1}	4.6 mg kg^{-1}
Spike Recovery[b]	97–106%	93–104%
BCR-191 found[c]	27.6 ± 1.0 µg kg^{-1}	38.2 ± 1.5 mg kg^{-1}
BCR-191 certified	28.4 ± 1.4 µg kg^{-1}	40.7 ± 2.3 mg kg^{-1}

[a] Limits expressed as mass of analyte per mass of sample considering a 0.25 g sample contained in a volume of 25 mL, i.e. dilution factor = 100.
[b] Spike recovery was determined for six real sample solutions spiked with 0.25 µg/l Cd and 250 µg/l Fe, respectively.
[c] Values for certified material are expressed as mean ± standard deviation, obtained by measuring six digests.

3.4. Validation studies

The figures of analytical merit are summarized in Table 2.

The limits of detection (LOD) and quantification (LOQ) were calculated as $3\,s/m$ and $10\,s/m$, respectively, where s is the standard deviation of the signal obtained by repeated analysis of the blank solution and m is the slope of the calibration graph. To cover the whole operation with real samples – digestion, dilution, etc., the procedural LOD and LOQ were calculated with s obtained from the analyses of six digestion blanks.

The accuracy of the method was tested by means of the analysis of the certified reference material BCR-191 Brown Bread in six replicates. Trueness, expressed as method bias, was −2.8% for Cd and −6.1% for Fe. Method precision, calculated as the relative standard deviation of concentrations determined in six digests, was 3.5% for Cd and 4.0% for Fe.

The accuracy of real sample analysis was further investigated by comparing the presented method with a different analytical technique. Fig. 3 presents a comparison of the results obtained by the presented HR CS GFAAS method and ICP-MS measurement. There was no significant deviation between the two methods according to the regression line slopes, which were close to 1 with negligible intercepts.

3.5. Real sample testing: Cd and Fe in cereal flakes

In total, 25 samples of cereal flakes were processed and analyzed using the presented method. Samples were brought into solution by conventional microwave-assisted digestion with a dilution factor of 1:100. The achieved detection limits (Table 2) corresponded to the use of the sensitive primary Cd line and a secondary Fe line with only 0.91% relative sensitivity. The working range that resulted from these parameters was shown to be appropriate for selected samples of cereal flakes and presumably also for other kinds of foodstuffs with similar levels and ratios of the elements (including, for example, fish muscle). The repeatability of the measurement, expressed as the relative standard deviation for five consecutive sample analyses, was < 5% for both elements in most cases.

Table 3
Contents of Cd and Fe in cereal flakes.

cereals	n	cadmium		iron	
		Range (µg.kg^{-1})	Median (µg.kg^{-1})	Range (mg.kg^{-1})	Median (mg.kg^{-1})
oat flakes (coarse)	6	16.0–53.0	45.3	34.8–53.1	48.3
oat flakes (fine)	4	16.0–150	39.8	32.8–58.2	34.3
spelt flakes	2	24.4–44.8	34.6	33.8–35.4	34.6
wheat flakes	2	19.6–21.9	24.2	19.2–31.3	25.2
rye flakes	2	5.6–15.4	10.5	23.0–23.5	23.3
millet flakes	2	6.3–7.4	6.9	7.3–20.3	13.8
buckwheat flakes	3	13.7–20.9	17.2	17.3–24.3	23.7
rice flakes	1	–	33.4	–	5.6
barley flakes	2	7.9–12.6	10.3	15.0–23.6	19.3
amaranth flakes	1	–	16.4	–	66.2

The results are summarized in Table 3. With regard to Cd content, one sample of fine oat flakes with a Cd content of 0.150 mg.kg^{-1} exceeded the maximum level set at 0.1 mg.kg^{-1} (European Commission Regulation (EC) No. 1881/2006 (as amended)). Regarding Fe, coarse cereals are generally considered to be a rich source (Kaur, Jha, Sabikhi, & Singh, 2014). Samples varied greatly in their contents of Fe, with amaranth flakes being the richest source of Fe (66.2 mg.kg^{-1}) and rice flakes being the least rich source (4.8 mg.kg^{-1}).

Oat flakes, which are especially popular in the Czech Republic, contained 32.8–58.2 mg kg^{-1} Fe. Although other cereals such as wheat and rice are consumed in higher quantities, oats are usually eaten as a whole grain cereal in porridge and also included in a variety of baked foods and muesli (Kaur et al., 2014; Rasane, Jha, Sabikhi, Kumar, & Unnikrishnan, 2015). This fact makes oats a more reasonable Fe source, since a significant proportion of the Fe located in the seedy parts other than endosperm is usually lost during milling (Shahzad et al., 2014). However, it should be stressed that, for the same reason, whole grains contain more Cd than milled and processed material (Alexander et al., 2009; Cubadda, Raggi, Zanasi, & Carcea, 2003).

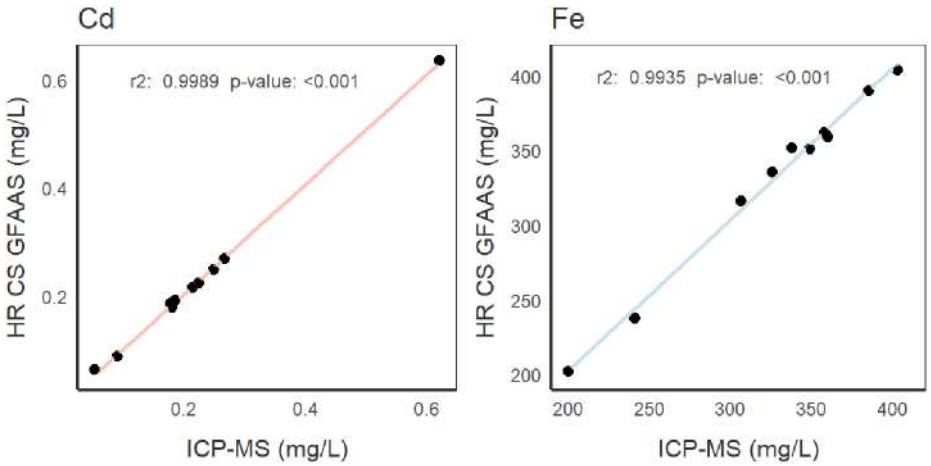

Fig. 3. Comparison of Cd and Fe concentrations in 10 randomly selected digests obtained by ICP-MS and the proposed HR CS GFAAS method (the curves' slopes are 1.0146 and 1.0134, respectively).

3.6. Conclusions: method overview

The presented method for the simultaneous determination of Cd and Fe was proven to work well during routine usage. In this approach, the two elements are determined in a single run. $Pd/Mg(NO_3)_2$ modifier is used for its thermal stabilization. The method is fast, simple, and does not require the use of any permanent modifier.

The accuracy of the method was verified by means of the analysis of certified reference material. The achieved sensitivity enabled the determination of Cd and Fe in all tested samples. Results were in excellent agreement with the comparative analysis of samples using ICP-MS.

The analysis of the two studied elements in one firing is faster and more economical than separate analyses. The method may be widely applicable in laboratories equipped with HR CS GFAAS spectrometers due to its simplicity and robustness and to the fact that both Cd and Fe are often of particular interest.

Acknowledgements

This work was financially supported by Masaryk University (projects MUNI/A/1288/2017, MUNI/A/1278/2018, and by funds from the Faculty of Medicine MU to junior researcher Ondřej Zvěřina) and the RECETOX research infrastructure (LM2015051 and CZ.02.1.01/0.0/0.0/16_013/0001761). The involvement of Pavel Coufalík was supported by the Institute of Analytical Chemistry of the CAS under the Institutional Research Plan RVO: 68081715.

Declaration of Competing Interest

The authors declare no competing financial interest.

References

Alexander, J., Benford, D., Cockburn, A., Cravedi, J., Dogliotti, E., Di Domenico, A., ... Verger, P. (2009). Scientific Opinion of the Panel on Contaminants in the Food Chain on a request from the European Commission on cadmium in food. *The EFSA Journal, 980*, 1–139. https://doi.org/10.2903/j.efsa.2009.980.

Cubadda, F., Raggi, A., Zanasi, F., & Carcea, M. (2003). From durum wheat to pasta: Effect of technological processing on the levels of arsenic, cadmium, lead and nickel–a pilot study. *Food Additives and Contaminants, 20*(4), 353–360. https://doi.org/10.1080/0265203031000121996.

Dos Santos, L. M. G., Araujo, R. G. O., Welz, B., Do, S., Jacob, C., Goreti, M., ... Becker-Ross, H. (2009). Simultaneous determination of Cd and Fe in grain products using direct solid sampling and high-resolution continuum source electrothermal atomic absorption spectrometry. *Talanta, 78*, 577–583. https://doi.org/10.1016/j.talanta.2008.12.006.

Dos Santos, L. M. G., Welz, B., Araujo, R. G. O., Jacob, S. do C., Vale, M. G. R., Martens, A., ... Becker-Ross, H. (2009). Simultaneous determination of Cd and Fe in beans and soil of different regions of Brazil using high-resolution continuum source graphite furnace atomic absorption spectrometry and direct solid sampling. *Journal of Agricultural and Food Chemistry, 57*(21), 10089–10094. https://doi.org/10.1021/jf9024773.

European Food Safety Authority Scientific Opinion (2012). SCIENTIFIC REPORT OF EFSA Cadmium dietary exposure in the European population 1. *EFSA Journal, 10*(1), 1–37. https://doi.org/10.2903/j.efsa.2012.2551.

EFSA Panel on Dietetic Products, Nutrition and Allergies (NDA) (2015). Scientific opinion on dietary reference values for iron. *EFSA Journal, 13*(10), 4254. https://doi.org/10.2903/j.efsa.2015.4254.

Ferreira, S. L. C., Bezerra, M. A., Santos, A. S., dos Santos, W. N. L., Novaes, C. G., de Oliveira, O. M. C., ... Garcia, R. L. (2018). Atomic absorption spectrometry – A multi element technique. *TrAC Trends in Analytical Chemistry, 100*, 1–6. https://doi.org/10.1016/J.TRAC.2017.12.012.

Heitmann, U., Becker-Ross, H., Florek, S., Huang, M. D., & Okruss, M. (2006). Determination of non-metals via molecular absorption using high-resolution continuum source absorption spectrometry and graphite furnace atomization. *Journal of Analytical Atomic Spectrometry, 21*(11), 1314. https://doi.org/10.1039/b607384k.

International Agency for Research on Cancer Monographs. (1993). Cadmium and cadmium compounds. Lyon. Retrieved from https://monographs.iarc.fr/wp-content/uploads/2018/06/mono100C-8.pdf.

Kaur, K. D., Jha, A., Sabikhi, L., & Singh, A. K. (2014). Significance of coarse cereals in health and nutrition: A review. *Journal of Food Science and Technology, 51*(8), 1429–1441. https://doi.org/10.1007/s13197-011-0612-9.

Leao, D. J., Junior, M. M. S., Brandao, G. C., & Ferreira, S. L. C. (2016). Simultaneous determination of cadmium, iron and tin in canned foods using high-resolution continuum source graphite furnace atomic absorption spectrometry. *Talanta, 153*, 45–50. https://doi.org/10.1016/j.talanta.2016.02.023.

Lepri, F. G., Dessuy, M. B., Goreti, M., Vale, R., Borges, D. L. G., Welz, B., & Heitmann, U. (2006). *Investigation of chemical modifiers for phosphorus in a graphite furnace using high-resolution continuum source atomic absorption spectrometry*https://doi.org/10.1016/j.sab.2006.08.001.

Lopez, A., Cacoub, P., Macdougall, I. C., & Peyrin-Biroulet, L. (2016). Iron deficiency anaemia. *The Lancet, 387*(10021), 907–916. https://doi.org/10.1016/S0140-6736(15)60865-0.

Rasane, P., Jha, A., Sabikhi, L., Kumar, A., & Unnikrishnan, V. S. (2015). Nutritional advantages of oats and opportunities for its processing as value added foods – A review. *Journal of Food Science and Technology, 52*(2), 662–675. https://doi.org/10.1007/s13197-013-1072-1.

Resano, M., Briceño, J., & Belarra, M. A. (2009). *Direct determination of phosphorus in biological samples using a solid sampling-high resolution-continuum source electrothermal spectrometer: Comparison of atomic and molecular absorption spectrometry*https://doi.org/10.1039/b907937h.

Resano, M., Flórez, M. R., & García-Ruiz, E. (2013). High-resolution continuum source atomic absorption spectrometry for the simultaneous or sequential monitoring of multiple lines. A critical review of current possibilities. *Spectrochimica Acta Part B: Atomic Spectroscopy, 88*, 85–97. https://doi.org/10.1016/j.sab.2013.06.004.

Rohr, U., Ortner, H., Schlemmer, G., Weinbruch, S., & Welz, B. (1999). Corrosion of transversely heated graphite tubes by mineral acids. *Spectrochimica Acta Part B: Atomic Spectroscopy, 54*(5), 699–718. https://doi.org/10.1016/S0584-8547(98)00254-7.

Shahzad, Z., Rouached, H., & Rakha, A. (2014). Combating mineral malnutrition through iron and zinc biofortification of cereals. *Comprehensive Reviews in Food Science and Food Safety, 13*(3), 329–346. https://doi.org/10.1111/1541-4337.12063.

Vergine, M., Aprile, A., Sabella, E., Genga, A., Siciliano, M., Rampino, P., ... De Bellis, L. (2017). Cadmium concentration in grains of durum wheat (Triticum turgidum L. subsp. durum). *Journal of Agricultural and Food Chemistry, 65*, 42. https://doi.org/10.1021/acs.jafc.7b01946.

Vignola, F., Borges, D. L. G., Curtius, A. J., Welz, B., & Becker-Ross, H. (2010). Simultaneous determination of Cd and Fe in sewage sludge by high-resolution continuum source electrothermal atomic absorption spectrometry with slurry sampling. *Microchemical Journal, 95*(2), 333–336. https://doi.org/10.1016/J.MICROC.2010.01.014.

Wennberg, M., Lundh, T., Nilsson Sommar, J., & Bergdahl, I. A. (2017). Time trends and exposure determinants of lead and cadmium in the adult population of northern Sweden 1990–2014. *Environmental Research, 159*, 111–117. https://doi.org/10.1016/j.envres.2017.07.029.

WHO. (1999). Prevention and Control of Iron Deficiency Anaemia in Women and Children. Retrieved from https://www.who.int/nutrition/publications/micronutrients/anaemia_iron_deficiency/UNICEF_WHO_ida_consutlation_report.pdf?ua=1.